Magma genesis and slab-wedge interaction across an island arc-continent collision zone, East Sunda Arc, Indonesia

J.A. Hoogewerff

Magma genesis and slab-wedge interaction across an island arc-continent collision zone, East Sunda Arc, Indonesia.

J.A. Hoogewerff

Magma genesis and slab-wedge interaction across an island arc-continent collision zone, East Sunda Arc, Indonesia.

Magmagenese en interactie tussen onderschuivende plaat en mantelwig in een eilandboog-continent botsingsgebied, Oostelijke Sundaboog, Indonesië.

(MET EEN SAMENVATTING IN HET NEDERLANDS)

PROEFSCHRIFT TER VERKRIJGING VAN DE GRAAD VAN DOCTOR
AAN DE UNIVERSITEIT UTRECHT
OP GEZAG VAN DE RECTOR MAGNIFICUS, PROF. DR. H.O. VOORMA,
INGEVOLGE HET BESLUIT VAN HET COLLEGE VOOR PROMOTIES
IN HET OPENBAAR TE VERDEDIGEN OP VRIJDAG 24 SEPTEMBER 1999
DES VOORMIDDAGS OM 10.30 UUR

DOOR

JURIAN ADRIAAN HOOGEWERFF

GEBOREN OP 25 JUNI 1960 TE UTRECHT

PROMOTOREN: PROF. DR. R.D. SCHUILING
               PROF. DR. J. HERTOGEN

CO-PROMOTOR: DR. M.J. VAN BERGEN

This thesis is dedicated to
the people of Adonara, Lembata,
Pantar, Treweg, Pura Besar, Ternate,
Kisu and Alor. Their „Menschlichkeit"
is as natural as the land they live on.

Contents

Foreword

This thesis is the fruit of almost ten years of fascination with magma-genesis in the subduction environment. During the first four years as a doctorate student at Utrecht University I was in the lucky circumstances to be able to collect a fine set of samples in east Indonesia and successively use many different analytical techniques resulting in a wealth of data. This wealth of data was a blessing and a curse at the same time as I was sure that this data-set might shed some light on great enigmas in subduction. This was also a curse as I was convinced that small parts of the holy subduction grail were in the data set and this made me unwilling to just quickly finish the thesis for the sake of a doctorate. In the years following the time in Utrecht I spend most of my free time wrestling with the data and now I feel I have some understanding of what is happening under eastern Indonesia.

For me the most important conclusion is that conservative bulk mixing of different mantle and crustal reservoirs does not provide a satisfactory explanation for the many observations in arc volcanism. In future we should be much more aware that groups of elements and individual elements all have their own geochemical characteristics and thus their own pathways, sinks etc. I hope that in this thesis I have shown that it is possible with simple mathematical models, systematic treatment of the different element groups and some unorthodox graphics to gain better understanding of magma-genesis in subduction zones.

During the years I have had much support and understanding from my wife, family, friends and colleagues who were all looking forward to see "het blauwe boekje" ("the little blue book": the thesis from Utrecht University). I hope it has been worth waiting for.

Fieldwork took place during the springs of 1989 and 1990. The islands are well populated (even the smallest) and the living conditions of the people vary from simple to poor depending on the availability of fresh water. Fresh water is very sparse on the island of Pantar and almost absent on the island of Treweg. Small dirt roads crossing the islands exist on Adonara, Lembata and Alor but usually trails had to be used with help of local guides, carriers and mules. Hospitality on the islands was heartwarming especially considering the poverty of the people. It is for this reason that this thesis is dedicated to the peoples of Adonara, Lembata, Pantar, Treweg, Pura Besar, Ternate, Kisu and Alor. The reality of their existence has given me a new perspective on being a scientist in a western country, a rare privilege indeed.

Concerning the scientific part of the study I thank my supervisor and co-promotor Manfred van Bergen for the support during all those years. He taught me to be an uncompromising researcher. I have to thank Conny van Bergen for being a great team-mate in Indonesia and being very understanding of Manfred and me during the last years. I thank Jan Hertogen and Olaf Schuiling for willing to be my promotors and their contribution to reviewing the manuscript and models used. I thank Pieter Vroon for sharing his knowledge in volcanology, mass-spectrometry, his interest in virtual flying and his support and friendship.

I thank Prof. Bernhard de Jong, and Prof. Jacques Touret for their critical reviews of the manuscript.

Summary

This thesis presents the results of a detailed trace element and isotope geochemistry study into the magma-genesis of volcanoes in the Adonara-Pantar Section (APS) of the East Sunda Arc in Indonesia, a setting where an oceanic island arc is colliding with a passive continental margin.

Sr, Nd, Pb, Ra, Th and U isotopes were analysed together with major and trace elements from five active and more than ten inactive volcanic centres on seven islands of the APS. In order to characterise the input into the subduction zone, literature data and additional analyses on samples of marine sediments from locations in front of the Timor Trough *(Vroon, 1982; Vroon et al., 1995)* were used.

The results of this study (1) identify different mantle and subduction-related components that contribute to the magma source region in the sub-arc mantle of the APS, (2) provide constraints for the mode of material transfer between the subducted slab and these magma sources, and (3) provide insight into spatial changes of this process as a function of the depth of the Benioff-Zone.

Careful consideration of isotope and trace element systematics suggests that one or two mantle components and three subduction-related components contribute to the magma generation in the APS. The mantle component consists of depleted Indian Ocean mantle (I-DM) which may contain enriched domains (I-EM), although their presence is not necessarily required to explain the observations. The subduction-related components consist of Subducted Continental Material (SCM), which changes systematically in composition from east to west, and crystalline Australian continental crust.

There appear to be different modes of mass transfer from the slab into the mantle wedge. At the frontal part of the APS arc, a hydrous fluid enriches the mantle wedge with only a selective group of elements. At the central and rear arc sections the subducting slab partially melts and a siliceous liquid subsequently enriches the mantle wedge.

The mantle wedge in the frontal part of the APS is depleted in trace elements and has a HFSE, REE and Nd-isotopic composition similar to that found in depleted Indian Ocean mantle (I-DM) close to the APS (e.g. DSDP261; *Weis and Frey, 1996*).

Pb isotopic signatures (e.g., elevated $^{208}Pb/^{204}Pb$ relative to I-DM) are difficult to explain by the subduction of sediments as represented by the cores taken in front of the arc. They can be attributed to local mantle characteristics or to involvement of subducted lithologies that have remained inaccessible for sampling. The presence of domains with the required I-EM-type signatures in the subarc-mantle would be consistent with mantle inhomogeneity in the NE part of the Indian Ocean as documented by Weis and Frey *(1996)*. Though theoretically conceivable, there is no need to invoke models for involvement of asthenospheric mantle that could rise through a slab window in response to incipient slab-detachment.

A more likely alternative to explain some of the more extreme lead isotopic data in the APS is involvement of subducted crystalline Australian crust. Evidence for subduction of the Australian continental margin is also provided by extremely radiogenic He-isotope ratios observed in the frontal volcanoes, as we have argued in Hilton et al.*(1992)*. Furthermore, Nd-isotope systematics as well as HFSE/HFSE and REE/HFSE ratios are consistent with a contribution from this source, even if an I-EM-type mantle would be present.

Across-arc systematics in U-series and other trace elements reflect a progressive down-dip change in the nature of the SCM-derived subduction component: a high U/Th, Ra/Th and LILE-enriched hydrous fluid in the shallow parts, and a siliceous-melt with a U/Th similar to

that of bulk SCM at greater depths.

Trace element modelling of the possible composition of a slab-derived melt demonstrates that a residual eclogitic composition (garnet + clinopyroxene) in the subduction SCM, with additional rutile (and possibly zircon), is capable of explaining most of the observed HFSE (Nb/Ta) and REE signatures in the central and rear arc sections. The stability of residual rutile during melting or dehydration of subducted sediment may thus explain the low HFSE/LILE ratios that the APS has in common with other subduction settings.

The combined spatial geochemical systematics in the APS volcanoes document that these changes in magmagenetic regimes occur at depths of the subducted slab between 100 and 250 km. Material transfer processes at the slab-wedge interface during progressive dehydration and melting produce variations in magma compositions that are dominated by changing mobilities of trace elements. Unlike models for more common oceanic island arcs, these slab components are largely derived from subducted sediments and continental lithologies, reflecting a setting with collision-induced involvement of a passive continental margin.

Samenvatting

Dit proefschrift bevat de resultaten van een gedetailleerd onderzoek naar het ontstaan van magma onder de vulkanen in de Adonara-Pantar sectie (APS) van de Oostelijke Sunda Boog in Indonesië middels de geochemie van sporenelementen en isotopen. De bestudeerde sectie is een relevant onderzoeksgebied, daar hier de Indonesische vulkanische eilandboog botst met het Australische continent. Dit heeft tot gevolg dat er een groot contrast is in de samenstelling van de mogelijke componenten die aan dit type van magmagenese bijdragen.

Van vijf actieve vulkanen en meer dan tien inactieve vulkanische centra zijn de isotopen van Sr, Nd, Pb, Ra, Th en U samen met hoofd- en sporenelementen geanalyseerd. Om het materiaal te karakteriseren dat in de Timor Trog in de subductiezone mee naar beneden gesleurd wordt is gebruik gemaakt van literatuurdata en extra analyses van monsters genomen tijdens de Snellius expeditie in 1985 *(Vroon, 1982; Vroon et al, 1995)*.

De resulaten van deze studie tonen: (1) de verschillende mantel- en subductie-gerelateerde componenten welke een rol spelen bij het ontstaan van magma in de mantelwig onder de vulkanen; (2) de processen die het meest waarschijnlijk het transport van materiaal van de subducerende plaat in de mantelwig bepalen; (3) de invloed van de diepte van de Wadati-Benioff-Zone op bovengenoemde processen.

Zorgvuldige afweging van de verschillende mogelijkheden leidt tot de conclusie dat één of twee mantelcomponenten en drie aan de subductie gerelateerde componenten de samenstelling van het magma in de Adonara-Pantar sectie bepalen.

De mantelcomponenten zijn een chemisch "verarmde" Indische Oceaan mantel en een "aangerijkte" Indische Oceaan mantel waarbij de aanwezigheid van de laatste niet absoluut noodzakelijk is om alle waarnemingen te verklaren.

De aan de subductie gerelateerde componenten bestaan uit: gesubduceed continentaal materiaal (SCM) dat parallel aan de boog een systematische samenstellingsverandering ondergaat en kristalijne Australische korst.

Uit de waarnemingen kan worden afgeleid dat er twee manieren zijn waarop materiaal van de gesubduceerde plaat (slab) in de mantelwig getransporteerd wordt. In het zuidelijke ondiepe deel van de boog wordt de mantelwig aangerijkt door een fluïdale oplossing welke opstijgt uit de ondergeschoven plaat. Deze oplossing transporteert slechts een beperkt aantal elementen. In het middelste deel en aan de achterzijde van de boog smelt de ondergeschoven plaat ten dele op en de ontstane silica-rijke smelt verrijkt de mantel met bijna alle sporen-elementen.

Omdat in het ondiepe gedeelte de oorspronkelijk mantelwig slechts aangerijkt wordt met beperkt aantal elementen kunnen de verhoudingen van de bepaalde andere elementen en Nd-isotopen gedetailleerd uitsluitsel geven over de oorspronkelijke mantelsamenstelling onder de onderzochte vulkanen. Deze gevonden samenstelling komt goed overeen met de samenstelling van "verarmde" Indische Oceaan mantel zoals die dicht bij de bestudeerde Adonara-Pantar sectie op DSDP lokatie 261 *(Weis and Frey, 1996)* in de Indische Oceaan gevonden wordt.

De lood-isotopen signaturen in de vulkanen (vooral $^{208}Pb/^{204}Pb$) laten zich niet verklaren door een combinatie van "verarmde" mantel en SCM alleen. Eén mogelijkheid is de aanwezigheid van "aangerijkte" manteldomeinen zoals die ook beschreven worden door Weis en Frey (*1996*). De "aangerijkte" mantel zou bijvoorbeeld door een breuk in de subducerende plaat in de mantelwig kunnen dringen. Een tweede, minder gecompliceerde verklaring, is dat

de rand van het kristallijne kontinent reeds diep genoeg in de mantel is doorgedrongen om deel te nemen aan het magmageneratie proces. Bewijs hiervoor hebben wij reeds gepubliceerd in Hilton et al. *(1992)* waar aangetoond is dat zeer lage He-isotopenwaarden het best verklaard kunnen worden door deelname van kristallijne korst aan het magma geneseproces. In de hier gepresenteerde studie wijzen ook Nd-isotopen en HFSE/HFSE- en REE/HFSE-ratios erop dat de rand van het Australische continent in de magma generatiezone is aangekomen.

De ruimtelijke systematiek van uraan en haar dochter-isotopen, in de richting van de subductie, duidt op een verandering in de aard van het materiaaltransport vanuit de ondergeschoven plaat in de mantelwig. In de ondiepe gedeelten wordt het transport bepaald door een fluïdale oplossing met hoge U/Th- en Ra/Th-ratios en hoge LILE-gehalten. In de diepere gedeelten transporteert een silica rijke smelt met U/Th-ratios gelijk die van SCM, materiaal vanuit de ondergeschoven plaat in de mantelwig.

Uit de modellering van de meest waarschijnlijke samenstelling van de silica rijke smelt blijkt dat de waargenomen HFSE en REE signaturen in de middelste en noordelijkste vulkanen het best verklaard kunnen worden met een ondergeschoven plaat waarvan de (voor sporenelementen relevante) residuaire mineralogische samenstelling bestaat uit granaat, clinopyroxeen en rutiel. De stabiliteit van het residuaire rutiel kan dus de lage HFSE/LILE ratios in de Adonara-Pantar sector en waarschijnlijk ook in andere eilandbogen verklaren.

De gecombineerde waarnemingen in de Adonara-Pantar sector tonen aan dat de waarnemingen en processen zoals boven beschreven gebeuren daar waar de onderschuivende plaat tussen 100 en 250 km diep onder de vulkanen ligt.

x

1 Introduction

The study of the processes operating at subduction zones is essential for the understanding of long-term global geochemical cycles of all natural elements. In general, three main subduction settings can be distinguished: intra-oceanic arcs, where oceanic crust is subducting under oceanic crust, destructive continental margins, where oceanic crust is subducting under continental crust, and continental collision, where (leading) parts of a passive continental margin collide with or are (partly) subducted under either an oceanic plate or another continent. The first two settings will always be present somewhere on earth, as oceanic crust production at mid-oceanic ridges demands destruction of older oceanic crust elsewhere. Continental collision happens where a drifting continent arrives at the trench of either an intra-oceanic arc or a destructive continental margin. Knowledge of the fate of subducted crustal material in any of these settings is crucial for the understanding of global geochemical cycles, as subduction of crustal material is a way to recycle it back into the mantle. An important question to answer is, if the recycling is a "bulk" process or if only certain elements return back into the mantle while others are preferentially transported to the overlying crust by the "subduction component".

In Figure 1.1 a generalised model for possible components and processes in a subduction setting is presented *(after Pearce and Peate, 1995)*. From Figure 1.1 it is clear that a complex set of processes might be involved in subduction magma genesis.
First there are the slab-related processes:
    1. shallow fluid loss through the accretionary wedge
    2. dehydration reactions and partial melting with increasing depth
Next transport of the slab component will become important:
    3. cryptic or modal enrichment of the down-dragged mantle by the slab component
    4. secondary dehydration caused by the breakdown of amphibole at about 100 km
    5. at deeper levels secondary dehydration through the breakdown of phlogopite
    6. melting of the mantle in the presence of water at T >1000 °C
    7. migration of small-volume hydrous melts
Mantle-source processes of importance are:
    8. mantle source depletion in the back arc through adiabatic melting
    9. replenishment of the arc-magma source with normal mantle and/or enriched domains
    10. mantle source enrichment by delamination of lithospheric mantle
Melt-column processes:
    11. buoyancy-driven counter flow
    12. decompression melting from 60 km upward
    13. selective tapping of the melting column
Lithosphere-melt interactions:
    14. melt segregation at the base of the lithosphere
    15. AFC processes within mantle lithosphere
    16. magma storage and segregation at the base of the crust
    17. AFC processes within the crust
This thesis will primarily deal with items 2, 3, 4, 5, 6, 7 and 9.
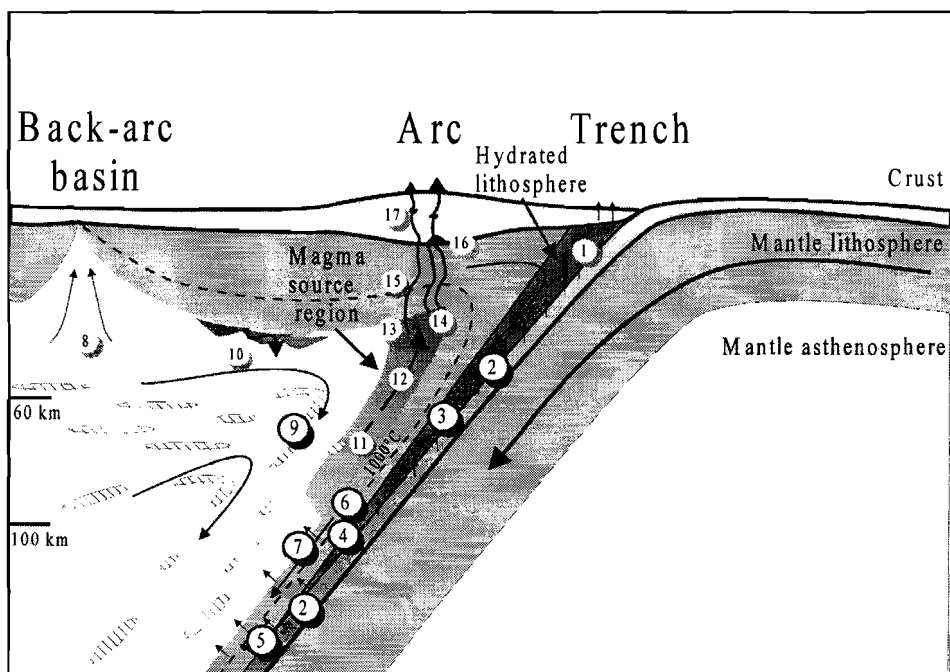
Figure 1.1. Overview of processes involved in arc magmatism *(after Pearce and Peate, 1995)*. Highlighted numbers refer to the slab mantle-interface processes treated in detail in this thesis. For explanation of the numbers see text.

In the light of the complexity mentioned above our research has focused on the Eastern Sunda volcanic arc (Fig. 1.2) because from the tectonic setting we expected a maximum geochemical contrast between subduction-related components and the sub-arc mantle, which would simplify the task of determining the mode of interaction between various endmembers that are potentially involved in arc magma genesis. The setting makes the area particularly attractive because the overriding plate consists of oceanic crust of the Banda Sea, whereas the subducting slab carries sediments derived from the ancient Australian continent and may even include the leading parts of the northward moving passive Australian continental margin (*Hilton et al. 1992*, this thesis). Furthermore, previous work has provided neither indication for the presence of continental slivers within the Adonara-Pantar Sector (APS) of the Banda Sea crust in the Eastern Sunda Arc (ESA) nor for any shallow-level crustal contamination that would obscure primary geochemical signals from magma sources. Major effects from Assimilation (A) and Contamination (C) processes 15, 16 and 17 in Fig. 1.1 can therefore be excluded. Finally, the favourable geographic distribution of active volcanoes in the APS allows us to detect changes in magma-genetic processes with increasing depth of the subducting plate.

The Adonara-Pantar Sector of the East Sunda Arc borders the volcanically inactive Alor-Wetar Sector, which separates the East Sunda Arc from the Banda Arc. Cessation of activity is assumed to be the result of a more evolved stage of collision between the island arc and the Australian continent *(Hamilton, 1979)*. Indeed, the smaller the distance to the inactive sector is,

2

Australian continent *(Hamilton, 1979)*. Indeed, the smaller the distance to the inactive sector is, the larger the contribution from a continental source to the geochemical signatures of the volcanics appears to be *(Van Bergen et al., 1993)*.

The islands in the APS have dimensions on the order of several tens of kilometres, and harbour a total of five active volcanoes and four to seven recently extinct volcanoes as well as older volcanic basement. The active volcanoes occur in an 80 km wide band on Benioff-Zone depth-contours ranging from 100 to about 300 km *(McCaffrey, 1989)*.
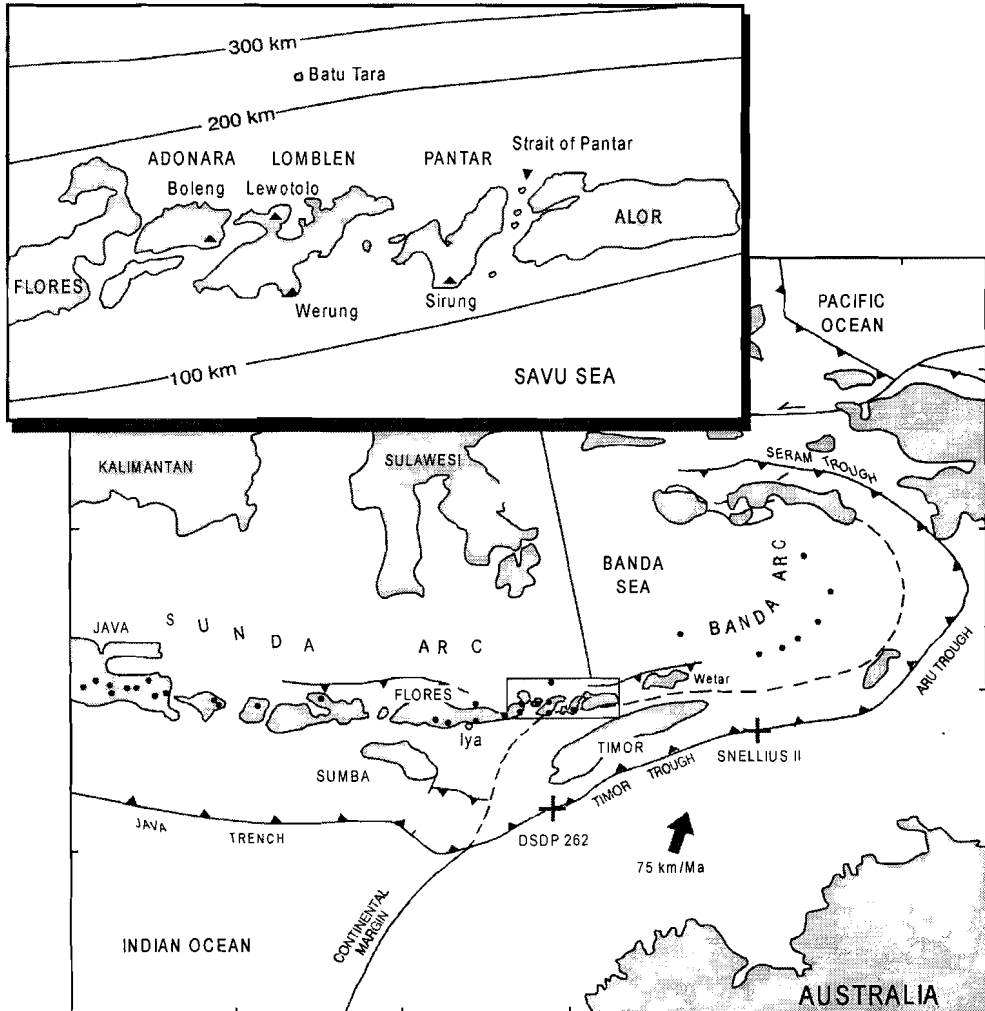
Figure 1.2. Overview of the area studied in Eastern Indonesia.

The structure of this thesis is as follows:

In chapter 2 a literature survey is given about across-arc systematics. The geological setting of the APS is discussed in chapter 3. Chapter 4 documents the field observations, petrography and major element geochemistry. In chapter 5 the possible within-suite variations will be discussed for each volcano.

On the basis of known isotopic (and selected trace element) characteristics of mantle and sedimentary components, the sources involved in magma genesis in the APS are identified in chapter 6. In chapter 7 U-series disequilibrium results are presented and used to evaluate the different subduction components, and to assess the time frame between dehydration of the slab to magma eruption at the surface.

In chapter 8 an attempt is made to integrate the results from the previous chapters with a detailed analysis of trace element behaviour in order to:

- quantify the dehydration and partial melting processes as a function of depth (2 in Fig. 1.1);
- determine the nature of the pre-subduction mantle wedge (9 and 10 in Fig. 1.1); and
- infer the mode of interaction between the subduction component and the mantle wedge (3, 4, 5 and 6 in Fig. 1.1).

4

2 Island-Arc Volcanism

2.1 Introduction

Although a large number of studies have attempted to explain the geochemistry of subduction-related lavas, there is still no unequivocal solution to the problem of distinguishing between the contributions of different sources and the role of magma-genetic processes *(Arculus, 1985; Arculus, 1994)*. Sources contributing to the formation of magma should lie either in the subducting slab, in the overriding mantle wedge or a combination of both *(see figure 1.1)*. Systematic changes in the geochemical signatures of volcanoes that form an array across an arc system are observed in many areas. In early papers they have been referred to as K-h relation, indicating an increase of potassium content (K) with increasing distance to the Benioff-Zone (h). These findings are evidence for the existence of down-dip variations in sources as well as processes. Here some of the parameters that are most relevant to this study are discussed. A general review of arc magmatism is given in Gill *(1981)*. Pearce and Peat *(1995)* reviewed and discussed all possible processes in arc magmatism.

The mantle wedge below arc volcanoes is generally considered to have characteristics of a MORB-source, which could be fertile or depleted by previous melt extraction (e.g. *Perfit et al.,1980; Woodhead et al., 1993)*. In the case of intra-oceanic arcs, the mantle wedge will most likely consist of a layer of Depleted Mantle down to depths of around 70 km underlain by more fertile mantle unaffected by previous MORB generation *(see Fig. 1.1)*. As arc magmatism coincides with Benioff depths between 100 and 300 km, both depleted and fertile mantle domains may be involved.

As an alternative hypothesis, it has been proposed that portions of the sub-arc mantle involved in magma genesis may have characteristics of an Enriched Mantle source *(Morris and Hart, 1983)*, whereas mixed MORB-source and enriched-mantle affinities have been considered as well *(Gill, 1984; Stern et al., 1991; Hickey-Vargas, 1992)*.

At active continental margins the sub-continental mantle is assumed to have geochemical characteristics distinct from the mantle-wedge reservoir in intra oceanic island arcs. The continental lithosphere has a thickness up to 140 km, whereas the oceanic lithosphere reaches a maximum of some 80 km *(Davidson et al., 1991; Wilson, 1989)*. The sub-continental lithosphere may have undergone multiple metasomatism events, and may thus be both enriched and depleted in certain elements.

2.2 The K-h relation

2.2.1 Historical

The systematic spatial distribution of alkaline rocks behind volcanic arcs and of andesitic rocks at the front of arcs was first described by Tomita *(1935)* in the Sakhalin-Japan arc. Tomkeiff *(1949)* described a similar trend in the Kamchatka-Kurile arc and acknowledged that there may be some tectonic control which causes the sub-alkaline magmas to be associated with folded "arcuate" mountains and the alkaline magmas with vertical

5

associated with folded "arcuate" mountains and the alkaline magmas with vertical movements and foundering of the earth's crust. Brouwer *(1940)* recognised the mineralogical trends in the APS from Werung via Lewotolo to Batu Tara without giving an explanation. Brouwer also already compared Batu Tara with the Muriah volcano on Java. Rittman (*1953)* discussed data from the whole Indonesian Sunda arc, and convincingly showed across-arc trends including the exceptionable composition of Batu Tara.

Wadati and Iwai *(1954)* were the first to suggest a relation between depth of the (what later would be named) Wadati-Benioff-Zone and genesis of magmas in the Japanese arc. At that time, however, the Wadati-Benioff-Zone had not yet been identified as the contact between slab and mantle wedge. Kuno *(1959)* believed that the melting process was responsible for the seismic disturbances. Attempts were made to find chemical parameters, which correlated consistently with depth *(Rittman, 1953; Kuno, 1959; Sugimura, 1960)*.

Benioff *(1954)*, independent from the work of Wadati, gave an overview of all major arcs, and envisaged a rigid oceanic block (650 km thick) sinking underneath the block on which an arc is situated. Benioff suggested that a part of the seismic energy that is released at the fault interface provides the energy for melting.

Oliver and Sacks *(1967)* were the first to suggest that the Wadati-Benioff seismic zones might be the upper surfaces of thick slabs of oceanic crust and upper mantle, carried beneath the arcs as part of a fundamental movement plan related to ocean floor spreading and continental drift.

The first modern papers, which not only showed a relation between the presence of a Wadati-Benioff-Zone and volcanism but also one between depth of the Wadati-Benioff (h) and potassium content (K) in the volcanics, were published by Dickinson and Hatherton *(Dickinson and Hatherton,1967; Hatherton, 1967; Hatherton and Dickinson 1969; Dickinson and Hatherton, 1975)*. In their 1969 article they suggested a Wadati-Benioff-Zone depth of 240 km for Lewotolo and 380 km for Batu Tara.

2.2.2 Contemporary research

Jakeš and White *(1972)* and Gill *(1981)* have given critical reviews of element abundances and across-arc systematics. Besides the increase in K across arcs, also an increase in K_2O/Na_2O, LILE and LREE was documented. Phenocryst assemblages showed across-arc trends, with biotite and hornblende appearing in the high-K series, consistent with increased amounts of H_2O and alkalis *(Gill, 1981)*. Several authors have discussed across-arc trends *(Gill, 1981; Tatsumi et al., 1991; Avdeiko et al., 1991; Tatsumi et al., 1992; Woodhead and Eggins, 1993; Stern et al, 1993)*. However, it should be noted, in the light of present day knowledge that in those cases where volcanic centres are not exactly aligned in one row perpendicular to the direction of subduction, rapid lateral changes in the composition of an endmember (e.g. the sediment; *Vroon, 1992; Van Bergen et al.,1993*) may obscure true across-arc source systematics.

As I will show in this thesis, it is possible to document significant changes in important chemical parameters (e.g. Ba/La) that correlate with only minor changes in the depth of the Benioff-Zone if geographic relations are well constrained. Without this condition it should be taken into account that some along-arc trends, e.g., as described in the Mariana Arc *(Lin et al., 1989; Woodhead, 1989)*, may in fact be across-arc trends.

There is consensus about the nominal increase of incompatible LIL, HFS and LRE-elements with increasing distance from the subduction trench *(Gill, 1981)*, which some authors have explained as evidence for increasing contributions from the subducting slab *(e.g., Kay, 1980; Stolz et al., 1990)* In contrast, LILE/HFSE and LILE/(L)REE ratios decrease from the trench to the back-arc in many arcs *(Gill, 1981)*. This combination of ratio changes and nominal increases implies that elements and/or groups of elements become fractionated from each other, or that magma sources change across the arc.

Isotope ratios are useful tracers of sources and processes. Gill *(1984)* documented a change in trace element- and isotopic ratios in the mantle wedge component from MORB source to OIB source in the Fijian arc. Stern et al. *(1993)* described across-arc systematics within the Kasuga chain of the Mariana arc and attributed the observed isotopic variations to decreasing amounts of melting in the source region, together with increasing involvement of OIB-like mantle sources in pockets, with increasing depth of the Benioff-Zone.

Isotopic across-arc variations that have been observed in the Kuriles *(Avdeiko et al., 1991)*, Izu-Bonin arc *(Tatsumi et al., 1992; Ishikawa and Nakamura, 1994)*, Sangihe arc *(Tatsumi et al., 1991)* show relatively high $^{87}Sr/^{86}Sr$ and $^{143}Nd/^{144}Nd$ ratios at the volcanic front and lower values behind the front. Hickey-Vargas *(1992)* could recognise a high U/Pb (HIMU=high μ) endmember in boninites in front of the Palu-Kyushu arc, but suggested that the behind-arc signal was 'swamped' by the slab contribution.

Systematic ^{238}U enrichment over ^{230}Th has been found at the front of several intra-oceanic arc systems, and equilibrium between these isotopes (within 10%) behind the front *(Newman et al., 1984, Gill et al., 1987; Gill and Williams, 1990; McDermott et al., 1991; Gill et al, 1993; Condomines et al., 1988; Condomines and Sigmarsson, 1993)*. The U enrichment shows that LILE elements are easily mobilised from the slab. Considering the apparent mobility of Pb, it is remarkable that Pb-isotopic compositions of most arc volcanics are intermediate between local MORB and sediments. Hence, the possibility of scavenging from the mantle has to be taken into account *(Hawkesworth et al., 1991; Hawkesworth et al., 1994)*.

Boron isotope data from the Izu arc in Japan *(Ishikawa and Nakamura, 1994)* show a decreasing flow of fluid from the altered oceanic crust with increasing depth of the Wadati-Benioff-Zone. The authors found evidence for a sediment-derived contribution to the fluid component in the fore arc.

2.3 Mineralogy of the mantle wedge and the subducting slab

The composition of arc magmas is largely determined by the mineral assemblages of the rock types that are involved in magma genesis near the slab-wedge interface. In principle, two domains should be distinguished: the (metasomatized) mantle wedge and the constituents of the subducting slab.

The mineral assemblage in the (pre-subduction) mantle-wedge consists of olivine, orthopyroxene, clinopyroxene (depending on the degree of depletion) and either plagioclase, spinel or garnet (depending on pressure) *(Wilson, 1989)*. Infiltration of a subduction component may add phlogopite *(Vidal et al., 1989; Maury et al., 1992)*, amphibole *(Foden and Green, 1992)* and/or apatite *(O'Reilly and Griffin, 1988)*.

The mineral assemblages in the slab depend on the original material and the metamorphic conditions. In intra-oceanic arcs the slab consists of oceanic crust, which will be

hydrothermally altered by seawater in variable degrees, resulting in Altered Oceanic Basalt (AOB). If a sediment cover is present, it can be (partially) subducted together with the AOB. In a collision zone the leading portion of AOB is gradually followed by (thinned) continental margin, as is the case in the East Sunda-Banda Arc.

It is generally accepted that the portion of the subducting slab that contributes to magma genesis is progressively metamorphosed from high-pressure amphibolite facies to eclogite facies conditions *(Arculus, 1994)*. If the subducted material consists of pelagic sediments, the mineral assemblage may contain garnet, clinopyroxene, mica, quartz/coesite and kyanite after partial dehydration *(Nichols et al, 1994)*. Experiments by Domanik and Holloway *(1994)*, who used compositions representative for a metapelite, yielded an assemblage of phengitic muscovite (white mica), topaz-OH, jadeite, garnet, coesite, lawsonite and a hydrous Mg-Al-silicate between 6 and 8 GPa, and disappearance of the coesite and formation of K-hollandite at >8 GPa.

Decarbonation of limestones under subduction conditions in absence of water would require very high temperatures *(Huang et al, 1980)*, but addition of water to a siliceous limestone lowers the melting temperature to below that of pelagic clays *(Nichols et al, 1994)*. Amphibolitic rocks consisting of amphibole and plagioclase react to garnet, (jadeitic) pyroxene and melt (no vapour) at high pressure, or to amphibole, clinopyroxene and vapour at even higher temperatures, until the break-down temperature of amphibole is reached *(Wyllie and Wolf, 1993)*.

Schreyer *(1995)* reviewed field observations on rock suites that have undergone ultra-high-pressure metamorphosis in a subduction zone. A well-studied example is the Dora-Maira Massif in the Western-Alps where metasediments have followed prograde P-T paths, typical for a mature subduction zone *(Chopin, 1984; Philipot, 1993)*. A diagnostic mineral for ultra-high-pressure metamorphosis is coesite, but mineral assemblages in the different Dora-Maira suites depend on the nature of the protolith. The most likely ultra-high-pressure equivalents of pelitic rocks are felsic garnet-bearing two-mica-gneisses *(Philipot, 1993)*. Pyrope in associated pyrope-quartzites has inclusions of coesite, kyanite, phengite, talc, paragonite, chlorite, ellenbergerite, apatite, zircon and rutile.

An important point to notice is that both the peridotitic mantle and the metamorphosed sediments may contain garnet and rutile, which will have consequences for the relative abundances of light REEs, heavy REEs and HFSEs in partial melts that are derived from these rock types.

2.3.1 Evidence for involvement of slab components in arc magmas

Although Hart and Staudigel *(1989)* have shown that subducted altered oceanic crust is probably not an important contributor to magma sources in most island arcs, models for some arcs do seem to favour involvement of altered oceanic crust *(Woodhead and Eggins, 1993)*. If a thin veneer of sediments is present, it can be subducted or scraped off and accreted onto the overriding plate. White and Dupre *(1986)* among many others *(e.g., Tera et al., 1986; Ellam and Hawkesworth, 1988; Woodhead 1989; Vroon, 1992)* have convincingly demonstrated the involvement of slab-derived sediments in magma genesis, mostly based on isotopic signatures (He, Be, Sr, Nd, Pb and Th). Depending on the areas studied, authors have invoked either a melt or a fluid as the medium that represents the slab component. In both cases the

8

mantle wedge is assumed to become enriched by metasomatic additions, but depletions, as a result of leaching by potentially aggressive fluids, should be taken into account as well *(Hawkesworth et al., 1994)*.

Plank and Langmuir *(1993)* used a mass-balance approach to demonstrate the importance of subducted sediments for the compositions of arc magmas world-wide. They showed that volcanic outputs reflect local sediment inputs in terms of trace element contents, if a correction for melting effects is applied. Their results show a good agreement between the input fluxes of incompatible elements like K, Ba, Sr,Th and K/Na, Ba/Na, Sr/Na, Th/Na ratios (taken at 6 wt% MgO) in the lavas. Arcs thus appear to have different inputs of trace elements, which is reflected by the geochemical signatures of their magmas.

2.4 Chemical characteristics of subduction-related magmas

2.4.1 The HFSE depletion

The most characteristic geochemical features of arc volcanics are high LILE/HFSE and LILE/REE ratios, and low abundances of the HFSE. This observation has been discussed extensively, but this 'HFSE problem' still remains to be solved. Generalised models point out that HFSE are preferentially retained by residual mineral phases during melting, or stress their poor mobility in slab-derived metasomatizing agents compared to other elements. The following papers have had a significant impact on the issue.

Green and Pearson *(1986)* concluded that a titanate phase may be stable in a low-temperature siliceous melt but not in mafic magmas under the conditions of melting in island arcs .

Ryerson and Watson *(1987)* suggested that it is unlikely for a residual titanate phase to be stable at the location of melt generation in the mantle but that such a phase may be present in the subducting slab. This would rule out the enrichment of a depleted mantle by interaction with a HFSE-bearing medium (melt or fluid) derived from the slab.

Ringwood *(1990)* stated that rutile will only be stable in the eclogitic subducting oceanic crust between 80 and 100 km depth. Melts would have SiO_2 contents of 63% or more, depending on how hydrous the melting conditions are. At depths between 150 and 300 km rutile will not be stable anymore, and Nb, Ta and Ti will partition into the less siliceous melt (55-60% SiO_2).

McCulloch and Gamble *(1991)* used Zr/Nb systematics to show that rutile is not stable in the mantle wedge nor in the slab.

Foley and Wheller *(1990)* argued that extraction of MORB melt from the mantle during an event prior to subduction would have depleted the residual mantle in Ca, Al, Na and other elements. Because primitive island-arc tholeiites still have high Al_2O_3 concentrations, a depletion event only is an unlikely explanation for the low Ti contents of arc magmas. Mixing between fluxes from different sources, each with their own HFSE control phases, might be a more plausible option.

Salters and Hart *(1991)*, using Hf-isotope systematics, demonstrated that the Hf-Zr depletion observed in arcs took place less than 250 Ma ago, but they also noted that it is not due to present-day magma genesis.

Vroon *(1992)* showed that sediments in front of the Sunda-Banda Arc have negative Nb, Ta,

Zr and Ti spikes in spidergrams, similar to the patterns of the volcanics, which suggests that the HFSE patterns might be largely derived from subducted sediments.

Brenan et al. *(1994, 1995)* presented convincing evidence for rutile as a refractory phase which preferentially retains HFSE relative to the LILE in the subducting slab. Only for rutile the solid/fluid distribution coefficients are sufficiently different to fractionate the HFSE from the LILE, whereas they are comparable for all common mafic silicates *(Brenan et al., 1995)*.

2.4.2 Zone refining, chromatographic effects and wall-rock interactions

Apart from the melting process, compositions of primary arc magmas are potentially modified by interaction with mantle or crustal material. Kelemen and co-workers *(1990, 1992)* argued that magma-wall rock interaction could explain many of the chemical features that are typical of subduction volcanics. According to their models the reaction of an olivine tholeiite with a depleted peridotite produces the major and trace element characteristics of calc-alkaline basalt, basaltic andesite and andesite, if the ascent of melt through narrow conduits is slow *(Kelemen et al., 1990)*. Thirlwall et al., *(1994)* pointed out that Kelemen's model cannot explain significant LREE/HREE variations with only minor major element variations in primitive lavas from the Lesser Antilles, as increasing LREE/HREE ratios should coincide with increasing silica content. Kelemen et al. *(1992)* also suggested that mantle rocks with less Ca-pyroxene than primitive mantle are not the result of a previous depletion, as is commonly assumed, but are the product of interaction between ascending basaltic magmas and the mantle lithosphere, which would cause dissolution of clinopyroxene and precipitation of orthopyroxene.

2.5 Melts or fluids as metasomatizing agents

From the discussion above it is obvious that the nature of the transport medium derived from the slab is crucial in determining the composition of subduction-related magmas.

2.5.1 Theory

Perhaps the most important issue in arc petrogenesis is the mode of element transfer from the slab to the mantle wedge. The nature of the transport medium has been hotly debated by many authors, but the topic is still not fully understood. It is loosely described as a fluid, a hydrous fluid, a hydrous melt or a melt, often without a clear definition. A reasonable criterion to distinguish between a fluid and a melt would be the amount of silicon versus H_2O or CO_2. Peacock *(1990)* defined a fluid as a low-viscosity medium containing C-O-H species such as H_2O, CO_2 and CH_4. "Under most subduction temperature and pressure conditions these species are supercritical fluids with characteristics of both liquids and fluids. However H_2O and CO_2 may also be dissolved in a magma or be bound in the crystal structure of minerals such as hydrous silicates, hydroxides and carbonates" *(Peacock, 1990)*.

Harte *(1987)* discussed the origin of fluids and melts in terms of metasomatism. In his definition, a melt is a fluid with a high silica content, whereas a (super-critical) vapour is the

10

best description for the hydrous fluid. Harte *(1987)* distinguished three kinds of metasomatism from observations in mantle xenoliths: (1) modal metasomatism where the relative abundance of minerals changes or new minerals appear or others disappear; (2) enrichment in major and minor elements without modal metasomatism; (3) isolated trace element enrichment. Gill *(1981 and references)* considered the fluid as a H_2O-CO_2-Cl system, in which the fluid may contain up to 40 wt% SiO_2. Melts under similar conditions may contain up to 30 wt% H_2O. Dehydration occurs beneath fore-arcs and volcanic fronts, and fusion could occur anywhere from fore-arc to the back-arc (or not at all), depending on the geothermal gradient *(Gill, 1981)*.

Holloway *(1987)* defined a fluid as a phase that consists of H_2O and other volatile molecules of low density at supercritical temperatures such as CO_2, CH_4, etc. It is distinct from silicate melts which have densities >2 $g.cm^{-3}$.

2.5.2 Experimental

Tatsumi et al. *(1986)* reported results of dehydration experiments on serpentinite at 12 kbar and 850 °C. They found increasing mobilities from Nb (0%) to Yb, Y, Tb, Sm and La (10-15%) to Sr and Ba (19-30%) to K, Rb and Cs (28-56%). The authors suggested a correlation between ionic radius and mobility, and not between ionic potential and mobility. Brenan et al. *(1994, 1995)* determined mineral-(aqueous) fluid partition coefficients for HFS and LIL elements, which provide some support for the presence of rutile in the subducting slab. Furthermore, significant differences between mineral-melt and mineral-fluid distribution coefficients were found for elements like U, Th and Nb, which suggests that they prefer the melt phase, whereas affinities of Ba, Sr and Pb for melt and fluid are similar. These findings agree with observations in the APS, and will be discussed in more detail in later chapters.

2.5.3 Xenoliths

Vidal et al. *(1989)* and Maury et al. *(1992)* studied rare island-arc xenoliths from Batan Island in the Philippines. The suite of xenoliths consists of harzburgites, dunites, lherzolites and pyroxenites, and contains undeformed grains of phlogopite, diopside, augitic clinopyroxene and scarce plagioclase. Although the xenoliths are not assumed to be source material of the host lavas, a common metasomatizing event may have affected xenoliths and magma source *(Maury et al., 1992)*. The metasomatic process introduced LREE, K, Rb and Ba. Lead isotopes point to a component with high time-integrated Th/U , "supposedly related to an old granulite facies type memory" *(Vidal et al., 1989)*. Maury et al. *(1992)* stressed the fact that the HFSE depletion in island arcs is a source characteristic resulting from earlier depletion of a MORB mantle. Because interaction of slab-derived melts with peridotitic mantle would produce Sr, Na, Al and Eu anomalies, their absence in the Bataan lavas makes a fluid as metasomatizing agent more likely *(Maury et al., 1992)*.

2.5.4 Fossil subduction zones

Several authors attributed petrological characteristics of exposed former mantle wedges on Catalina Island *(Sorensen and Barton, 1987; Bebout and Barton, 1989; Sorensen and Grossman, 1989; Moree, 1998)* and in the Alps *(Philipot and Selverstone et al., 1991)* to subduction-related processes. On Catalina Island low-salinity $H_2O \pm NH_4$ - bearing fluids may have actively transported elements from the slab into the hanging wall of a subduction zone at 25-45 km depth. Philipot and Selverstone *(1991)* analysed inclusions in omphacite in eclogitic veins in the Monviso ophiolitic complex in the Western Alps, and concluded that "the daughter mineral suite in the Monviso samples indicates high solubilities of Na, K, Ca, Mg, Fe, Si, Al, Zr, Ti, P, Ba, Ce, La, Th and S in aqueous brines at a minimum pressure of 10-11 kbar." The presence of monazite, rutile and sphene indicates increasing REE and Ti solubilities with increasing Cl molalities, pressure and salinity *(Philipot and Selverstone, 1991)*.

The observations on Catalina Island and in the Western Alps indicate that HFSE may be mobile under subduction conditions, and therefore conflict with the experimental findings of Tatsumi et al. *(1986)*. Philippot et al. *(1995)* studied fluid inclusions from the Dora-Maira Massif in the Western Alps, and demonstrated the concurrent presence of (a) fluid and melt during prograde ultra-high-pressure metamorphism, and (b) a saline and a water-rich fluid during retrograde metamorphism. Moree *(1998)* stressed the fact that most interpretations (e.g. peak of metamorphism, channelled flow versus pervasive flow, and high versus low-salinity fluid) in the terrains mentioned above might be based on local phenomena which are difficult to scale up to the dimensions of an entire arc system.

2.5.5 Circumstantial evidence

Additional evidence for the role of hydrous fluids in subduction-related magmatism has been obtained from B-Be systematics. These elements have similar distribution coefficients during melting, but boron is far more mobile in aqueous fluids than Be *(Ryan and Langmuir, 1993; and references therein)*. Across-arc trends in B/Be ratios show a decrease with increasing depth of the subducting slab, which can be interpreted as a progressive depletion of boron during advancing dehydration. Edwards et al. *(1992)* determined B and Be concentrations in volcanics just west of the Adonara-Pantar Sector, and found a decreasing B/Be ratio with increasing depth of the Benioff-Zone. Ryan et al. *(1995)* argue, on the basis of across-arc systematics of B, Cs, As and Sb in the Kurile arc, that H_2O-fluid dehydration is likely at shallow depths at the front of the arc, whereas a SiO_2 rich fluid is active in deeper parts.

2.6 Summary

Current ideas on the processes which generate the chemical characteristics of island-arc magmas are not uniform. Although empirical data on arc rocks, experimental results and theoretical considerations have not yet produced unequivocal answers, the importance of a slab-derived medium in generating typical arc-type chemical signatures is being recognised.

The following points are important for a better understanding of the problem: partitioning of elements between various phases involved near the slab-wedge interface, the role of minor residual mineral phases in the slab and in the sub-arc mantle and the changing conditions down the dip of the subducting slab. Every model proposed will have to be tested in well-defined tectonic settings. The Adonara-Pantar Sector is such a well defined setting.

3 Geological Setting and Geochemical Characteristics of the Adonara-Pantar Sector

3.1 Introduction

The Adonara-Pantar Sector (APS) of the Eastern Sunda Arc (ESA) is situated in a part of the Sunda-Banda Arc where the Indian-Australian plate collides with the Asian plate *(see Fig. 3.1)*. The volcanic arc of the APS is formed on the oceanic crust of the Banda and Flores Seas in a tectonic framework similar to that of an intra-oceanic subduction system *(Karig et al., 1987)*. Different hypotheses have been proposed for the origin of the oceanic crust of the Banda and Flores Seas. Some authors suggest that it was formed by back-arc spreading in the Neogene *(e.g., Hamilton, 1979)*, while others believe that the crust represents an old (Cretaceous) trapped piece of the Indian Ocean *(Bowin et al., 1980; Lee and McCabe, 1986; Beiersdorf and Hinz, 1979)*.

The subducting Indian-Australian plate changes from an oceanic to a continental domain near the APS *(Hamilton, 1979)*. Australian continental crust underlying the Timor trough is up to 40 km thick *(Jacobsen et al., 1978)* and consists of Precambrian crust overlain by Phanerozoic sediments *(Powel and Mills, 1978)*. The continent moves in a NNE direction at 75 km/Ma *(Minster and Jordan, 1978; DeSmet, 1989)*. Seismic studies *(e.g., McCaffrey, 1989)* show that the slab dips gently down to 200 km, then steepens to 60-70 degrees, and flattens again below 500 km. In the Alor-Wetar sector just east of the APS no active volcanoes are found. This sector is also marked by seismic quiescence between 50 and 380 km depth *(McCaffrey, 1989)*. Volcanic activity in the Alor-Wetar sector started at least 12 Ma ago as an intra-oceanic arc, and ceased about 3 Ma ago, which is thought to coincide with collision of the arc with the continent *(Abbot and Chamalaun, 1981)*. In more detail McCaffrey *(1985)* puts the western end of the collision zone south of Pantar island and suggests that the continental crust or its rifted margin has subducted to depths of 150 km. Some authors argue that the leading oceanic crust has detached from the continental margin in the subduction zone at depths between 70 and 100 km *(McCaffrey, 1985; Charlton, 1991)* but not all seismic evidence supports this hypothesis *(McCaffrey, 1989)*. Considerable recent uplifts at Timor *(DeSmet et al., 1989)* are consistent with the arrival of subducted but relatively buoyant continental crust under the outer arc *(Hamilton, 1979)*.

The oldest rocks in the APS are supposed to be of Miocene age and consist of lavas, tuffs and limestones *(Noya and Koesoemadinata, 1986)* but have never been investigated in any detail. Five active volcanoes are located in the APS: Boleng on Adonara, Lewotolo and Werung on Lomblen (also called Lembata), Batu-Tara Island and Sirung on Pantar. Two more recent but extinct volcanoes are found on Lomblen: Labalekan close to Werung and Kedang in the north-east of the island. Four recent volcanic centres form a NNE-SSW array in the Strait of Pantar between Pantar and Alor. Of these islands Pura Besar has an intact summit caldera which points to a relatively young age. Some lavas from Boleng, Lewotolo, Kedang, Sirung and Pura Besar have been incorporated in regional petrologic studies earlier *(Whitford, 1975a; Whitford et al., 1977; Wheller, 1986; Wheller et al., 1987; Varne and Foden, 1987; Varekamp et al., 1989; Vroon, 1986; Stolz et al., 1990)*, only Batu Tara has been investigated in

15

more detail *(Stolz et al., 1989; Van Bergen et al , 1992)*. The Werung volcano was discovered in 1911 *(Beckering, 1911)*, much later than the discovery of Lewotolo around 1775 *(Schouten, 1775)*, and has remained inaccessible since, except for isolated visits by Hartman *(1935)* and Brouwer *(1940)*. The rock compositions presented in this thesis are the first modern data for this volcano, and extend the remarkable across-arc geochemical trend signalled earlier by Varekamp et al. *(1989)*.
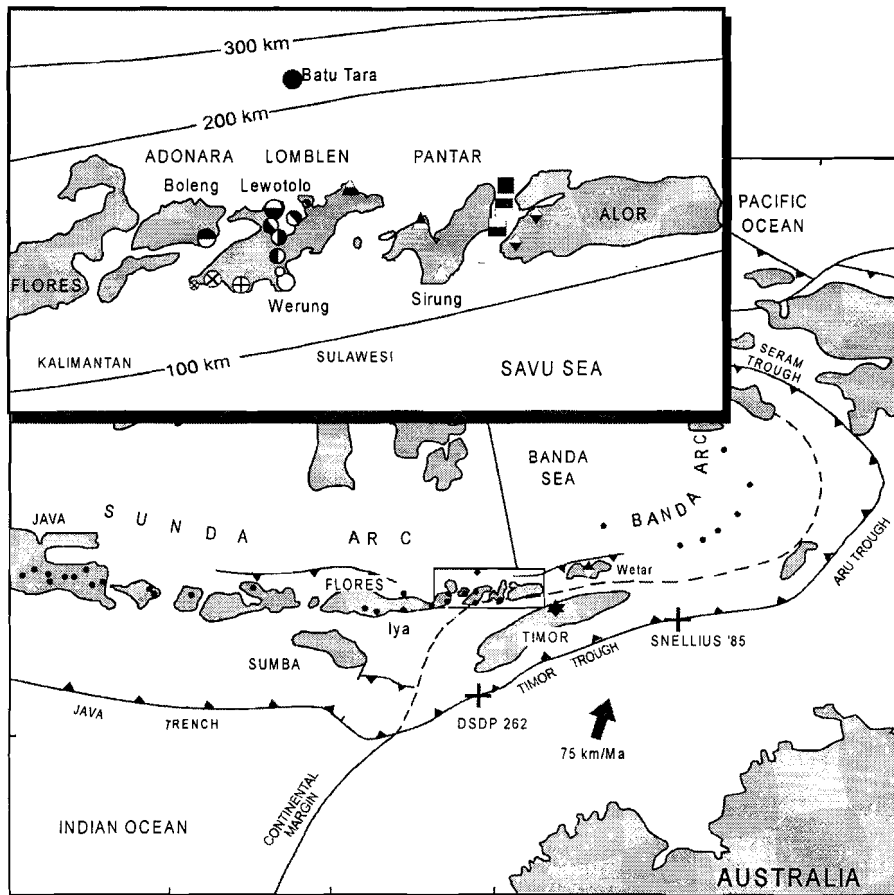
Figure 3.1. Setting of the Adonara-Pantar Sector in the Sunda-Banda Arc system and volcanic centres from which samples have been studied in this thesis. Sediment compositions from DSDP-262 and Snellius '85 sites have been discussed by Vroon *(1992)*. See also Figure 4.1.
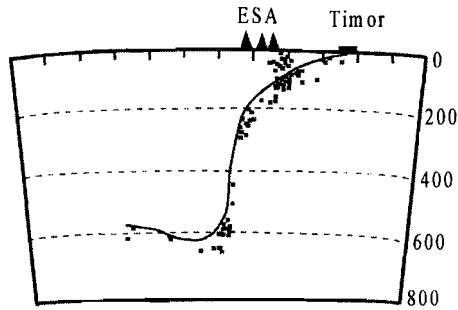
Figure 3.2. Trace of subducting slab at the APS according to McCaffrey *(1989)*.

3.2 Geochemical data in literature concerning the APS

As noted first by the studies of Whitford and co-workers *(Whitford et al., 1977; Whitford and Jezek, 1979; Whitford and Jezek, 1982; Whitford et al., 1981)* East Indonesian arc lavas have relatively extreme isotopic compositions, which suggest similarities rather with an Andean type of volcanism than with an oceanic island arc type. However, whereas assimilation or contamination of magmas en-route to the surface is probably an important cause of the 'crustal' isotopic ratios in the Andes *(Davidson et al., 1991)*, contamination of the mantle source by fluxes from subducted sediments or continental crust, prior to or during magma generation, determines the isotopic composition of most of the magmas in Eastern Indonesia *(Vroon, 1992; Hilton et al., 1992)*.

3.2.1 Sunda-Banda

Although the APS is part of the greater Sunda-Banda Arc system, it has distinct geochemical characteristics most likely related to its tectonic setting. As a whole the Sunda-Banda Arc is characterised by a clear subduction component of sedimentary origin in the magma sources *(Whitford et al., 1977; Magaritz et al., 1978; Whitford and Jezek, 1979; Whitford and Jezek, 1982; Whitford et al., 1981; Morris, 1984; Varne and Foden, 1986; Wheller et al, 1987)*.

Regional studies of the Sunda Arc have shown that the East Sunda Arc has higher $^{87}Sr/^{86}Sr$ ratios *(Whitford et al., 1977; Varekamp et al., 1989; Stolz et al., 1990; Vroon, 1986)*, a more radiogenic helium isotopic composition *(Poreda and Craig; 1989; Hilton and Craig; 1989; Hilton et al., 1992)* and higher $^{206}Pb/^{204}Pb$ ratios *(Ben Othman, 1989)* than the western part of the Sunda Arc. Using a compilation of literature data and data from this thesis, Van Bergen et al. *(1993)* have shown a convincing correlation between the composition of the material being subducted and the composition of the volcanics along the Sunda and Banda Arcs *(see also Fig. 6.6.)*. The active APS volcanoes display the strongest sedimentary or even 'continental' signal *(Hilton et al., 1992; this thesis)*, which coincides with their position closest to the collision between the arc and the Australian continent. Pb-isotope systematics in the Banda Arc reveal an increase of the crustal signal from the Banda Archipelago via Manuk, Serua, Nila, Teon, Damar and Romang to the inactive Alor-Wetar segment *(Vroon, 1992)*. The same

17

systematics have been found in the sediments in front of the trench, which provides strong evidence for their involvement in magma genesis *(Vroon, 1992)*.

Previous authors have suggested that three or four major components are involved in magma genesis of the Sunda-Banda Arc *(Wheller et al., 1987; Stolz et al., 1990; Vroon, 1992)*. Stolz et al. *(1990)* proposed three mantle components: Indian MORB source, depleted Indian MORB source and Indian OIB source, and a single subduction component: Indian Ocean sediment. The documented change in the composition of the subduction component along the arc *(Van Bergen et al., 1993)* demonstrates that there must be at least two sedimentary sources that make up the subduction component: Indian Ocean pelagic sediment and detrital Australian shelf sediment. Hilton et al. *(1992)* inferred the presence of Australian continental crust at magma-generation depths, thus adding a third potential subduction component. In theory the subduction components may even add up to six, if hydrous fluids and melts derived from slab material are treated as separate components. In contrast, Edwards et al. *(1993)* have interpreted B/Be results and isotope systematics along a 1500 km long stretch of the arc in favour of a homogeneous subduction component.

With respect to the MORB-type source component, Stolz et al. *(1990)* have shown that frontal tholeiitic lavas in the Flores part of the East Sunda Arc have ^{143}Nd/^{144}Nd ratios close to, or overlapping with, Indian MORB values. Evidence for a depletion of the MORB mantle comes from the LREE and HFSE abundances in these lavas, which are lower than in normal MORBs and are consistent with a previous melt-extraction event.

Data on Pb and Nd isotopes and selected trace elements (e.g. Zr/Nb) provide some indications for the presence of an OIB-like source (or at least an old Enriched Mantle source relative to MORB) underneath the high-K series volcanoes in the vicinity of the inactive collision zone *(Stolz et al., 1989; Van Bergen, 1992)*. However, as noted by Van Bergen et al. *(1993)*, it is difficult to explain why the amount of involvement of an OIB-like source would correlate with the tectonically controlled increasing supply of sedimentary and/or continental material.

3.2.2 Adonara-Pantar Sector

Brouwer *(1940)* was the first to study the geochemistry and petrology of volcanics in the APS. Modern geochemical data on samples from a limited number of centres in the area were presented by Whitford et al. *(1977)*. The systematic mineralogical trends across the arc that were documented by Brouwer *(1940)* agree well with the extreme geochemical range in magma compositions from low-K tholeiitic through medium- and high-K calcalkaline to ultra-potassic rocks *(Stolz et al., 1988; Stolz et al., 1990)*. Varekamp et al. *(1989)* have shown that active volcanoes in the APS erupt lavas that range in composition from low-K tholeiitic at the frontal Sirung volcano of the arc to ultra-potassic at Batu Tara behind the arc. None of the lavas has Mg numbers greater than 50 (except some samples from Batu Tara), which is a common feature in arc settings *(Gill, 1981)*. The LILE and LREE contents were found to systematically increase from the front to the rear of the arc. As opposed to some of the Banda-Arc volcanoes *(Vroon et al., 1993)*, no isotopic evidence has been put forward for a major role of crustal assimilation in the APS *(Stolz et al, 1990; Van Bergen, 1992)*.

18

3.3 Depth of Wadati-Benioff-Zone in the Adonara-Pantar Sector

Figure 3.3. demonstrates the existence of a systematic increase in total alkali contents from South to North across the APS. The alkali contents are plotted versus latitude (Fig. 3.3a) and versus the inferred depth of the Wadati-Benioff-Zone (Fig. 3.3b) following the shape of the subduction slab in the ESA according to McCaffrey et al. *(1985)* and McCaffrey *(1989)*. Using the strike of the WBZ (N65°E), the position of the slab below each of the volcanic centres studied here was reconstructed from Figures 3 and 8 in McCaffrey et al. *(1985)*. The results of this reconstruction are shown in table 3.1

Tandjung	160	Hadakewa	170	B. Waspila	160
Mingar	160	SE of Lewotolo	175	Sirung	140
Labalekan	160	Lewotolo	180	Treweg	145
Boleng	180	Noehanera	170	Pura Besar	150
Werung	150	Dalaleng	180	Ternate	160
Labala Penins.	160	Kedang	180	Kisu	170
Inl. Lembata	165	Batu Tara	220	Alor	150

Table 3.1. Calculated depths of the Wadati-Benioff-Zone underneath each volcanic centre in km.

The accuracy of this approach is debatable. As Figure 3.3b illustrates, the use of the calculated WBZ depths results in different across-arc trends in the Werung-Lewotolo-Batu Tara, Sirung-B.Waspila-Kedang and Strait of Pantar transects. This may be a real feature, dictated by local geological/tectonic controls or an artefact of the procedure followed, as it is conceivable that slight changes in subduction geometry caused by the collision occurred after subduction-induced modification of mantle sources had started. Given this uncertainty and the better coherence shown in Fig. 3a, the latitude of volcanic centres rather than depth of the WBZ will be used in diagrams.
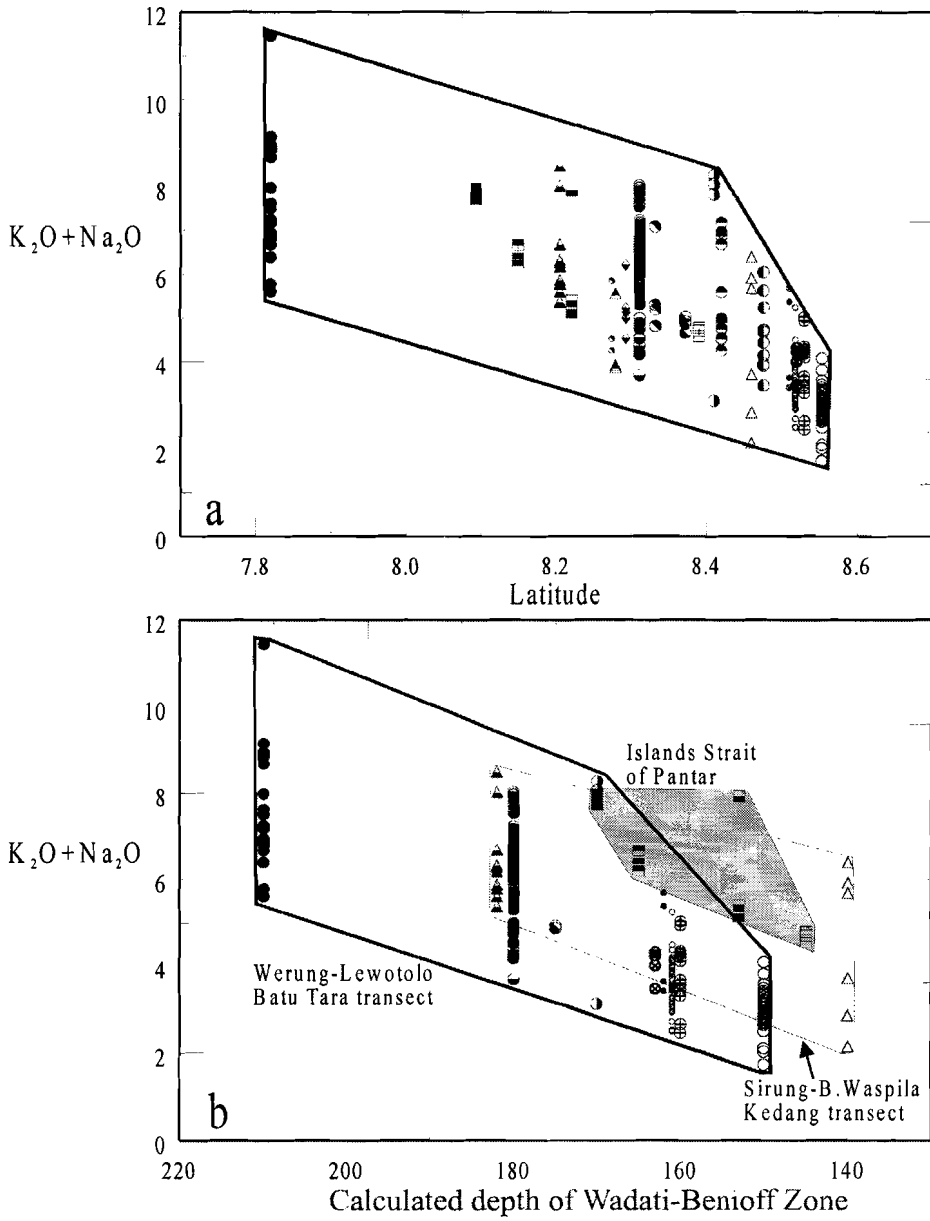
Figure 3.3. Alkali content versus latitude and versus calculated Wadati-Benioff-Zone depth.

4 Sample Locations and General Petrography

4.1 Introduction

In this chapter the sample locations, sampling procedures, the mineralogy and the major element chemistry of the Adonara-Pantar Sector will be discussed. In the next chapter the variations within each suite will be treated. Most of the more than 400 samples studied were collected during fieldwork campaigns in 1989 (Lembata and Adonara) and 1990 (Pantar, Islands in the Strait of Pantar and Alor). Some additional data were obtained on samples collected during the 1984 Snellius Expedition *(Van Bergen et al, 1989)*, mainly from Batu Tara, Boleng, Sirung and Lewotolo.
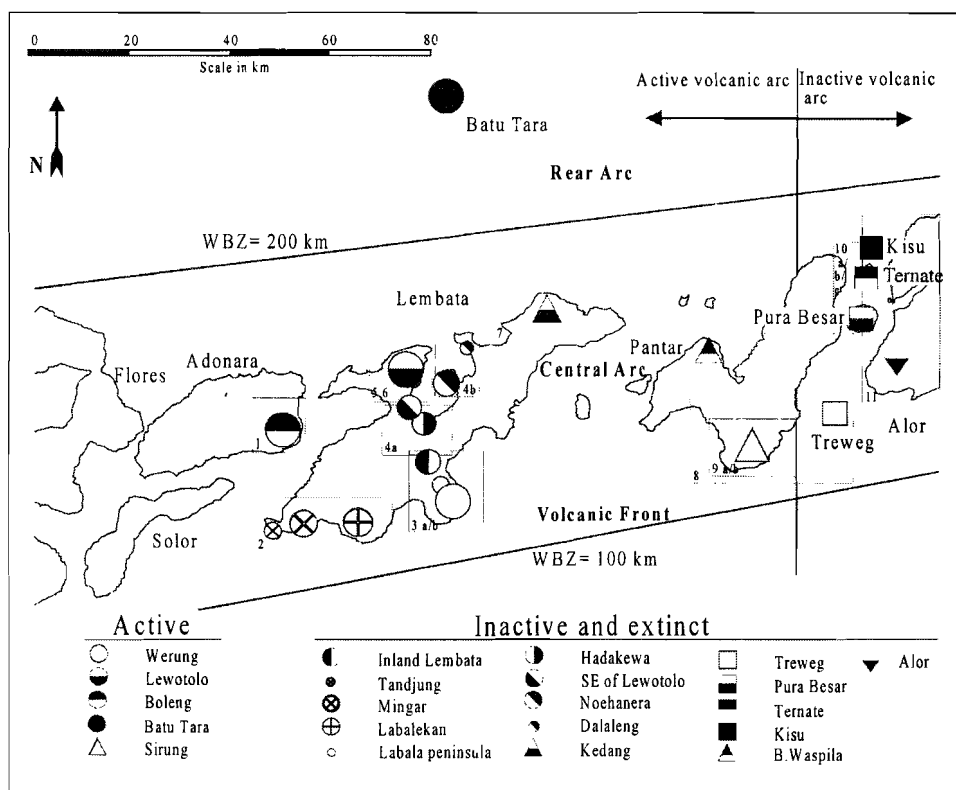
Figure 4.1. Overview of active and inactive or extinct volcanoes. Numbers relate to detailed maps to be found in the appendix. WBZ is Wadati-Benioff-Zone.

The sample strategy was based on five criteria:
-to cover the area between eastern Flores and Alor.
-to obtain samples from multiple across-arc transects including Lembata, Adonara, Pantar and the Strait of Pantar.
-to collect a representative set of samples for each volcano in terms of geographic distribution.
-to obtain samples of the most recent products for each volcano.
-to supplement the samples taken during the Snellius II expedition.

In this thesis the notations „VF", „CA" and „RA" will be used for the Volcanic Front volcanoes (Werung, Sirung, Treweg, Labalekan and Mingar), the Central Arc volcanoes (Lewotolo, Boleng, Kedang, Pura Besar, Ternate, Kisu and B. Waspila) and the Rear Arc volcano (Batu Tara), respectively *(see Fig. 4.1)*.

4.2 Sample locations

Figure 4.1 shows the study area and the detailed sample location maps given in appendix 1. The quality of available topographic maps of the fieldwork area is poor. A 1:250,000 (Pulau Lomblen, SC 51-3, 1963) map by the Army Map Service, Corps of Engineers, U.S. Army covers the whole fieldwork area. For the 1989-fieldwork on Lembata (also called Lomblen) and Adonara we used the 1:100,000 "Verkenningskaart van de onderafdeling Oost-Flores en Solor-eilanden, oostblad" from the Dutch colonial topographic service in Batavia (Jakarta), which was printed in 1931. For different sections of the individual volcanoes we used blown-up sections of this map (1:12,500). Comparison of the Lewotolo section of this map with a SPOT satellite image revealed discrepancies in the order of a few hundred metres. For the island of Pantar and the small islands in the Strait of Pantar we used the "blad 88-89/XLIII-XLIV, Algemene Schetskaart van Nederlands Indië, 1:200,000, 1940", which is of poor quality. For the fieldwork on Alor we resorted to the U.S. Army map. Detailed sketch maps of Werung, Lewotolo and Sirung volcanoes were available from internal reports of the Indonesian Volcanological Survey *(Wiriosoemarto, 1960a, 1960b; Rohi, 1978)*. A SPOT image of the Geological Research and Development Centre, Bandung (GRDC) enabled us to plan fieldwork around Lewotolo and Werung, as different flows units could be recognised. Airborne photography of Werung volcano clearly shows the different units present in the area (Fig. 4.2).

The samples were processed at the Faculty of Earth Sciences, Utrecht, for petrographic study and analysis. Major and trace elements were measured in Utrecht using XRF. Neutron activation analyses were carried out at IRI, Delft and by J. Hertogen at the University of Leuven, Belgium. Sr-Nd-Pb isotopes were measured at the Isotope Laboratory of the Free University, Amsterdam. U-series measurements at the University of Leuven were performed in co-operation with J. Hertogen and A. Sneyers. ^{226}Ra was analysed by R. Wordel and D. Mouchel at EU-JRC, IRMM in Geel, Belgium. Helium isotope analysis on minerals separated in Utrecht, was carried out at the Free University of Berlin with the help of D. Hilton. All analyses, except INA and gamma-spectrometry, were performed by the author in co-operation with the specialists on site.
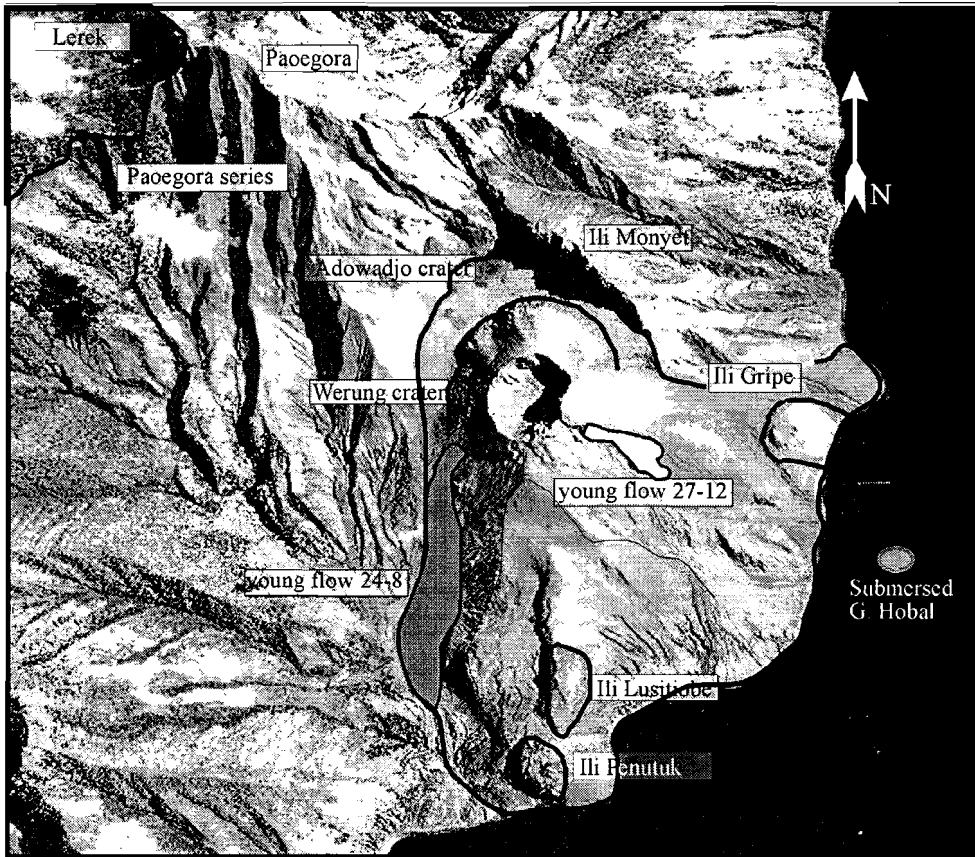
Figure 4.2. Aerial picture of Werung volcano and surroundings showing young lava flows.

4.3 Petrography

Systematic variations in phenocryst assemblages across the APS coincide with changes in major and trace element contents. A listing of the phenocryst assemblages in the samples collected for this study can be found in appendix 2. The petrography of some additional samples from the collections of Brouwer and the 1984 Snellius-II expedition that have been used as well can be found in the respective reports. The Snellius-II samples from Lewotolo, Sirung and Batu Tara have been described by Vroon *(1986)*, Varekamp et al. *(1989)* and Van Bergen et al. *(1989, 1992)*. Petrographic descriptions of the Brouwer samples from Boleng and Batu Tara are given in Brouwer *(1940)*.

4.3.1 Volcanic Front

Tholeiitic basalts of the Werung, Sirung, Labalekan and Mingar volcanoes are predominantly porphyritic (10-80%), and carry phenocrysts of plagioclase (pl), orthopyroxene (opx). Olivine (ol) contents range from abundant to absent, and crystals sometimes appear to be resorbed. The opx frequently has overgrowths of cpx. Hydrous phenocrysts are absent.

4.3.2 Central Arc

Older volcanic products between Werung and Lewotolo document a transition from the tholeiitic series at the volcanic front to the high-K series of the central-arc volcanoes through the appearance of amphibole (amph) and phlogopite (phl) in addition to cpx, opx and pl. Interestingly, some lavas contain both ol and amph. This feature is also observed in the CA volcanoes Lewotolo, Kedang and Pura Besar. In general, the CA volcanics contain olivine at low SiO_2 levels, whereas amphibole and phlogopite are commonly found at more elevated SiO_2 levels. Phlogopite is often associated with cpx and opx.

De Hoog *(1996)* distinguished three series in the lavas of Lewotolo: mafic, low alkaline and high alkaline, each with different mineral assemblages. The mafic series contain calcic plagioclase, augitic clinopyroxene, olivine, Mg-Al-rich Fe-Ti oxides, orthopyroxene, amphibole, fluorine-rich phlogopite, monazite and zirconolite. The high-alkaline series contain calcic to intermediate plagioclase, augitic clinopyroxene, scarce olivine, Ti-rich Fe-Ti oxides, apatite as inclusions and some amphibole. The low-alkaline series contain calcic to intermediate plagioclase, augitic clinopyroxene, Fe-rich Fe-Ti oxides, abundant apatite and amphibole, some phlogopite, monazite and zirconolite *(see table 7.1 in De Hoog, 1996)*.

4.3.3 Rear Arc

A detailed petrography of ultrapotassic rocks from Batu Tara discussed in this thesis can be found in Van Bergen et al. *(1992)* and Brouwer *(1940)*. The Batu Tara rocks contain leucite, clinopyroxene, olivine, plagioclase, Ti-magnetite, minor apatite and occasionally biotite, sanidine and amphibole as phenocrysts. They can be subdivided into two different series *(Brouwer, 1940; Stolz et al., 1988; Van Bergen et al., 1992)*: older leucite-basanite lavas and leucite-tephrite dikes, and younger biotite-leucite-tephrite lavas. The biotite-leucite-tephrites lavas are characterised by the absence of olivine, (micro-) phenocrysts of biotite and groundmass sanidine *(Van Bergen et al., 1992)*. The older series contain large phenocrysts of clinopyroxene and olivine, and leucite, olivine Ti-magnetite, apatite and some biotite and/or amphibole in the groundmass. The less mafic rocks of the older series also contain plagioclase.

24

4.3.4 Strait of Pantar and Alor

The islands in the Strait of Pantar show a petrographic trend that is similar to that of the western APS transects. Phenocrysts of olivine (with plag, opx and cpx) are found in the lavas at the front, whereas amphibole and phlogopite appears in the more northern volcanoes. Although the origin and age of the Alor samples is not well constrained, similar systematics may be valid in the western part of this island.
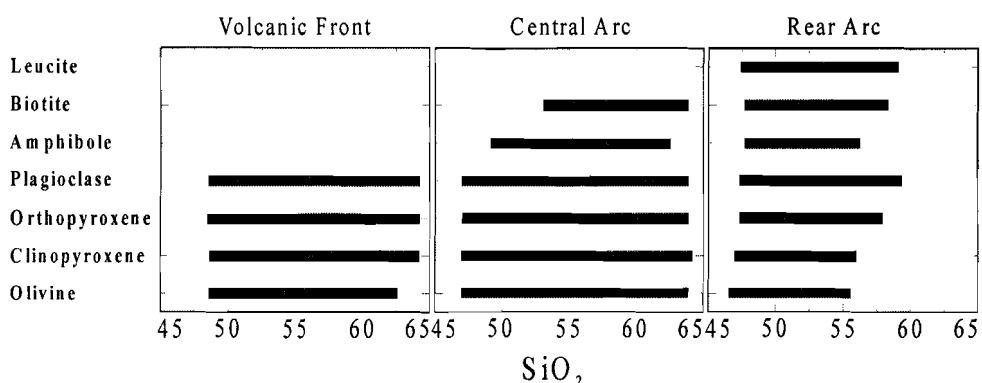
Figure 4.3. Generalised distribution of phenocryst assemblages in volcanics (including xenoliths) across the ESA as a function of SiO$_2$ contents.

4.3.5 Comparison with adjacent sectors in the Sunda Arc

The systematics in phenocryst assemblages in the APS are comparable to those observed in the more western parts of the Sunda Arc. Basaltic andesites from volcanoes in Java and Bali contain plagioclase, augite, olivine and Ti-magnetite and orthopyroxene that may be replaced by pargasitic amphibole. Andesites and dacites contain strongly zoned plagioclase, augite, orthopyroxene/pargasitic amphibole and phlogopitic-biotite. Lavas from the mostly mafic high-K series carry olivine, Ca-rich clinopyroxene, calcic-plagioclase, rare leucite, pargasitic amphibole and rare Ti-rich garnet *(Whitford et al., 1979)*. Highly porphyritic low-K tholeiites at the volcanic front in Flores contain phenocrysts of plagioclase, orthopyroxene, minor clinopyroxene and Ti-poor magnetite. The medium-K rocks from centres on this island carry plagioclase, clinopyroxene, some orthopyroxene and hornblende *(Stolz et al., 1990)*.

Rock types on the small island of Atauro, east of the APS, include low-K basaltic andesite that contain opx, cpx, plag and rare ol, high-K dacite and hornblende andesite *(Abbott and Chamalaun, 1981)*. On the island of Wetar, further to the east, exposures of an intrusive suite of diorites and granodiorites with dolerite dykes have been found. Most remarkable are rhyolites with relicts of cordierite *(Abbott and Chamalaun, 1981)*.

5 Major and Trace Elements: Within-Suite Variations and Spatial Geochemical Systematics

5.1 Introduction

This chapter documents major and trace element variations within each suite and across the arc that are of interest to assess the characteristics of magma sources in the Adonara-Pantar Sector. For each volcanic centre element concentrations were determined from the local compositional trend at a constant SiO_2 level of 55 wt%, and results were plotted as a function of latitude in order to detect across-arc trends that are independent of magma evolution at shallow crustal depths. At the end of the chapter it is shown that any effects of assimilation of wall-rock material in the ascending magmas en route to the surface are minimal in the APS, in agreement with previous findings (*Stolz et al., 1990; Van Bergen et al., 1992*).

5.2 Major element chemistry

Detailed results of the geochemical analysis can be found in appendix 4 and a description of the sample preparation, analytical methods and results obtained on reference materials in appendix 3. Volcanic centres in the APS have SiO_2 contents of 45-65 wt%, except for some older rhyolitic pumice deposits near Hadakewa that contain 70-75 wt% SiO_2. The lowest SiO_2 contents can be found in the most primitive lavas from Werung (49 wt%), Lewotolo (47 wt%), Boleng (50 wt%, based on a limited number of samples), Batu Tara (45 wt%) and Sirung (47 wt%).

K_2O and Na_2O+K_2O

In Figure 5.1 K_2O (Fig. 5.1b) and Na_2O+K_2O (Fig. 5.1a) contents are plotted against SiO_2, which results in a well defined trend for each of the active volcanoes except Batu Tara. The slope of the SiO_2-K_2O trends (Fig. 5.1b) systematically increases with increasing average K_2O contents at SiO_2=55 wt%. It is not clear how to interpret this; do all the magma series start at a common SiO_2 concentration and if so, is this the composition of the magma source? On the other hand in the K_2O+Na_2O versus SiO_2 diagram the intercept along the y-axis tends to increase with increasing depth. On closer inspection, several different evolutionary series can be recognised in the Lewotolo rocks (*De Hoog, 1996*): two relatively evolved series with slightly different total alkali contents and a series of low SiO_2 rocks, which could be parental to the series with the highest total alkali content. The mixing of different magma series as explanation for the observed heterogeneity in the Batu Tara rocks has been discussed by previous authors (*Stolz et al., 1988; Van Bergen et al., 1992*). It is noteworthy that five of all the volcanoes are presently active. Thus, the variation in alkali content is contemporaneous and represents one of the largest compositional ranges in an active arc today.
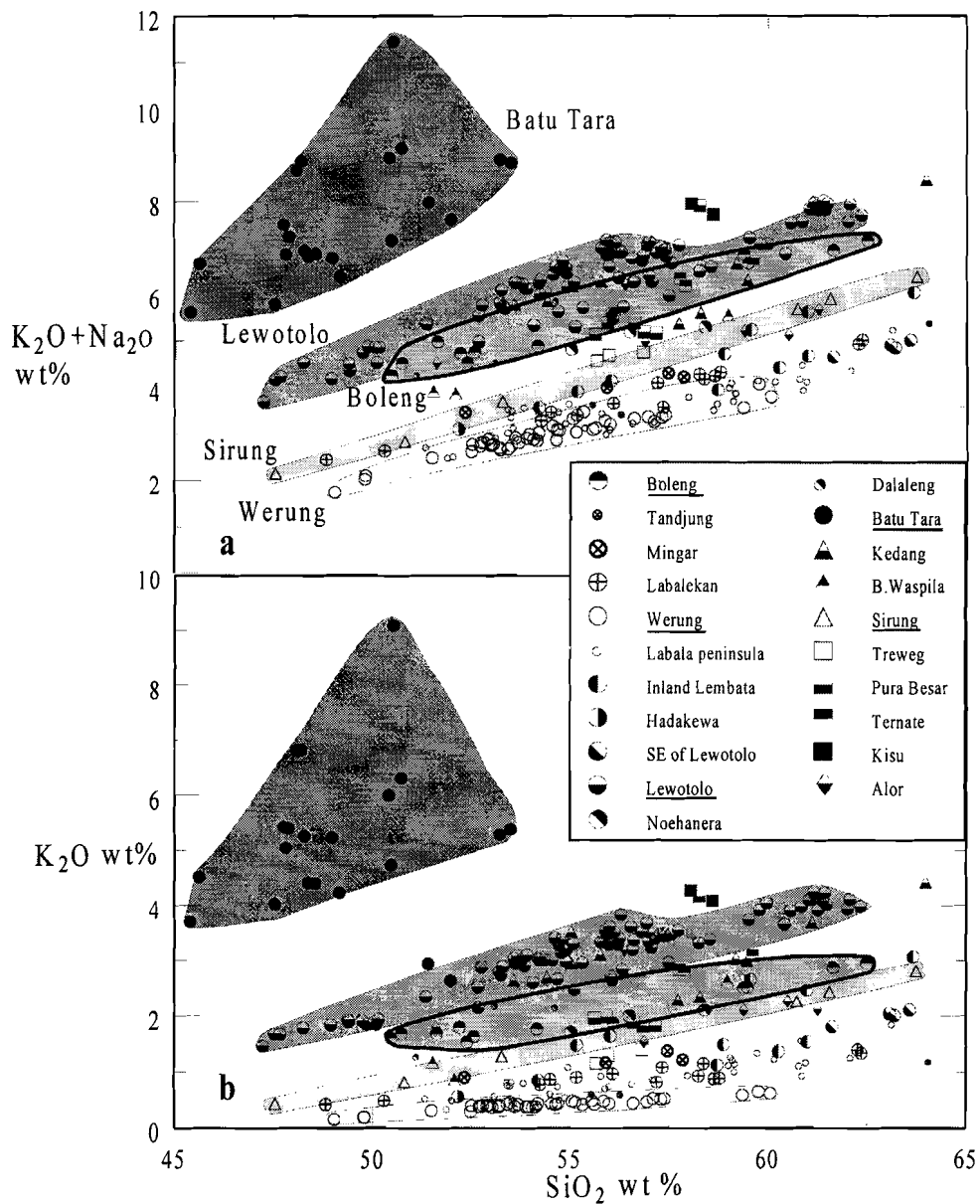
Figure 5.1. K_2O and K_2O+Na_2O contents of volcanics in the Adonara-Pantar Sector versus SiO_2. Fields indicate the active volcanoes.
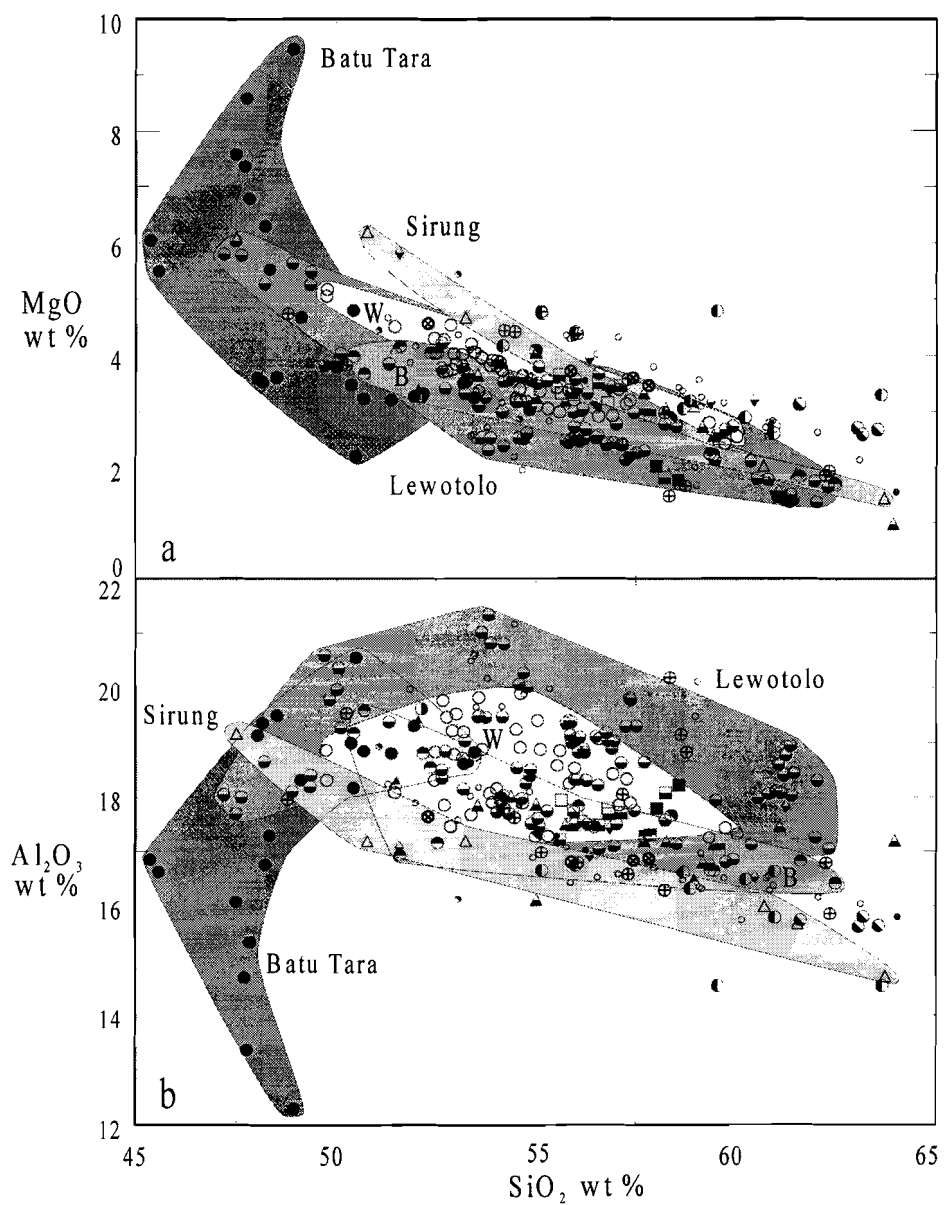
Figure 5.2. MgO and Al$_2$O$_3$ contents of volcanics in the Adonara-Pantar Sector versus SiO$_2$. Symbols according to Fig. 5.1.

MgO

Only Batu Tara has several rocks with MgO contents >6 wt% (Fig 5.2a) and a Mg-number (not shown) >0.5 (0.63). The samples from Lewotolo and Werung have Mg numbers around 0.47 and 0.41, respectively, and their MgO contents systematically decrease with increasing SiO_2, consistent with pyroxene fractionation. The rocks from Sirung have a maximum Mg-number of 0.48, and MgO values decreasing stronger than in the other series. Lavas from Boleng have a maximum Mg-number of 0.41 and MgO values fitting within the array formed by the other samples.

Al_2O_3

Batu Tara samples have the lowest Al_2O_3 concentrations in the APS (Fig. 5.2b), which correspond with the highest MgO values. The other series show a general decrease in Al_2O_3 contents with increasing SiO_2.

CaO

CaO contents show an across-arc trend with high CaO at the volcanic front to low values behind the front for a given SiO_2 content (Fig. 5.3a). Except for Batu Tara, all the active volcanoes show well-defined within-suite trends of decreasing CaO contents with increasing SiO_2. Both the series that can be distinguished in the relatively evolved lavas of Lewotolo tend to be different in CaO contents as well.

Fe_2O_3 (all iron expressed as Fe_2O_3)

The low-K frontal rocks from Werung, Labalekan and the Labala peninsula show trends that are shifted to higher Fe_2O_3 contents relative to the series of Lewotolo and the other MA volcanoes (Fig. 5.3b). All series show decreasing Fe_2O_3 contents with increasing SiO_2. The Batu Tara rocks are the most depleted of the low-SiO_2 rocks. The relative iron enrichment in the frontal rocks is consistent with the compositions of other tholeiitic arc suites *(Gill, 1981)*.

TiO_2

The K-rich volcanoes all show a normal decrease of TiO_2 with increasing SiO_2 (Fig. 5.4a) due to crystallisation of titanipherous magnetite. Boleng lavas have a relatively high TiO_2 content compared to the other volcanoes. The data for Werung suggest that the onset of titanipherous-magnetite crystallisation in the magmas of this volcano takes place between 50 and 53 wt% SiO_2. Sirung shows an anomalous increase in TiO_2, which is not compatible with magnetite fractionation. This makes it difficult to interpret the trend and deduce the original Ti-level of mantle-derived magma by extrapolation.
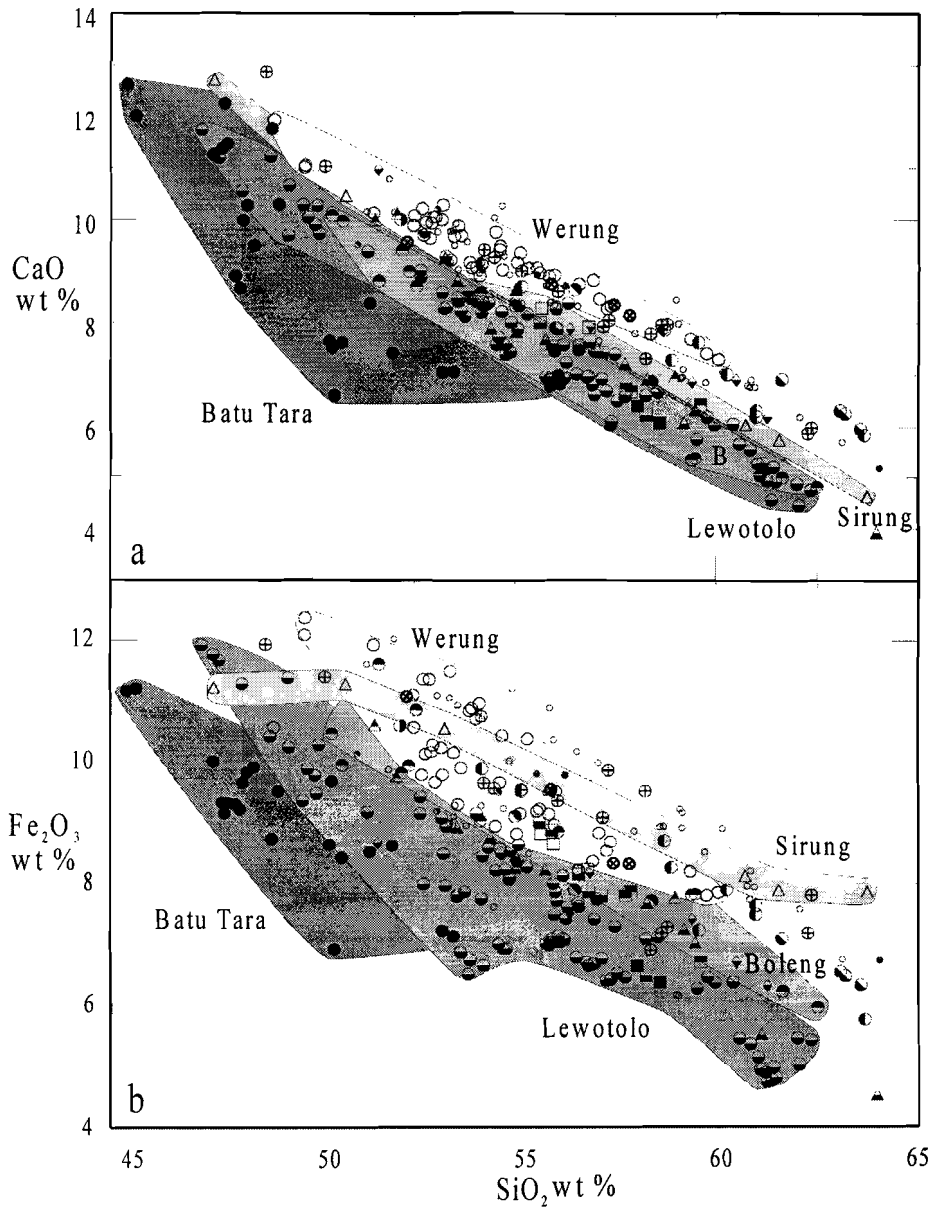
Figure 5.3. CaO and total Fe as Fe_2O_3 contents of volcanics in the Adonara-Pantar Sector versus SiO_2. Symbols according to Fig. 5.1.
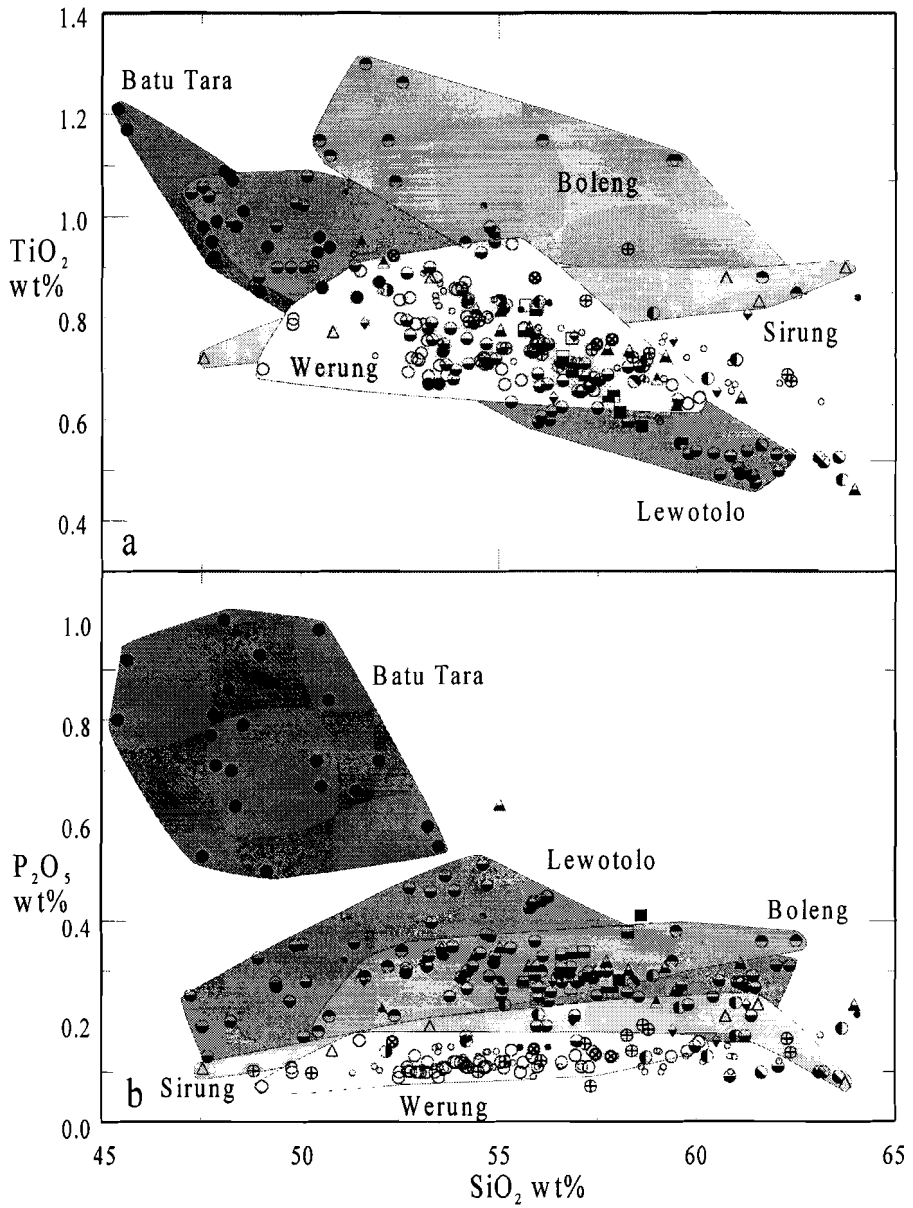
Figure 5.4. TiO₂ and P₂O₅ contents of volcanics in the Adonara-Pantar Sector versus SiO₂. Symbols according to Fig. 5.1.
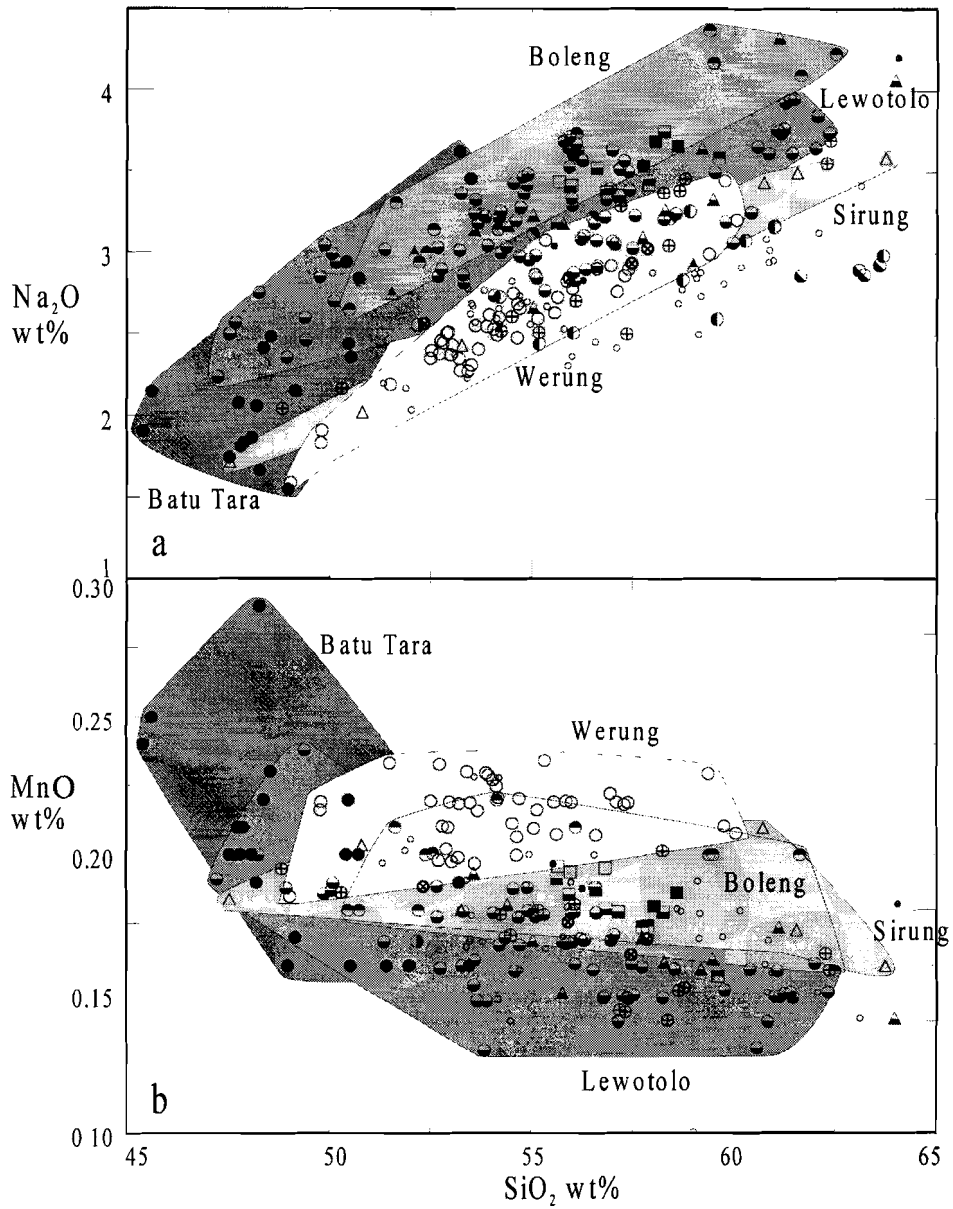
Figure 5.5. Na₂0 and MnO contents of volcanics in the Adonara-Pantar Sector versus SiO_2. Symbols according to Fig. 5.1.

P₂O₅

P$_2$O$_5$ levels scatter but are clearly highest in the Batu Tara samples (Fig. 5.4b). In the Lewotolo series the onset of apatite crystallisation occurs at about 55 wt% SiO$_2$. The frontal volcanoes demonstrate an incompatible behaviour of phosphorous and no crystallisation of apatite.

Na₂O

There is a clear positive correlation between Na$_2$O and SiO$_2$ for all volcanoes (Fig. 5.5a). In general, sodium contents appear to increase in a direction away from the trench, although the samples from Batu Tara show much scatter and do not follow this trend. Unusually high Na$_2$O contents in two of the Batu Tara samples are probably due to secondary alteration *(Van Bergen et al., 1992)*.

MnO

Batu Tara shows a decline in MnO contents (Fig. 5.5b) from 0.3 to 0.16 wt% with increasing SiO$_2$. Other volcanoes scatter between 0.12 and 0.25 wt% with the frontal volcanoes at the high end, Lewotolo and other MA volcanoes having relatively low values that follow the iron systematics.

5.3 Classical petrologic diagrams characterising the different suites

Classification diagrams confirm the distinct chemical characteristics of the APS suites. The AFM plot (Fig.5.6a) demonstrates the tholeiitic character of the frontal volcanoes; they are enriched in Fe relative to the more northern volcanoes, in agreement with observations in other arcs *(Gill, 1981)*. The Batu Tara rocks show the other extreme and plot in the calc-alkaline field, but they are clearly distinct from the Lewotolo and Boleng series that form well-defined trends. Note that the lavas from Sirung deviate and crosscut the boundary between the tholeiite and calc-alkaline fields.

Molar normative CIPW abundances of quartz, anorthite, diopside and nepheline are plotted in Figure 5.6b for the different suites. The Batu Tara rocks are clearly distinct from the other series by their silica undersaturated character. Four Lewotolo samples also plot in the nepheline field, but petrographic analysis *(De Hoog, 1995)* did not reveal the leucite-bearing phenocryst assemblages that are typical for Batu Tara.

5.4 Across-arc systematics of the major elements

In Figures 5.7.1-5.7.3 the across-arc changes in major element contents are demonstrated by the comparison of the average for individual series at a SiO$_2$ concentration of 55 wt%. In the case of Batu Tara this implies an extrapolation outside the observed compositions.

34
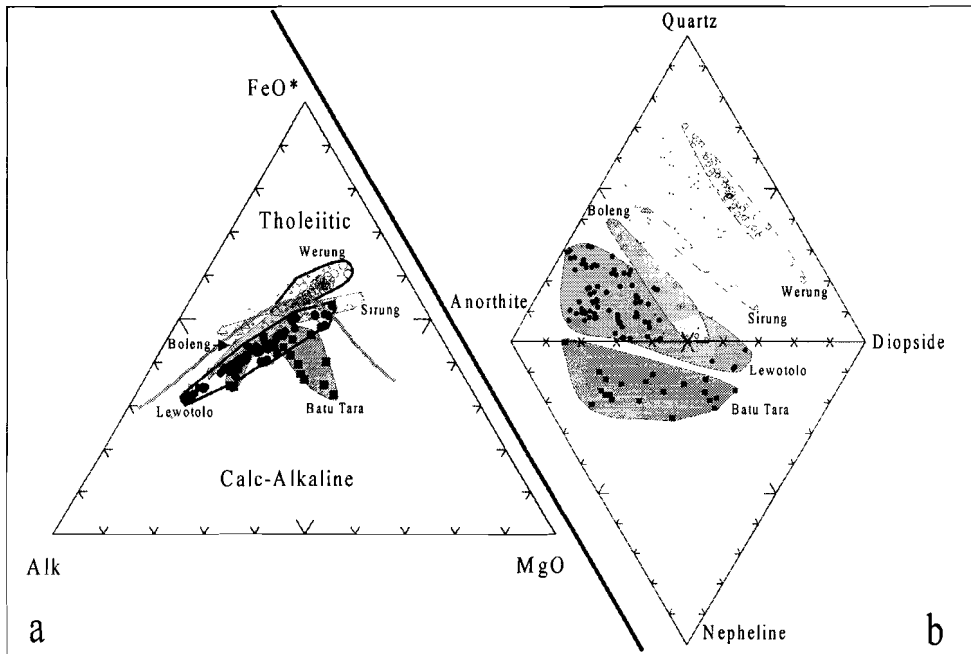
Figure 5.6. a: AFM plot of APS rocks and **b:** normative CIPW values. Fig. 5.6a shows a systematic across-arc transition from tholeiitic to calc-alkaline rocks, and Fig. 5.6b a change from quartz-saturated to quartz-unsaturated series. Small dots represent inactive centres.

This method was chosen, however, to enable comparison among the APS series as well as with data from other arcs *(e.g., Woodhead and Johnson, 1993)*. For each volcanic centre linear regression calculations were performed with the „SPSS„ software program in order to calculate element concentrations at 55 wt% SiO_2 and associated 95% confidence intervals. In the figures the calculated element contents at 55 wt% SiO_2 are indicated by horizontal bars, and the 95% confidence intervals by vertical shaded bars. If no bar is drawn, the number of samples was too small and/or the confidence interval exceeded the vertical scale.

K_2O demonstrates a smooth convex increase across the arc in the west from Werung (right) to Batu Tara (left), and a concave increase in the eastern transect. MnO in Figure 5.7.2 has a slightly decreasing curve across arc. The expected value for Na_2O rises with increasing Benioff-Zone depth and CaO shows the opposite trend. MgO at 55 wt% SiO_2 is remarkably constant as is Al_2O_3 in the next Figure 5.7.3. The Boleng samples have a higher TiO_2 content than those of the other centres, which could indicate a different source mineralogy. Iron as Fe_2O_3 slightly decreases in the western part of the APS. P_2O_5 systematically increases across the arc and as the 55 wt% point lies in the middle of the true observations also this seems to be due to a magma source characteristic.
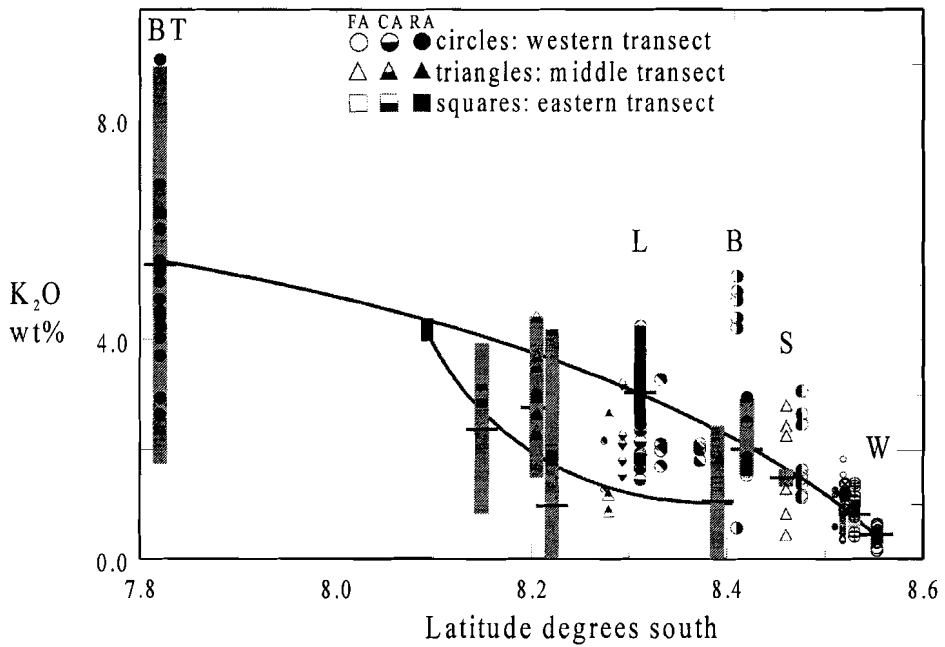
Figure 5.7.1. Across-arc trends in K_2O contents. Note the different trends for the western and eastern transects in the APS. Symbols are individual samples, circles for the western transect, triangles for the middle transect and squares for the eastern transect. Short horizontal bars indicate interpolated K_2O values at $SiO_2=55$ wt% from linear regression analysis. Shaded bars represent 95% confidence intervals. No bar was drawn when its length would exceed the plot boundaries. Symbols as in Figure 5.1.
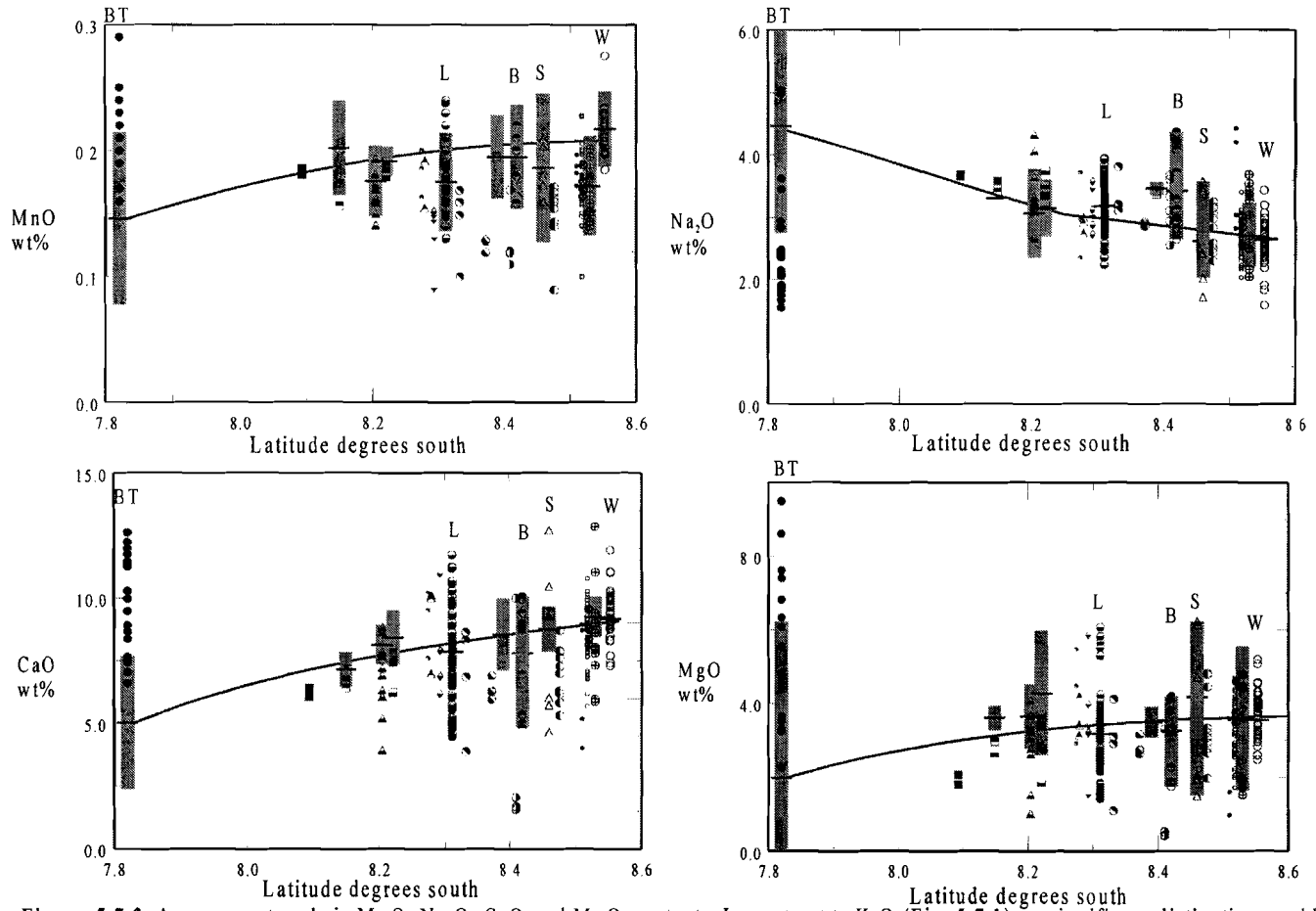
Figure 5.7.2. Across-arc trends in MnO, Na₂O, CaO and MgO contents. In contrast to K₂O (Fig. 5.7.1) no significant distinction could be made between the eastern and western transects. Symbols as in Figure 5.1.
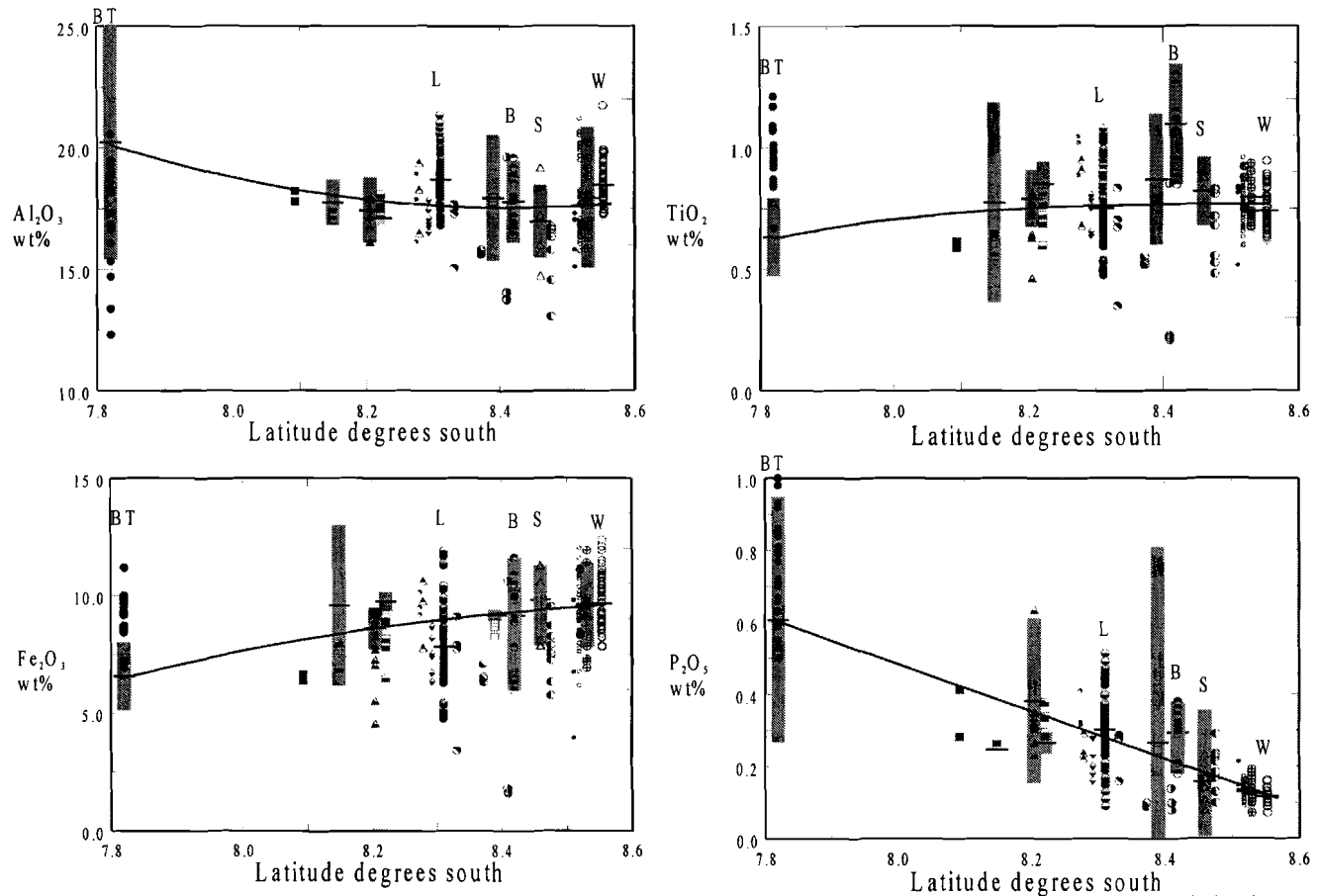
Figure 5.7.3. Across-arc trends in Al_2O_3, TiO_2, Fe_2O_3 and P_2O_5 contents. In contrast to K_2O (Fig. 5.7.1) no significant distinction could be made between the eastern and western transects. Symbols as in Figure 5.1.

5.5 Trace element chemistry

Analytical methods and trace element results can be found in appendix 4. In Figures 5.8.1-5.8.6 trace element concentrations are plotted versus SiO_2 concentration.

5.5.1 The elements Sc, V, Cr, Co, Ni, Cu, Zn, Ga

Vanadium and Gallium have not been determined for Lewotolo and Batu Tara, but show strong compatible behaviour (Fig. 5.8.1b) in the other volcanoes. Scandium (no data for Batu Tara are available) shows compatible behaviour and its concentration decreases away from the front (Fig. 5.8.1a). The contents of Ni, Cr and Co are highest in Batu Tara (20-110, 10-300 and 10-70 ppm, respectively) as illustrated in Figure 5.8.1c,d and 5.8.2a. Sirung volcano shows a very large range in concentrations of Ni, Cr and Co compared to the other frontal volcanoes, from 50 to < 5 ppm with increasing SiO_2. Lewotolo samples have relatively high Cr contents (>30 ppm) in the most mafic rocks, but these values rapidly decrease to < 10ppm when SiO_2 exceeds 50 wt%. Nickel concentrations were below detection limits in Werung and other volcanoes at the front. Copper concentrations are most elevated in the Batu Tara rocks (up to 170 ppm) and show compatible behaviour in the other suites (Fig. 5.8.2b). Zinc increases with increasing SiO_2 in Sirung (Fig. 5.8.2c) but decreases in the other volcanoes.

5.5.2 The LIL elements Ba, Sr, Pb, Rb, U, Th

In agreement with the northward increase in K_2O and Na_2O across the arc (Fig. 5.7.1 and 5.7.2), the other (trace) LIL elements follow suit. On closer inspection there are some differences between the singly and doubly charged cations:

Barium contents increase with increasing SiO_2 within individual volcanoes but also increase across the arc at increasing distances from the trench (Fig. 5.8.3a). The values found at Boleng completely overlap those of Lewotolo. The rocks from Kisu in the Strait of Pantar show the highest Ba concentrations. The difference with the levels at Batu Tara indicates that the across-arc increase of Ba does not follow the same systematics in each of the transects, which can also be observed in Figure 5.9.3. Strontium contents increase northward across the arc (Fig. 5.8.3b and 5.9.3b). Within-suite trends can easily be explained by the role of plagioclase fractionation. The Sr contents tend to drop with increasing SiO_2 in the MA volcanoes, but the Werung series exhibit a modest increase. Boleng shows Sr contents intermediate between frontal Sirung and Werung on the one hand and Lewotolo on the other. Treweg in the Strait of Pantar is richer in Sr than would be expected from comparison with Sirung and Werung. Lead contents are highest in Boleng and Lewotolo but not in Ternate or Pura Besar which are situated on similar WBZ contours (Fig. 5.8.3c). It is of interest to note that Ce, which has a similar bulk distribution coefficient as Pb in MORB environments *(Sun and Mcdonough, 1989)*, shows a different behaviour as it is not highest in Boleng. Lavas from Werung have the lowest Pb contents. The Pb-SiO_2 trends suggest incompatible behaviour of lead for virtually all volcanoes.
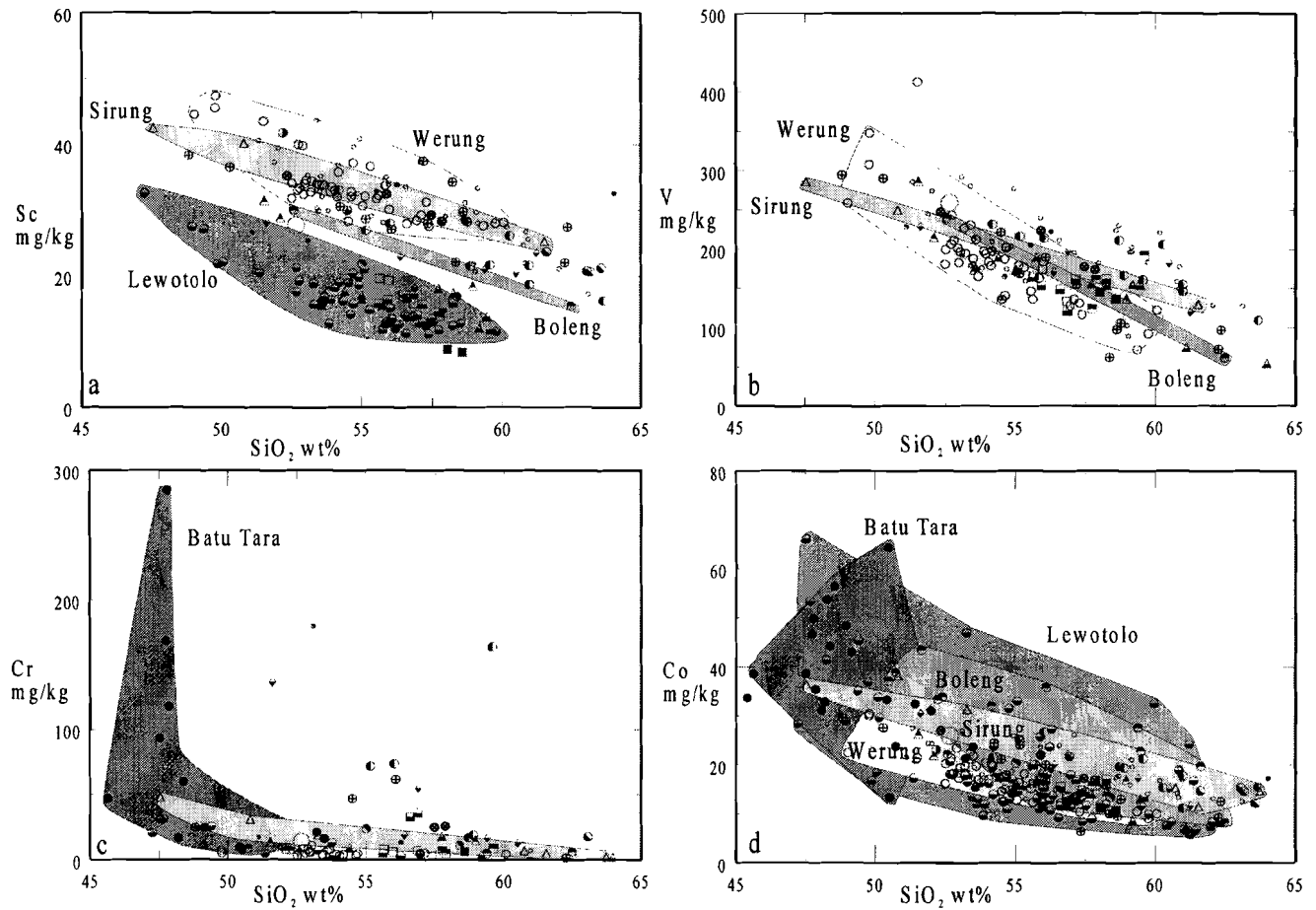
Figure 5.8.1. Plots of Sc, V, Cr and Co contents versus SiO2. Symbols as in Fig. 5.1.
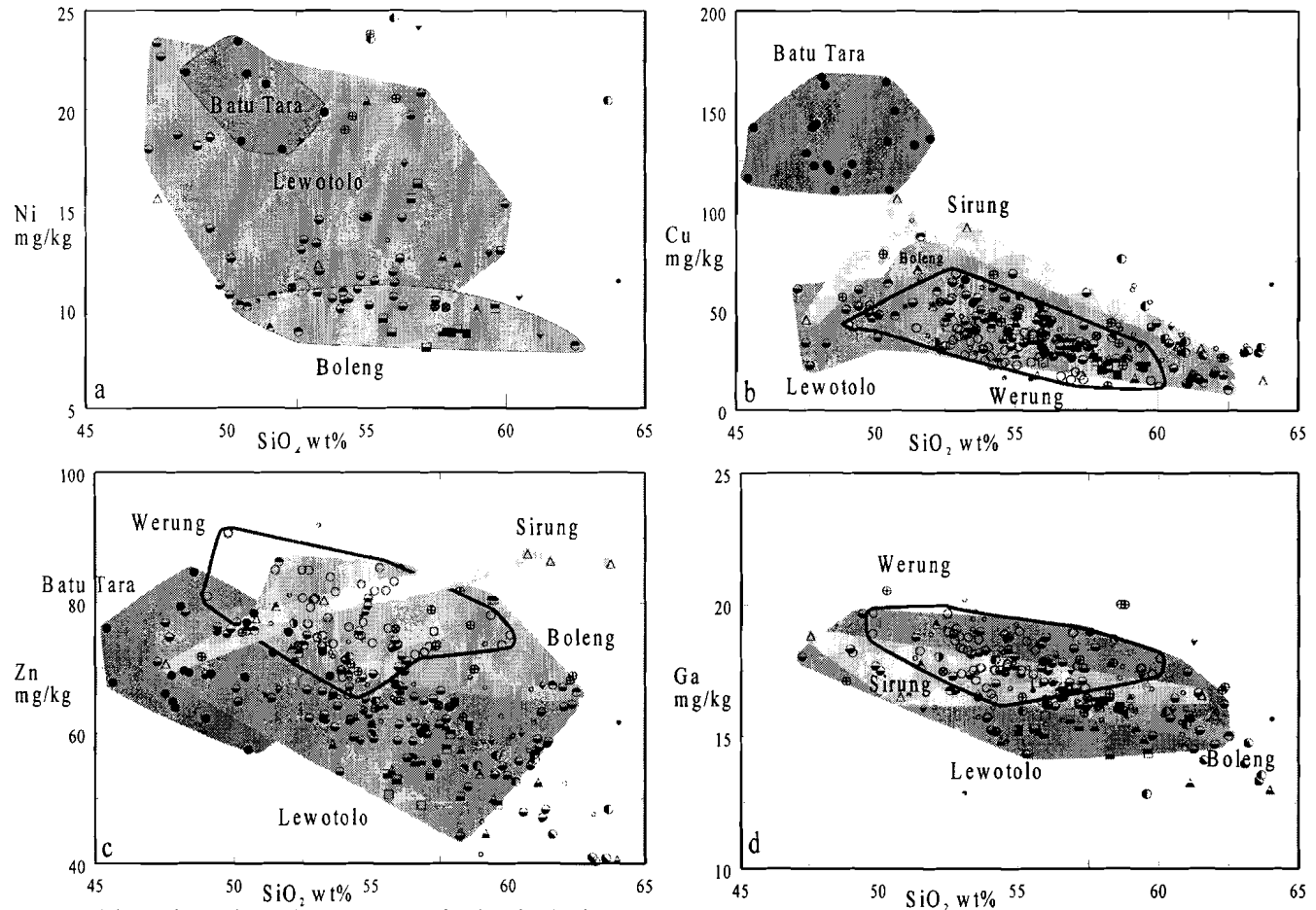
Figure 5.8.2. Ni, Cu, Zn and Ga contents of volcanics in the Adonara-Pantar Sector versus SiO$_2$. Symbols according to Fig. 5.1

41
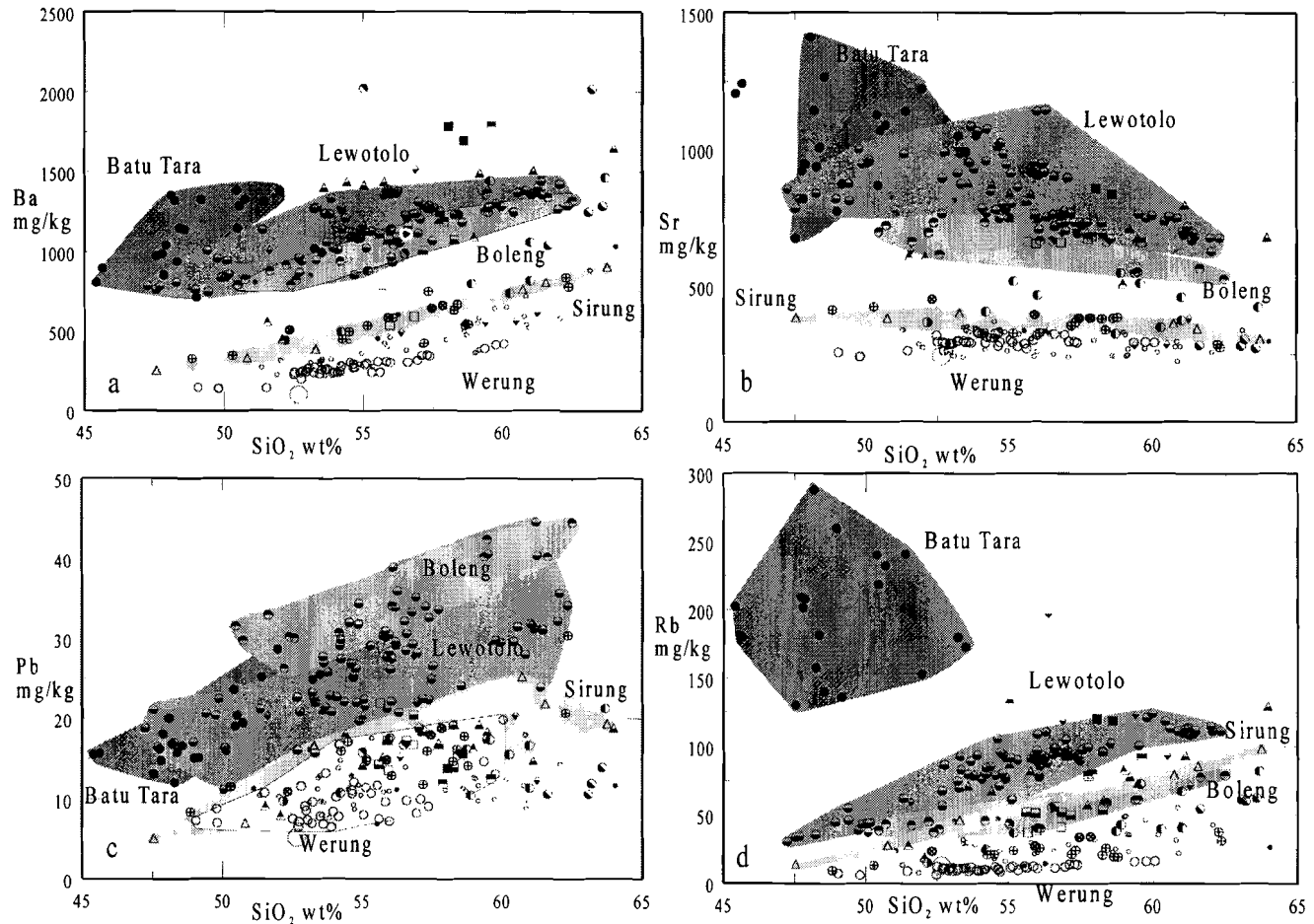
Figure 5.8.3. Ba, Sr, Pb and Rb contents of volcanics in the Adonara-Pantar Sector versus SiO$_2$. Symbols according to Fig. 5.1
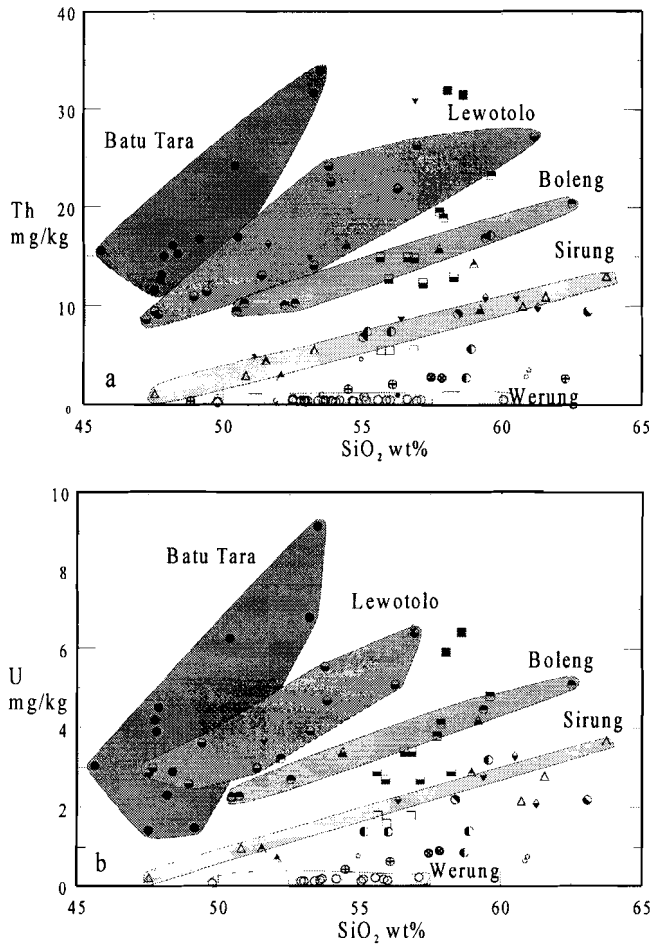
Figure 5.8.4. Th and U contents of volcanics in the Adonara-Pantar Sector versus SiO₂. Symbols according to Fig. 5.1.

The behaviour of rubidium follows that of potassium (Fig. 5.8.3d) and shows increasing values within each suite, except Batu Tara, as well as increasing contents across the arc with increasing WBZ depth. There is no overlap between concentrations at Boleng and Lewotolo. The Sirung suite forms a steep array versus SiO_2. Th-SiO_2 trends become systematically steeper with increasing distance from the trench (Fig. 5.8.4a). Uranium behaves similar to Th (Fig. 5.8.4b), and a general increase from the frontal volcanoes to Batu Tara can be observed. Both elements behave incompatible within each suite, except Batu Tara, where Th/U ratios can be correlated with Th and Sr isotope compositions (see chapter 7).
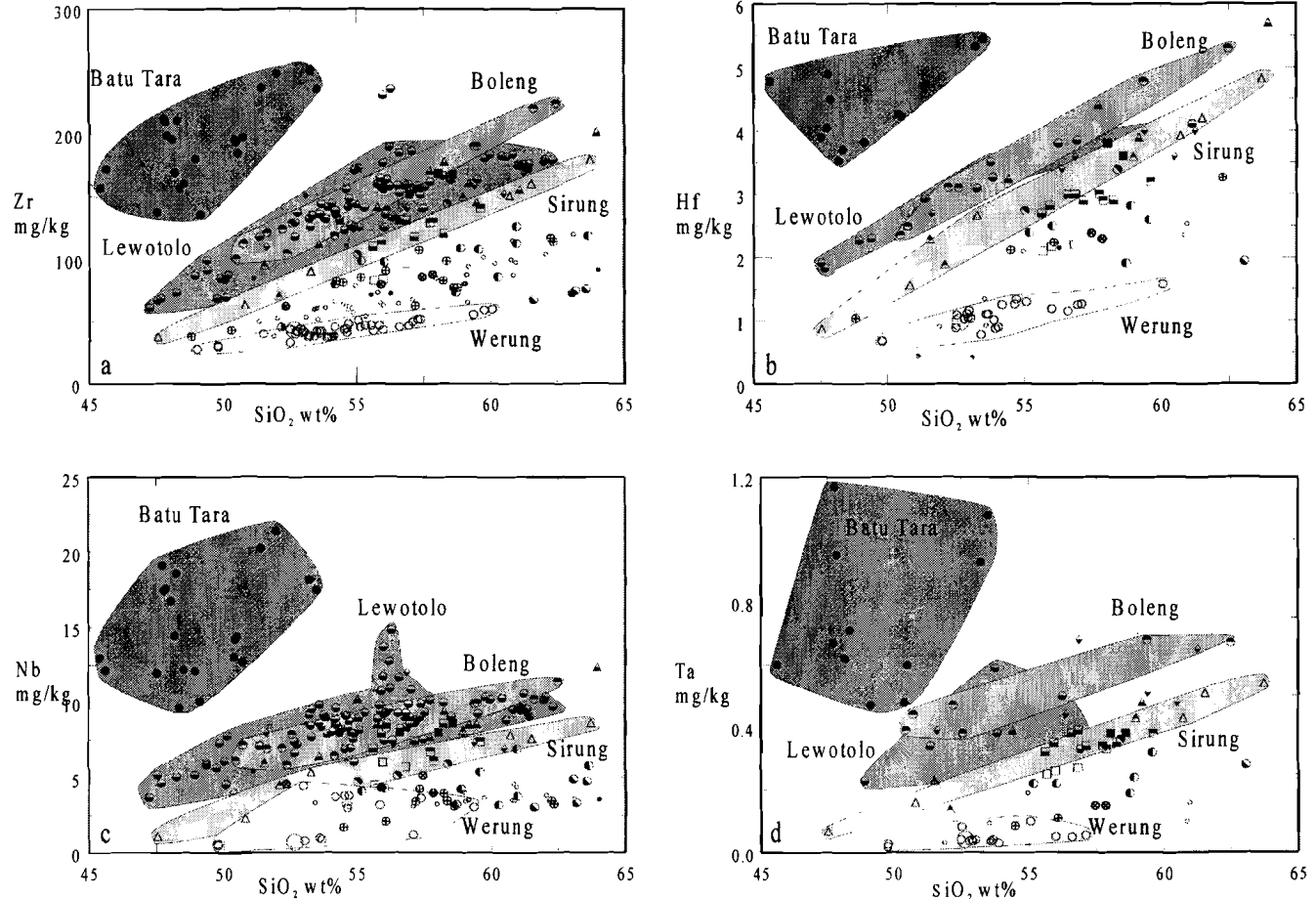
Figure 5.8.5. Zr, Hf, Nb and Ta contents of volcanics in the Adonara-Pantar Sector versus SiO$_2$. Symbols according to Fig. 5.1
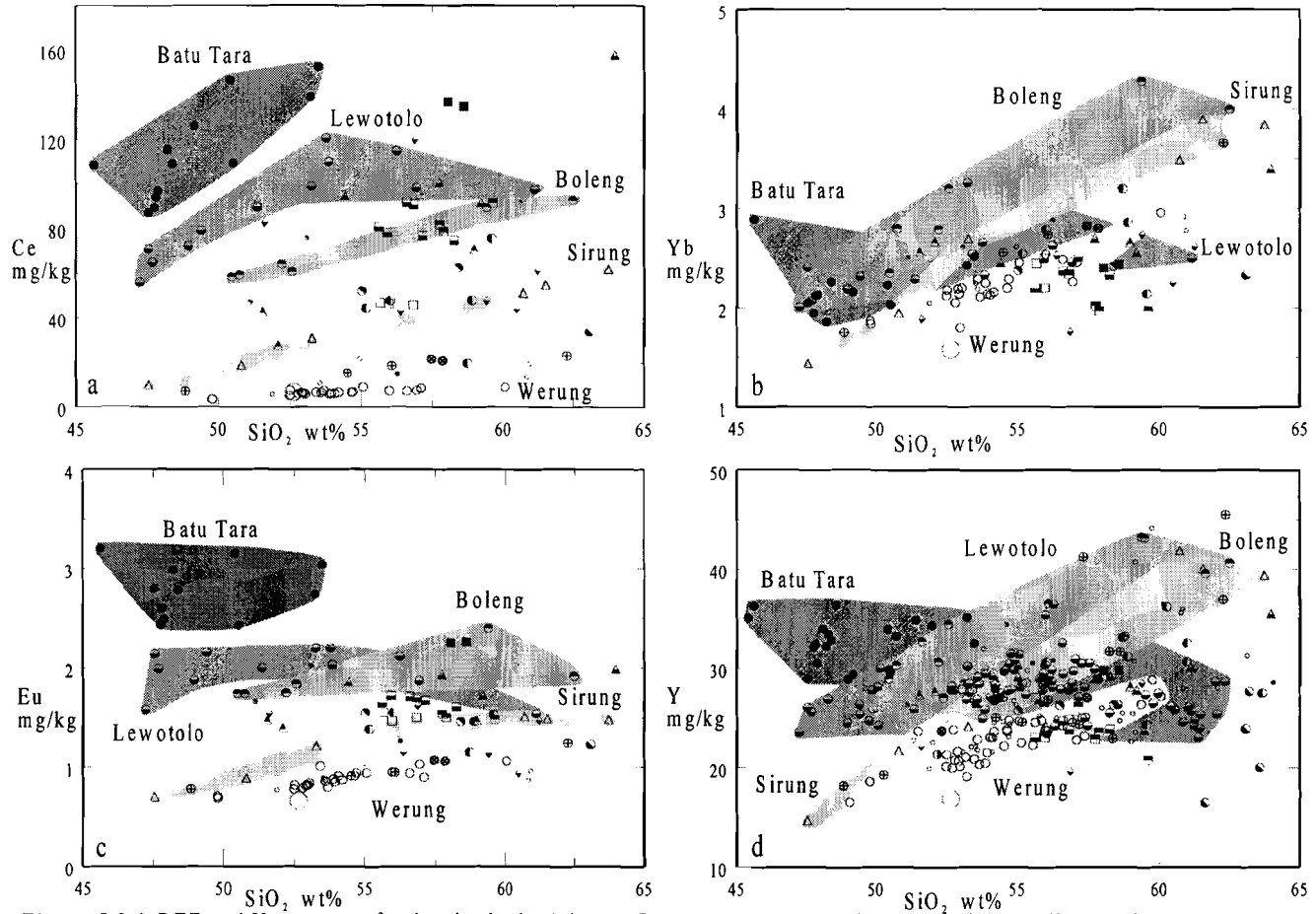
Figure 5.8.6. REE and Y contents of volcanics in the Adonara-Pantar Sector versus SiO_2. Symbols according to Fig. 5.1

5.5.3 The high field strength elements Zr, Hf, Nb and Ta

The contents of zirconium and the other high-field-strength elements systematically increase across the arc as well as within each suite (Fig. 5.8.5). Some lavas from Lewotolo show positive Zr and Nb anomalies (similar anomalies may be present for Hf and Ta, but these samples were not analysed by INAA). De Hoog *(1995)* discovered zirconolite in several Lewotolo lavas. This HFSE-rich mineral probably formed during late-stage degassing, which could explain the Zr and Nb anomalies.

5.5.4 The REE group and Y

The light rare earth elements (LREE) become systematically more abundant in the direction away from the trench (Fig. 5.8.6). The heavy rare earth elements (HREE) and Y show a strong positive correlation with SiO_2 in Werung, Sirung, the other frontal volcanoes and Boleng. At Werung the lavas are depleted in the LREE relative to the HREE compared to other arc settings. The oldest lavas are even depleted relative to N-MORB *(see Fig 6.6)*. Most interestingly, the depletion diminishes with increasing maturation of the volcano, as the Ce/Yb ratio increases (at constant Yb) with stratigraphic position *(see Fig. 6.7)*. Europium is remarkably constant in the Lewotolo and Batu Tara suites and increases slightly in the VF volcanoes and Boleng, in agreement with the behaviour of Sr.

5.6 Across-arc systematics of the trace elements

In Figures 5.9.1-5.9.6 the across-arc systematics of the trace elements are presented after following the same procedures as outlined in 5.3.1 for the major elements. The most important features have already been discussed in the previous part of this chapter, but some additional remarks should be made.

Concentrations of predominantly compatible elements shown in Fig 5.9.1 remain fairly constant across the arc, except for Sc, which decreases away from the trench. The concentrations of bivalent LILEs Ba, Sr, and Pb (Fig. 5.9.3a-c) exhibit relatively strong increases near the volcanic front, whereas the monovalent LILEs K and Rb (Figs. 5.7.1 and 5.9.3d) increase more gradually. Lead appears to have a maximum at some point not far behind the volcanic front. Thorium and Uranium (Fig. 5.9.4) show a gradual increase in concentrations. Furthermore, it seems that the eastern transects (triangles and squares) are characterised by overall concentrations of Th and U that are lower than in the western transect (circles). This phenomenon also emerges in the data of the other LILEs but is much less obvious.

The gradual increase in element concentration across the arc is also observed in the HFSEs (Fig. 5.9.5). The HFSE enrichment in the western relative to the eastern transect is more pronounced than that of the LILEs.

46
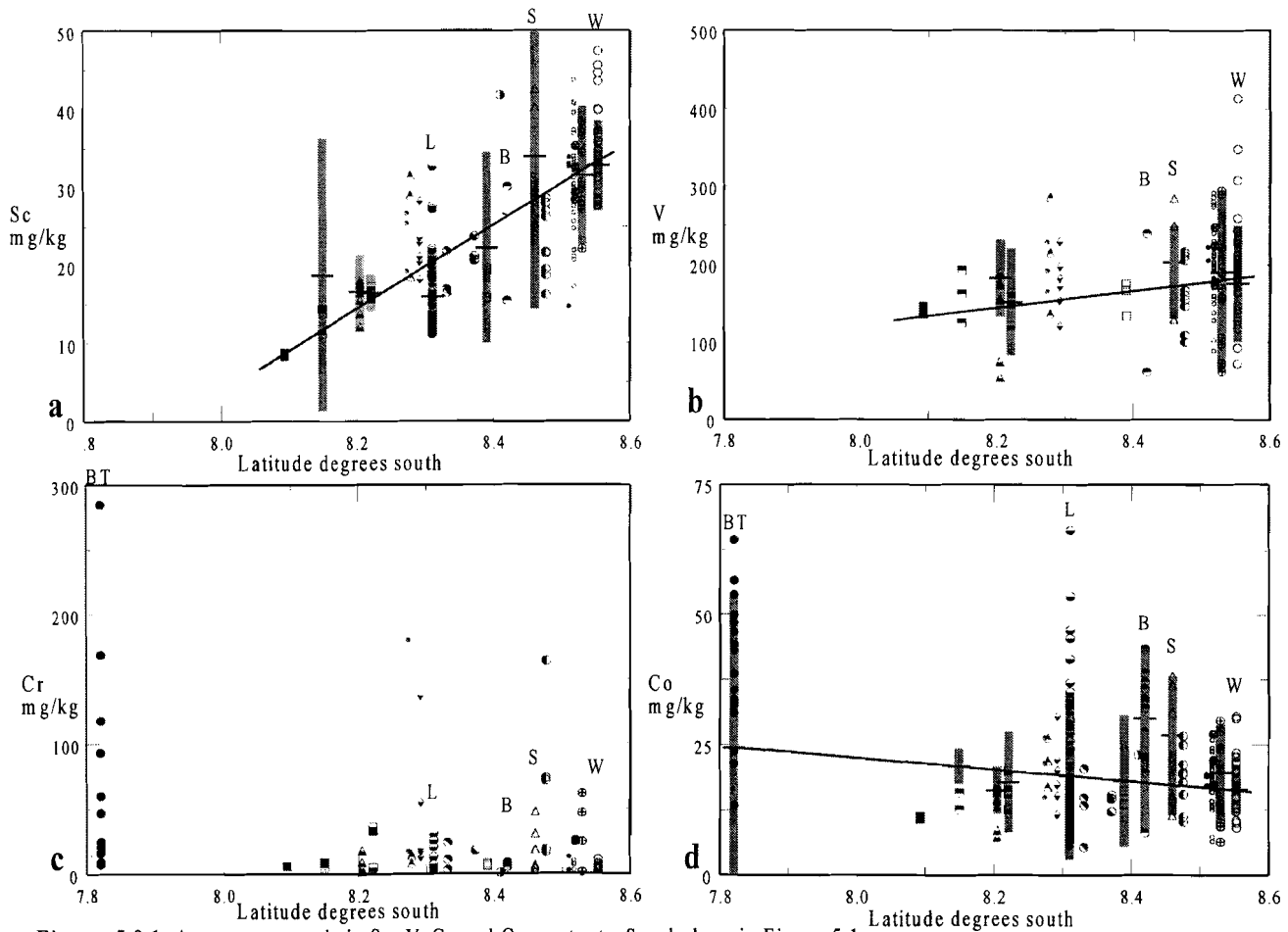
Figure 5.9.1. Across-arc trends in Sc, V, Cr and Co contents. Symbols as in Figure 5.1.
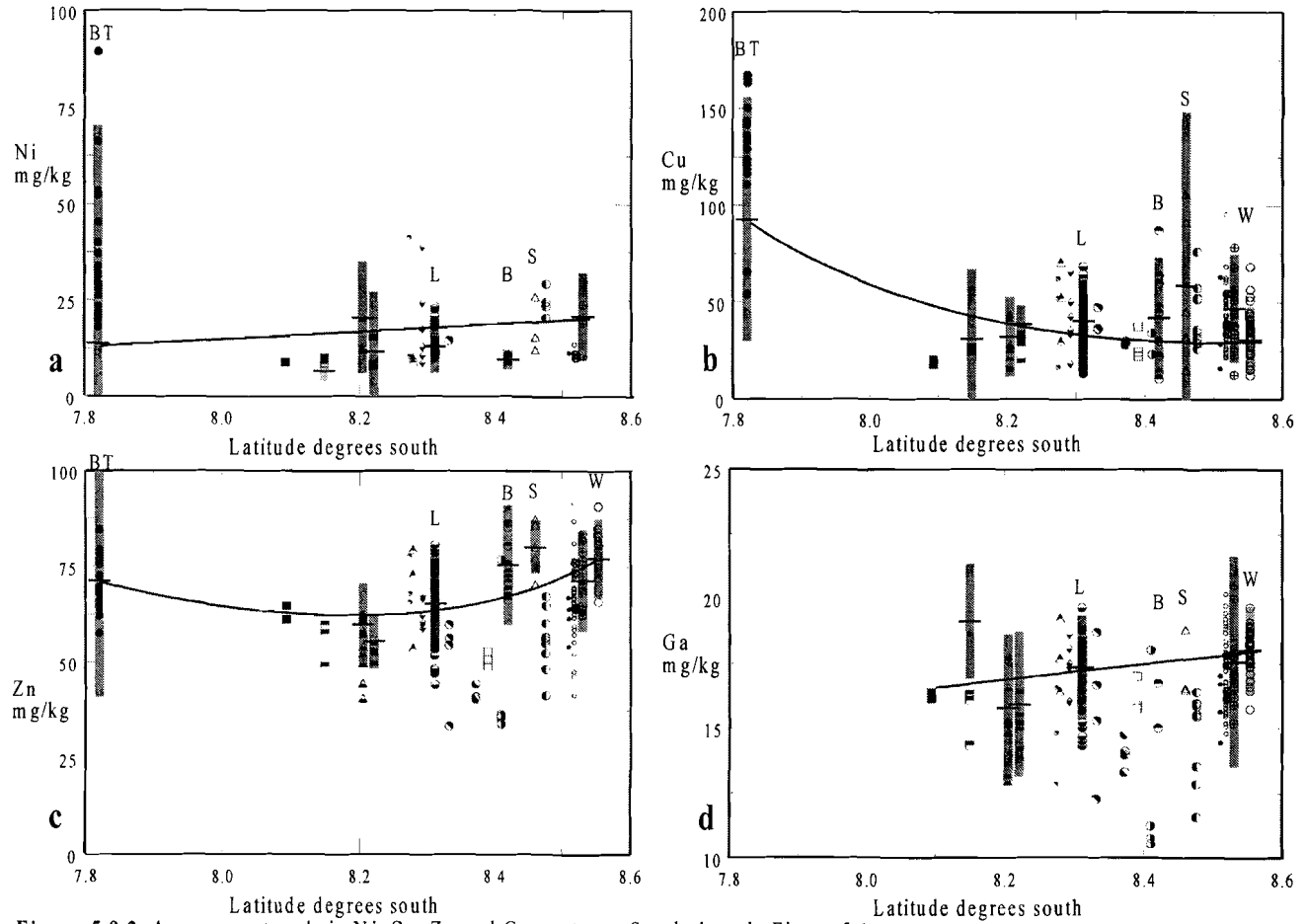
Figure 5.9.2. A cross-arc trends in Ni, Cu, Zn and Ga contents. Symbols as in Figure 5.1.
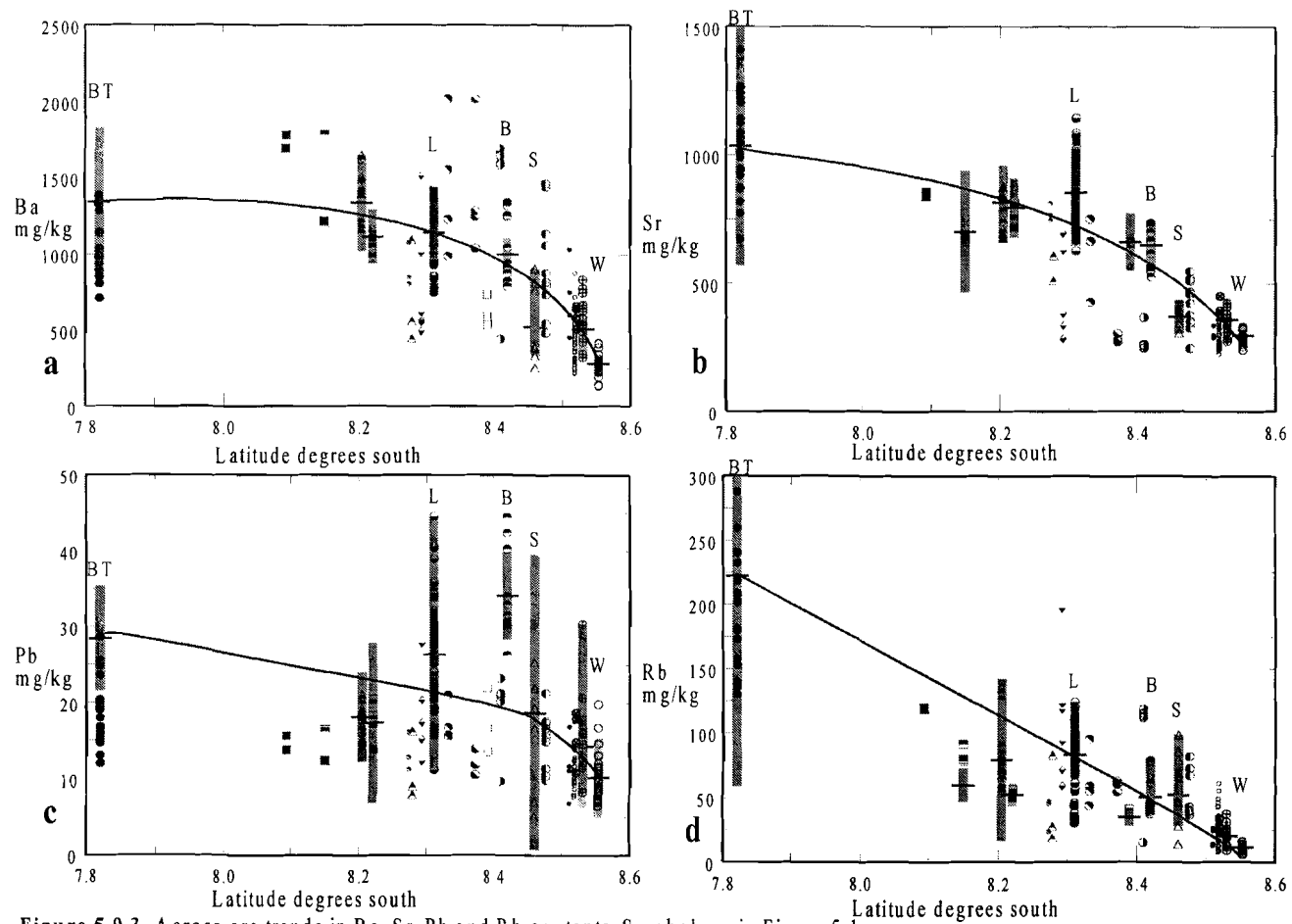
Figure 5.9.3. Across-arc trends in Ba, Sr, Pb and Rb contents. Symbols as in Figure 5.1.
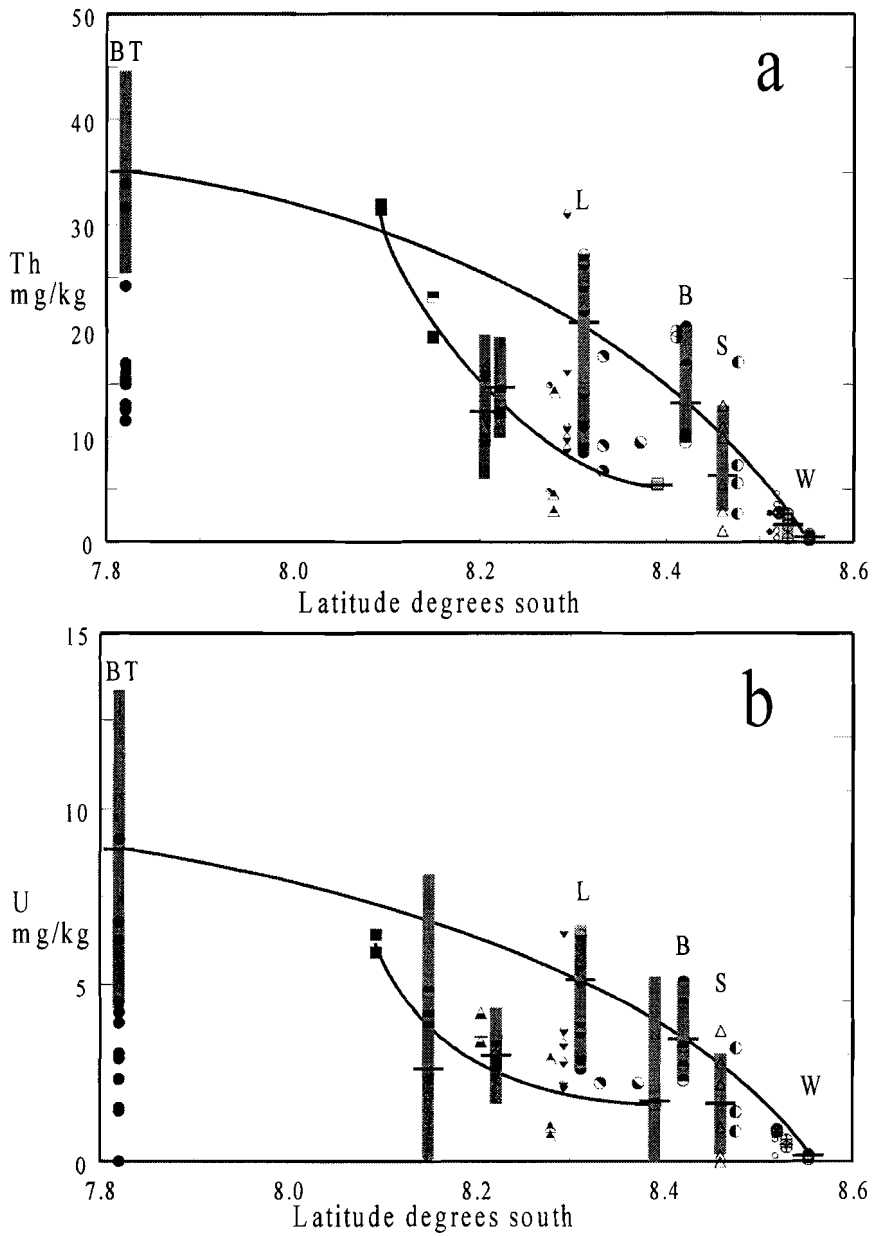
Figure 5.9.4. Across-arc trends in Th and U contents. Symbols as in Figure 5.1.
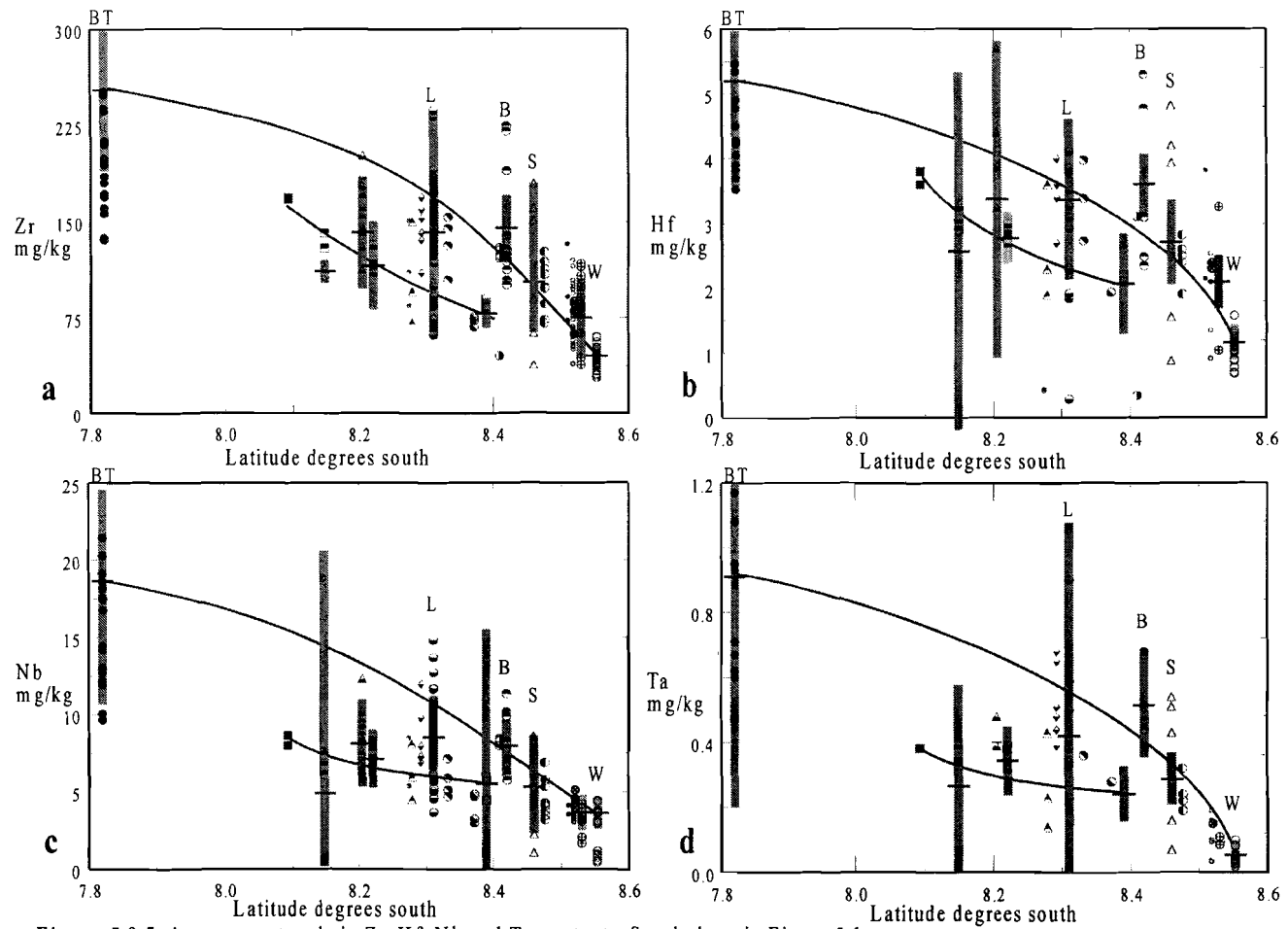
Figure 5.9.5. Across-arc trends in Zr, Hf, Nb and Ta contents. Symbols as in Figure 5.1.
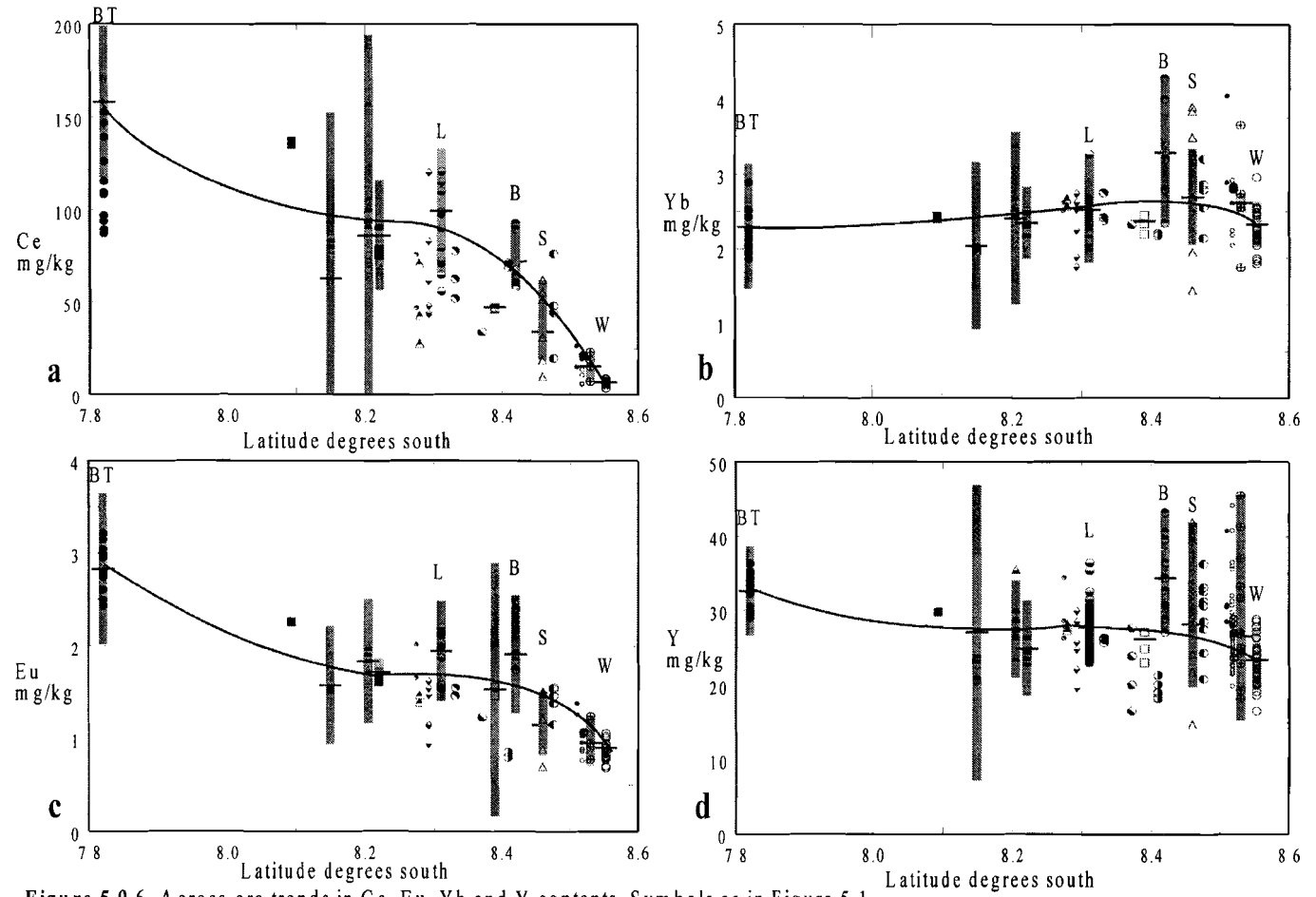
Figure 5.9.6. A cross-arc trends in Ce, Eu, Yb and Y contents. Symbols as in Figure 5.1.
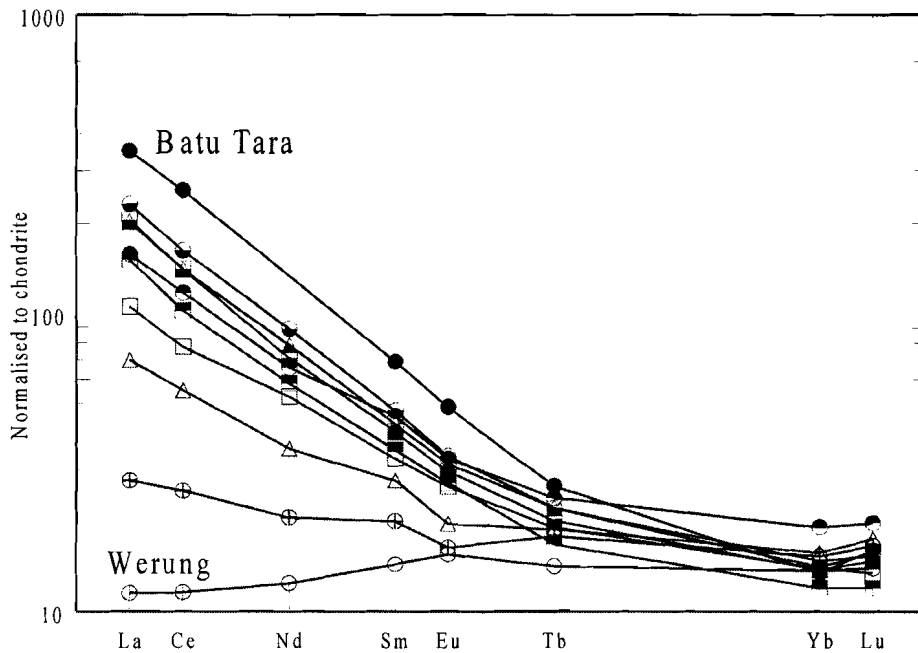
Figure 5.9.7. Average chondrite-normalised REE patterns for the APS series at 55 wt% SiO_2. Symbols as in Fig. 5.1.

Light REE concentrations (Fig. 5.9.6a) increase gradually across the arc. Europium and the middle REEs increase as well, but to a lesser extent (Fig. 5.9.6c). Heavy REEs (Fig. 5.9.6b) remain relatively constant (with the exception of Boleng and Sirung), a feature that is usually confined to continental arcs (*cf., Gill, 1981*). In a transect across the New Britain island arc, Yb concentrations increase twofold due to changing magma-genetic parameters (*Woodhead and Johnson, 1993*). Concentrations of Y in the APS centres slightly increase from Werung to Batu Tara. The Y concentrations in the lavas of Sirung and Boleng follow the behaviour of Yb in these volcanoes. Figure 5.8.7 documents chondrite-normalised REE patterns at 55 wt% SiO_2, highlighting the LREE-depleted signature of Werung and the systematic increase of the LREE and MREE across the arc.

5.7 Trace elements versus Isotopes

An effective way to explore for indications of assimilation of crustal wall rock-material and its influence on the chemical composition of the rocks of interest, is to test for a correlation between a differentiation index and isotopic signals. In Figure 5.10 SiO_2 and the inverse of the Sr concentration are plotted against $^{87}Sr/^{86}Sr$.
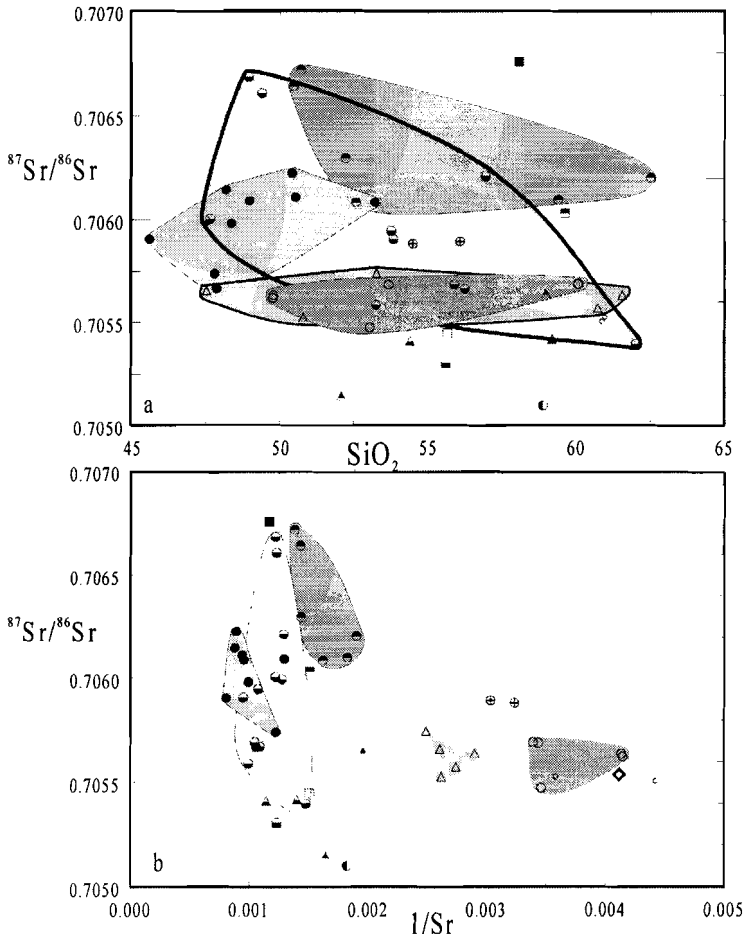
Figure 5.10. Sr isotopes versus SiO_2 and Sr isotopes versus 1/Sr.

The frontal rocks show little or no correlation between $^{87}Sr/^{86}Sr$ and SiO_2. The Batu Tara samples show a significant variation in $^{87}Sr/^{86}Sr$ ratios, but there is no correlation with SiO_2 contents. The Lewotolo and Boleng samples show a broad inverse correlation with SiO_2,

54

which is opposite to what would be expected in the case of (shallow) assimilation of crustal rocks that are enriched in radiogenic strontium relative to the magma.

In Figure 5.10b mixtures of magma and wall-rock should fall on straight (diagonal) lines for individual volcanoes, as both variables have the same denominator. In contrast, the Boleng, Batu Tara and Lewotolo samples show remarkable variations in $^{87}Sr/^{86}Sr$ at almost constant Sr concentrations, which is inconsistent with crustal contamination at shallow depths. In a similar plot of $^{143}Nd/^{144}Nd$ versus 1/Nd (Fig. 5.11) mixing of ascending magma with crustal wall-rock should produce straight lines, but individual suites tend to lie on a hyperbola.

Van Bergen et al. *(1992)* presented oxygen isotope results for the Batu Tara samples, which show mantle or near-mantle values, and argued that assimilation was unlikely for these samples. Preliminary oxygen isotope data of whole-rock samples from Werung *(De Groot, pers. comm.)* fall in the same range as the Batu Tara rocks.

This combination of evidence indicates that crustal assimilation has had little or no influence on elemental and isotopic compositions of lavas in the Adonara-Pantar Sector, and that first-order differences between individual volcanic centres shown by the least evolved magmas can be attributed to source characteristics and/or melting processes.
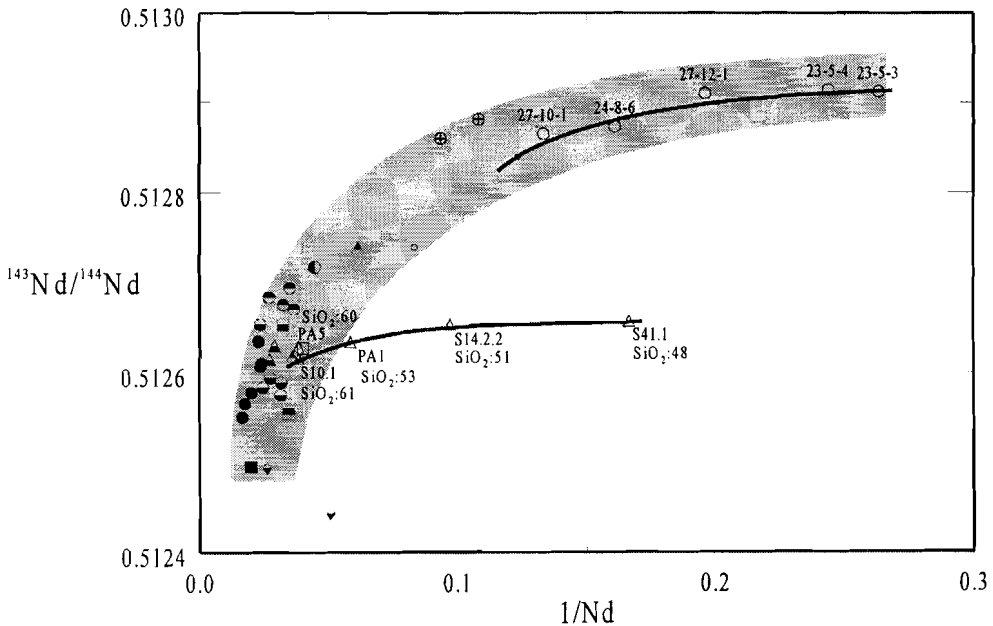
Figure 5.11. Plot of $^{143}Nd/^{144}Nd$ ratios versus 1/Nd. The field encompasses all APS centres except Sirung. The curvature implies that wall-rock contamination cannot be responsible for the observed variations as in that case a straight array would be present. The $^{143}Nd/^{144}Nd$ ratios of Sirung lavas tend to decrease with increasing Nd and SiO_2 contents. Symbols as in Figure 5.1.

55

6 Magma Sources, Evidence from Isotope Systematics

6.1 Introduction

In chapter 2 the historical development of the understanding of the origin of arc magmas has been reviewed and in chapter 3 the geology and geochemistry of the APS (Adonara-Pantar Sector) has been addressed. From these starting points the principal objective of this chapter is to assess the possible different source materials that participate in the genesis of the APS magmas. Because relations exist between the nature of a source material and the processes acting on it, some of these processes are briefly discussed.

6.2 Results

The results for major elements, trace elements and Sr, Nd, Pb isotopes are given in appendices 3 and 4. In Figure 6.1 the relation between the isotope systems and SiO_2 is presented and used to discuss the results in the APS also in relation to previously published data. In all, our results agree with the previous, less detailed, studies in the Eastern Sunda Arc. Strontium isotopes in the APS are more radiogenic than those in the more western part of the Sunda Arc. This has been interpreted as being caused by involvement of sediments or even continental crust *(Whitford et al., 1977)* at this location. The more detailed Nd and Pb isotope data in the APS presented in this study agree with recent studies by other authors *(Vroon, 1986; Varekamp et al., 1989; Stolz et al., 1990)*. The most important additional observations are the very high, close to mantle, Nd isotope values in contrast with the extremely radiogenic (crustal) He isotope values in the Werung volcano. Furthermore, the Sr, Nd, Pb and Th isotopes display a more crustal character when approaching the inactive Alor-Wetar sector. This observation agrees with results for the Sunda Arc between Java and the APS presented by Ben Othman *(1989)*.

6.2.1 Sr isotopes

All frontal volcanoes have $^{87}Sr/^{86}Sr$ lower than 0.7059 (Fig. 6.1a). Lowest $^{87}Sr/^{86}Sr$ ratios at the front of the arc are found at Werung (0.70548-0.70569) and Waroe (0.70510). The CA volcanoes and Batu Tara range between 0.7051 and 0.7067. The samples from the inactive zone, Alor and Atauro (including Atauro samples from *Whitford et al., 1977*), display increased values (>0.707). Lewotolo and Boleng samples have a remarkable inverse correlation between SiO_2 and $^{87}Sr/^{86}Sr$ at low SiO_2. The frontal volcanoes show no change in $^{87}Sr/^{86}Sr$ with increasing SiO_2. The islands in the Strait of Alor (Treweg, Pura Besar, Ternate) display an across-arc increase in $^{87}Sr/^{86}Sr$ away from the trench. It is of interest to note that the highest values are not found in high-K rocks but in the lavas of Lewotolo and Boleng. This coincides with trace element results in chapter 8 where the highest Sr/HFSE ratios also occur at Lewotolo.
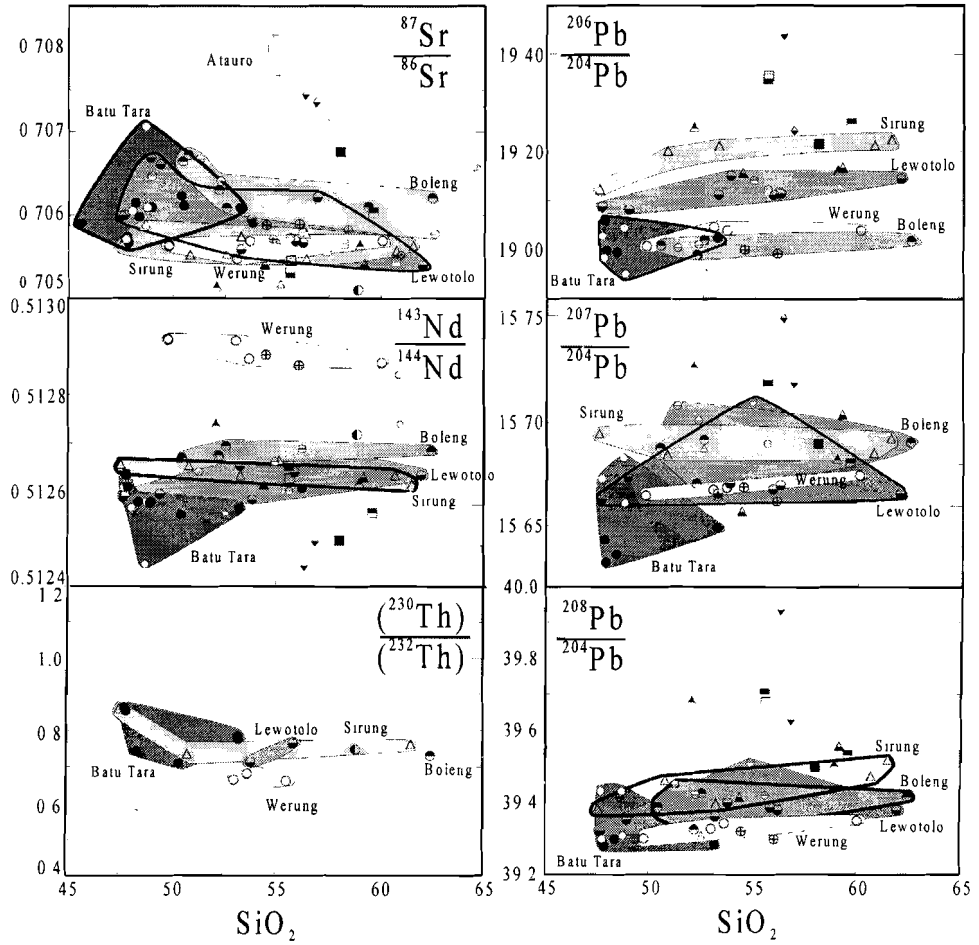
Figure 6.1. Sr, Nd, Th and Pb isotopes versus SiO2 of APS samples including literature data *(Whitford et al., 1997; Stolz et al., 1988; Stolz et al., 1990)*. Fields indicate data from the five active volcanoes in this study. In the Sr isotope plot the upper-right field represents Atauro samples from the inactive Alor-Wetar sector *(Whitford et al., 1997)*.

58
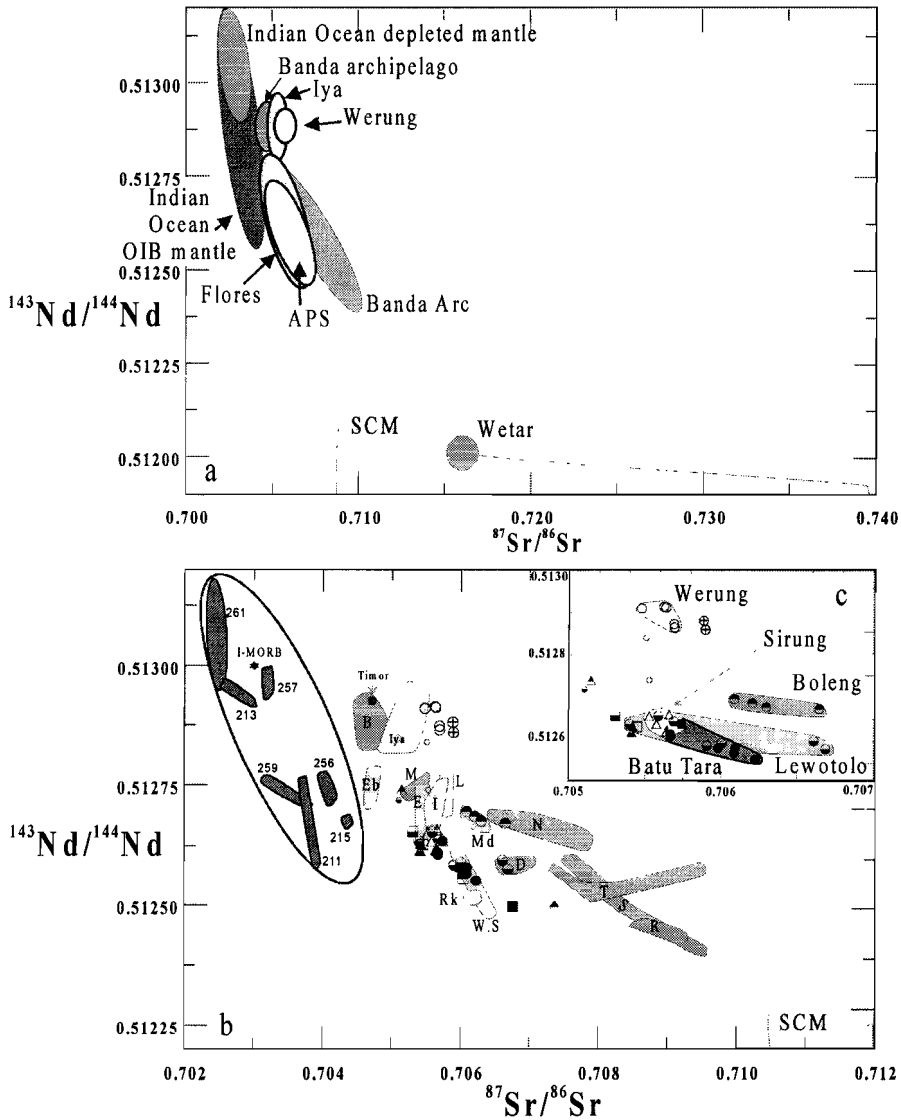
Figure 6.2. Nd versus Sr isotopes. **a:** The values of the APS samples are within the range of those of Flores *(Stolz, 1990 and pers. comm.)* and have lower $^{87}Sr/^{86}Sr$ (except for frontal rocks) at similar $^{143}Nd/^{144}Nd$ compared to the Banda Arc rocks *(Vroon, 1992)*. SCM stands for subducted continental material. **b:** Individual APS samples in relation to Flores and Banda Arc centres; Flores: Iya, Eb=Ebulobo, L=Lewotobi, I=Inerie, E=Egon, Md=Mandiri, Rk=Rokatenda, W.S.=Wai Sano. Banda Arc: B=Banda, M=Manuk, N=Nila, D=Damar, T=Teon, S=Serua. R=Romang. Indian Ocean fields; numbers in Fig.b indicate DSDP and ODP sites from *Weis and Frey, 1996.* **c:** Enlargement shows fields for the active APS volcanoes. Literature data from: *Bergman et al., 1996; Edwards, 1990; Edwards et al., 1993; Edwards et al., 1994; Gerbe et al., 1992; Hoogewerff et al., 1997; Hutchison and Jezek, 1978; Gasparon, 1993; Gasparon et al., 1994; Magaritz et al., 1978; McCulloch et al.,*

59

1983; McDermott and Hawkesworth, 1991; Morris et al., 1983; Morris et al., 1983; Morris et al., 1984; Stolz et al., 1988; Stolz et al., 1990; Tatsumi et al., 1991; Varne and Foden, 1987; Vukadinovic and Nicholls, 1989; Vukadinovic and Sutawidjaja, 1995; Whitford et al., 1977; Whitford et al., 1979; White and Patchet, 1984.

6.2.2 Nd isotopes

The Nd isotopes display the expected inverse relation with Sr isotopes with low ratios in the inactive segment (<0.5125) in Fig. 6.2. High ^{143}Nd/^{144}Nd values at Werung, Labalekan and the Labala Peninsula *(see Fig. 6.1b)* almost coincide with I-MORB values *(Ito et al., 1987; Weis and Frey, 1996)* in Fig 6.2b. This is also observed in similar low K tholeiites from Iya on Flores *(Stolz et al., 1990)*. The Werung samples seem to define a negative trend against SiO$_2$, which is not observed in the other centres. Again the locations close to the inactive Alor-Wetar sector have the least radiogenic signal down to 0.51245.

6.2.3 Sr and Nd isotopes

The combined Sr and Nd isotope systematics in Fig. 6.2a show two arrays with slightly different angles between a high ^{143}Nd/^{144}Nd, low ^{87}Sr/^{86}Sr endmember and a high ^{87}Sr/^{86}Sr, low ^{143}Nd/^{144}Nd (crustal-) sedimentary endmember. The high ^{143}Nd/^{144}Nd and intermediate ^{87}Sr/^{86}Sr values at Werung, Labalekan, the Labala peninsula, Iya and the Banda archipelago, relative to the other locations, appear to be a significant feature. In Sr and Nd space the APS rocks lie on the same trend as the Flores rocks, whereas the Banda Arc rocks (including inactive Wetar) have higher ^{87}Sr/^{86}Sr at similar ^{143}Nd/^{144}Nd than the APS-Flores rocks. This suggests that the inactive Alor-Wetar segment is not only a tectonic border, but that magma sources or magmagenetic processes in the APS are somewhat different from those in the Banda Arc.

In Figure 6.2b different eastern Indian Ocean DSDP and ODP data *(Weis and Frey, 1996)* are plotted to outline the composition of depleted (sites 261, 257, 213) and enriched Indian Ocean mantle (sites 259, 256, 215, 211). The trace element compositions of 261 and 211 will be used in chapter 8. In Fig 6.2c the Boleng samples show relatively elevated Sr isotope values within the APS central arc (CA) and rear arc (RA). The Lewotolo samples form an array with a slightly negative slope, as do the Batu Tara samples.

6.2.4 Pb isotopes

The Batu Tara samples have the lowest ^{208}Pb/^{206}Pb and ^{207}Pb/^{206}Pb compositions *(Van Bergen et al., 1992)*. The centres nearest to the inactive Alor-Wetar sector show the most radiogenic Pb compositions (Fig. 6.1d,e,f). Thus the conspicuous East-West trend in ^{206}Pb/^{204}Pb observed in the sediments in front of the arc is mirrored in the volcanics *(Van Bergen et al., 1993; Vroon, 1992; Ben Othman et al., 1989)*. All volcanic centres seem to display a small but significant increase in ^{208}Pb/^{204}Pb with increasing SiO$_2$.
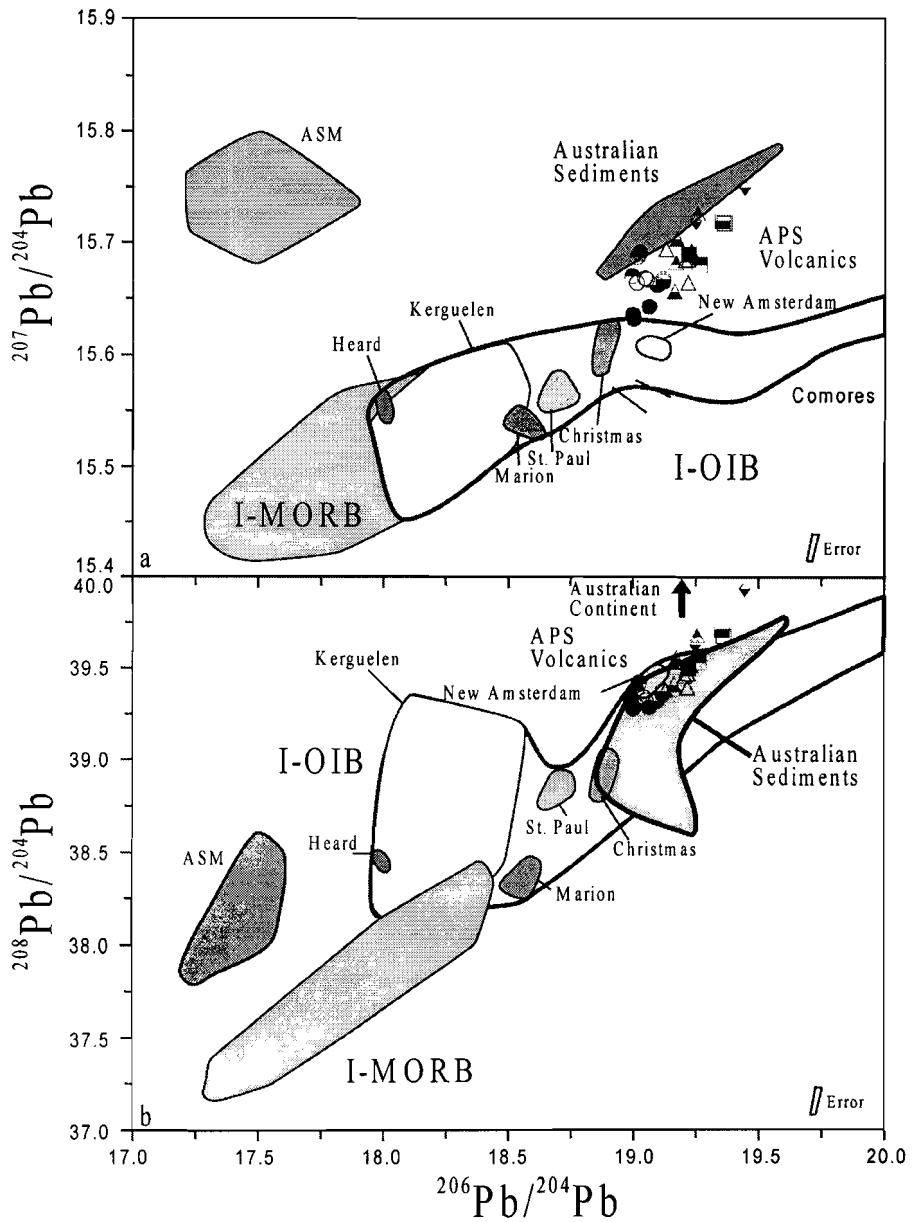
Figure 6.3. ^{208}Pb/^{204}Pb and ^{207}Pb/^{204}Pb versus ^{206}Pb/^{204}Pb and fields for Indian-MORB, Indian OIB, Australian Subcontinental Mantle (ASM) and local sediments (for references see text).
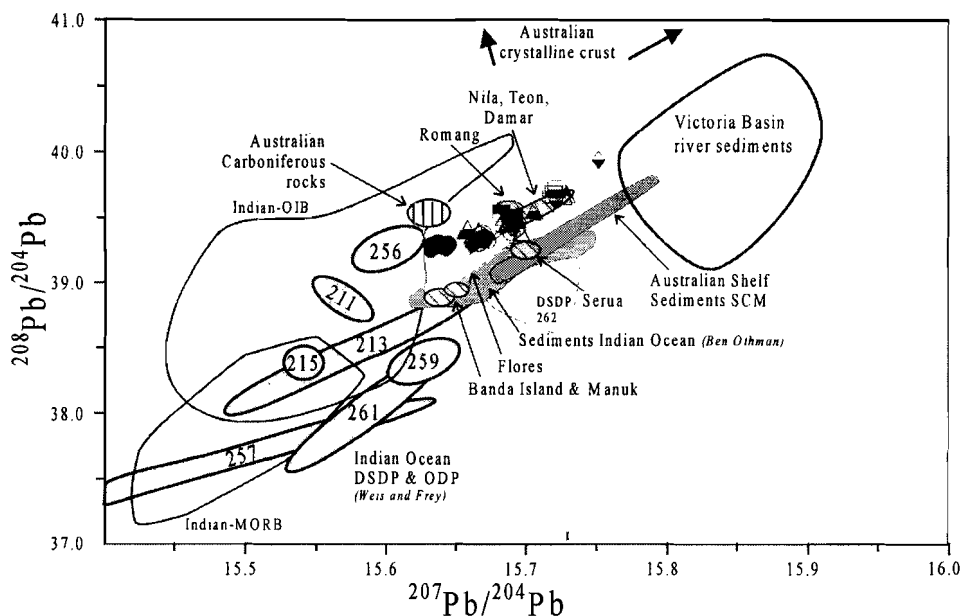
Figure 6.4. $^{208}Pb/^{204}Pb$ versus $^{207}Pb/^{204}Pb$ showing the necessity of a high $^{208}Pb/^{204}Pb$ component other than the Indian Ocean sediments or Indian Ocean mantle (for references see text).

The volcanics have higher Pb isotope values than I-MORB (Fig. 6.3a,b) and do not systematically overlap with the I-OIB fields. A significant S-N tendency is not observed (except for the lower $^{208}Pb/^{206}Pb$ and $^{207}Pb/^{206}Pb$ values at Batu Tara).

6.2.5 Th isotopes

The results of Th isotope analysis of the active volcanoes have been reported in Hoogewerff et al. *(1997)* and will be more extensively discussed in chapter 7. The available data show no significant trends with SiO_2 (in Fig. 6.1c) but values for Batu Tara and Lewotolo correlate with Sr and Nd isotopes.

6.2.6 He isotopes

He isotope values from the Sunda-Banda Arc *(Poreda and Craig, 1989; Hilton and Craig, 1989)* are intermediate between the mantle reservoir with 8.Rᴀ (Rᴀ= air $^3He/^4He$) and radiogenic values <0.01.Rᴀ. We *(Hilton et al., 1992)* have reported helium isotope data for olivines and clinopyroxenes from recent lavas for eleven volcanoes from Flores in the East Sunda Arc through the inactive segment between the APS and Banda Arc, to Banda Island at the northern end of the Banda Arc. In the APS $^3He/^4He$ ratios vary between 4.5 Rᴀ for Batu Tara volcano to a remarkably low radiogenic ratio of 0.0075 Rᴀ at Werung. Lavas from the inactive segment have a narrow range between 3.9 Rᴀ at Kisu (APS) to 1.0 Rᴀ at Romang

62

(most eastern part of the inactive segment). Also the sample from Banda archipelago has a moderately radiogenic value of 3.1 RA indicating involvement of crustal material in magma genesis in the entire Sunda-Banda Arc system from Flores (Iya) to Banda.

In our study *(Hilton et al., 1992)* we combined Sr and He isotopes results to argue that degassing of the Australian crust is responsible for the low ^{3}He/^{4}He. Terrigenous sediments are an improbable source, as they are unlikely to retain helium during subduction and subsequent heating. Crystalline crust, however, is capable of carrying the radiogenic signal to depths that are relevant for magma genesis.
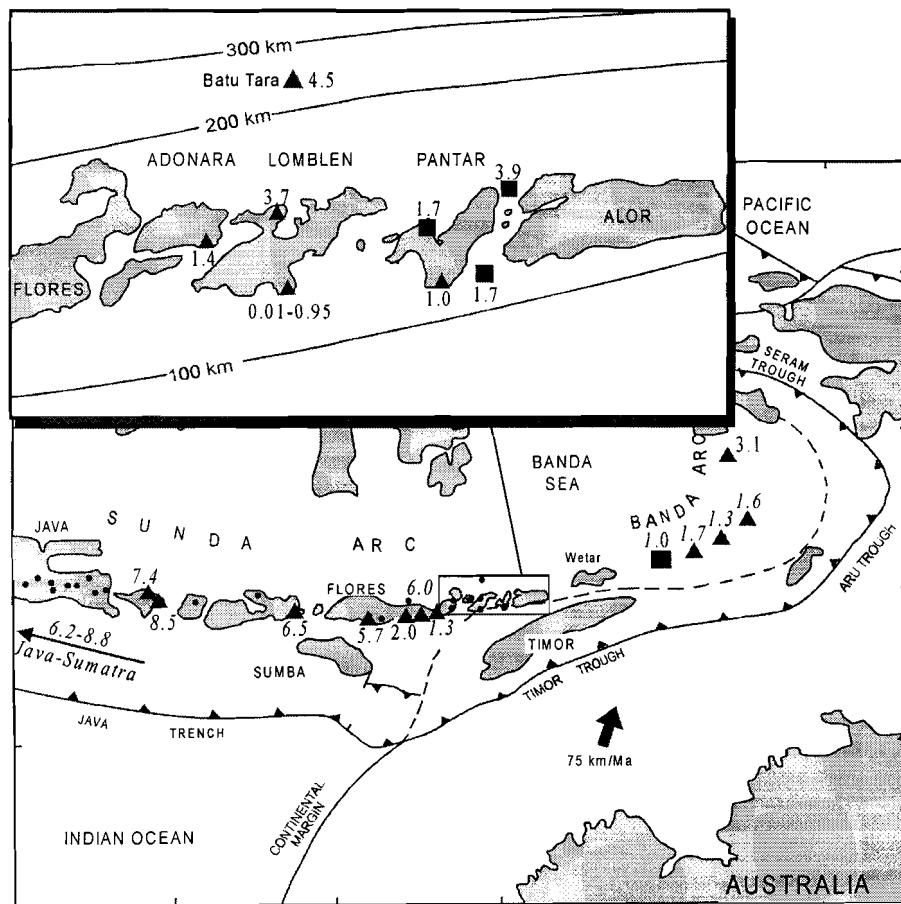
Figure 6.5. He isotopic ratios (RA) in fumarols and mineral separates from the literature (*Poreda and Craig, 1989; Hilton and Craig, 1989:* italics in figure) and our study *(Hilton et al., 1992)*.

6.2.7 O isotopes

Volcanics in the Banda Arc (to the east of the APS) have $\delta^{18}O$ values between 5.6 ‰ and 9.2 ‰ *(Magaritz et al., 1978)* together with high Sr and low Nd isotope ratios. Magaritz et al. *(1978)* explained this by addition of 50 % sedimentary material to the mantle wedge. Vroon *(1992)* argued, however, that mixing curves in Sr-O isotope diagrams such as used by Magaritz et al. strongly depend on the relative Sr and O concentrations in the endmembers, which would make it difficult to interpret the Banda Arc array in terms of source mixing. One preliminary whole rock $\delta^{18}O$ result from Werung is about 8 ‰ *(De Groot, pers. comm., 1992)*.

6.3 Discussion

I will start the discussion of potential endmembers with the 'non-mantle' components because of their dominant role in arc magmatism.

6.3.1 Sedimentary and crustal sources

There are five possible non mantle sources: Banda Sea crust (1), Indian Ocean pelagic sediments (2), Indian Ocean terrigenous sediments (3), Australian continental crust (4) and the leading oceanic part of the Indo-Australian continent (5).

6.3.1.1 Banda Sea crust

Assimilation of Banda Sea crust in APS volcanism is highly unlikely, as has been discussed in chapter 5.

6.3.1.2 Indian Ocean pelagic sediments or Indian Ocean terrigenous sediments

Sediments in front of the trench (Australian Shelf Sediments or SCM in Figures 6.3 and 6.4) *(Ben-Othman et al., 1989; Vroon, 1992; Van Bergen et al., 1993)* show a decreasing $^{206}Pb/^{204}Pb$ trend away westwards from the Australian continent, which corresponds to the trend observed in the volcanics (Fig. 6.5 after Van Bergen et al., *(1993)*). Furthermore, Sr, Nd, Th and He isotopes have the most SCM-like values near the Alor-Wetar collision zone (this thesis).

Because of the changing isotopic signals, the sedimentary component must be a mixture of at least two endmembers. The most likely candidates are a pelagic endmember with low U/Pb in the west and one more terrigenous endmember with high U/Pb *(Weaver, 1991)* in the east.

64
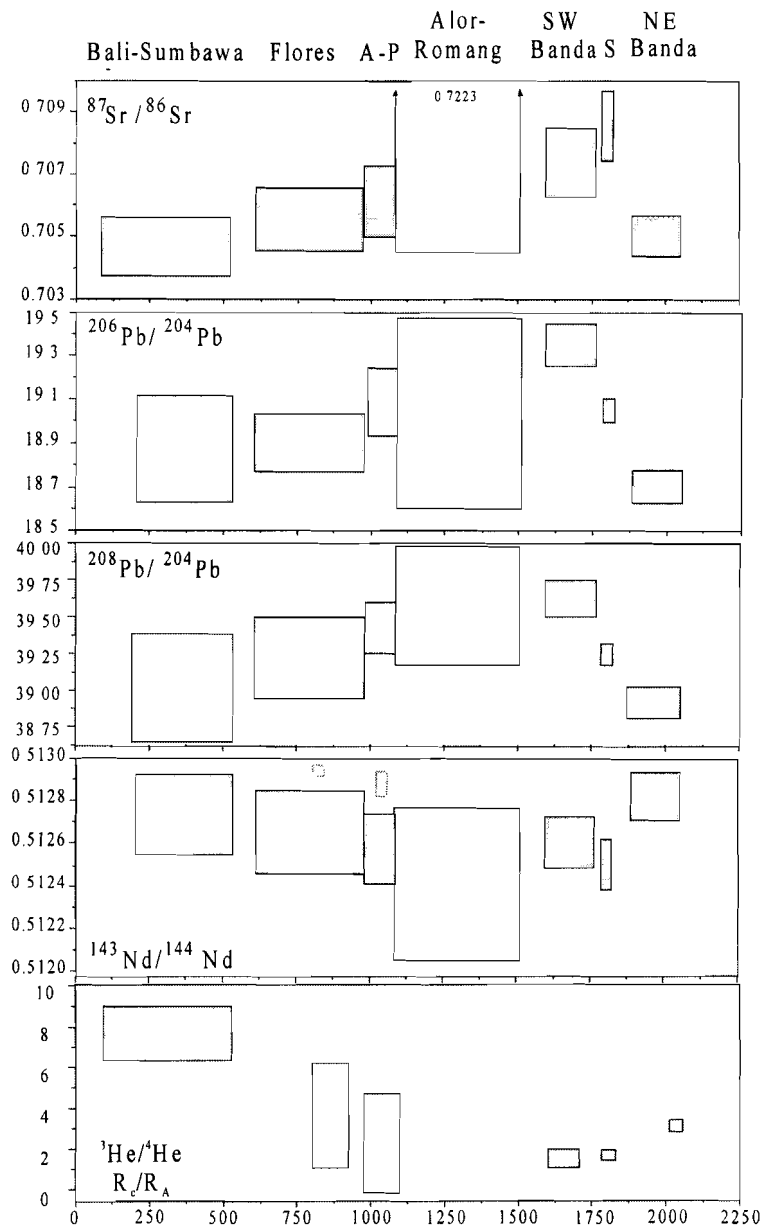
Figure 6.6. After Fig. 3 from Van Bergen et al., *(1993)*. Dominance of the SCM signal near the collision zone between the Sunda and Banda Arc appears from the isotope ratios of Sr (high values), Pb (high values), Nd (low values) and He (low values). X-axis represents distance east of Bali in km.

The $^{206}Pb/^{204}Pb$ trend in the sediments is not due to volcanoclastics, because the cited sediments have no volcanic component (except G5-6-123 *(Vroon, 1992)*). However, mixing of two sedimentary endmembers represented by the most extreme values from Ben Othman et al. *(1989)* and Vroon *(1992)* cannot explain all the volcanic Pb isotope values, especially the high $^{208}Pb/^{204}Pb$ component close to the Alor-Wetar sector (Fig. 6.3b). Hence, an extra SCM source must be involved. The same systematics are observed in the Southern Banda Arc *(Vroon, 1992)* where the volcanic and sedimentary signals are parallel but do not overlap in all Pb plots. The component required, which must have $^{208}Pb/^{204}Pb$ higher than any of the plotted endmembers (Fig. 6.3b), will be discussed below.

6.3.1.3 Australian continental crust

Hilton et al. *(1992)* suggested the possibility of subduction of Australian crust underneath the ESA on the basis of apparent involvement of radiogenic He isotopes in magma genesis. We must therefore assess the influence of this continental crust on the Pb isotopes in the ESA volcanics. The correlation of Pb/Ce ratios *(Hilton et al., 1992; Hoogewerff et al., 1997)* with radiogenic helium suggests a common origin for He and Pb, at least in the frontal volcanoes. High $^{208}Pb/^{204}Pb$ requires a sustained high Th/Pb ratio, and as the $^{206}Pb/^{204}Pb$ and $^{207}Pb/^{204}Pb$ are less extreme, the data also suggest a high Th/U ratio. A high Th/U hints to a crustal source, which would be in agreement with the radiogenic helium values.

In a first approximation it is reasonable that the sediments present in front of the subduction zone are representative for the material going down into the mantle. However, deeper parts of the subducted crust may have no equivalent in the hinterland and are thus not necessarily represented by the sediments on the shelf. This is supported by sparse new data from river sediments from the Victoria Basin in Northern Australia *(unpublished data Elburg and Vroon, 1994)*. Victoria Basin data plotted in Fig.6.7 indicate the presence of a high $^{208}Pb/^{204}Pb$ component that has no equivalent on the shelf.

There is limited whole rock Pb isotope data available from the western and northern parts of Australia *(Fraser K.J. et al., 1985/86; Nelson D.R. et al., 1986; McCulloch M.T. et al.,1983; Perring and Rock, 1991)*. More data are available from the eastern Cenozoic *(Ewart et al., 1988; Stolz and Davies, 1988; Rudnick and Goldstein, 1990; Fletcher et al., 1991)*. Most of the volcanics and xenoliths from eastern Australia show low values, not radiogenic enough to explain the high $^{208}Pb/^{204}Pb$. They are also a tectonically less likely endmember because they consist of volcanics associated with Cenozoic accretion terrains in the east, and are different from the old cratonic crust of west and north Australia. Although the eastern rocks may have a similar isotopic signal as a subcontinental mantle component, it cannot be involved in the APS magmatism. Limited data from carboniferous country rocks *(Ewart et al, 1988)* overlap with the Batu Tara values in each of the Pb isotopic plots, and the presence of such rock types in the subducted slab cannot be excluded. The Shaw Batholith in the western Pilbara Block and the Kambalda goldfield show a large range of lead isotopes including extremely radiogenic values *(Bickle et al, 1989; Perring et al, 1991)*. But although the occurrences are substantial, they are present over tens of kilometres, it is very difficult to asses the relative importance of the different occurrences in a subducting slab. The northern Australian Subcontinental Mantle (ASM), as tapped by kimberlites and lamproites *(Fraser et al, 1985/86; Nelson et al, 1986)*, has no relation with volcanism in the APS, as can be deduced from Figures 6.3 and 6.4. Using an average of the Pb isotopic compositions of the Leuco-Adamellites and Granites

66

from the Shaw Batholith we would find that this average could be a U-Pb depleted crustal source with high Th/Pb *(Rudnick et al, 1985)*. This source could explain the relatively high $^{208}Pb/^{204}Pb$ in the volcanics close to the inactive Alor-Wetar sector. It is therefore plausible, in conjunction with the He isotope results, that the Australian crust takes part in magma genesis below the APS.
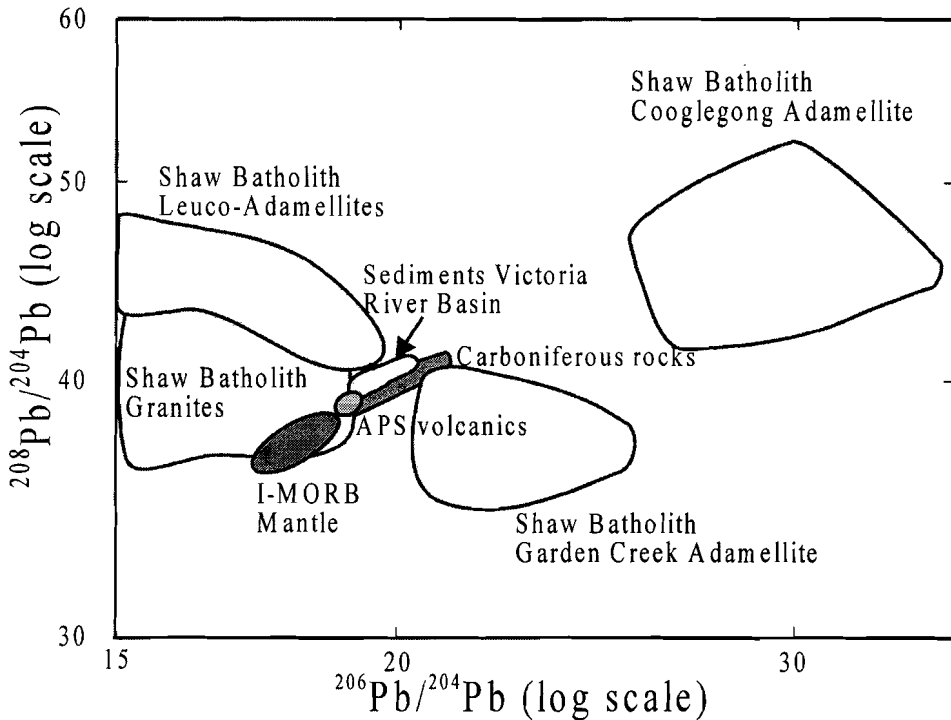
Figure 6.7. Pb isotope systematics showing potential Australian crustal endmembers.

6.3.1.4 Leading oceanic part of the Indo-Australian Crust

The leading part of the Indo-Australian plate most likely consists of oceanic crust, which may be in an altered state. The oldest oceanic crust on earth is found in this region and is supposedly of Late Jurassic-Early Cretaceous *(DSDP site 261, Veevers et al., 1974; ODP site 765, Gradstein et al., 1990)*. Recent data *(Weis and Frey, 1996)* of samples from DSDP 261 (in front of the APS) point to the presence of depleted Indian MORB close to the APS. More to the west at site 211, enriched Indian Ocean mantle is present *(Weis and Frey, 1996)*. The Indian Ocean mantle thus has inhomogeneities on more than 1000 km scale. Accepting that at least 700 km of oceanic crust has been subducted *(McCaffrey et al., 1989)* both depleted and enriched Indian Ocean mantle could be present under the APS.

Christmas Island *(Hart, 1988)* is situated close to site 211. It has been suggested *(Varne, pers. comm. 1991)* that this is not an ocean island of the hotspot type but a remnant part of an uplifted ridge segment due to bending in the subducting plate and therefore has Indian MORB isotopic characteristics. It might even be of similar age as the subducted crust under the APS, as might be roughly deduced from magnetic anomalies *(Heitzler et al., 1978; Lapouille et al., 1985; Hartono, 1990)*. If volcanics similar to Christmas Island (with an age of 150 Ma, Late Jurassic) would be altered (assuming the μ of altered oceanic crust to be four times the fresh value and the $\kappa/\mu \sim$ Th/U to be between 2 and 3 *(Albarede and Michard, 1987)* a value less than that of fresh Indian MORB, which has a ratio of 4), its present day Pb isotope composition would overlap with that of Batu Tara and the pillow basalts from Timor *(Vroon, 1992)*. Hart and Staudigel *(1987)*, however, suggested that the Th/U ratio in altered oceanic crust should be lower and close to 0.2. In that case altered oceanic crust would be an unlikely endmember. The altered oceanic crust hypothesis would conflict with Th isotope systematics because our models show a slab-derived component with high Th/U at Batu Tara, in contrast with what would be expected from altered oceanic crust *(Hoogewerff et al., 1997; this thesis)*.

6.3.2 Mantle sources

Major mantle sources to be considered are an Indian Ocean MORB-type mantle and an Indian Ocean enriched OIB-like mantle.

6.3.2.1 Indian MORB mantle source

The first option to be explored is that the mantle component consists of an Indian-MORB like source, which may be in a depleted state. In Figures 6.2 to 6.6 the APS samples could be lying on mixing lines between the subduction component (SCM) and either I-MORB or an enriched I-OIB mantle. Which of the two mantle components is the most likely cannot be simply deduced from these figures as the contribution from the subduction component is too large. From Figure 6.8 it is clear that at least the mantle involved underneath the frontal volcanoes must have a depleted character relative to Indian-MORB in the HFSE and REE. The relative enrichment in the LILE is due to the contribution of the subduction component *(cf. Gill, 1981)*.
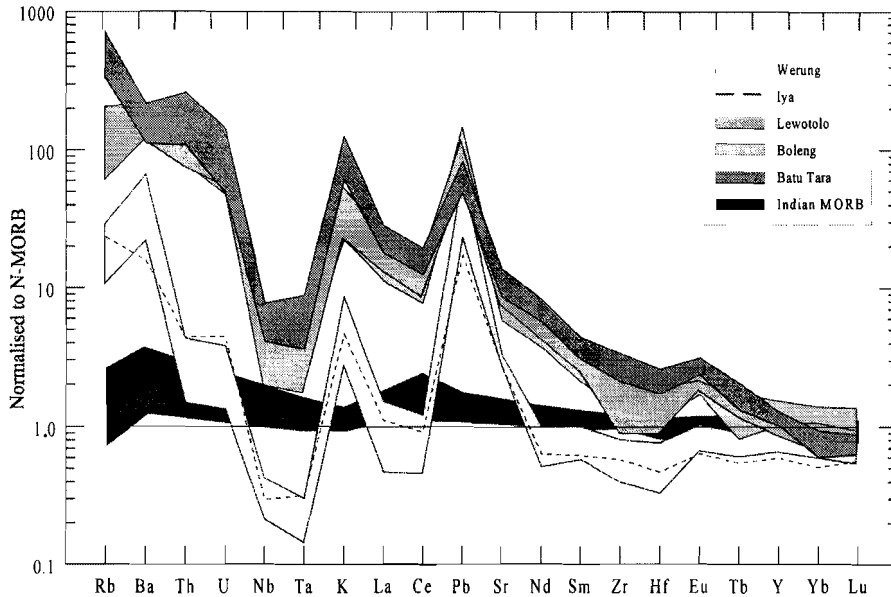
Figure 6.8. Trace element patterns showing the depletion of HFSE and REE relative to Indian MORB at Werung in comparison to the more northern volcanoes. Elements are listed in order of decreasing incompatibility according to Sun and Mcdonough *(1989)*.

6.3.2.2 Arguments for an isotopically Enriched Mantle component

Tie-lines in Fig. 6.9 between the extremes of the volcanic field and the sediment fields suggest that enriched Indian Ocean mantle sources should be considered if it is assumed that just one subduction and one mantle component are involved, because in such a case any mixing line is straight in Pb-Pb plots. As discussed above, contribution of radiogenic crustal component to the subduction component must also be evaluated. Taking the most extreme values from the Victoria Basin river sediments, some of the volcanics lie on a mixing line with Indian MORB but most of the APS volcanics still need the Enriched Mantle component. The correlation between the $^{206}Pb/^{204}Pb$ in the sediments and in the volcanics mentioned earlier argues against a single extreme radiogenic Australian crustal endmember. Thus on the basis of Pb isotopes the most likely mantle endmember in a two-component model would be an isotopically Enriched Mantle. Vroon *(1992)* has argued for a mantle component involved in the southern Banda Arc with a Pb isotopic composition similar to the source of 6-7 Ma pillow lavas on Timor *(Abbot and Chamalaun, 1981; Carter et al., 1976)*. Their Pb-isotope composition is similar to that of site 211 and Christmas Island, situated in the Indian Ocean close to the Sunda Arc. The trace element composition of the pillow lavas is similar to Indian MORB. These pillow lavas are probably only minimally influenced by a subduction component. The differences in Pb isotope values between VF, CA and RA are negligible, although it seems in Fig.6.9a that Batu Tara has a smaller contribution of ^{207}Pb from the subduction component compared to Werung, Lewotolo and Boleng, which all have similar $^{206}Pb/^{204}Pb$ values.
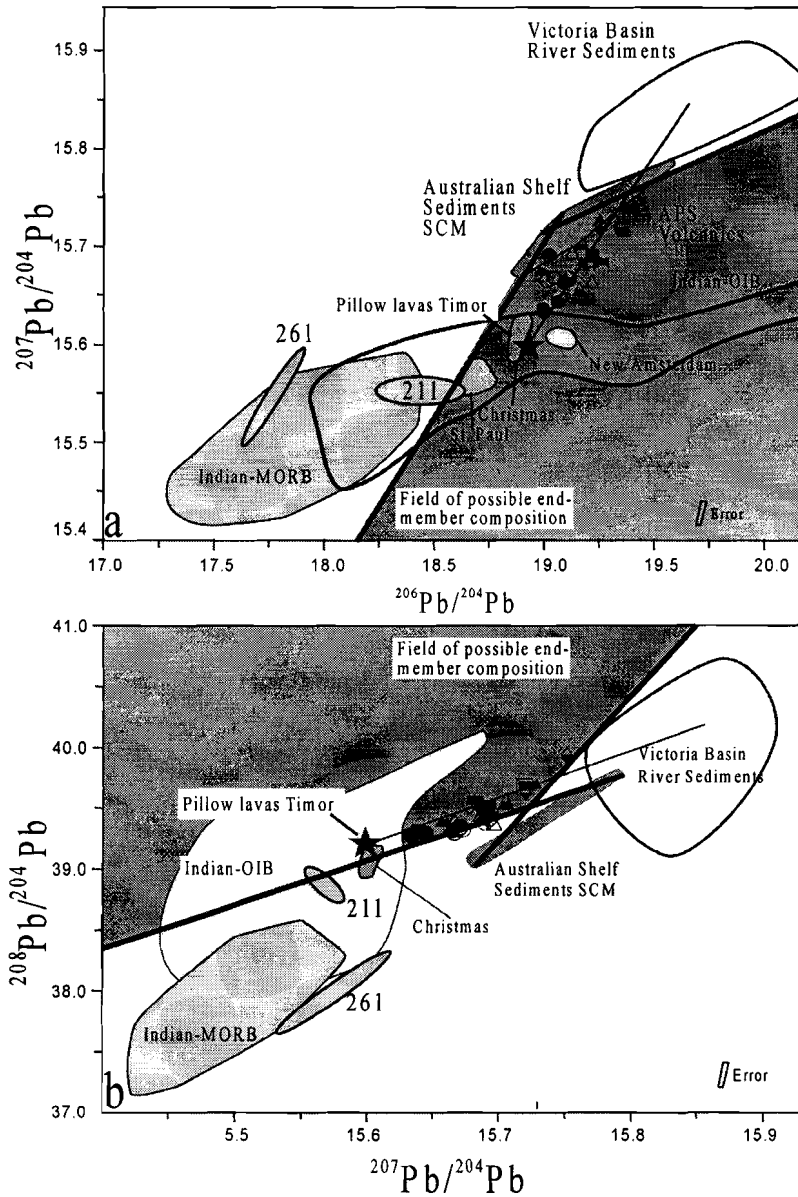
Figure 6.9. Connecting the most extreme Pb isotope compositions in the APS with those in the Australian Shelf Sediments demonstrates that SCM and Enriched Mantle (Indian-OIB) would be the most likely endmembers in a two-component mixing model. If more than two components would be involved, a combination of SCM + Indian MORB mantle + Australian crust ± Indian-OIB could explain the observations.
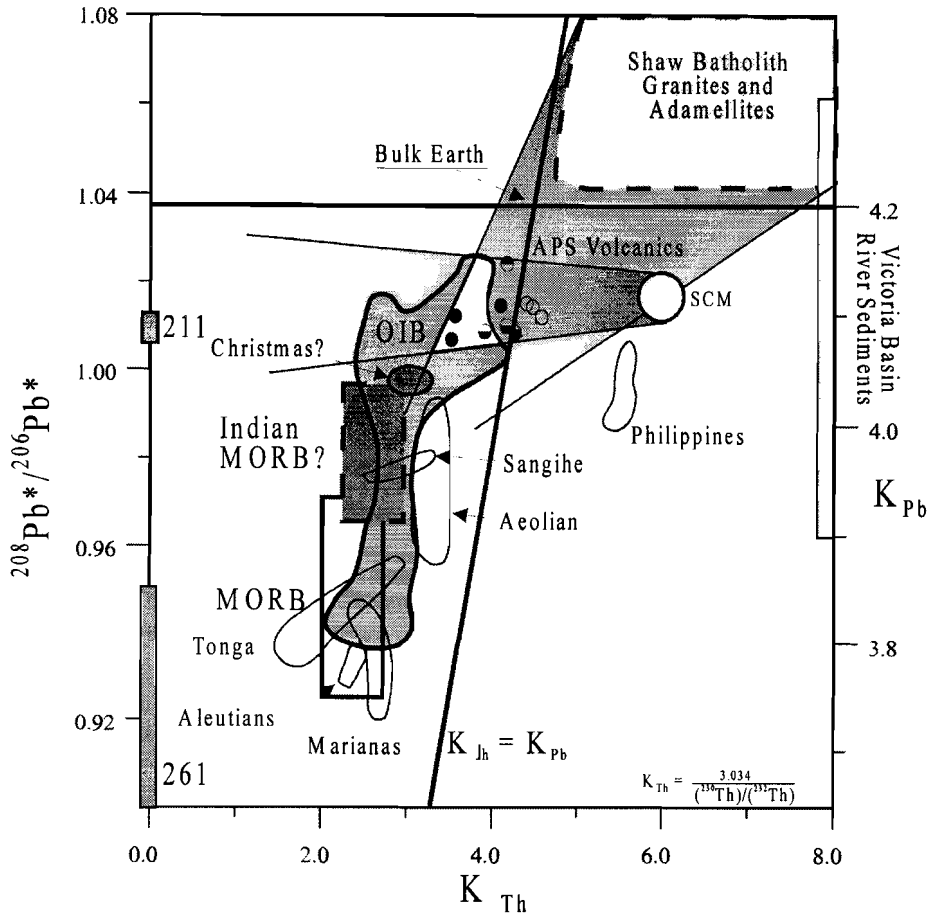
Figure 6.10. Radiogenic lead component $^{208}Pb*/^{206}Pb*$ versus source Th/U *(Fig. after McDermot et al., 1991)*. Fields on axis give ranges of $^{208}Pb*/^{206}Pb*$ for these samples as no Th and/or U data are available. As in Figure 6.9 Indian-OIB is required in a two-component model. In a three-component model (SCM + Indian MORB mantle + Australian crust) enriched Indian Ocean mantle would not be required.

As noted by other authors *(Stern and Ito, 1983; Morris and Hart, 1983; Gill, 1984; Lin et al., 1990; Hickey Vargas, 1992)* most island arcs seem to require an isotopic Enriched Mantle component. On Java in the western Sunda Arc, the rear arc volcano Muriah *(Edwards et al., 1991)* shows even more extreme Enriched Mantle source characteristics but also has lower $^{206}Pb/^{204}Pb$ as could be expected from its more western position where the influence from the oceanic slab would still be large.

Mixing between Indian MORB with $^{208}Pb*/^{206}Pb*$ *(Allégre et al., 1986)* ranging from 0.964 to 0.998 *(Ito et al., 1987)* and the local sediments (0.980 to 1.017) results in values below or only partly overlapping with the values observed in the APS volcanics (1.002-1.032). When using Christmas Island with $^{208}Pb*/^{206}Pb*$ between 0.98 and 0.99 *(calculated from Hart, 1988)*

71

as an endmember, not all the APS data plot on a mixing line either (see also y-axis Fig. 6.10). Some of the Indian Ocean OIB's have sources with acceptable $^{208}Pb*/^{206}Pb*$ values to explain all the APS data as a result of a two-component source mixing between SCM and OIB: Kerguelen 0.979-1.115, Crozet 0.981-1.041, Heard 1.033-1.044. However, parts of the Australian continental crust also appear to be capable of generating high $^{208}Pb*/^{206}Pb*$ ratios. Hence, the APS data can be equally well explained as the result of a two-component mixing between the Australian crust and the Indian MORB source as well.

Further possible evidence for involvement of a high $^{208}Pb/^{204}Pb$ component might be derived from combined $^{208}Pb*/^{206}Pb*$ and Th isotopes (Fig. 6.10). $^{208}Pb*/^{206}Pb*$ is a measure of the average Th/U since the formation of the earth and will therefore reflect old and sustained variations in Th/U *(Allégre et al., 1986)*. Th isotopes reflect short term Th/U ratios (< 30ka). In general, Fig. 6.10 displays the oceanic character of the Tonga, Aleutian and Mariana arcs compared to the stronger influence of crustal material in the Aeolian, Sangihe and Philippine arcs and in the APS. The K_{Th} of Indian MORB is assumed to be slightly higher than that of N-MORB. Limited $(^{230}Th)/(^{232}Th)$ data from the Indian Ocean *(Othman and Allegre, 1988)* and measured Th/U ratios from Kerguelen *(Gautier et al., 1990)* constrain the initial Th isotope composition of the Indian Ocean sources between 0.9 and 1.3.

Again, as can be seen in the plot of Fig. 6.10, the APS signatures can be generated by involvement of rock-types such as exposed on the Australian continent (e.g., Shaw Batholith) without the need to invoke an Enriched Mantle.

6.3.3 Bulkmixing models

Edwards et al. *(1993)* presented B/Be data from volcanics in the Sunda Arc and concluded that the subduction component along the Flores section has a constant composition and is made up of 20% sediment and 80% altered oceanic crust. In their view, the observed variation in isotopic compositions only reflect changes in the contribution from different mantle domains. However, the Sr-Nd isotope relations displayed in figure 6.11 are difficult to reconcile with a homogeneous subduction component. The composition proposed by the authors seems inadequate to produce the isotopic signatures of the volcanics in the APS and Flores, and mixing models suggest that subduction components with, at least, different Sr/Nd ratios are required to generate the observed isotopic variation. Because volcanoes with the highest B/Be ratios are those at the shallowest WBZ contours (Kelimutu and Lewotobi), an alternative interpretation to that given by Edwards et al. *(1993)* is that these ratios, although they were obtained from samples distributed over a large distance along the arc, reflect cross-arc trends that are connected with relative changes in the release of these elements from the downgoing slab.

72
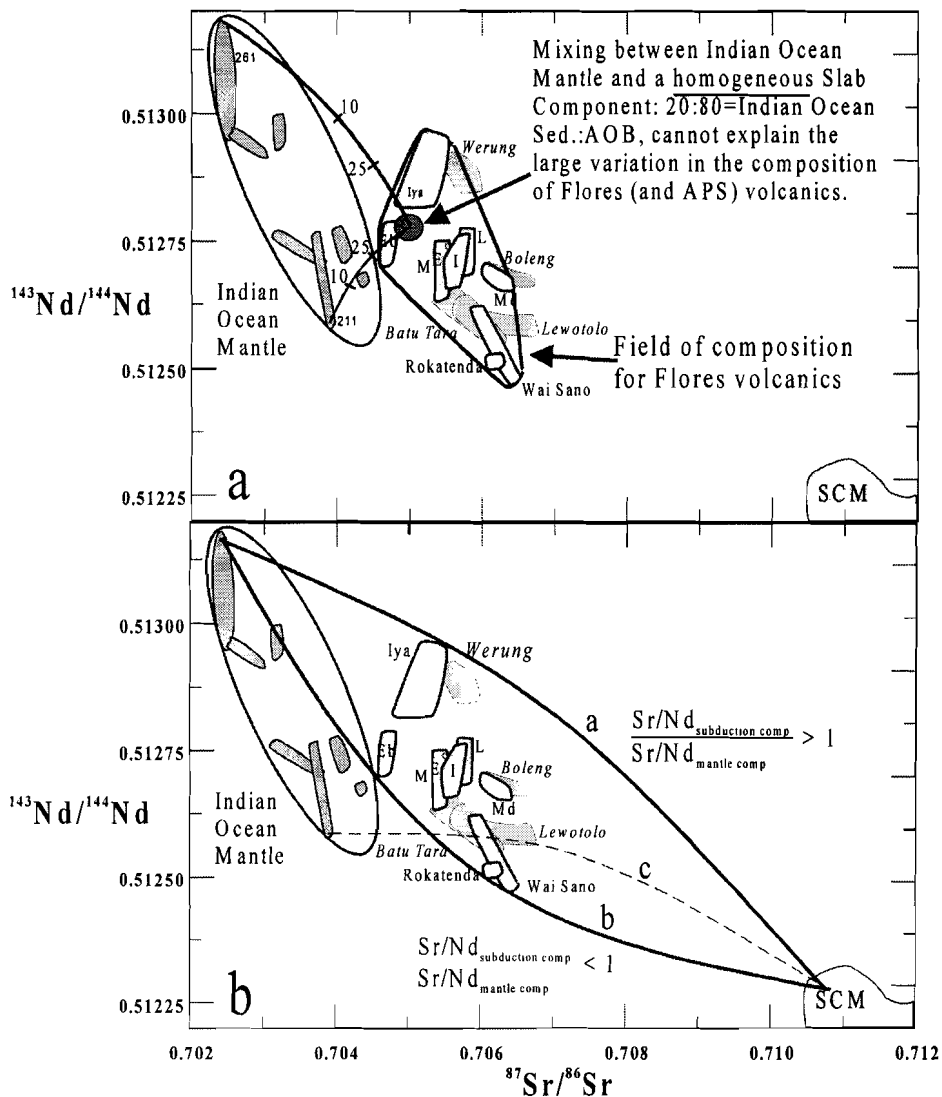
Figure 6.11 a: This figure demonstrates that mixing between a homogeneous subduction component with a composition as proposed by Edwards et al. *(1993)* and any endmember in the field of Indian-Ocean mantle cannot explain the observed Sr-Nd isotopic variation in volcanics of the APS and Flores. **b:** This figure shows that at least two subduction components with different Sr/Nd (LILE/LREE) ratios (but similar isotopic compositions) are required, irrespective of possible mantle inhomogeneity. Mixing curves for a homogeneous subduction component are inconsistent with observations in the plot. The Sr/Nd ratio for enriched Indian Ocean is larger than the ratio for depleted Indian Ocean mantle, which predicts less curvature for curve c than for curve a, if a homogeneous subduction component would be assumed. Furthermore, the volcanics would have the same Sr/Nd ratio across the arc, which is not the case (see Fig. 6.13).

In order to circumvent the problem addressed above, I shall express the contribution from the SCM source incorporated in a given sample (in %) as a function of the isotope ratio (R) of the endmembers according to:

Percentage of subduction component = $(R_{sample}-R_{mantle})/(R_{slab}-R_{mantle})$ x 100

In this model the Pb-isotopic composition of the pillow basalts from Timor *(TTVF; Vroon, 1992)* is used as mantle endmember, although it should be noted that it may not represent the "extreme-end" endmember. The rationale is that the TTVF composition was also used in previous work on the Banda Arc *(Vroon, 1992)*. The isotopic composition of the SCM component is taken from terrigenous samples from the Snellius II expedition *(Vroon, 1992)*. The $^{206}Pb/^{204}Pb$ of SCM is assumed to be 19.1 in front of Werung, Boleng, Lewotolo, Batu Tara and the older volcanics in this area and 19.57 in front of Sirung, Kedang and the other more eastern volcanoes.

Figure 6.12 presents the calculated subduction-related fractions of Sr, Nd and Pb in the samples. At first, one might be surprised by the high percentages of contribution from SCM, but elemental amounts are similar as in a weighed mixing calculation. In a weighed mixing calculation, however, little bulk sediment is needed due to the high element concentrations relative to those in the mantle. Only 1 % bulk addition means that 50 % of the Sr, Nd and Pb in a sample is derived from the subducting slab.

The SCM contribution for strontium appears to be more or less constant across the arc with some significant variation within the Lewotolo suite. The contribution for neodymium is minor from the slab at Werung and Labalekan but it increases up to 50 % with only slightly increasing depth of the WBZ (decreasing latitude). There is great scatter in the calculated contribution for lead. The result that >100 % of the lead should come from the slab at Lewotolo confirms that a component with an isotopic ratio ($^{206}Pb/^{204}Pb$) higher than SCM is needed to explain the observations. If a $^{206}Pb/^{204}Pb$ ratio of 20.237 from the Victoria River Basin in North Australia *(Elburg and Vroon unpublished, 1994)* and a ratio of 18.48 from enriched Indian mantle (DSDP 211; *Weis and Frey, 1996*) are used in the calculation, only between 35 and 40 % of the lead would be derived from the slab.

The large scatter in lead results within each volcano does not correlate with Sr isotope ratios. This points to heterogeneity in the plumbing systems, which is also suggested by the significant variations in initial ($^{238}U)/(^{230}Th$) activity ratios between different lavas of Werung volcano (see next chapter).
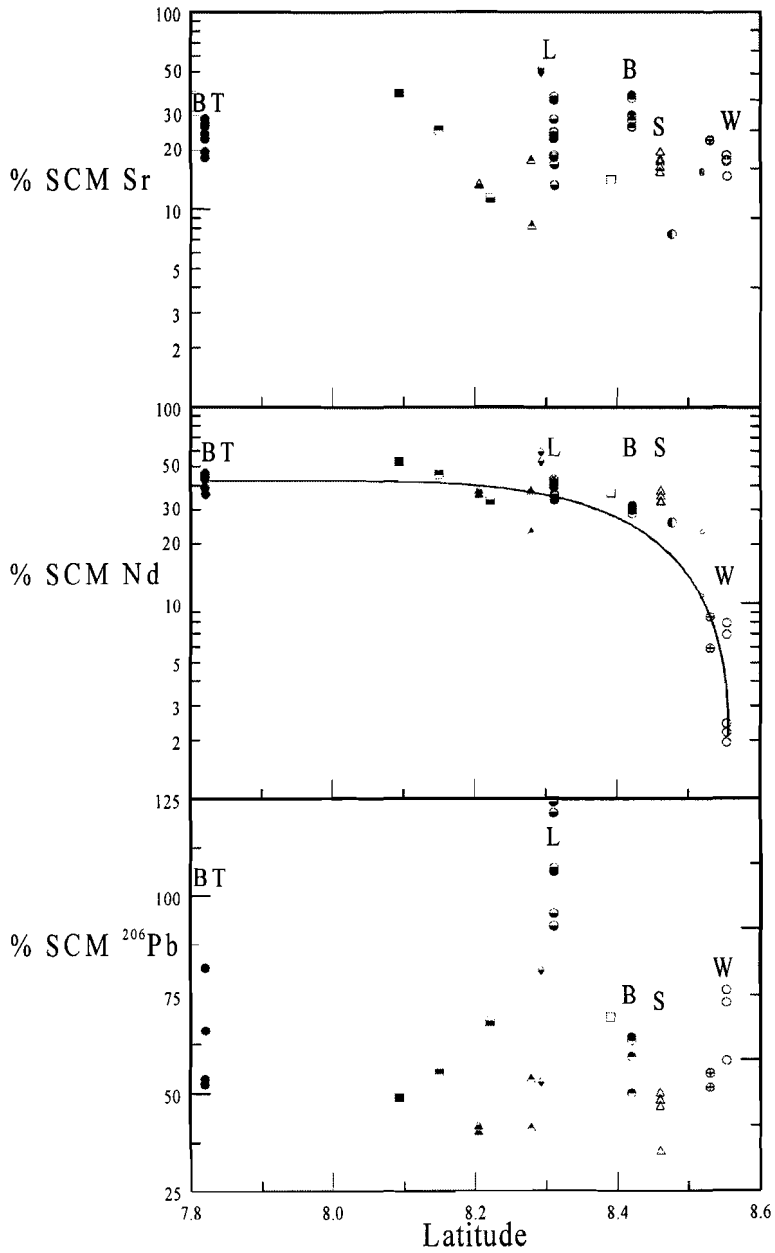
Figure 6.12. Calculated contributions of Subducted Continental Material to magma sources for Sr, Nd and Pb, assuming a TTVF-type mantle source (Timor) below the Adonara-Pantar Sector. Symbols as in Fig. 5.1
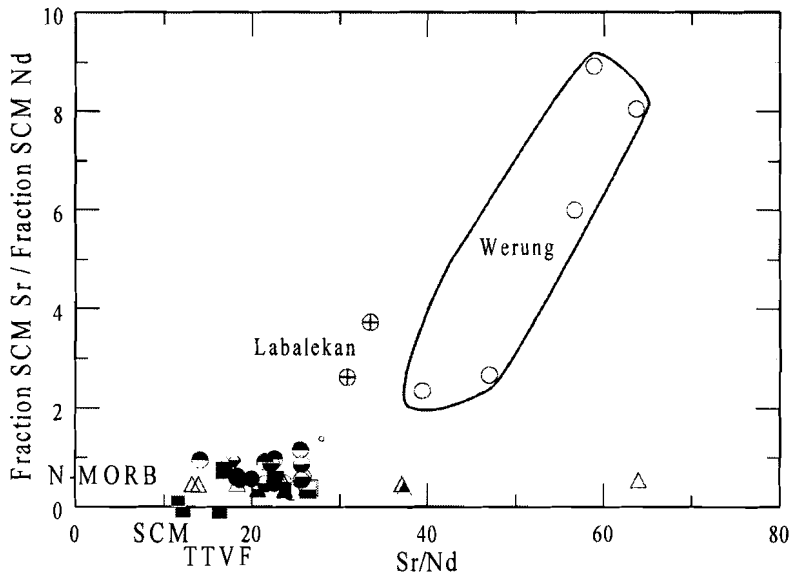
Figure 6.13. Trend between the ratio of Sr and Nd fractions incorporated in magma sources and Sr/Nd ratios in the lavas, suggesting a fractionation of these elements in the slab under Werung.

Figure 6.13 shows a trend between observed Sr/Nd ratios in the lavas and the calculated ratio of SCM fractions for Sr and Nd at Werung and Labalekan, indicating that the responsible process is source related. The samples from Sirung also show elevated Sr/Nd ratios but no fractionation of Sr and Nd isotopic ratios in the source, suggesting that Sr/Nd fractionation must have occurred after segregation of the subduction component from the slab.

6.4 Conclusions

On the basis of REE systematics it must be assumed that at least underneath Werung the mantle wedge has a depleted character. The age of the depletion is difficult to constrain.

In the volcanics a concurrent west-east change in $^{206}Pb/^{204}Pb$ in the composition of the subducted sediments from pelagic to detritic getting closer to the inactive zone can be observed.

The samples closest to the inactive zone indicate the existence of one more component with high $^{208}Pb/^{204}Pb$ not found in the sediments in front of the arc. I suggest that this may be due to involvement of truly crystalline Australian crust, which would agree with occurrence of radiogenic He values in the sector.

This suggests that possibly four or five endmembers are involved in the APS: a combination of depleted Indian Ocean mantle, with or without enriched domains, SCM with E-W compositional differences and crystalline Australian crust.

The subduction component is not only isotopically heterogeneous but also chemically and/or physically.

In the next chapter the nature of the transfer of material from the slab into the wedge and magma source regions will be discussed. In chapter 8 trace elements systematics are used to further constrain the relative importance of the mentioned endmembers.

7 Uranium Series Disequilibrium in the APS

7.1 Abstract

In this study U-series, Sr-Nd-Pb isotope and trace element results of a regional study of geochemical systematics across an island arc-continent collision zone in the East Sunda Arc of Indonesia are presented. Samples from four active volcanoes exhibit a striking compositional range from low-K tholeiitic to ultrapotassic, but all are characterised by high $^{87}Sr/^{86}Sr$ (0.7053-0.7067), radiogenic Pb isotope ratios ($^{206}Pb/^{204}Pb$=18.99-19.15), low ($^{230}Th/^{232}Th$) (0.66-0.85) and low $^{143}Nd/^{144}Nd$ (0.51255-0.51272), except for high $^{143}Nd/^{144}Nd$ (>0.51286) ratios at the volcanic front. Low (^{230}Th)/(^{232}Th) ratios are also found in terrigenous sediments in front of the arc, which, in combination with Sr-Nd-Pb isotopic constraints, indicates that subducted continental material contributes to magma sources in this arc sector. The volcanoes close to the trench show a large excess of ^{238}U over ^{230}Th (up to 80%) and of ^{226}Ra over ^{230}Th (up to 800%). In addition, they are enriched in elements thought to be mobile in hydrous fluids during slab-wedge transfer, such as Ba, Pb and Sr. In contrast, U-Th-Ra systematics are close to equilibrium in the volcanoes behind the front. Abundance patterns of incompatible trace elements in these rocks are similar to those of the terrigenous sediments, so that in comparison with the arc-front lavas, they possess low Ba/La, Ba/Th, La/Th, Pb/Ce and Zr/Nb ratios. Higher concentration levels and less inter-element fractionation form conspicuous differences with the front volcanics.

The combined isotopic and trace element data are consistent with three-component mixing whereby a slab-derived hydrous fluid and a siliceous melt are both added to the sub-arc mantle source. The hydrous fluid largely controls the input in the shallow part of the subduction zone, whereas the siliceous melt dominates the flux at deeper levels. Sedimentary material is considered to be the primary source of both. The large U-Th-Ra disequilibria at the front suggest that element transfer is a currently active process associated with present-day subduction of continental material.

7.2 Introduction

The Uranium series disequilibrium system is a powerful tool for identifying the nature of magma-genetic processes in active subduction settings (*Capaldi et al., 1976; Newman et al., 1984; Krishnaswami et al., 1984; Condomines et al., 1988; Gill and Williams, 1990; Sigmarsson et al., 1990; McDermott and Hawkesworth, 1991; Gill and Condomines, 1992; Gill et al., 1993; Condomines and Sigmarsson, 1993; Chabaux and Allègre, 1994; Reagan et al., 1994*). Despite increasing consensus that infiltration of mantle sources by material released from subducting

slabs is a key process in the origin of arc magmas, the mechanism and time-scale of element transfer remain little understood. The presence of excess ^{238}U over ^{230}Th in subduction-related volcanics has been attributed to recent enrichment of magma sources in uranium by slab-derived fluids *(Condomines et al., 1988; Gill and Williams, 1990; Sigmarsson et al., 1990; McDermott and Hawkesworth, 1991; Gill and Condomines, 1992; Gill et al., 1993; Condomines and Sigmarsson, 1993)*. However, uranium enrichment has been found in less than half of the cases studied *(Gill and Williams, 1990)*, and tends to be more common at volcanic fronts. The reason for frequent absence of enrichment is obscure *(Gill and Condomines, 1992; Condomines and Sigmarsson, 1993)*. This paper reports the existence of important systematic variations within a single across-arc transect, ranging from extreme excesses of ^{238}U and ^{226}Ra over ^{230}Th to equilibrium. I use the U-series results together with Sr-Nd-Pb-He isotopic and trace element data from both the volcanics and sediments in front of the arc, to argue that a down dip change in the nature of the slab-derived flux controls the composition of the magmas. The Adonara-Pantar Sector (APS) of the Sunda-Banda Arc is an unique setting in which to study the behaviour of U, Th, Ra and other trace elements in a subduction regime. It forms part of a region of ongoing collision between the eastern oceanic end of the Sunda Arc and the northern passive continental margin of Precambrian Australia *(Hamilton, 1979)*. Consequently, there is a maximum geochemical contrast between subducted components and mantle components involved in magma genesis, which facilitates the identification of slab-derived elements in volcanic products. Systematically distributed across this arc sector, active volcanoes have produced suites with the largest range of composition known in any island arc: from low-K tholeiites at the southern volcanic front to ultrapotassic lavas to the north behind the arc *(Whitford et al., 1977; Stolz et al., 1988; Varekamp et al., 1989; van Bergen et al., 1992)*. 'Enriched' Sr-Nd-Pb-He isotope signatures *(Whitford et al., 1977; Stolz et al., 1988, 1990; Varekamp et al., 1989; Van Bergen et al., 1992; Hilton et al., 1992; Vroon, 1992; Vroon et al., 1993)* in this part of the Sunda-Banda Arc coincide with the locus of collision near Timor *(Van Bergen et al., 1993)*, which provides strong evidence for the involvement of Subducted Continental Material (SCM), either as sediment or continental crust, in magma genesis for all the APS volcanoes.

7.3 Sample selection and analytical procedures

Samples were selected from four active volcanoes across the arc (Werung, Lewotolo, Boleng and Batu Tara), situated at Benioff-Zone depth contours between 100 and 250 km. One extra sample from the Iya volcano at the volcanic front on Flores Island (west of the APS) was analysed as we had included this sample also in our He study *(Hilton et al., 1992)*. In order to define the composition of the subducted source component, we also selected seven sediments from the Timor Trough and the Australian continental shelf from Deep Sea Drilling Project-Site 262 *(Veevers et al., 1974)* and the Snellius-II Expedition *(Vroon, 1992)*. Chemical and Sr-Nd-Pb isotope data for the sediments are reported in Vroon et al. *(1995)*, who also give details on lithologies and sampling strategy. Major and trace element compositions of the volcanics were determined by standard XRF techniques in Utrecht *(Vroon, 1992)*, and INA results were obtained at IRI, Delft and KU, Leuven *(de Bruin, 1983 and Pedersen and Hertogen, 1990, respectively)*. Sr-Nd-Pb isotopic compositions were determined at the Free University (Amsterdam), the Université Libre (Brussels) and Royal Holloway University (London), according to methods referred to in Vroon *(1992)*, Vroon et al. *(1993, 1995)* and Thirlwall et al. (1996). High-precision Nb XRF analyses of 'low-abundance' samples were carried out at Royal Holloway, following

80

Jochum et al. *(1990)*. Samples selected for U-series analysis are restricted to recently erupted lavas from each volcano, as based on field appearances. Th-U activity ratios and concentrations were determined by α-spectrometry according to Vanlerberghe *(1987)*, using decay constants from Gill and Williams *(1990)*. The "Harwell" spike was used with a $(^{228}Th)/(^{232}U) = 1.017 \pm 0.006$ (measured at IRMM, Geel, Belgium). Errors are 1 standard deviation from counting statistics. Blanks showed no peaks for relevant nuclides. Because Th and U α-spectrometry concentrations were some 5% higher than INAA data (or isotope dilution data for 'low-abundance' Werung lavas) from the same samples, all concentrations have been corrected accordingly. Values thus obtained for sample KO3A agree well (differences <1% for activity ratios and concentrations) with results from the same sample reported in Gill and Williams *(1990)*.

Sample	$\frac{(^{238}U)}{(^{232}Th)}$	$\frac{(^{230}Th)}{(^{232}Th)}$	$\frac{(^{234}U)}{(^{238}U)}$	$\frac{(^{238}U)}{(^{230}Th)}$	$\frac{(^{226}Ra)}{(^{230}Th)}$	U (ppm)	Th (ppm)	$\frac{Th}{U_{source}}$	$\frac{Th}{U_{rock}}$
Volcanics									
Werung									
24-8 q	1.22±0.05	0.68±0.01	0.98±0.04	1.8±0.1	8.0±0.7	0.18±0.02	0.45±0.03	4.46	2.5
					7.6±0.5				
27-12-1d	0.95±0.05	0.67±0.03	1.03±0.05	1.43±0.08		0.12±0.01	0.38±0.01	4.46	3.17
30-01-01	1.08±0.05	0.66±0.03	1.04±0.04	1.62±0.07		0.14±0.01	0.38±0.01	4.6	2.71
Lewotolo									
14-06-01	0.72±0.04	0.71±0.01	0.97±0.02	1.01±0.06	1.25±0.08	5.16±0.09	21.8±0.3	4.27	4.22
LO8A d	0.77±0.03	0.76±0.01	1.02±0.02	1.01±0.04		5.15±0.08	20.2±0.2	3.99	3.92
LO18A	n.d.	0.78±0.02	n.d.	n.d.		n.d.	12.4±0.2	3.9	n.d.
Boleng									
34-4-1	0.82±0.03	0.73±0.01	1.00±0.02	1.12±0.04		5.28±0.08	19.7±0.2	4.16	3.73
Batu Tara									
KO1A d	0.93±0.05	0.85±0.03	1.01±0.02	1.08±0.06		4.47±0.07	14.7±0.3	3.57	3.29
-leu	1.06±0.07	0.95±0.05	1.06±0.07	1.12±0.07		0.22±0.01	0.62±0.02	-	2.82
-px	0.47±0.02	0.77±0.03	0.97±0.03	0.61±0.02		0.15±0.01	1.00±0.02	-	6.67
KO2L	0.71±0.03	0.78±0.02	1.01±0.02	0.90±0.04		8.4±0.1	36.3±0.6	3.89	4.32
KO3A d	0.94±0.04	0.86±0.02	1.00±0.02	1.09±0.05	1.12±0.08	4.19±0.07	13.6±0.2	3.53	3.25
KO5C d	0.68±0.02	0.75±0.01	1.03±0.03	0.91±0.03	0.96±0.06	3.27±0.06	14.7±0.1	4.05	4.5
KO6D	0.65±0.03	0.71±0.02	1.02±0.03	0.92±0.04		5.7±0.1	26.7±0.4	4.27	4.68
Iya (Flores)									
IYA	1.14±0.05	0.69±0.03	1.03±0.04	1.65±0.08		0.22±0.01	0.58±0.01	4.4	2.64
Sediments									
Snellius II					%CaCO3				
G5-6-134B	0.47±0.02	0.51±0.02	0.97±0.03	0.93±0.05	1.6	3.74±0.07	23.9±0.4	-	6.39
G5-6-136B	1.85±0.06	1.41±0.03	1.05±0.02	1.31±0.04	23.7	8.6±0.1	14.2±0.2	-	1.65
G5-6-145P	0.97±0.03	0.96±0.02	1.02±0.02	1.02±0.03	21.5	3.68±0.06	11.5±0.2	-	3.13
G5-6-147B	1.01±0.04	1.29±0.04	1.02±0.03	0.78±0.03	26.3	3.21±0.07	9.7±0.2	-	3.02
G5-6-149P	1.90±0.07	1.47±0.04	1.07±0.02	1.29±0.04	32.5	5.24±0.06	8.4±0.2	-	1.6
G5-6-157B	2.56±0.09	1.19±0.04	1.12±0.02	2.15±0.07	37.7	6.56±0.07	7.8±0.2	-	1.19
DSDP262 Core 14-5 69-71cm	0.66±0.03	0.63±0.03	0.92±0.03	1.04±0.05	24.6	2.21±0.05	10.2±0.3	-	4.62

Table 7.1. U-series disequilibrium results for the active APS volcanics.

The age of KO1A is 30±5 Ka with a source composition of $(^{230}Th)/(^{232}Th)= 0.85\pm0.06$, according to the isochron method *(Allègre, 1968)*, using mineral separates and whole rock data. An imprecise Rb/Sr date from leucite-plagioclase agrees with this age *(Van Bergen et al., 1992)*. Sediment samples from piston- or box-cores *(Vroon, 1992)* show considerable disequilibrium. Sediments with the highest Th and lowest $CaCO_3$ concentration show the lowest $(^{230}Th)/(^{232}Th)$ ratio; in others, the terrigenous fraction (SCM) is diluted by carbonate. In the absence of exact eruption dates for even the youngest lavas in this remote area, samples selected for Ra analysis only represent what in the field appeared to be the latest products of each volcano. ^{226}Ra activity was determined by g-spectroscopy using the 352.0 keV of ^{214}Pb after allowing for ingrowth of this nuclide *(Graustein and Turekian, 1990)*, following procedures described in detail in Wordel et al. *(1994)*. Ra data for 24-8 are from two separate determinations. Our (^{226}Ra) of KO3A from γ-spectroscopy shows slightly less excess over (^{230}Th) than in Gill and Williams *(1990)*: 1.29±0.06 where (^{226}Ra) was obtained from ^{210}Po by α-spectroscopy. Loss of Rn seems an unlikely explanation because our containers were tightly closed and left standing for more than five times the half live of ^{222}Rn. Comparison of the ^{226}Ra 186keV line with the 295keV or 352keV of ^{214}Pb also seems to rule out Rn loss within analytical precision.
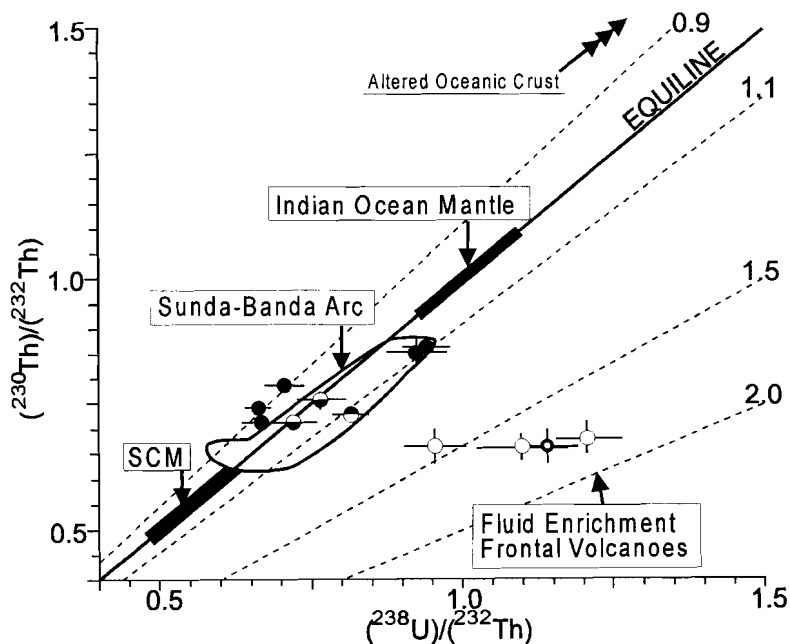
Figure 7.1. $(^{230}Th)/(^{232}Th)-(^{238}U)/(^{232}Th)$ systematics. Werung at the volcanic front of the across-arc transect and Iya in Flores (heavy open circle) show a large ^{238}U excess (up to 80%). $(^{230}Th)/(^{232}Th)$ ratios plot between SCM (the most terrigenous, carbonate-poor sediments analysed) and Indian Ocean mantle *(Williams and Gill, 1990; Ben Othman and Allègre, 1990)* which includes both MORB and OIB-type compositions. Shaded field represents volcanics from other regions in the Sunda-Banda Arc *(Rubin et al., 1989; Gill and Williams, 1990; McDermott and Hawkesworth, 1991; Condomines and Sigmarsson, 1993)*. Dashed lines indicate ^{238}U enrichment versus ^{230}Th. Note that AOC is an unlikely source component.

82

7.4 U-Th-Ra Results

U-series data are presented in Table 7.1 and Figure 7.1. The APS volcanics yield $(^{230}Th)/(^{232}Th)$ ratios between 0.66 and 0.85 from Werung to Batu Tara (Fig. 7.1). These values are low compared to other arcs *(c.f. Gill and Williams, 1990; McDermott and Hawkesworth, 1991)* and have been observed before in the Sunda-Banda Arc *(Rubin et al., 1989; Gill and Williams, 1990; McDermott and Hawkesworth, 1991; Condomines and Sigmarsson, 1993)*. The $(^{230}Th)/(^{232}Th)$ ratios in the local sediments range from 0.5 (at 2% $CaCO_3$) to 1.5 (at 32% $CaCO_3$). The lower values apparently represent the terrigenous fraction, and are close to the lowest ratios of the volcanics.

   The data further reveal the presence of large excesses of U and Ra over Th at the frontal low-K tholeiitic Werung volcano: $(^{238}U)/(^{230}Th)$=1.4-1.8 and $(^{226}Ra)/(^{230}Th)$=7.8, with an apparent source $(^{230}Th)/(^{232}Th)$ ratio of about 0.67. The sample from Iya, a low-K volcano at the front in central Flores shows a similar excess U (heavy open circle). These excesses are the largest found in the Sunda-Banda Arc to date, and are similar to those found in the Mariana and Tonga arcs *(Newman et al. 1984; Gill and Williams, 1990; McDermott and Hawkesworth, 1991)*. The radium excess is the largest observed in any island arc so far. The medium- and high-K calc-alkaline volcanoes on intermediate Benioff contours (Lewotolo and Boleng) have $(^{230}Th)/(^{232}Th)$ ratios between 0.71 and 0.76, little or no U excess and, based on one sample, little Ra excess. The ultrapotassic lavas from Batu Tara behind the arc have slightly higher $(^{230}Th)/(^{232}Th)$ ratios between 0.71 and 0.86, very little U or Th excesses and, on average, no Ra excess.

7.5 Within-suite isotopic variations

The Batu Tara rocks display significant within-suite isotopic variations (Fig. 7.2), which can be attributed to source heterogeneity (cf. *Stolz et al., 1990; Van Bergen et al., 1992*). The latter authors distinguished a 'low-Th' and a 'high-Th' series, which are not related by a closed-system differentiation process. The high-Th magmas were considered to be derived from a source, which is most influenced by SCM, as they have the highest $^{87}Sr/^{86}Sr$ ratios. These samples also have the lowest $(^{230}Th)/(^{232}Th)$ and $^{143}Nd/^{144}Nd$ ratios. Both ratios show an inverse correlation with $^{87}Sr/^{86}Sr$ (Fig. 7.2), which provides evidence for involvement of magmas originating from mantle sources with different SCM contributions. Isotopic variations at Lewotolo and Boleng are also likely to reflect source heterogeneity. The three samples from Lewotolo that were analysed for Th isotopes show similar Sr-Nd-Th correlations as the Batu Tara rocks, but offset to lower $^{87}Sr/^{86}Sr$ and higher $^{143}Nd/^{144}Nd$. Samples with the highest $^{87}Sr/^{86}Sr$ belong to the lower part of the stratigraphic sequence and were therefore not selected for U-series analysis.
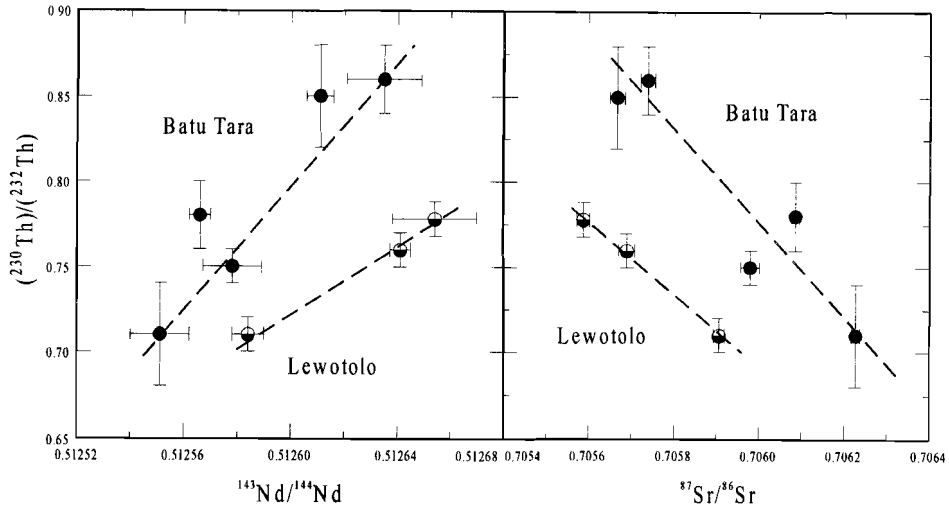
Figure 7.2. Within-suite isotopic variations for Batu Tara and Lewotolo samples showing a positive correlation between $(^{230}Th)/(^{232}Th)$ and $^{143}Nd/^{144}Nd$, and a negative correlation between $(^{230}Th)/(^{232}Th)$ and $^{87}Sr/^{86}Sr$. These variations are attributed to source heterogeneity with the lowest $(^{230}Th)/(^{232}Th)$ and $^{143}Nd/^{144}Nd$, and highest $^{86}Sr/^{87}Sr$ values being indicative for sources which are most influenced by SCM.

7.6 Discussion

7.6.1 Isotopic evidence for involvement of subducted continental material

The combined Sr-Nd-Pb isotopic data presented here and in earlier work *(Whitford et al., 1977, 1981; Magaritz et al., 1978; Whitford and Jezek, 1979; Stolz et al., 1990; Vroon, 1992; Vroon et al., 1993)* point to a dominant role of terrigenous sediments in magma genesis in the East Sunda-Banda Arc. Strong support for this conclusion has recently been obtained from the observed parallel along-arc variations in the Pb-Nd isotopic ratios of volcanics and sediments in front of the trench *(Vroon et al., 1993, 1995; Van Bergen et al., 1992)*. Accordingly, we prefer to interpret the overall low $(^{230}Th/^{232}Th)$ ratios in the APS volcanics as largely derived from a mixture of sub-arc mantle and Subducted Continental Material (SCM). As Fig. 3 illustrates, the volcanics in the transect also have isotopic compositions between mantle and SCM values, with $(^{230}Th)/(^{232}Th)$ tending to increase down the dip of the subduction zone. Although low $^3He/^4He$ ratios are a general characteristic of the East Sunda-Banda Arc *(Hilton et al., 1992)*, the exceptionally radiogenic values in the APS suggest that the leading edge of the subducted continental margin may have reached the sub-arc mantle East of central Flores. The Australian margin, up to 40 km thick when entering the Timor trough *(Jacobsen et al., 1978)*, consists of presumably Precambrian-aged crust covered by Phanerozoic sediments with a thickness up to 10 km *(Powel and mills, 1978; Hamilton, 1979)*, and thus could be an (additional) source of SCM-derived elements. Mass-balance considerations confirm the possibility for involvement of the subducted Australian margin in magma genesis *(Van Bergen et al., 1993)*.

84
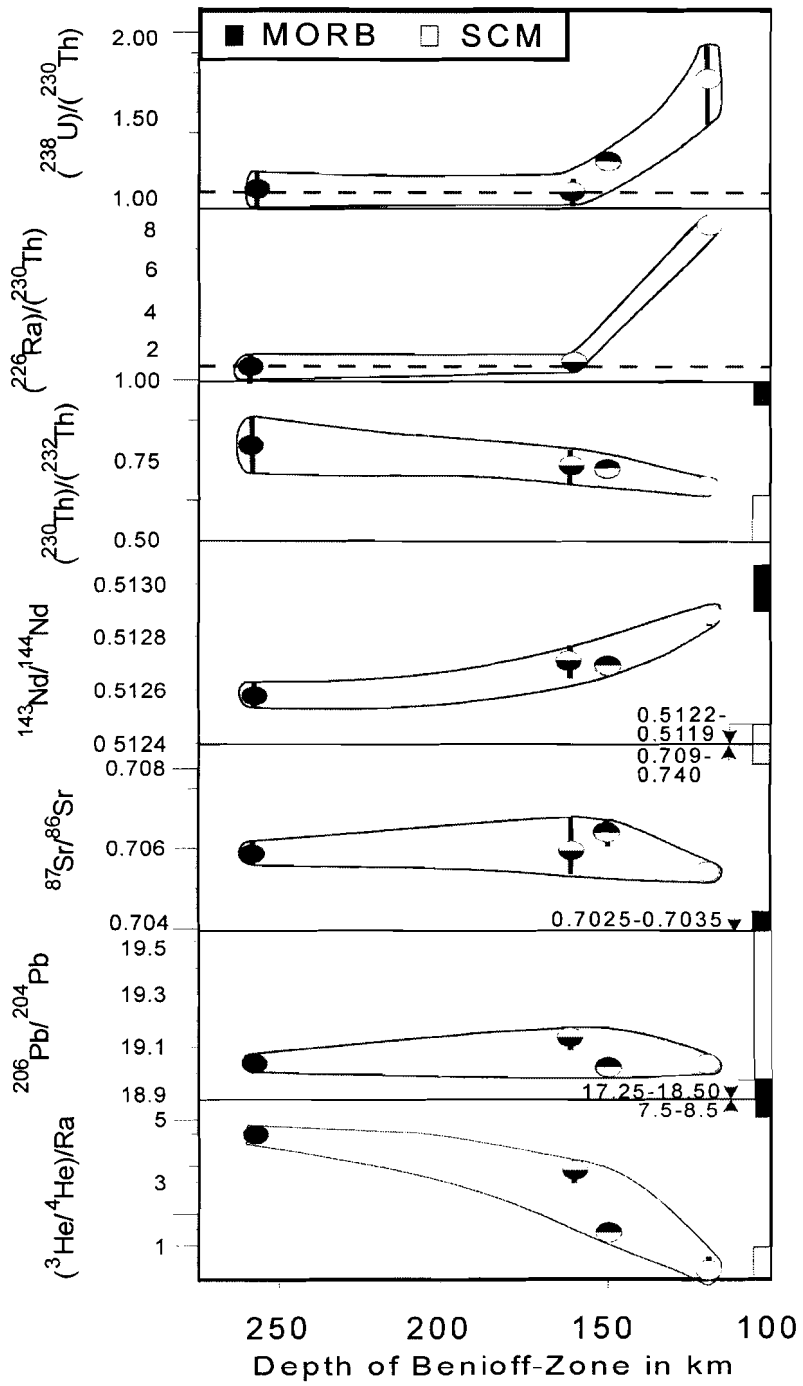
Figure 7.3. (previous page) Across-arc systematics of U-Th-Ra activity ratios and Sr-Nd-Pb-He isotopes, and comparison with SCM (local carbonate-poor sediment) and MORB mantle. Extreme selective enrichment of U and Ra over Th by fluids is confined to Werung at the volcanic front (dashed line represents equilibrium). Werung also has the lowest Th isotope ratios, which indicates that much of the thorium is also derived from SCM. Sr and Pb isotopes seem insensitive to discriminate between fluid and melt. He isotopic ratios at the front are the most radiogenic (crustal) ever measured in an island arc *(Hilton et al., 1992)*, which corresponds with the highest excess U and Ra. Bars indicate within-suite ranges.

This influence of the SCM component varies along the arc and culminates near the APS, which is difficult to reconcile with the hypothesis that magma sources in the Sunda Arc are composed of variable mantle components and one homogeneous subduction component derived from a mixture of altered oceanic crust and sediments *(Edwards et al., 1993)*. The combination of low $(^{230}Th)/(^{232}Th)$ and low $^3He/^4He$ in all APS volcanics (including the alkaline rocks) and Iya *(Hilton et al., 1992)* precludes a major role of (altered) basaltic oceanic crust in the collision region. Moreover, the correspondence between Pb and Nd isotopic compositions of volcanics and sediments in front of the trenches along the Sunda-Banda Arc *(Ben Othman et al., 1989; Vroon, 1992; Vroon et al., 1993; Van Bergen et al., 1993)* is controlled by the provenance of terrigenous fraction *(Vroon et al., 1995)*, and argues against homogeneity of the subduction component. Though Enriched Mantle-like characteristics are locally observed in East Sunda-Banda Arc volcanics and may be indicative of mantle inhomogeneity *(Stolz et al., 1990; Van Bergen et al., 1992; Vroon, 1992; Vroon et al., 1993)*, trace elements derived from subducted material (including U, Th and Ra) largely dominate the chemical signatures of the magma sources (cf., *Vroon et al., 1995*).

7.6.2 Mixing relationships and implications for across-arc changes in element transfer

As a first approximation, simple two-component bulk mixing models, using I-MORB mantle and local sediment compositions as endmembers, seem adequate to generate the observed signatures of the volcanoes behind the front for various combinations of isotope systems. According to the Nd-Pb and Nd-Sr systematics illustrated in Fig. 7.4, some 2% addition of sediment would be required to obtain their isotopic signatures. However, the Werung data fall off the bulk-mixing curves. This volcano only fits mixing models, if in the Sr-Nd diagram a convex upward mixing line, and in the Pb-Nd diagram one with a stronger curvature is assumed. Such models are consistent with a slab-derived component having higher Sr/Nd and Pb/Nd ratios than bulk terrigenous sediment. In view of the greater mobility of Sr and Pb relative to Nd in fluids (cf. *Tatsumi et al., 1986*), we infer that source contamination at the front below Werung is controlled by fluid-controlled preferential transfer of SCM-derived elements.
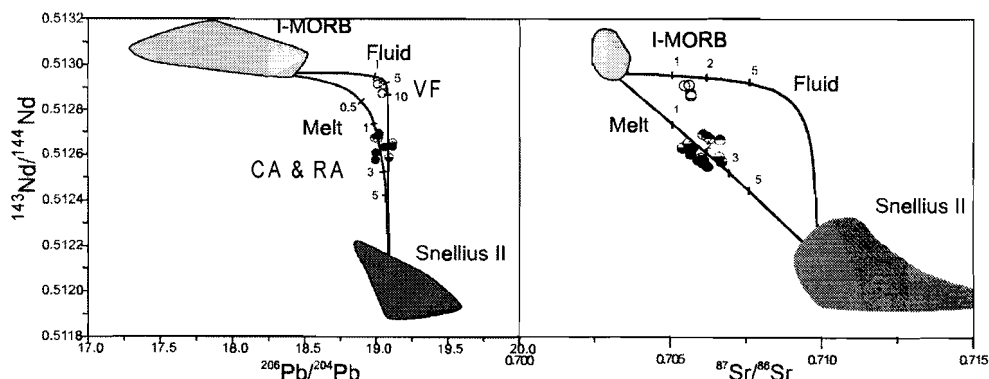
Figure 7.4. $^{206}Pb/^{204}Pb$-$^{143}Nd/^{144}Nd$ and $^{87}Sr/^{86}Sr$-$^{143}Nd/^{144}Nd$ diagrams showing schematic models for mixing between I-MORB and local sedimentary material. Curves for bulk mixing fit the data for behind-the-front volcanoes. Werung, at the volcanic front, plots close to hypothetical 'Fluid' lines, which link the same endmembers in terms of isotopic compositions but require higher Pb/Nd (22) and Sr/Nd (62) for the sedimentary endmember. These values are estimated assuming an eclogite-facies mineralogy in SCM (presence of garnet, clinopyroxene and minor mica) and $D^{mineral/fluid}$ data largely based on Brenan et al. *(1995)*. Werung, at the volcanic front, plots close to hypothetical 'Fluid' lines, which link the same endmembers in terms of isotopic compositions but imply higher Pb/Nd and Sr/Nd ratios for the sedimentary endmember, in accordance with enrichment of Pb and Sr relative to Nd in fluids. I-MORB endmember: Sr=9ppm, Pb=0.03ppm, Nd=0.73ppm, $^{206}Pb/^{204}Pb$=18.28, $^{143}Nd/^{144}Nd$=0.51297, $^{87}Sr/^{86}Sr$=0.70309; sediment endmember: Sr=367ppm, Pb=21ppm, Nd=27ppm, $^{206}Pb/^{204}Pb$=19.1, $^{143}Nd/^{144}Nd$=0.51215, $^{87}Sr/^{86}Sr$=0.710, based on Vroon et al. *(1993)* and Vroon et al. *(1995)*. Tick marks indicate percentages of bulk sediment added. Note that even if a more radiogenic Sr isotopic composition of the sediment endmember would be assumed, no mixing line would fit the Werung data without invoking a high fluid-type Sr/Nd ratio. A sediment endmember with more radiogenic $^{206}Pb/^{204}Pb$ could be taken to construct a bulk mixing line through Werung in the Pb-Nd diagram, but this would imply a down-dip change in the isotopic composition of the subducted sediments.

Alternative interpretations are less convincing. The Sr/Nd ratios could also be raised by contributions of subducted carbonate. However, a dominant role of carbonate is difficult to reconcile neither with the conspicuous fluxes of many other trace elements, nor with the low $(^{230}Th)/(^{232}Th)$ ratios observed. Fumarole compositions in the East Sunda-Banda Arc do not show CO_2 enrichments compared to other arcs, despite the presence of carbonate intercalations in the shelf sediments and the evidence for abundant sediment subduction (*Poorter et al., 1991; Varekamp et al., 1992*). In the Pb-Nd isotope diagram, the Werung data could be fitted in a mantle-sediment bulk mixing model, but this would require involvement of terrigenous sediments with isotopic ratios, which are considerably different from those added to the sources of the other volcanoes in the transect and thus seems an unlikely scenario. As discussed in Hilton et al. *(1992)*, the strontium-helium pair shows an even stronger decoupling. The $^{87}Sr/^{86}Sr$ and $^{3}He/^{4}He$ ratios of the East Sunda-Banda volcanoes only fit two-component mixing models if the Sr/He ratio in the subduction component is variable. This variation is systematic as increasing Sr/He ratios are required when going from the low-K to the (ultra) high-K volcanics.

88
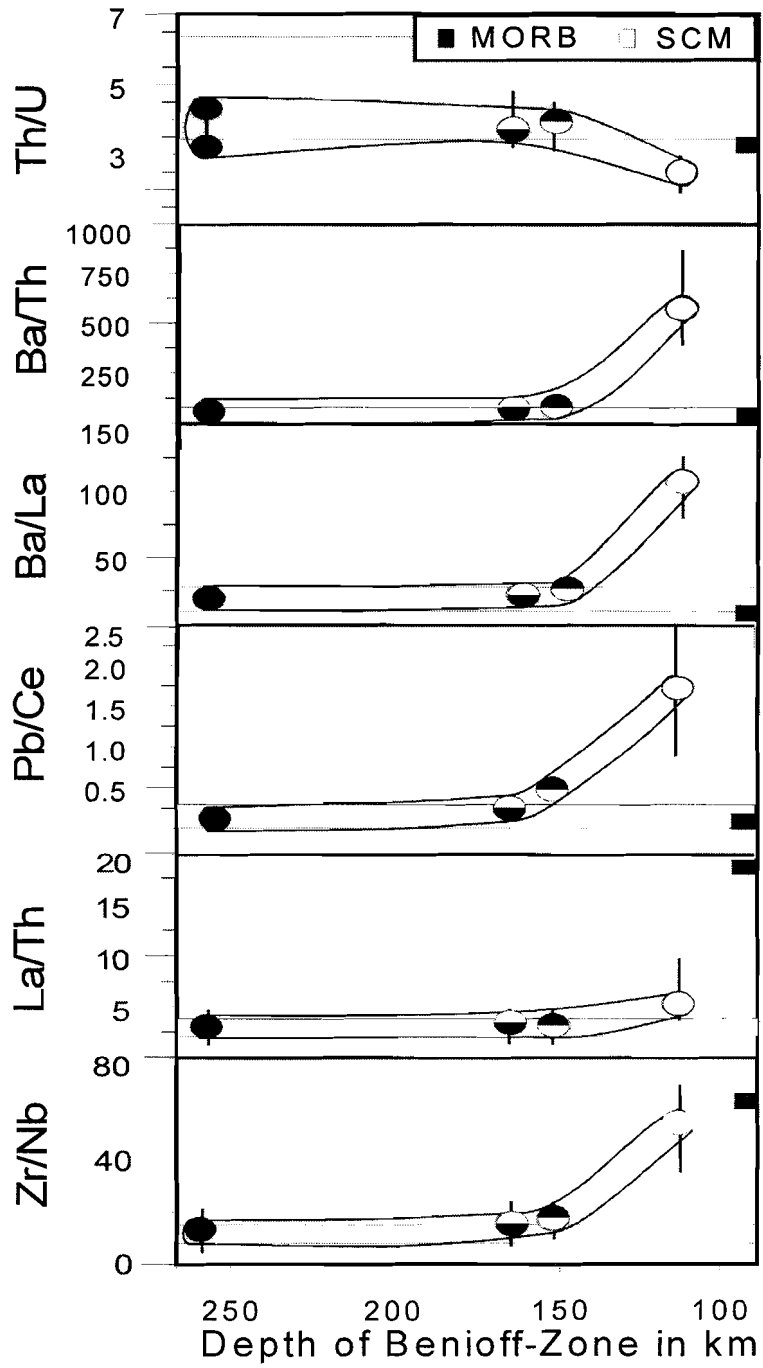
Figure 7.5. (Opposite page) Across-arc trace element systematics in comparison with SCM (shaded fields) and MORB-mantle values. SCM field for Th/U: lower limit is average of sediments with less than 30% $CaCO_3$, upper limit is from the most terrigenous sample analysed; note that this field includes the value of average upper continental crust. See Vroon *(1992)*, Vroon et al. *(1993, 1995)* for SCM data and references for MORB and upper crust. Symbols represent element ratios at 50% SiO_2. Bars indicate within-suite ranges. The behaviour of Th/U, Ba/Th, Ba/La and Pb/Ce is consistent with a transition from selective transfer of elements to mantle sources by fluids below the volcanic front to melt-controlled transfer behind the front. The La/Th ratios illustrate the dominant control of SCM in generating the trace element signatures of the APS volcanics. The Zr/Nb ratios indicate little or no transfer of HFSE at the front, but mobility in SCM melts behind the front.

The Th-U-Ra disequilibrium of the frontal volcanoes also indicates that bulk mixing of source components is inadequate to describe the across-arc behaviour of all trace elements in detail. A more realistic mechanism seems to be that of preferential enrichment of U and Ra with respect to Th by the addition of a high U/Th, Ra/Th medium to the source regions closest to the trench *(see Fig. 7.5)*. Because U and Ra are thought to preferentially partition into a hydrous fluid relative to Th *(Gill, 1981; Eggler, 1987; Gill and Williams, 1990; Keppler and Wyllie, 1991)*, their behaviour points to dehydration of the slab at relatively shallow depths. The observed decreasing fractionation between Th and U to the north can be explained by changes in the nature and transport capacity of the slab-derived medium with increasing pressure and temperature (cf., *Bailey and Ragnarsdottir, 1994*). When this medium has the character of an SCM-derived siliceous melt, mobilisation of elements can be expected to be least selective behind the front (if residual mineral assemblages do not exert a dominant control on element partitioning). I infer therefore that the slab-derived medium is a high U/Th, Ra/Th hydrous fluid in the South and a low U/Th silicate melt more to the North.

Our interpretation implies that the across-arc change in $(^{230}Th/^{232}Th)$ ratios (Fig. 7.3) reflect variations in source characteristics. As an alternative, it could be hypothesised that the modest increase of observed $(^{230}Th/^{232}Th)$ ratios with increasing depth of the Benioff-Zone results from an increasing period of time needed for the melt to rise to the surface. If this is sufficiently long, decay to equilibrium in a melt originating from sources with U excess and low initial $(^{230}Th/^{232}Th)$ ratios could yield a down-dip trend. However, the within-suite correlations with Nd and Sr isotopes at Batu Tara and Lewotolo (Fig. 7.3), where transport distances are largest, argue in favour of source-related Th isotope signals. Furthermore, the small Ra excess at Lewotolo also suggests that transport of melt to the surface is sufficiently rapid to preclude major deviations from initial $(^{230}Th/^{232}Th)$ ratios behind the front.

The observation that $(^{230}Th/^{232}Th)$ ratios are closest to SCM at Werung (Fig. 7.3) seems difficult to reconcile with the above inferred lower mobility of Th in hydrous fluid at the front. However, even if the amount of Th transported by an SCM-derived fluid is relatively small, it will dominate the isotope signature of the magma source, particularly if the mantle below Werung has a depleted character (Th<0.1 ppm). Similar to what has been proposed for arc tholeiites in other regions, the source below Werung may have been depleted relative to MORB mantle as a result of a melt extraction event prior to the recent addition of slab-derived components (cf., *Woodhead et al., 1993*).

The inferred down-dip change in the transporting agent occurs within 80 km of the across-arc section, and is consistent with a S-N change in the ratios of incompatible trace elements (Fig. 7.5). Whereas the low-K volcanics in the South have Ba/La, Ba/Th and Pb/Ce ratios higher than the local sediments, which is compatible with hydrous-fluid enrichment (*Gill,*

89

1981; Tatsumi et al., 1986), the incompatible-element ratios of the medium-K and high-K centres to the North fall largely within the sediment field, which corresponds to the transfer of SCM-derived siliceous melt. Similarly, the ^{143}Nd/^{144}Nd ratios being highest at the front (and close to Indian MORB, Fig. 7.3) are consistent with the expected lower mobility of the REE in slab-derived hydrous fluids *(Tatsumi et al., 1986)* than in silicate melts. The same change in the slab-derived medium is also consistent with the northward decrease in B/Be observed in an adjacent cross-arc section in East Flores *(Edwards et al., 1993)*, as B is probably more mobile than Be in a hydrous fluid *(Morris et al., 1990)*.

Consistent with earlier observations in the Banda Arc, some trace element ratios are particularly diagnostic for involvement for SCM-derived melt, as they deviate from common island-arc and mantle values but overlap with or are close to the local sediments: e.g., low La/Th, K/Rb, Ba/La, Ba/Th behind the front (Fig. 7.5, cf. *Vroon et al., 1995*). Of particular interest is the behaviour of the HFS elements. These are commonly considered as immobile or 'conservative', in the sense that they do not contribute significantly to element fluxes from the slab to the sources of arc volcanism *(Pearce and Peate, 1995)*. However, as these authors emphasise, the behaviour of HFSE will strongly depend on whether the subduction component is a siliceous melt or a hydrous fluid. Along the Banda Arc a positive correlation exists between ^{143}Nd/^{144}Nd and Zr/Nb, with high values of both ratios representing uncontaminated mantle and low values coinciding with the terrigenous sediments *(Vroon et al., 1995)*.

In the APS these systematics are similar but are observed across the arc: the high ^{143}Nd/^{144}Nd lavas of Werung have high Zr/Nb, which is probably close to the local mantle, whereas this ratio falls in the sediment field for the low ^{143}Nd/^{144}Nd volcanoes behind the front (Fig. 8). I conclude that mobilisation of Zr, Nb and other HFSE is virtually absent, when hydrous fluids escape at the front, but is promoted after SCM has started to melt at deeper levels. At Batu Tara, where the slab is deepest, the within-suite isotopic variations (Fig. 7.3) also apply to the HFSE, as there is an inverse correlation between Zr/Ta and ^{143}Nd/^{144}Nd (not shown here). Hence, both on the scale of the arc transect and within individual volcanic centres, sources rather than processes appear to be dominant in controlling the HFSE systematics. Similar to the SW Banda Arc *(Vroon et al., 1995)*, the Zr/Nb ratios of Batu Tara largely overlap with SCM at values lower than MORB (Fig. 7.5), consistent with the dominant role of the sedimentary source. However, whether bulk mixing between SCM and mantle can explain the HFSE (and REE) systematics in all details is questionable. Firstly, the Batu Tara compositions do not plot on mixing curves between a mantle component and bulk sediment, if HFSE and Sr isotopes are used to constrain these endmembers. For example, Zr/Nb ratios are significantly lower than predicted by mixing between MORB mantle and SCM in Zr/Nb- ^{87}Sr/^{86}Sr space *(Van Bergen et al., 1992)*. These authors proposed that the Batu Tara magmas represent mixtures of a SCM-contaminated arc-type melt and a low Zr/Nb melt derived from an Enriched Mantle. Secondly, Batu Tara's Zr/Ta and Nb/Ta ratios are generally higher than those of SCM (cf. *Vroon et al., 1995*). Thus, the combined HFSE relations within this group of elements are difficult to explain by involvement of multiple sources alone, and call for an additional process capable of raising Zr/Ta and Nb/Ta while having little effect on Zr/Nb. A plausible scenario is that partial sediment melts, which fertilise the magma source are relatively depleted in Ta. As rutile is probably stable in siliceous rocks at the pressure and temperature conditions of a subducting slab (cf. *Vielzeuf et al., 1990*), we hypothesise that this mineral may be responsible for preferentially retaining Ta in the SCM residue.

90

Our findings are qualitatively consistent with recent experimental results on the partitioning of elements between minerals and hydrous fluid at high pressure and temperatures *(Brenan et al., 1995)*, which indicate that Ba, Pb and Sr will be preferentially mobilised by a fluid, relative to Th, U and Nb. From a comparison between $D^{mineral/melt}$ and $D^{mineral/fluid}$ for these elements, Brenan et al. *(1995)* concluded that metasomatism by a hydrous fluid will lead to enrichment in alkaline earth elements relative to highly charged cations, and that inter-element fractionations will be considerably less in siliceous melts than in hydrous fluids. Although this evidence is primarily based on equilibria with mantle-type mineral assemblages, the widespread stability of garnet and clinopyroxene in continental crust and terrigenous or pelagic sediments under subduction-zone conditions *(Nichols et al., 1994; Irifune et al., 1994)* lends support to the supposition that it also applies to the high-pressure metamorphic equivalents of SCM-type lithologies.

The APS results are to a large extent in agreement: behind the front, where SCM-derived melts are considered to dominate, the similarity of trace element patterns of volcanics and sediments agrees with only limited inter-element fractionation. At the volcanic front, where the slab-derived medium is inferred to be a hydrous fluid, considerable fractionation is observed, given the enrichment of Ba (as well as Ra), Sr and Pb, relative to Th, Nb and the REE.

The experiments by Brenan et al. *(1995)* predict little difference in the behaviour of uranium and thorium, which seems at variance with the strong ^{238}U excess at Werung, and the contention that U-Th fractionation, occurring when fluid escapes from the slab, can be held responsible for U excesses in island-arc basalts (e.g., *Gill and Williams, 1990* and other references given above). Brenan et al. *(1995)* argue, however, that dehydration of an oceanic slab with an eclogite mineralogy will produce U excesses, provided that the garnet content in the residue is low and the oxygen fugacity sufficiently high. In the case of the APS, the association of largest U-Ra excesses and lowest ^{3}He/^{4}He ratios at the front suggests that the subducted leading edge of the Australian continent may be a common source of U, Ra and radiogenic He. The dehydration behaviour may therefore be controlled by eclogite facies assemblages in a sedimentary/continental lithology rather than in oceanic crust, but with similar effects in terms of the preferential release of uranium relative to thorium.

Quantitative estimates on the composition of the transfer medium in subduction zones have been given by McCulloch and Gamble *(1991)*, and Stolper and Newman *(1994)*, which were derived from data on Pacific island arc basalts and the Marianas back-arc respectively. Conspicuous differences in geochemical signatures between these regions exist, as the Mariana lavas show larger enrichments in Th, U, Nb, Ta, Ba, Pb and Sr as well as less inter-element fractionation. Brenan et al. *(1995)* suggested that these differences can be attributed to the distinctions between mineral-fluid and mineral-melt partitioning: the metasomatic agent of McCulloch and Gamble *(1991)* may represent a hydrous fluid and that of Stolper and Newman *(1994)* a silicate melt.

In the light of our cross-arc systematics, and given that the melt signature in the Marianas was inferred from a back arc, it appears that fluid-to-melt transitions down the dip of subduction zones can explain differences within and between various island-arc settings, irrespective of the nature and amounts of sediments involved.

7.6.3 Three-component mixing

Difficulties in modelling combined isotopic and trace element signatures of subduction related basalts as simple two-component mixing between a mantle-wedge source and a single subduction component, have led to the hypothesis that more than one slab-derived medium may be involved in arc magma genesis. Ellam and Hawkesworth *(1988)* provided arguments supporting three-component mixing, whereby contributions of both a high Sr/Nd fluid, derived from the dehydration of subducted oceanic crust, and a low Sr/Nd component from subducted terrigenous sediment can explain systematics in various subduction-related magmas world-wide. From regional trace element and isotopic variations in the North Luzon arc, McDermott et al. *(1993)* concluded that, in addition to the mantle wedge, a high LILE/HFSE hydrous fluid as well as bulk addition of terrigenous sediments are required to explain the observed intra-arc trends. Based on REE systematics, Bau and Knittle *(1993)* provided evidence that the tholeiitic lavas of Mt. Arayat, situated behind the front of Batan segment in the Taiwan-Luzon arc, originated from a source, which was infiltrated by fluids, whereas its calc-alkaline lavas were derived from a source affected by both fluids and melts. Vroon et al. *(1993)* explained minor deviations from simple two-component bulk mixing between the mantle wedge and subducted sediments in the Banda Arc (e.g., relatively high Sr/Nd and Pb/Nd in the volcanics) by an additional role of fluids derived from the sediments. This fluid is most evident in the Banda Archipelago, the suite with the lowest potassium level, furthest away from the collision zone North of Timor. For similar reasons we also consider three-component mixing an attractive scenario for the APS. Despite the reasonable fits in mantle-fluid and mantle-bulk sediment mixing models for the front and behind-the-front volcanoes respectively (Fig. 7.2), closer observations suggest that both fluid and melt play a role in all cases, though in clearly different proportions. This is illustrated in the $^{143}Nd/^{144}Nd$ vs. Ba/Th diagram of Fig. 7.6, showing models, which assume an eclogite-facies mineralogy for the sedimentary material *(cf., Nichols et al., 1994)*. All volcanoes in the transect fall in the field enclosed by the two mixing curves between the mantle wedge (MORB source) and melt derived from the local sediment (SCM), and between the mantle wedge and sediment-derived hydrous fluid. Werung, at the front, plots close to the fluid curve and requires only very little melt. The reverse situation holds for the volcanoes behind the front, which tend to plot at only slightly higher Ba/Th values than the mixing line connecting SCM melt and MORB mantle, consistent with a minor role of hydrous-fluid. The Ba/Th ratios are low compared to those in many other oceanic arcs, indicating that the sediment (melt) imprint is dominant, a characteristic, which the volcanoes behind the APS front share with the SE Banda Arc centres *(Vroon et al., 1993)*.

This three-component mixing scenario thus implies that some fluid is retained in the subducting slab behind the front, but precise controls are difficult to assess. Experimental and theoretical studies concerning the transport and release of volatiles in subduction zones have mainly focused on peridotitic, basaltic and andesitic systems *(Peacock, 1990; Poli and Schmidt, 1995)* using various models for the thermal structure of down-going oceanic crust (e.g., *Davies and Stevenson, 1992; Peacock et al., 1994)*. They show that fluids can be transported to depth behind the front by hydrous phases either in the slab itself or in down-dragged portions of the overlying mantle being hydrated by slab-derived fluids at relatively shallow levels *(Tatsumi, 1989)*.
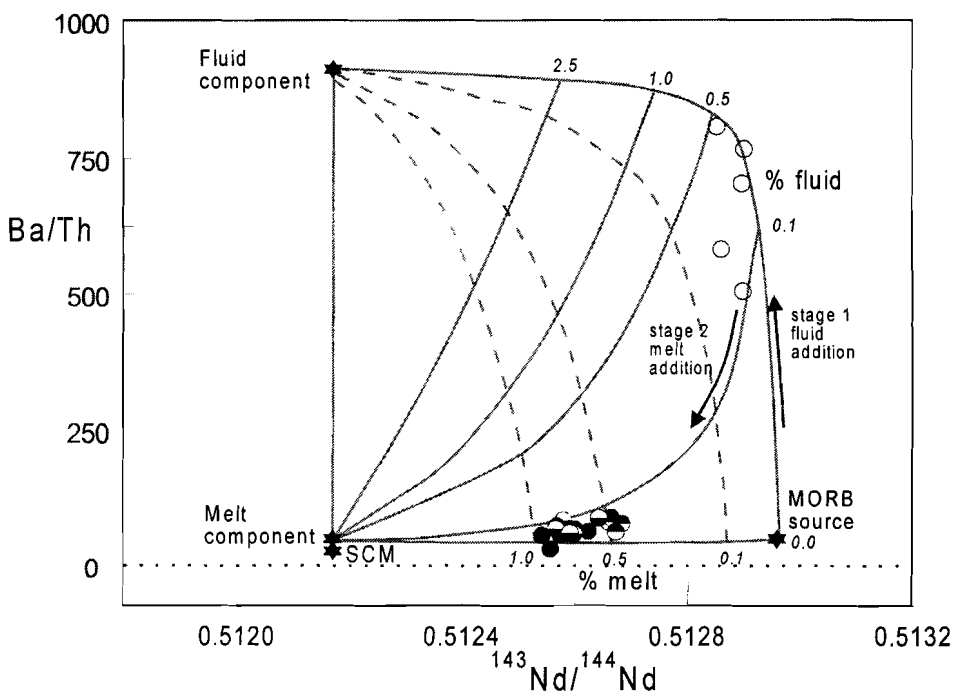
Figure 7.6. Three component mixing model in which a fluid and a melt, both derived from SCM, are added to a MORB mantle source. Up to 0.5 % percent fluid together with less than 0.1 % melt can explain the composition of Werung at the volcanic front, whereas that of the volcanoes behind the front requires addition of less than 0.1% fluid together with 0.25-1% melt. These percentages will be less, if the mantle source is more depleted than assumed here. Note that the percentages of added melt are lower than in the case of bulk SCM. Data and references for MORB mantle and SCM can be found in Vroon et al. *(1995)*. Concentrations in MORB mantle (ppm): Ba=0.63, Th=0.12, Nd=0.73; SCM-bulk: Ba=608, Th=12.6, Nd=27; SCM-fluid: Ba=22461, Th=25, Nd=27; SCM-melt: Ba=2183, Th=52, Nd=85. Compositions of the slab-derived components are based on the 'batch' production of 10% fluid (*Nichols et al., 1994*) and 25% melt (*Johnson and Plank, 1993*) respectively from a SCM source with an eclogite facies mineral assemblage (cf., *Nichols et al., 1994*): garnet, clinopyroxene and minor mica (59.5:39.5:1). Quartz/coesite and kyanite were considered to have no effect on the trace element contents. Mineral/fluid partitioning coefficients: $D^{gnt/fluid}$ and $D^{cpx/fluid}$ for Ba, Sr, Pb and Th from Brenan et al. *(1995)*, for Nd assumed to be 1; $D^{mica/fluid}$ assumed to be 1 for Ba, Pb, Sr, 0.1 for Nd and 0.01 for Th based on Rosenbaum and Wilson *(1993)*. Mineral/melt D's from McKenzie and O'Nions *(1991)*, Beattie *(1993)* and Latourette *(1994)*. Symbols as in Fig. 1.

For cases where a thin veneer of sediment covers oceanic crust, the experiments of Nichols et al. *(1994)* on pelagic clays suggest that there may be a considerable depth interval near the levels of arc magma genesis, where melting occurs within sediments but not within underlying (dehydrating) gabbroic crust. According to Ryan et al. *(1995)*, white mica potentially plays an important role in retaining fluids and controlling element transfer across the Kurile arc and elsewhere. Similar to our conclusions, these authors hypothesise from

93

across-arc trace element systematics that a mixed slab flux, consisting of hydrous fluid and sediment melt, infiltrates the sub-arc mantle, and that down-dip changes in their proportions can explain observed variations in element ratios.

If the small Ra excess found in our behind-the-front samples can also be attributed to a contribution from slab-derived fluid, similar to what we infer for the large excess at Werung, it has implications for the question of whether the fluid signature is introduced at shallow levels and transported down-dip in hydrated mantle *(Tatsumi, 1989)*, or at the depth of each magma source behind the front. Assuming that fluid escapes from the slab below Werung, and taking convergence rate, travel distance, and the short Ra half-life into account, any Ra excess in the other APS volcanics cannot reflect an inherited fluid signal in down-dragged mantle. Instead, slab-wedge transfer, magma generation and transport to the surface must have occurred very recently, perhaps less than 8,000 y ago (cf., *Gill and Williams, 1990; Gill et al., 1993*). In this respect, it is also of interest to note that low ^{3}He/^{4}He ratios (R/Ra=4.5) have been found at Batu Tara *(Hilton et al., 1992)*, which indicates that SCM-derived, highly mobile elements such as helium may still escape from the slab far behind the front.

7.7 Conclusions

The array of active volcanoes across the arc-continent collision zone in the East Sunda Arc shows systematic geochemical variations in terms of U-series, Sr-Nd-Pb-He and trace element compositions, which can be attributed to changes in the mechanisms of element transfer and in the magnitude of fluxes at the slab-wedge interface.

(^{230}Th)/(^{232}Th), ^{87}Sr/^{86}Sr, ^{143}Nd/^{144}Nd, Pb isotopes and incompatible trace element signatures of the volcanics, as well as marked correspondences with local terrigenous sediments, all point to subducted continental material as a dominant source of slab-derived material.

Low-K Werung volcano at the front is characterised by large excesses of ^{238}U and ^{226}Ra over ^{230}Th, high Ba/La, Ba/Th, Pb/Ce, and high ^{143}Nd/^{144}Nd ratios, as well as depleted HFSE and REE patterns. On the other hand, high-K calcalkaline and ultrapotassic Boleng, Lewotolo and Batu Tara behind the front have little or no U and Ra excess, and values for incompatible trace element ratios (such as low Ba/La, Ba/Th, Pb/Ce, La/Th) are similar to those in the terrigenous fraction of the local sediments.

From these systematics we conclude that the across-arc systematics of Th-U-Ra and other trace elements reflect a change in the nature of the SCM-related magma source component: a high U/Th, Ra/Th and LILE-enriched hydrous fluid in the shallow parts, and a siliceous-melt with a U/Th similar to that of SCM at greater depths. Hence, both U and Th must be added to the mantle wedge, though in different and variable proportions. This process is a recent event associated with the present-day subduction of ancient continental material under the East Sunda Arc. Given the importance of subducted sediments in generating trace element characteristics of island-arc volcanics *(Plank and Langmuir, 1993)*, and the apparent dominance of the slab-derived metasomatic component in the U and Th budgets of their mantle sources, the influence of melts as transfer medium behind volcanic fronts may be more significant than realised so far and be responsible for the frequently absent disequilibrium in volcanic arcs *(Condomines and Sigmarsson, 1993)*.

8 Across-arc Processes of Magma Genesis in the Adonara-Pantar Sector: an attempt to synthesise isotope and trace element data

8.1 Introduction

In chapter 6 I concluded the following concerning the components, which contribute to magma sources in the Adonara-Pantar Sector (APS):
- The pre-subduction frontal mantle wedge is depleted in trace elements and, on the basis of Nd and Sr isotopes, similar to depleted Indian Ocean domains (e.g. DSDP261).
- The high Pb isotope ratios can be explained by a combination of (a) Indian Ocean Depleted Mantle (I-DM) with Australian deep crustal material and Subducted Continental Material (SCM) or (b) an Indian Ocean Enriched Mantle (I-EM, similar to DSDP211 or Christmas Island) with the same Australian deep crustal material and SCM.

In chapter 7, combined Th-U disequilibrium, isotope and trace element results demonstrated that simple bulk-mixing of the mantle wedge component and the subduction component cannot explain the observations in the APS, but that cross-arc changing contributions from slab-derived fluid and melt represent a more plausible model.
In this chapter I shall try to answer four important questions left open:
- is an I-EM component really needed to explain the isotope systematics in the APS?
- is it possible to determine the trace element characteristics of the slab-derived melt and fluid?
- is it possible to identify a residual mineral assemblage that controls the behaviour of HFSE?
- do across-arc systematics in LILE signatures enable identification of hydrous phases in the mantle wedge?

Using simple batch models, I will evaluate the HFSE, REE and LILE systematics to come to an overall model for the across-arc geochemical observations in the APS.

8.2 Components revisited

Central to this chapter are the element distribution coefficients between minerals and melt and between minerals and fluid, which influence trace element behaviour during melting, dehydration and fractionation.

8.2.1 Model parameters

In the following discussion, the distribution coefficients used for the calculation of solid/melt and solid/fluid equilibria are compiled in table 8.1 and table 8.2. Data homogeneity and

relevance for subduction-related magmagenesis have been the principal justifications for the choice of distribution coefficients from the vast amount of data published in the literature. The same set of coefficients has been used for slab melting models, which is a compromise, as no comprehensive database is available for high-pressure eclogite-facies dehydration and melting reactions.

	Olivine	Orthopyroxene	Clinopyroxene	Plagioclase	Spinel	Garnet	Amphibole	Phlogopite	Rutile
Plagioclase peridotite	0.636	0.263	0.012	0.089	-	-	-	-	-
Spinel peridotite	0.578	0.27	0.119	-	0.033	-	-	-	-
Garnet peridotite	0.598	0.211	0.076	-	-	0.115	-	-	-
Amphibole peridotite	0.599	0.247	0.038	-	-	-	0.116	-	-
Phlogopite peridotite	0.599	0.247	0.038	-	-	-	-	0.116	-
SCM Eclogite	-	-	0.4	-	-	0.6	-	-	-
SCM Eclogite + Rutile	-	-	0.395	-	-	0.595	-	-	0.01
SCM Ecl. + Ru + Phlog	-	-	0.39	-	-	0.59	-	0.01	0.01

Table 8.1 Modal mineral fractions used in model calculations. Plagioclase, spinel, garnet and amphibole peridotites from McKenzie and O'Nions *(1991)*, phlogopite peridotite adapted from the amphibole peridotite; SCM eclogites after Nichols et al. *(1994)*.

	Olivine	Orthopyroxene	Clinopyroxene	Plagioclase	Spinel	Garnet	Amphibole	Phlogopite	Rutile
Ba	0.01	0.01	0.00068	1.0	0.1	0.00001	0.15	4.0	*0.0001*
Th	0.0001	0.0001	0.0080	0.05	0.1	0.0015	0.004	0.0015	*0.001*
U	0.0001	0.0001	0.0034	0.11	0.1	0.0096	0.004	0.001	*0.001*
Nb	0.01	0.001	0.05	0.01	0.5	0.25	0.1	0.1	52.6
Ta	0.01	0.001	0.1	0.05	0.5	0.25	0.1	0.1	99.5
Ce	0.0005	0.003	0.098	0.2	0.01	0.021	0.1	0.03	0.73
Pb	0.0001	0.0013	0.01	0.36	0.001	0.00001	0.1	0.1	*0.0001*
Sr	0.00019	0.007	0.067	2.0	0.25	0.0006	0.3	0.15	0.518
Nd	0.001	0.0068	0.21	0.14	0.01	0.087	0.2	0.01	*0.0001*
Zr	0.05	0.01	0.12	0.1	0.5	0.4	0.3	0.015	4.76
Yb	0.0015	0.049	0.28	0.031	0.01	4.0	0.5	0.015	*0.0001*

Table 8.2. Mineral/melt distribution coefficients. The mineral/melt distribution coefficients were taken from: Beattie *(1993)* (Sr, Ba, Pb, Th and U in garnet), Latourette *(1994)* (amphibole and phlogopite), Rosenbaum and Wilson *(1993)* (LILE, amphibole and phlogopite), Adam et al. *(1993)* (Sr, REE amphibole), Thirlwall et al. *(1993)* (LREE/Nb in phlogopite), Green *(1994)* (Nb/Ta, amphibole), Klein et al. *(1997)* (Zr/Ta amphibole), Jenner et al. *(1993)* (rutile). Other data were taken from McKenzie and O'Nions *(1991)* or Green *(1994)*. Data in italics are estimates based on heuristic assumptions.

The rutile/fluid distribution coefficients for Nb, Ta, and Zr were used from Brenan et al. *(1994)*. An average value of 200 was taken for Nb and 150 for Ta, being about ¾ of the Nb value in all their experiments (cf. Table 1 in *Brenan et al. (1994)*. Because only a few of their experiments included zirconium, the Zr solid/fluid coefficient (471) preferred here represents a value relative to Nb and Ta: (206/471)*150≈66. In this manner it is ensured that the direction in which calculated trace element ratios will develop are consistent with empirical observations.

The bulk distribution coefficients for an eclogite with 1% rutile yield mobility factors similar to those defined by Tatsumi et al., *(1986)* for the LILE elements. The REE are less mobile as a result of residual garnet in the eclogite, whereas Tatsumi et al., *(1986)* used pure

96

serpentine in their experiments. This is obviously inadequate to represent the mineralogy of high-grade metamorphosed subducted sediment.

	Cpx/fluid	Garnet/fluid	Rutile/fluid	Phlog/fluid
Ba	0.0008	0.0001	0.001	1.00
Th	2.5	0.13	*0.01*	0.01
U	0.3	0.7	*0.01*	-
Nb	0.05	0.09	200	0.10
Ta	0.09	0.09	150	0.10
Ce(La)	1	0.02	0.1	-
Pb	0.02	0.003	*0.01*	1.00
Sr	0.5	0.002	0.01	1.00
Nd	2	0.09	0.5	0.10
Zr	0.1	0.08	66	-
Yb(Lu)	9	4.0	1	-

Table 8.3. Mineral/fluid partitioning coefficients:). $D^{gnt/fluid}$ and $D^{cpx/fluid}$ from Brenan et al. *(1995)* and Ayers et al. *(1997)*. $D_{Ta}^{cpx/fluid}$ and $D_{Ta}^{gn/fluid}$ calculated from $D_{Nb}^{min/fluid}$ and $D_{Nb}^{min/melt}/D_{Ta}^{min/melt}$. $D^{rutile/fluid}$ from Brenan et al. *(1994)* and Ayers et al. *(1997)*. $D^{phlog/fluid}$ assumed to be 1 for Ba, Pb and Sr, 0.1 for Nd and 0.01 for Th, based on Rosenbaum and Wilson *(1993)*. Data in italics are heuristic estimations.

8.2.2 HFSE as tracers of the mantle component

The systematic depletion of the high field strength elements (HFSE) Nb, Ta, Zr, Hf, V and Ti, relative to LILE and LREE, distinguishes arc volcanics from MORBs, and has spurred many discussions. During melting of normal mid-oceanic mantle, Nb is about as incompatible as U *(Hofmann et al.,1986; Sun and McDonough, 1989)*, but U/Nb ratios in arc volcanics are much higher than in MORBs. To explain this, it has been proposed that a residual titanate mineral would retain the HFSE in either the slab *(Saunders et al, 1980; Ringwood, 1990)* or the mantle wedge *(Green 1980; Morris and Hart, 1983)*. An alternative hypothesis is that a higher mobility of the LILEs during slab dehydration results in magma sources that are enriched relative to the HFSE *(McCulloch and Gamble, 1991)*. In the latter case, the HFSEs would represent the nature of the unmodified mantle *(Ryerson and Watson, 1987)*.

Vroon *(1992)* has pointed out that bulk SCM addition to mantle sources can also result in HFSE depletions, based on the observation that sediments entering the Banda Arc have spidergrams with negative Nb, Ta, Zr and Ti anomalies that match the patterns in the volcanics. Although this explanation can be valid in arc-continent collision settings, HFSE depletion is a common feature in intra-oceanic arcs, irrespective of involvement of subducted sediments. Also HFSE depletion is not necessarily less pronounced in 'sediment-starved' intra-oceanic arcs, as for example the New Brittain Arc *(Gill et al., 1993; Woodhead and Johnson, 1993)*. Hence, until it will be demonstrated that sediment subduction plays a more important role in generating the HFSE anomalies in collision settings than in intra-oceanic arcs, it could be argued the mantle wedge is the principal source of HFSEs in both cases.
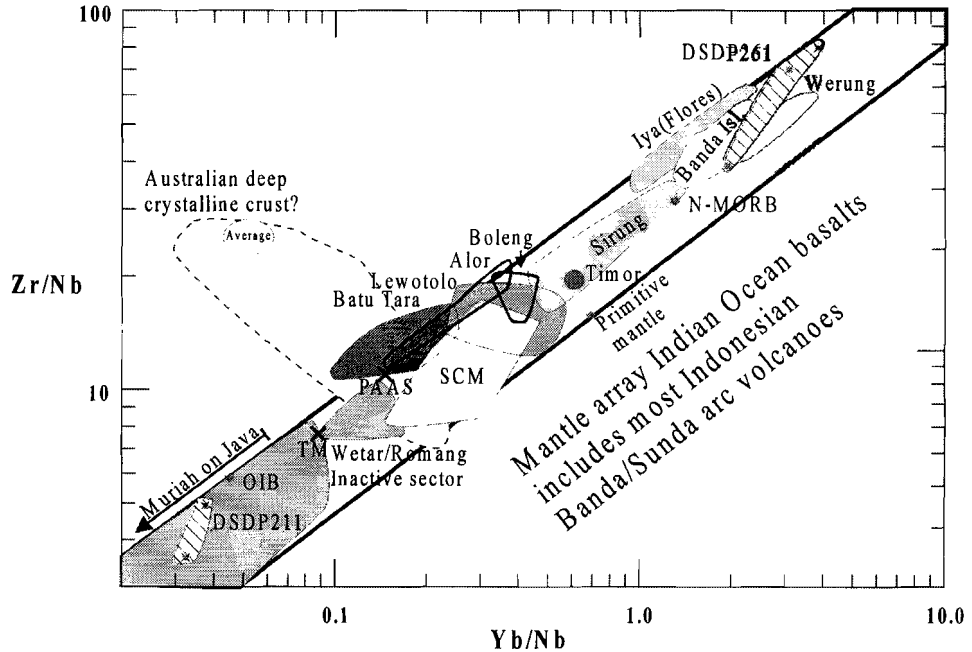
Figure 8.1. Zr/Nb versus Yb/Nb diagram showing relations between Indian Ocean mantle and Indonesian volcanics. *(Data from: Bergman et al., 1996, Edwards, 1990; Edwards et al., 1993; Edwards et al. 1994; Gerbe et al. 1992; Hoogewerff et al., 1997; Hutchison and Jezek, 1978; Gasparon, 1993; Gasparon et al., 1994; McCulloch et al., 1983; McDermott and Hawkesworth, 1991; Morrice et al., 1983; Morris et al., 1983; Morris et al., 1984; Stolz et al., 1988; Stolz et al., 1990; Tatsumi et al., 1991; Varne and Foden, 1987; Vukadinovic and Nicholls, 1989; Vukadinovic and Sutawidjaja, 1995; Whitford et al., 1977; Whitford et al., 1979; Magaritz et al., 1978; White and Patchet, 1984; Vroon, 1992; Vroon et al., 1993; Vroon et al., 1995).*

As an introduction to the HFSE systematics in the APS Figure 8.1 gives an overview of the relation between the active APS volcanoes, other relevant Indonesian volcanics, the Indian Ocean mantle sources, sediments and continental crust in Zr/Nb and Yb/Nb space. The Indian Ocean data from Weis and Frey *(1996)* form a mantle array, which also encompasses the N-MORB, Primitive Mantle and OIB compositions of Sun and McDonough *(1989)*. The compositions of average crust (TM in Fig. 8.1) and PAAS *(both from Taylor and McLennan, 1985)* plot also within the mantle array, as does the SCM field based on sediments from the Australian margin in front of the APS *(Vroon, 1992; Vroon et al., 1995)*.

The data of nearly all Indonesian volcanics (not shown for clarity) fall within the mantle array and are concentrated between average N-MORB and OIB. The basalts from Timor *(Vroon, 1992)* have an intermediate mantle composition. In general, rocks from Flores and Banda Arc have similar values as the APS rocks. Most of the frontal low-K LREE-depleted rocks extend up to the most depleted values of I-DM at DSDP site 261 *(Weis and Frey, 1996)*. The Werung volcano is as depleted as the Banda Archipelago in the Banda Arc and Iya volcano on Flores. The high-K Muriah volcano on Java *(Edwards, 1990)* has Zr/Nb and Yb/Nb

values lower than those of I-EM at DSDP site 211 *(Weis and Frey, 1996)*. The high-K Batu Tara volcano appears to be an exception, as it falls partly outside the mantle array. Because mixing relations in this plot are defined by straight lines, a source that is different from both SCM or Indian mantle is required. Although data on the trace element compositions of the West Australian batholiths (see chapter 6) are limited, in number these lithologies should be considered as conceivable endmembers as they plot at a position, which could explain the Batu Tara compositions.

8.2.2.1 Frontal volcanoes

As has been discussed in the previous chapters, the mantle source of the frontal volcanoes, and especially Werung, is metasomatized by a fluid from the slab. Brenan et al. *(1994)* and Tatsumi et al. *(1986)* have experimentally shown that HFSE are not mobile in a fluid under subduction conditions. The HFSE signature of Werung seems therefore most appropriate as indicator of the pre-subduction mantle in the wedge.

In Figure 8.2 Zr and Yb are normalised to the Ta concentration in order to compare the APS data with the mantle array defined by these elements. Ta instead of Nb is chosen as the number of Ta analyses in the APS is larger and the Ta data have a better precision. All the Werung samples have Zr/Ta and Yb/Ta higher than N-MORB, similar as in Figure 8.1. Using the Zr, Yb and Nb data from *(Weis and Frey, 1996)* and assuming that Nb/Ta of the Indian Ocean basalts is around 17 (range 14-20; *F. Frey personal communication, 1997)*, the Zr/Ta and Yb/Ta ratios of depleted Indian Ocean mantle would encompass the extreme Werung values.

The following model calculations show that a Werung-type magma source could have been generated by previous melt extraction. Modal mineral abundances from table 8.1 and mineral/melt distribution coefficients from table 8.2 were used to calculate the composition of a batch melt (named „second melt" in figures) extracted from different possible MORB-restites. These restites have been calculated first, assuming 10% batch melt extraction from an N-MORB source. While a Plagioclase-restite source would not fit, the melts from an Amphibole-, Spinel- or Garnet-restite source fall within the field defined by the Werung samples and depleted I-DM in Figure 8.2. Not only the trace element ratios but also the HREE abundances from a melt derived from any of these restite sources are within the range of the Werung samples. More sophisticated melting models like dynamic- and continuous-melting *(Williams and Gill, 1989)* would yield even more extreme values.
These findings thus support the hypothesis that the frontal mantle wedge could have undergone an earlier depletion event.

The presence of a titanate phase in the melting column could strongly enhance the Zr/Ta and Yb/Ta ratios as well, as it is assumed that the D for Ta and Nb is much larger than the D for Zr and Yb in these phases (Table 8.2; *Jenner et al., 1993; Thirlwall et al., 1994)*. The presence of residual titanates in two magma components in the APS has also been suggested by Foley and Wheller *(1990)*. These authors suggest that one rutile might be present at the slab-wedge interface, where silicic melts interact with the mantle and the second rutile in the peridotite wedge or in K-rich vein domains of the wedge.

In the above calculation of the 2nd stage melts, it was assumed that the original mantle mineralogy does not change significantly. However, because the subduction component may alter the modal assemblages, we have to discuss the effects of other relevant minerals. Evidence for potential role of hydrous minerals in arcs has been provided by Vidal et al. *(1989)*, who documented depleted harzburgite xenoliths with both cryptic and modal metasomatism (addition of phlogopite and amphiboles and new growth of clinopyroxenes).

As can be observed in Figure 8.4 the highest Zr/Ta ratio seems to correspond with the lowest SiO_2 concentration in the Werung rocks. This poor trend of decreasing Zr/Ta with SiO_2 cannot be explained by fractional crystallisation of olivine or pyroxene, as the observed decrease per SiO_2 unit seems much too large. Amphibole should, however, be considered.
Experimentally determined D_{Zr}/D_{Ta} and D_{Yb}/D_{Ta} ratios (3 and 5 res.) for amphibole *(Green, 1994; Klein et al., 1997)* would indicate that its presence in the source could lower the Zr/Ta and Yb/Ta ratios in the magma.

Low-pressure fractionation of amphibole would also lower both Zr/Ta and Yb/Ta, but it has not been observed in any of the frontal lavas. It thus seems that the decrease of Zr/Ta and Yb/Ta ratios from extremely depleted I-DM to N-MORB values could only be explained by different abundances of amphibole in the mantle source. This would agree with observations by Ionov and Hofmann *(1995)* who documented variable amounts of amphiboles in metasomatized mantle fragments. However, Ionov and Hofmann *(1995)* also observed extremely high $D_{Nb,Ta}$ in natural amphiboles resulting in D_{Zr}/D_{Ta} and D_{Yb}/D_{Ta} ratios less than unity. If this would also be the case in the APS, then the decrease of Zr/Ta and Yb/Ta (and Zr/Nb) in Figures 8.4. (and 8.3) could not be explained by residual amphibole during melting. Instead, it would require breakdown of the amphibole in the mantle source, as this would release a low Zr/Ta and Yb/Ta component.

It must be stressed, however, that inhomogeneity in the pre-subduction mantle remains a conceivable alternative, given the variations in I-MORB as documented by Weis and Frey *(1996)*. This alone would be sufficient to explain the observed HFSE signatures within the frontal APS volcanoes, without the need to invoke amphibole fractionation or breakdown.

The possible role of rutile

The frontal rocks as well as the Banda Archipelago (BA) *(Vroon, 1992)* show a positive correlation between Zr/Ta and Nb/Ta (Fig. 8.6). Neodymium isotopes in the Banda Archipelago ($^{143}Nd/^{144}Nd$ = 0.5126-0.5128) also correlate positively with these ratios, but they show a scatter in the Werung samples (0.5128-0.5129). A further difference is that Nb/Ta ratios of the BA series plot between the mantle array (14-20, *F. Frey pers. comm., 1997*) and sediment/crustal values, whereas the Werung frontal rocks have high ratios that tend to fall at the opposite side of the mantle array. This may imply that mixing of different source components is responsible for the BA trend but that the enhancement of Nb/Ta ratios at Werung might be controlled by a local melting process.

Because, as discussed above, the variation of Zr/Ta can be explained by the composition of the pre-subduction mantle, this process must fractionate Nb from Ta and Zr, and be related to active subduction. There are several options:

(a) Addition of fluid to the magma source

This explanation is inadequate, as the low mobility of all HFSE in hydrous fluid is unlikely to influence any of their ratios to a significant extent. Furthermore, addition of a high Nb/Ta component would enhance the Nb concentration in the source, which is inconsistent with the observations. Still, it is conceivable that rutile exerts a control on HFSE ratios in a slab-derived fluid. However, as pointed out by Stolz et al. *(1996)*, the experiments of Brenan et al. *(1994)* indicate that a fluid in equilibrium with rutile would have Nb/Ta lower than its source. The observed ratios are higher than any of the potential sources of the fluid, be it SCM (average Nb/Ta=11) or Indian Ocean-type basaltic crust (Nb/Ta~17.5).

(b) Amphibole control during melting

Ionov and Hofmann *(1995)* suggested that $D_{Nb/Ta}$ for amphibole in natural systems could be larger than 2 and $D_{(Nb,Ta)/Zr}$ much greater than unity. Melting in presence of residual amphibole would thus result in lower Nb/Ta and higher Zr/Ta in the melt, and produce a trend perpendicular to the observed trend. This also rules out amphibole breakdown as explanation as this would produce a trend in the opposite direction.

(c) Rutile control during melting

The above arguments leave a residual phase with $D_{Nb/Ta} < 1$ as the most plausible alternative. Rutile is a likely candidate as it is capable of retaining both elements in the required proportions. However, it must be stressed again that these points in favour of rutile in the mantle wedge are critically dependent on assumptions on the pre-subduction Nb/Ta ratio of the mantle, which is poorly known in I-DM.
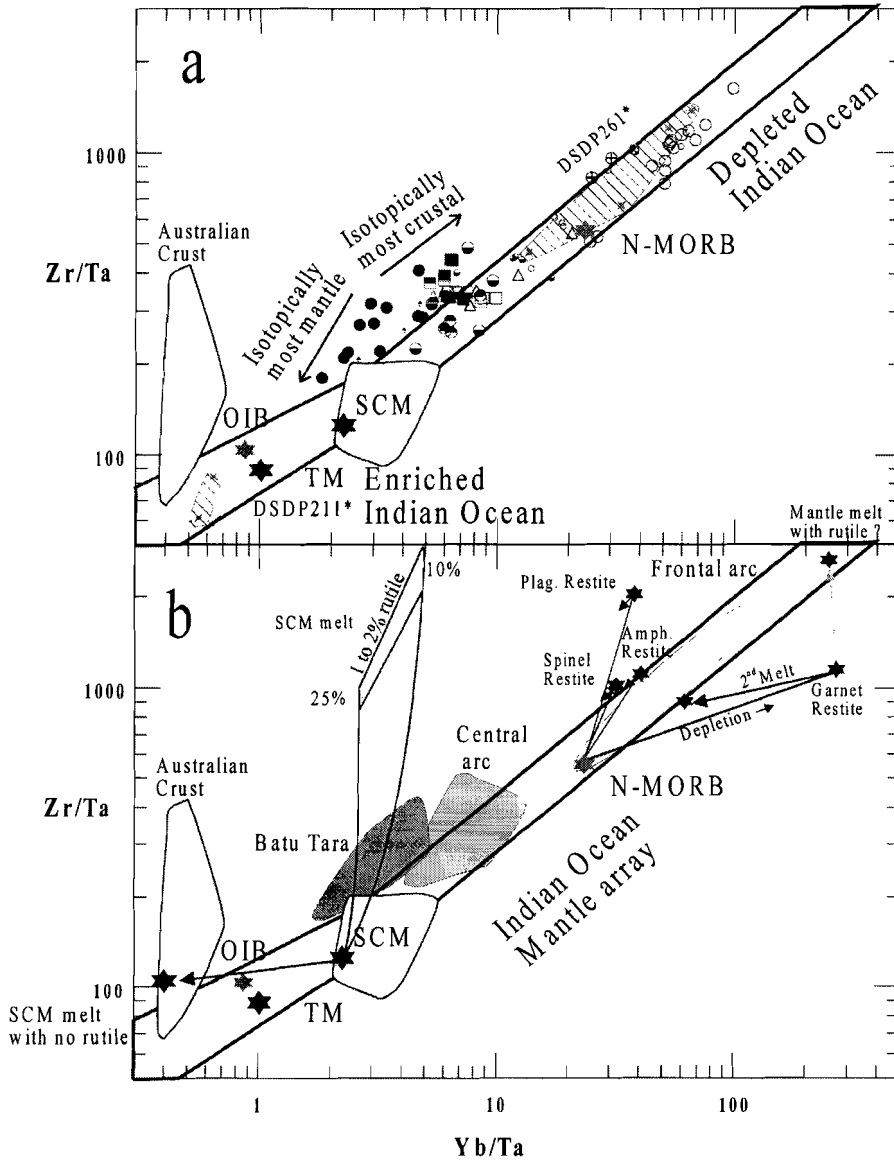
Figure 8.2. a: Zr/Ta versus Yb/Ta of the APS volcanoes in relation to the Indian Ocean mantle array (calculated from Weis and Frey *(1996))* assuming Nb/Ta=17 *(Frey pers. comm. 1997))*, bulk SCM, SCM melt and Australian crust. Samples from Werung and other frontal centres fall in the depleted Indian Ocean Field. **b:** results from melting models.

8.2.2.2 Non-Frontal volcanoes

The trace element systematics in the APS generally agree with general island arc characteristics in the sense that low abundances of the HFSE coincide with Ti/Zr, V/Ti and Sc/Y ratios higher than in MORBs (cf., *Woodhead et al., 1993*). This is consistent with derivation of the magmas from relatively depleted sources, as Zr and V are more incompatible than Ti, and Sc is more incompatible than Y. In the APS the samples with the highest Zr/Ta also have the lowest Ta.

Zr/Nb-Nb relations

Figure 8.3 shows that there is a systematic down-dip decrease in Zr/Nb with increasing Nb in the APS. Following Woodhead et al. *(1993)* (who used Ti/Zr vs. Zr instead), this should reflect decreasing degrees of melting with increasing WBZ depths. However, within-suite variations of Zr/Nb ratios in the central and rear arc volcanoes show correlations with Sr, Nd, Pb or Th isotopic ratios, which favours local source inhomogeneity, as discussed in chapter 6. Hence, it is more reasonable to assume that source mixing is responsible for across-arc changes in Zr/Nb.
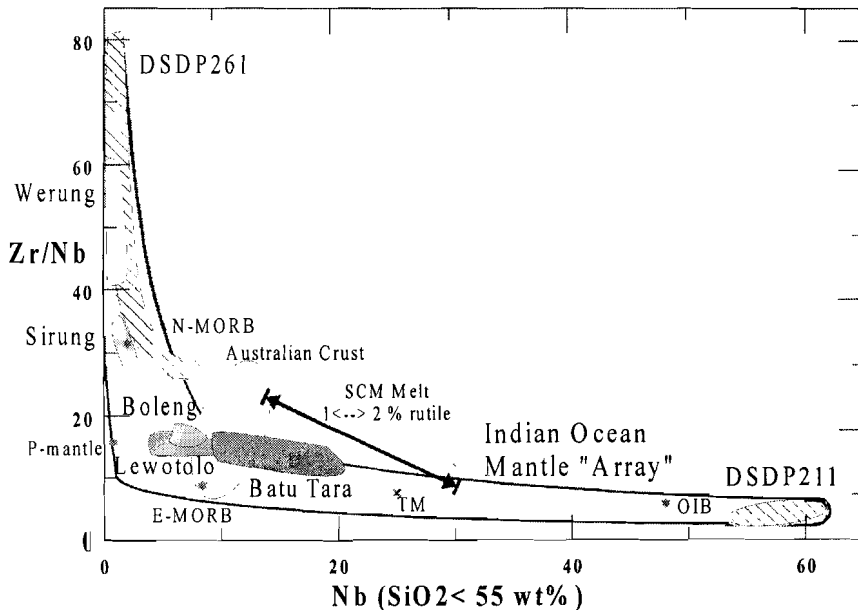
Figure 8.3. Zr/Nb versus Nb plot in which, after Woodhead et al. *(1993)*, the concave trend is indicative for different degrees of melting of the mantle during active volcanism between the sources of the different suites of the APS volcanoes. In the APS this explanation is not sufficient as within-suite isotopic trends in the non-frontal centres indicate that their sources are enriched by HFSE from the slab.

The Zr/Ta ratio (as well as the Yb/Ta ratio) in the central and rear arc appears not to be influenced by crystal fractionation, as the data plot at a horizontal array versus SiO_2 (Fig. 8.4). Within the suites there is also no correlation between Zr/Ta and Zr or Ta concentration, indicating that, although the element concentration may be controlled by (AF)C processes, the Zr/Ta ratio is controlled by the source characteristics.

In fact, Zr/Ta and Yb/Ta correlate well with the Nd and Th isotopic ratios and less significant with the Sr and Pb isotopic ratios. Figure 8.5 shows an inverse correlation between $^{143}Nd/^{144}Nd$ and Zr/Ta in Batu Tara and Lewotolo, suggesting involvement of a component with low $^{143}Nd/^{144}Nd$ and high Zr/Ta, compared to normal mantle values. From Figure 8.2 it can be deduced that bulk addition of SCM to I-DM would not explain these mixing arrays, as the Zr/Ta ratio of bulk SCM would be too low. Involvement of a mantle component with an elevated Zr/Ta ratio due to an ancient depletion event is also unlikely, as this would result in lower $^{87}Sr/^{86}Sr$ and higher $^{143}Nd/^{144}Nd$ ratios, opposite to what is observed.
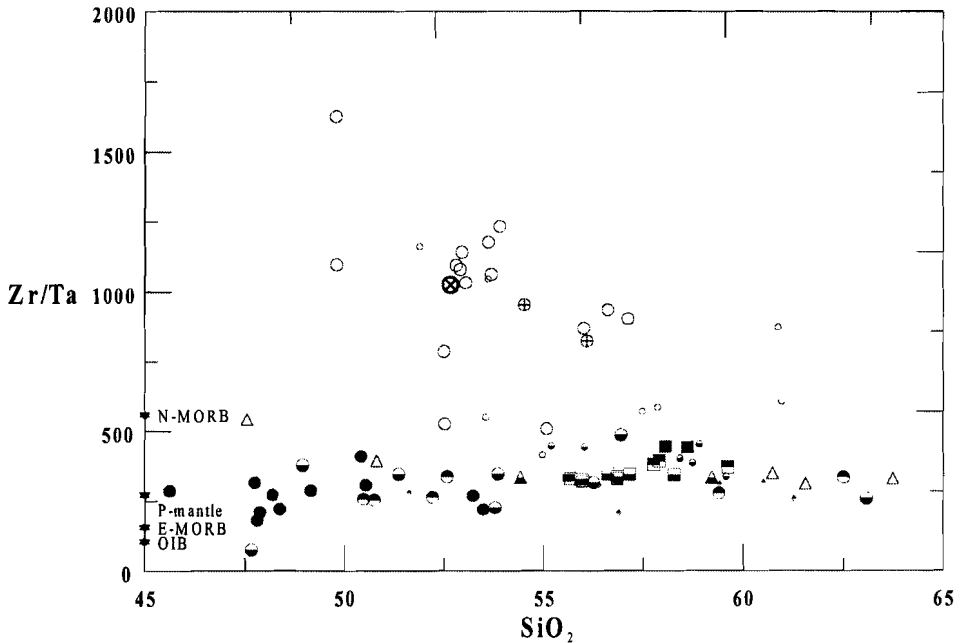
Figure 8.4. Zr/Ta versus SiO_2 demonstrates that there is no influence from crystal fractionation on Zr/Ta ratios in the non-frontal rocks. Also the frontal rocks (open circles) do not contain mineral phases or assemblages that could be responsible for ~80% fractionation in Zr/Ta between 50 and 65%wt SiO_2.

Models involving melts from subducted material

In the previous chapter arguments have been presented for melting of subducted material in the deeper parts of the subduction zone. Brenan et al. *(1994)* have argued that siliceous melts are better transporters of the HFSE than hydrous fluids, which can be deduced from the smaller D's for mineral/melt than for mineral/fluid fractionations. This hypothesis has been tested by the following modelling calculations.
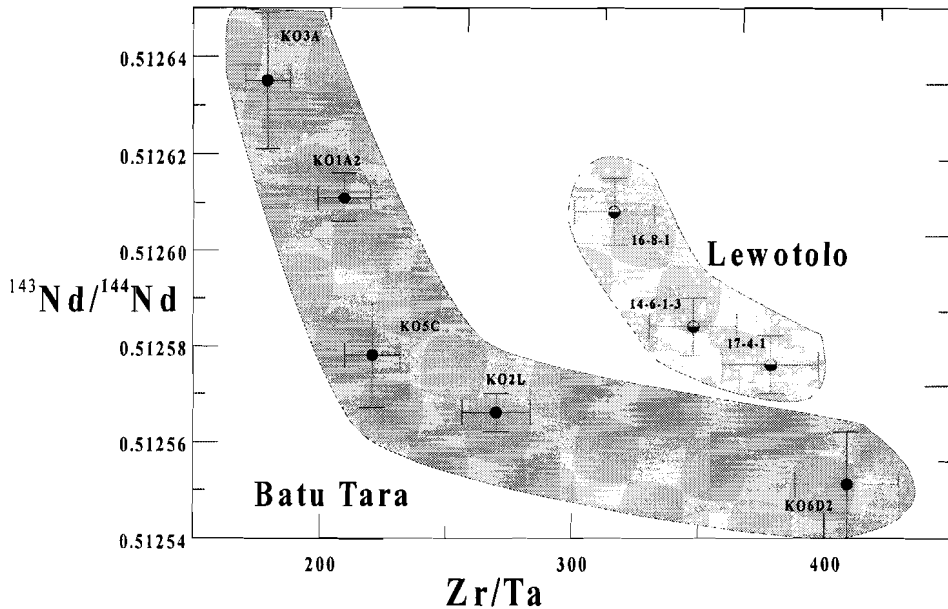
Figure 8.5. Zr/Ta versus Nd isotopes revealing a relation between Nd isotopes and Zr/Ta indicating that the variation of Zr/Ta is source bound.

8.2.2.3 HFSE signature of an SCM-derived melt component

Simple 25% batch melting of an SCM source (eclogite from chapter 7, based on Johnson and Planck, *1993*) without a titanate phase would result in a melt with Zr/Ta too low to be an acceptable candidate (see Fig 8.2b). However, if the same source would contain 1 or 2 wt% rutile, a melt can be produced with Zr/Ta in an order of magnitude necessary for a subduction component. In Figure 8.2 a ratio D^{Zr}/D^{Ta} of 0.05 (5/100) for rutile was chosen according to Jenner et al. *(1993)*. The presence of rutile in the APS slab is not unlikely, as rutile-bearing eclogites have been documented in paleo-subduction settings and HP terrains *(Nelson, 1995, Sorensen and Barton, 1987; Philippot and Selverstone, 1991; Vielzeuf et al., 1990)*, and has been predicted to be stable during melting of material with crustal compositions *(Green, 1986)*. Although experimental data about Nb/Ta fractionation is still sparse *(Jenner et al., 1993)* and the precision of low-level Nb measurements remains a challenge, the study of Nb/Ta ratio in

105

arc rocks is probably the most promising way to resolve the question concerning the role of a residual titanate phase (rutile). In a recent paper Stolz et al. *(1996)* included some of the APS rocks in a comparison of Nb/Ta ratios in different settings and found that Nb/Ta ratios (25-30) in K-rich alkaline rocks deviated from bulk earth/mantle values (17.5).
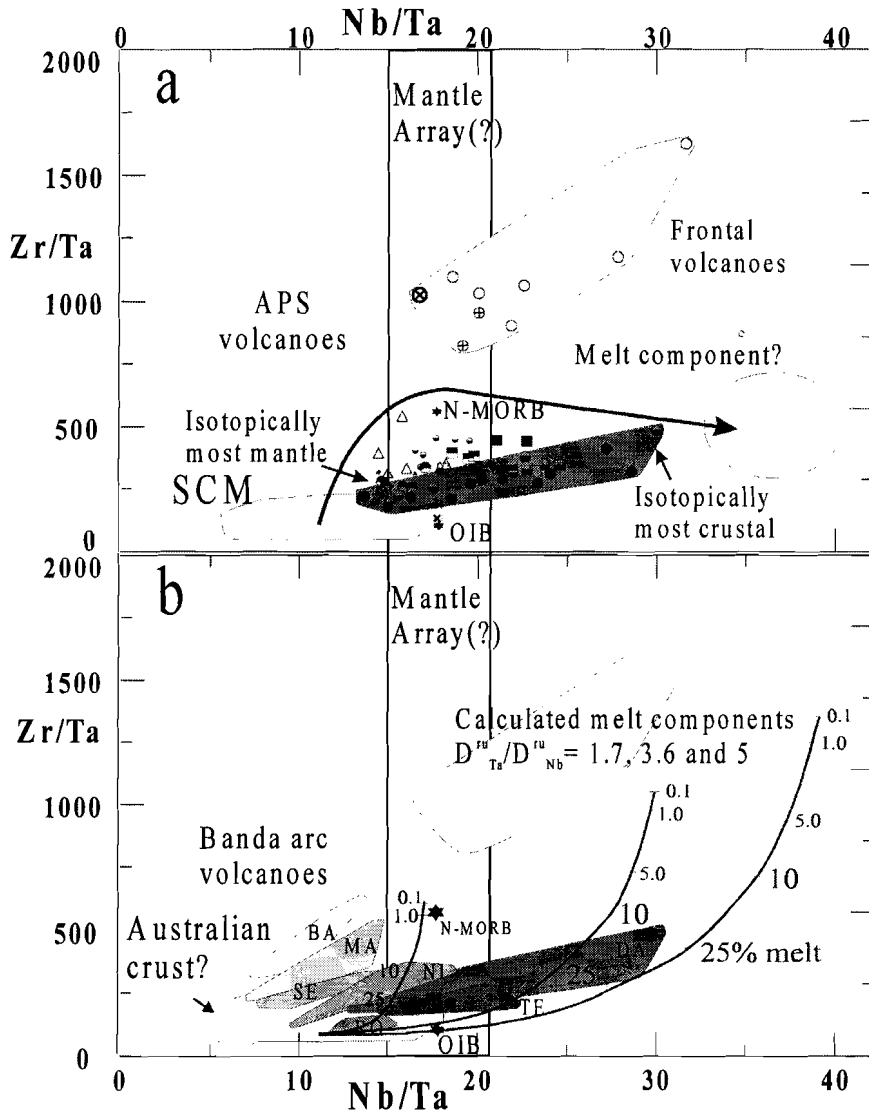
Figure 8.6. a: Plot of Zr/Ta versus Nb/Ta ratios. The Nb/Ta signatures point to 3 different components: Depleted Mantle, a melt component with high Nb/Ta and Australian crust.
b: The composition of SCM melt from an eclogite with 1% residual rutile was calculated for three different ratios of D^{ru}_{Ta}/D^{ru}_{Nb} on the basis of arguments discussed in the text.

Figure 8.6 shows a plot of Zr/Ta versus Nb/Ta, illustrating the possible influence of rutile in the APS. The following observations are important:

First: There appears to be a consistent behaviour of HFSE in the APS and the Banda Arc, suggesting that similar components are involved.

Second: Nb/Ta ratios in the non-frontal volcanoes correlate with isotopic tracers, as is the case for Zr/Ta (Figure 8.5), implying that the component most influenced by SCM has also the highest Nb/Ta values. Important to note is that the average Nb/Ta ratio of *bulk* SCM would again be too low, indicating that extraction of a high Nb/Ta *partial melt* from the SCM source is required.

In order to identify the residual mineral responsible for Nb/Ta fractionation during SCM melting, the effect of relevant minerals on bulk distribution coefficients in simple batch melting scenarios has been explored:

Rearranging the formulas for simple batch melting shows that:

$$\frac{(Nb/Ta)_{melt}}{(Nb/Ta)_{source}} = \frac{D_0^{Ta} + \dfrac{f}{1-f}}{D_0^{Nb} + \dfrac{f}{1-f}}$$

where D_0 is the **bulk** distribution coefficient and f is mass fraction of melt produced. The formula demonstrates that only if one or both D_0 values are significantly larger than $f/(1-f)$, a change in the ratio of the melt relative to the source can expected.

For example, for 25 % melt generation *(Johnson and Planck, 1993)* the formula becomes:

$$\frac{(Nb/Ta)_{melt}}{(Nb/Ta)_{source}} = \frac{D_0^{Ta} + 0.33}{D_0^{Nb} + 0.33}$$

The most extreme Nb/Ta value observed in the high-K APS rocks is 30 but as this value is already the value of a mixture of SCM-melt and mantle, the actual Nb/Ta in the SCM-melt may even have been higher and therefore the value used is a minimum estimate.

The average SCM value of 10 is close to crustal values of 11 *(Green, 1995)* and can therefore be taken as representative for continental-type slab material in a first approximation. Using these values it appears that a bulk distribution coefficient ratio of *at least* 3 is needed, as:

$$\frac{30}{10} = \frac{D_0^{Ta} + 0.33}{D_0^{Nb} + 0.33}$$

In similar fashion, the constraints for the relation between the distribution coefficients of Zr/Ta and Nb/Zr can be calculated. Comparison of these results with experimental

distribution coefficient ratios will then allow us to identify residual minerals that are possibly present during melt generation.

	D^{Ta*}/D^{Nb*}	D^{Zr*}/D^{Ta*}	D^{Nb*}/D^{Zr*}	$D^{HFSE} > 1$
SCM Bulk APS	**3**	**0.25**	**1.8**	**+**
Olivine	1	1.1	0.9	-
Opx	1	1	1	-
Cpx	1.1	1	0.8	-
Garnet	1	1.25	0.8	-
Phlogopite	1	0.8	1.3	-
Amphibole	1	1.5	0.7	-
Rutile solid/melt	1.9	0.05	11	+
Rutile solid/fluid	0.75	0.4	3	+

Table 8.4. Relations between HFSE distribution coefficients enabling to predict the direction in which the melt composition will change during progressive melting. Asterisk indicates that corrections were applied for f/(1-f) = 0.33. All are solid/melt distribution coefficients except for rutile solid/fluid D.

As the data in Table 8.4 show, only rutile is capable of producing the right effect, although in this simple model the D^{Nb*}/D^{Zr*} ratio seems larger than required. New results from Hf-isotope analyses by P.Z. Vroon *(pers. comm., 1999)* suggest the additional presence of residual zircon. Because this will lower the bulk $(D^{Nb*}/D^{Zr*})_0$, it is conceivable that a rutile-zircon combination would bring the ratio within the required limits *(Vroon et al., 1998)*.

The conclusion that rutile is dominating the control over the HFSE budgets is in agreement with the findings of Brenan et al. *(1994)*. However, from the APS data it can be inferred that the $(D^{Ta}/D^{Nb})_0$ ratio for rutile may be somewhat larger than the 1.25-2 value measured by Brenan et al. *(1994)*. Calculations using the eclogite (Table 8.1) with 1 wt% rutile, 25% melting *(Johnson and Planck, 1993)* suggest that the $(D^{Ta}/D^{Nb})_{rutile}$ may be about 3.6 instead of 2, in order to obtain a bulk $(D^{Nb}/D^{Ta})_0$ of 3 or less. Based on these constraints the possible composition lines for the melt component were drawn in Figure 8.2b and 8.6b, using values of 99.5, 190 and 250 for $(D^{Ta})_{rutile}$.

Two-stage process?

An alternative way to create a high Nb/Ta magma envisions a two-stage model *(pers. comm. J. Hertogen, 1999)*. In this model the mantle wedge is infiltrated by a melt with Nb/Ta = 19 *(see Fig. 8.6b)*. Subsequent melting of this fertilised mantle in the presence of residual rutile is able to raise the Nb/Ta ratio to the required 30. However, at the same time, too high Zr/Ta ratios (above 3000) would occur, unless this ratio would again be buffered by residual zircon. In absence of supporting evidence this option remains highly speculative.

Similarity with the Banda Arc

In Fig. 8.6b, data from the Banda Arc *(Vroon, 1992)*, including re-measured high-precision data for Nb *(P.Z. Vroon, pers. comm.)*, complement the trends observed in the APS. The Banda

Archipelago and Manuk plot on a line between the more extreme Werung samples and a low Nb/Ta component. The other Banda-Arc centres lie more between the suggested SCM-melt component and the same low Nb/Ta component. Note that these trends are not low-pressure differentiation trends, as both Zr/Ta and Nb/Ta show no correlation with SiO_2 or other differentiation indices. Furthermore, the ratio trends correlate with isotopic changes.
These observations suggest that magmagenetic processes that govern the behaviour of HFSE in the APS are similar to those in the Banda Arc.

8.2.2.4 Low Nb/Ta component

After the above discussion on the origin of the high Nb/Ta component, the question remains, which of the components thus far proposed for the APS could represent the low Nb/Ta component.

1st: Altered oceanic crust? A potential source could be the leading oceanic part of the Indian-Australian plate that has been subducting before arrival of the Australian continental margin. As mentioned in chapter 6, there is a lack of high-quality data on HFSE in altered oceanic crust. Recent data presented by Staudigel et al. *(1996)* indicate that HFSE abundances in altered MORB are close to those in pristine MORB, implying little or no change in the Nb/Ta ratio during alteration. Although the element compositions of the Indian Ocean mantle domain differ from the Atlantic and Pacific domains, and Nb/Ta ratios do scatter in the Indian Ocean domain (*F. Frey, pers. comm. 1997)*, these ratios are certainly not less than 10. This clearly excludes oceanic crust as the source of the low Nb/Ta component.

2nd: I-EM? Some Enriched Mantle-type volcanics appear to have Nb/Ta ratios lower than chondritic values. In a compilation by Green *(1995)* relatively low Nb/Ta ratios (but >10) are reported in more silicic series of Oceanic islands, a feature that was attributed to ilmenite fractionation. In the APS all rocks types have low Nb/Ta and the arrays point to a component with Nb/Ta below 5. This makes such an OIB-related component highly unlikely.

3rd: SCM? The average Nb/Ta ratio of SCM is 13 ± 4, which is higher than the Nb/Ta value of the component searched for. It can be hypothesised that the SCM residue that remained after extraction of a high-Nb/Ta melt is involved. However, given the high distribution coefficients for Nb and Ta (> 1) in the residual assemblage, no significant fractionation of Nb/Ta can be expected as long rutile remains a stable phase.

4th: Fluid? As documented by Brenan et al. *(1994)*, Ta has a greater affinity for the fluid than Nb. Thus, infiltration of a slab-derived fluid could potentially lower the Nb/Ta ratio of a magma source region. However, the following observations argue against this option. Samples with low Nb/Ta ratios do not have the high Ba/Th and Ba/La ratios and extreme ^{238}U excess of the frontal volcanoes, signatures that we attributed to the activity of a hydrous fluid in chapter 7. Furthermore, low Nb/Ta samples of Batu Tara have the highest concentrations of Nb and Ta, which is consistent with siliceous melt as a transport medium of HFSE rather than a hydrous fluid *(Brenan et al., 1994)*.

109

5th: Local mantle wedge? In the discussion of the frontal volcanoes it was pointed out that there is no evidence for a low Nb/Ta component in Indian Ocean mantle domains. A mineralogical control during the melting process is also unlikely. It is inconsistent with the co-variation of Nb/Ta and $^{143}Nd/^{144}Nd$ observed in the Banda Arc. Furthermore, although an across-arc decrease in K/Rb could reflect a change from breakdown of amphibole to breakdown of phlogophite *(Tatsumi, 1992)*, the Batu Tara samples do not show within-suite correlations between K/Rb and Nb/Ta ratios. These would be expected if hydrous minerals control the HFSE fractionation.

6th: Australian continental crust? Lithologies within continental crust can have the required low Nb/Ta signatures. Crustal values between 5 and 15 have been reported for the central parts of California and the Andes *(Green, 1995 and ref. therein)*, where an inverse correlation between Nb/Ta and Nb concentration in volcanics suggests crustal contamination or crustal melting. Absence of continental crust in the upper block in the APS precludes contamination of magmas en-route to the surface, which leaves involvement of the subducted continental margin as the only alternative. Because many samples of the Shaw Batholith in western Australia *(Bickle et al., 1989, see also chapter 6)* have Nb/Ta below 10 and Zr/Ta below 20, Australian continental basement should be considered as a candidate with the appropriate HFSE signature.

HFSE resume:

The HFSE systematics thus favour a scenario of a depleted mantle wedge, which, in the source regions behind the front, is mixed with a subducted component that presumably consists of Australian crustal material. As mentioned in chapter 6, there is little need to invoke an enriched Indian Mantle source, if Australian continental crust is involved. To this mixture a high Nb/Ta siliceous melt is added. This probably originates from partially melted SCM in the presence of residual rutile, possibly associated with zircon. Until it is unequivocally proven that high Nb/Ta ratios do occur in depleted Indian Ocean mantle, it cannot be ruled out that rutile is also present in the mantle-wedge source region at the front. Given the significant differences between HFSE distribution coefficients for amphibole and phlogophite obtained from experiments *(Green, 1994)* and natural samples *(Ionov and Hofmann, 1995)*, the importance of these minerals in controlling HFSE behaviour in the APS sources is difficult to evaluate.

8.2.3 The REE/HFSE relations as indicators for the nature of the contributing components

As shown in the previous section, the Yb/Ta can be used do discriminate between the different sources. In a plot of Ce/Ta versus Yb/Ta (Fig. 8.7) an attempt is made to investigate the behaviour of the lanthanides in magma genesis across the arc. Note that mixing relations are represented by straight lines. In Figure 8.7a the pronounced increase of the LREE/HREE ratio across the arc is depicted by the tangent of the array formed by each centre. The depleted nature of the frontal rocks is demonstrated by the low angle Ce/Yb ratios. The most notable features in Figure 8.7 are:

1st: the good separation between frontal and non-frontal rocks and,
2nd: the fact that the frontal rocks have Ce/Ta values higher than MORB and/or the mantle array.

8.2.3.1 The frontal centres

It is commonly assumed that the LREE can be transported in hydrous fluids to a certain extent. However, large-scale Ce enrichment by a fluid of the frontal APS sources is very unlikely as a high-Ce fluid would have very high Ce/Ta and extreme Ce/Yb ratios in combination with a low Yb/Ta. Furthermore, this fluid would have concentrations of Ce and Nd more than 100 times that of a depleted mantle (calculated using the 10% fluid from an eclogite as before). This would conflict with the observed high $^{143}Nd/^{144}Nd$ mantle-like values in the most depleted Werung samples, which indicates that there is no large addition of REE (and certainly not of HREE) from the slab at the front.

Weis and Frey *(1996)* described the composition of basalts at the DSDP 261 and 259 sites as typical depleted Indian MORBs. Plotting these and other Indian Ocean data from Weis and Frey *(1996)* in Figure 8.8 it is clear that the frontal Werung samples are within the boundaries of the depleted Indian MORB field for Yb/Ta. The slightly higher LREE/HFSE (Ce/Ta, Ce/Nb) could be due to a melting control.

The Ce/Ta ratios of Werung are higher than I-DM *(Weis and Frey, 1996)* but they do not correlate with fluid indicators like Ba/Th and Sr/Nd (chapter 7). This may imply involvement of a residual phase, which suggests that the higher than I-DM *(Weis and Frey, 1996)* Ce/Ta in the APS mantle wedge might be due to a phase with more affinity for the HFSE than the light and heavy REE. Because garnet, amphibole and phlogopite all have $D^{Ce}/D^{Ta} < 1$, they should be considered as possible candidates. Melting of an I-DM source (0.1x DSDP261, garnet-, amphibole- or phlogophite-peridotite, (see Table 8.1) would yield a melt with slightly enhanced Ce/Ta in the required range (between 100 and 150).
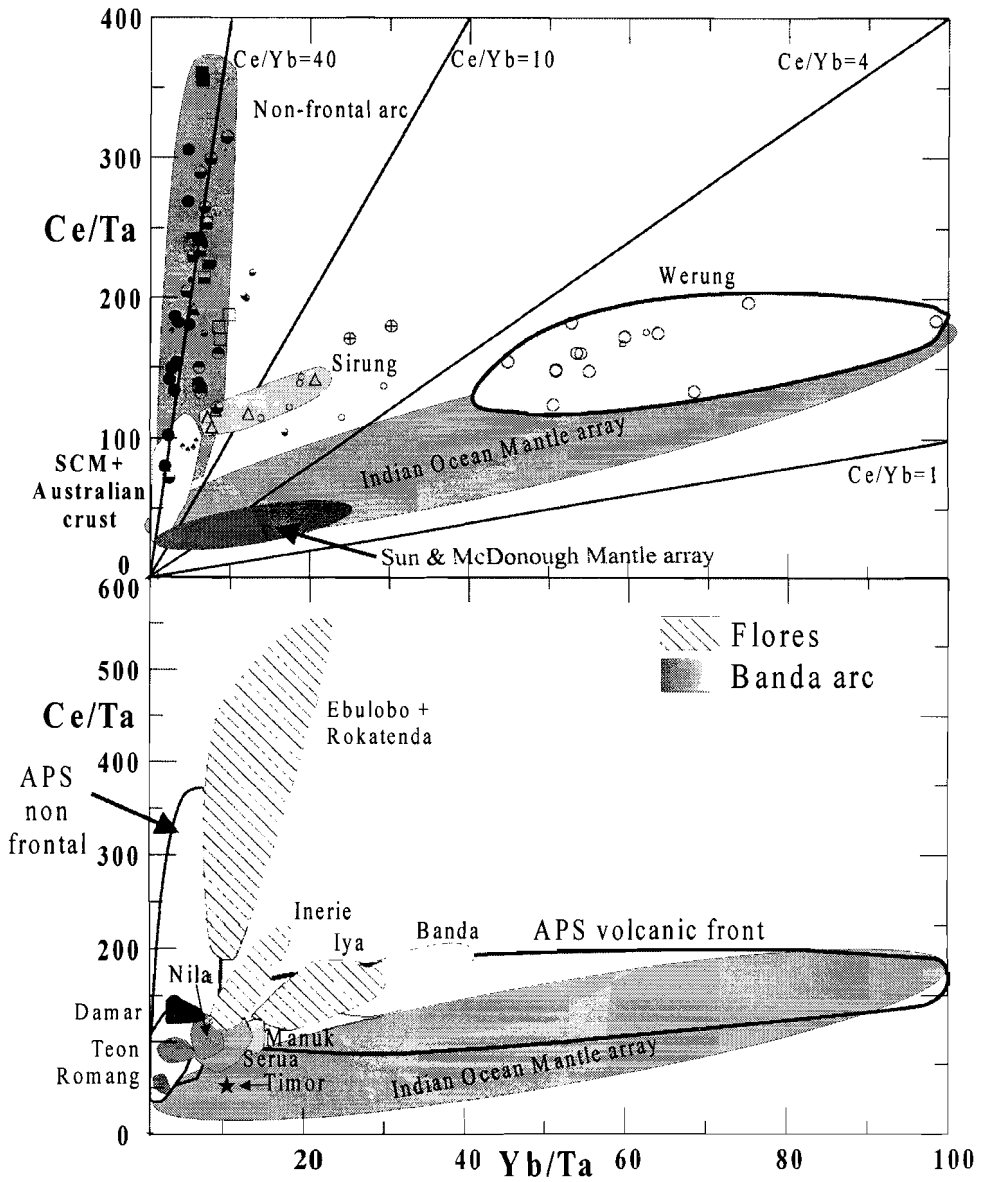
Figure 8.7. Ce/Ta versus Yb/Ta in the APS (a) and Eastern Indonesia (b). Indian Ocean Mantle array calculated from Nb data from Weis and Frey *(1996)* and F. Frey *(pers. comm., 1997)*. Banda Arc data from Vroon *(1992)* and Flores data from Stolz et al. *(1990)*.
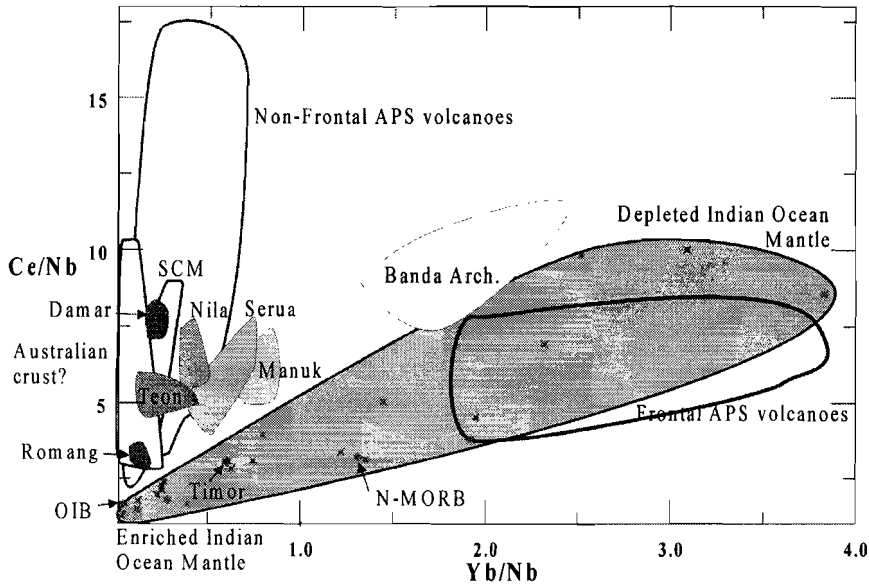
Figure 8.8. Ce/Nb versus Yb/Nb showing the presence of I-DM at the front. High Ce/Nb in the non frontal samples cannot be explained by components alone and must be due to mineralogical control during melting in the slab. Indian Ocean Mantle array from Weis and Frey *(1996)*

8.2.3.2 The non-frontal centres

In Figure 8.7 and 8.8 the data are fanning from the frontal rocks upward to the non-frontal rocks. This hints at increasing involvement of a component with elevated LREE/HFSE and low HREE/HFSE characteristics. The central and rear arc rocks have increasingly higher Ce/Yb and Ce/Ta ratios. The Ce/Ta and Ce/Yb ratios of the non-frontal rocks shows no systematic behaviour in a plot versus SiO_2, thus ruling out significant crystal-fractionation effects on the Ce/Ta and Ce/Yb composition of the magma.

The Banda Arc volcanics match the APS results in Figure 8.7b and 8.8. The Banda Archipelago is probably underlain by a depleted mantle wedge like the frontal APS volcanoes. The rocks from the islands Damar, Teon and Romang individually show the same tendencies as found in the APS. The Flores samples from Stolz et al. *(1990)* also comply with the APS observations in Figure 8.7b: volcanoes with depleted character at the volcanic front (e.g. Iya) and volcanoes with extremely high Ce/Ta are also present (Rokatenda, Ebulobo), although their signatures are less well constrained due to the limited data set. There is a correlation between the Ce/Ta ratio and Nd (Fig. 8.9), Sr and Th isotopes, indicating a relation between Ce/Ta variation and source characteristics.
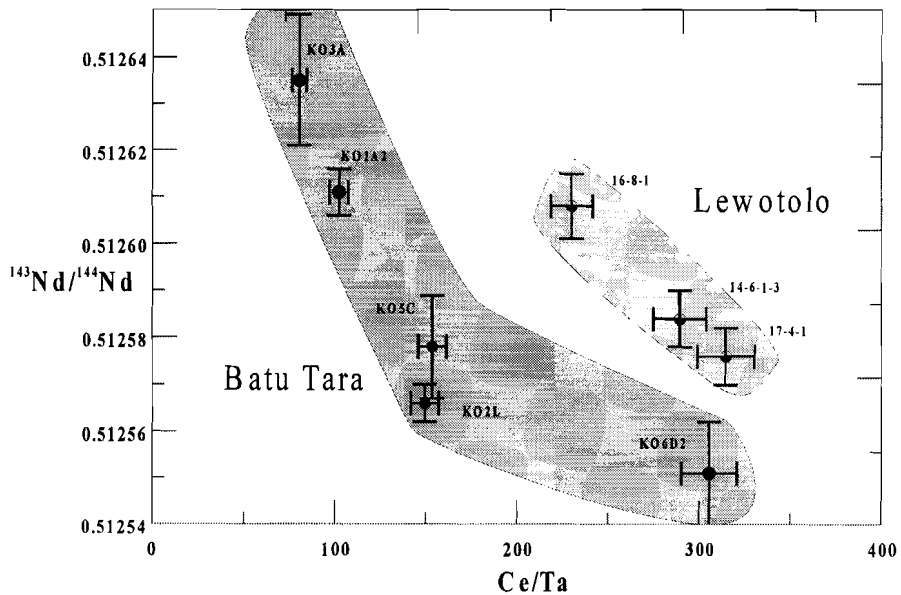
Figure 8.9. Ce/Ta versus Nd isotopes demonstrating that a high Ce/Ta ratio is a magma source characteristic.

Which are the endmembers for the non-frontal rocks?

8.2.3.3 The high Ce/Ta component

The result of simple batch melting of SCM with a rutile-free eclogite-facies mineral assemblage falls within the boundaries of the non-frontal array, but this model does not explain the most extreme Ce/Ta ratios. When residual rutile is added, a melt composition with a sufficiently high Ce/Ta ratio can be generated. Mixing of this high Ce/Ta component with a low Ce/Ta component can explain the array of the central and rear arc volcanoes.

8.2.3.4 The low Ce/Ta component

The most problematic question again concerns the origin of the low Ce/Ta (LREE/HFSE) and low Nb/Ta component. Using the same order as in the HFSE discussion, the following potential endmembers are discussed:

1st: Altered oceanic crust? Not likely, since Staudigel et al. *(1996)* have documented an increase in Ce/Ta in the altered oceanic crust to values between 60 and 75, compared to NMORB with 57.

114

2nd: Enriched Indian Ocean mantle? This domain has Ce/Ta ~30, Ce/Nb>1.3 and Yb/Ta~0.8 due to the relatively high HFSE content compared to NMORB. Because these values are also observed in the crustal material, they are not sufficiently diagnostic.

3rd: SCM?
Bulk SCM has Ce/Ta, Ce/Nb, and Yb/Ta ratios that fall within the required range.

4th: Fluid?
A hydrous fluid would have elevated Ce/Ta around 400, which is too high for the low Ce/Ta component.

5th: Local mantle wedge?
If a (depleted) mantle similar to that below Werung is assumed, there is need for a component with an even lower Ce/Ta ratio.

6th: Australian crust?
Australian continental crust has only slightly lower Ce/Ta than SCM, and thus could also be a possible source.

8.2.3.5 Three component mixing?

From the above analysis it can thus be concluded that Enriched Indian Ocean mantle, SCM or Australian continental crust could all be responsible for the low Ce/Ta and Nb/Ta signal. The best way to discriminate between SCM and Australian continental crust would be to combine the two ratios with an isotopic tracer. Lead isotopes would be the most suitable, as they provide evidence for an along-arc variation in the subduction component. They show, however, no co-variations with Ce/Ta or Nb/Ta, presumably due to swamping of mantle sources with slab-derived Pb (Figure 6.11). Nd isotopes do show such trends, as documented above, and are therefore preferred here.

Figure 8.10 shows the APS samples and fields for Banda Arc, Flores, Indian Ocean, SCM, Australian crust and relevant endmember compositions in a $^{143}Nd/^{144}Nd$-Nb/Nd diagram. The advantage of this diagram is that these parameters are insensitive for the fluid component. All samples lie within a triangle formed by a depleted Indian Ocean mantle, SCM-melt (+rutile) and a bulk crustal component.

In order to test the possible endmember combinations quantitatively, two mixing models were constructed: (A) Depleted Mantle with I-EM like mantle and the rutile controlled SCM melt (Fig. 8.11a), and (B) Depleted Mantle with Australian crust and the rutile-controlled SCM melt (Fig. 8.11b). Model A encompasses all the volcanic data except a result from the island of Wetar in the inactive collision zone *(Vroon and Hoogewerff, unpublished)*. The samples from the pillow lavas complex on Timor *(Vroon, 1992)* can be explained as purely mantle-derived (at least as far as Nd and Nb are concerned). Model B accommodates the Wetar sample but not the Romang samples. The latter could be included if a higher Nb/Nd for the local crustal source is assumed.
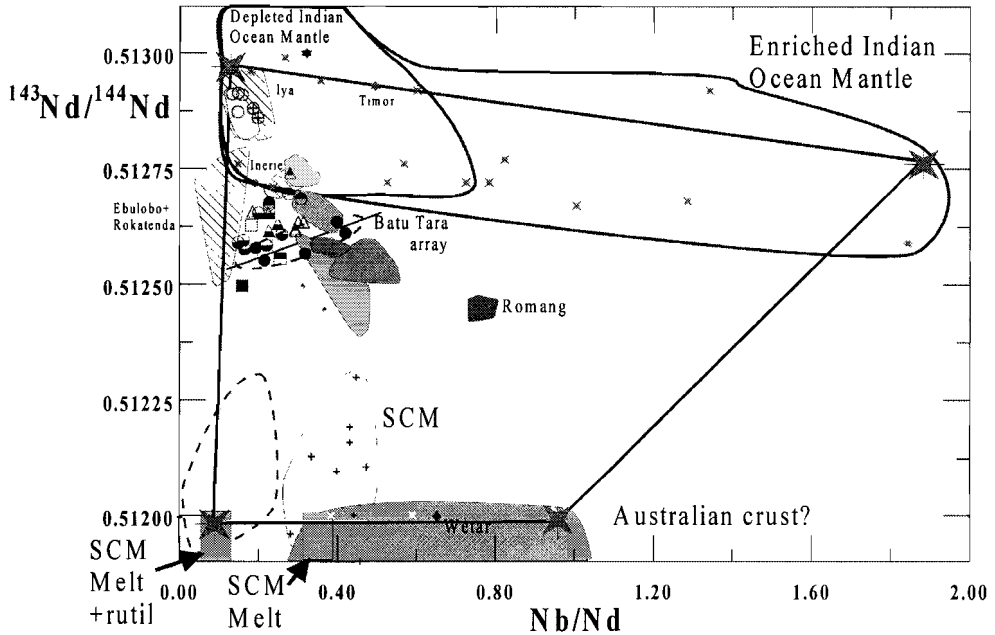
Figure 8.10. A plot of $^{143}Nd/^{144}Nd$ versus Nb/Nd in which mixing relations should be straight lines. The four relevant endmembers are indicated by stars: Indian Ocean Mantle both depleted and enriched, Australian crust and SCM melt with residual rutile.

Model B would favour the domination of the SCM-melt component around Flores and greater affinity for the crustal component in the Banda Arc. Most remarkable are the Batu Tara rocks from the APS, which span the range from the melt side to the crustal side of the triangle (Fig. 8.11b). The large variation in incompatible trace element concentrations (including Nd and Nb) within the Batu Tara samples cannot be explained by simple crystal fractionation *(Stolz et al, 1988; Van Bergen et al, 1992)*, but rather reflects source mixing.

In model A, the within-suite array of Batu Tara can be explained by an increasing influence of the Enriched Mantle component, while the contribution of SCM-melt remains more or less constant.

116
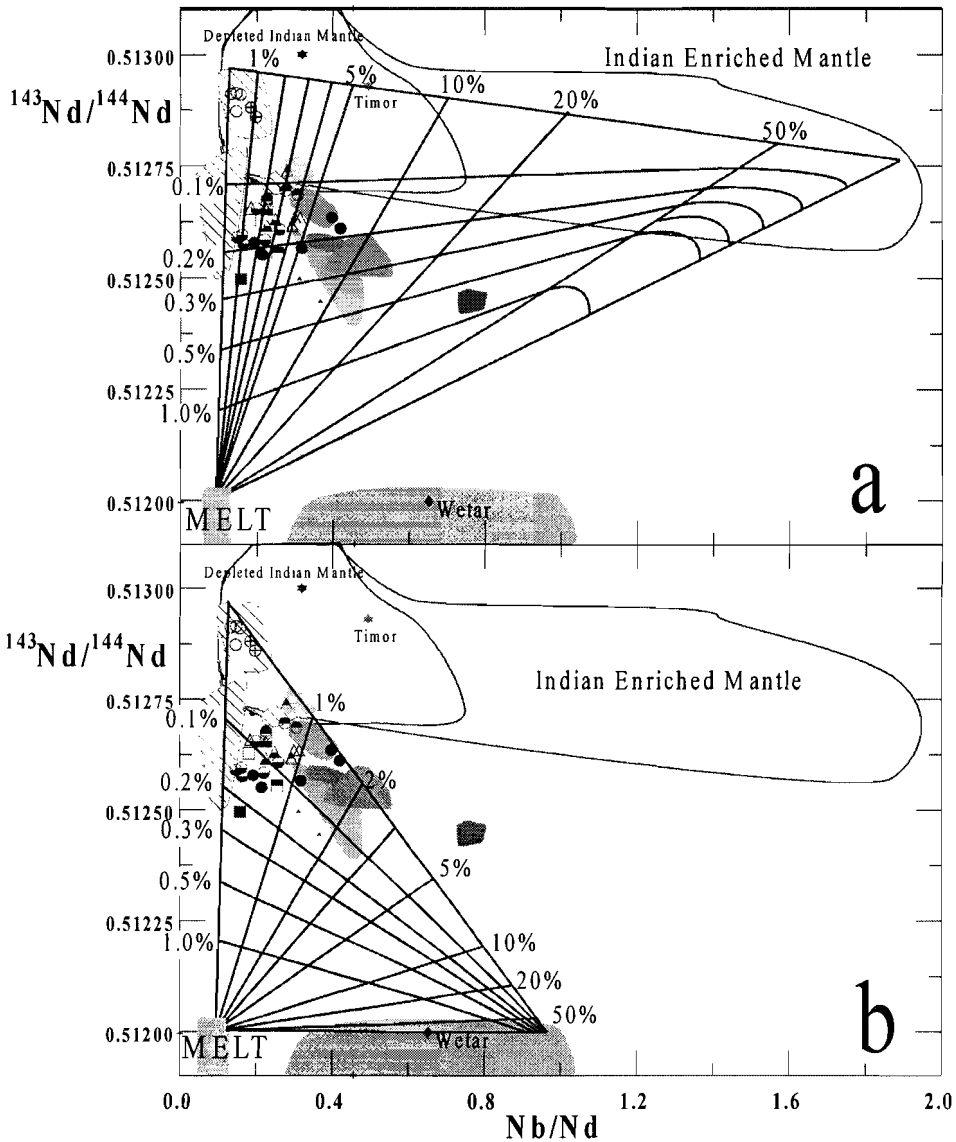
Figure 8.11. a: Mixing between two Indian Ocean mantle components and the rutile-controlled SCM melt. **b:** Mixing between depleted Indian Ocean mantle, rutile-controlled melt and Australian crust. Percentages refer to a three-component system: % melt + % I-EM or % Crust + % depleted Indian Ocean mantle (= 100 - % melt - % (I-EM/Crust)).

117

The combination of Nb/Nd and ^{143}Nd/^{144}Nd alone thus seems not able to provide a conclusive answer to the preferred scenario. In order to find a more decisive answer, the ^{143}Nd/^{144}Nd and Nb/Nd ratios of each individual Batu Tara sample were used in an inverse three-component model (see appendix of this chapter) that predicts the fractions of the various endmembers involved. The mathematical formulation was developed in such a manner that it is only a function of the element ratios in the endproduct and of the concentrations in the sources, thus eliminating the influence of fractionation on the incompatible-element concentrations in the rocks (see the appendix of this chapter).

Then for each sample the most likely Nb and Nd concentrations of its source were calculated. The most plausible model is inferred from the fit between these calculated source concentrations and the observed concentration trends.

The Batu Tara samples with the highest ^{143}Nd/^{144}Nd have the lowest Nd content. Fig. 8.12 shows that the calculated source concentration and the values observed in the samples agree better in the crust-model (B) than in the enriched-mantle-model (A). Differences in the slopes of observed and modelled trends can be attributed to a too low Nd_{crust}/Nd_{mantle} ratio assumed in the model. In theory, difference in degree of melting (calculated from the ratio of observed concentration divided by the model source concentration and assuming simple batch melting) could also explain some of the Nd concentration variations. However, the degree of (simple batch) melting in the A-model would have to vary by a factor of 10 (0.1-1%) to match the calculated source values with the measured values, which seems unlikely for a single volcano. Moreover, it does not explain the isotopic variations.

The B-model does allow for the isotopic trends and predicts more homogenous melt percentages (0.5-0.8%), which seem more realistic. Both models can explain the variation in Nb concentrations (not shown), but again the A-model requires large differences in the degrees of melting. In the B-model extremely little SCM-melt (<0.01%) contributes to the source of KO1A and KO3A, increasing to 0.1% for KO6D. The crust contribution in the B-model ranges from 13% to 4%, respectively. In the A-model the variations of the contributions are less extreme: about 0.2% SCM-melt and 7-2 % Enriched Mantle can reproduce the data.

Although the crust-model (B) is the most attractive and fits with the continental He-isotope signature, it would be interesting to check models that include both an inhomogeneous mantle and an extra crustal reservoir. Several attempts were made to model a four-component mass-balance calculation using the Nd isotopes, Nb/Nd and either Ta/Nd, Zr/Ta or Yb/Ta. However, as the crustal component and the enriched-mantle component are very similar in HFSE and REE trace element ratios, no meaningful results were obtained.

End member input parameters			
	Nd	Nb	$^{143}Nd/^{144}Nd$
Depleted Mantle	0.71	0.09	0.51297
Enriched Mantle	3.24	6.1	0.51276
Melt SCM	265	25	0.51200
Crust	2.6	2.5	0.51200

Observed values in Batu Tara				
			Input parameters	
	Nd	Nb	$^{143}Nd/^{144}Nd$	Nb/Nd
KO1A	42	17.6	0.512611	0.42
KO3A	44	17.4	0.512635	0.4
KO5C	50.5	9.6	0.512578	0.2
KO2L	58	18.2	0.512566	0.32
KO6D	61	13.1	0.512551	0.19

Results of 3-component model calculations				
Enriched Mantle model				
	%SCM Melt	% D-mantle	% E-Mantle	Nb	Nd
KO1A	0.2	92.7	7.1	0.56	1.33
KO3A	0.1	93.6	6.3	0.50	1.26
KO5C	0.2	97.8	2.0	0.24	1.24
KO2L	0.2	94.8	5.0	0.44	1.37
KO6D	0.2	98.2	1.7	0.26	1.31

Crust model				
	% SCM Melt	% D-mantle	% crust	Nb	Nd
KO1A	< 0.1	86.8	13.2	0.41	0.98
KO3A	< 0.1	88.0	12.0	0.38	0.95
KO5C	0.1	95.2	4.6	0.22	1.14
KO2L	0.1	89.9	10.0	0.35	1.09
KO6D	0.1	96.0	3.9	0.24	1.19

Table 8.4. Input parameters and results for three-component models evaluating the most likely source configuration for Batu Tara volcano (for model see appendix of this chapter).

It is generally accepted that Enriched Mantle may have become enriched by addition of crustal material, which is consistent with the lack of „ratio contrast" *(see also Weaver, 1991)*. Enriched Mantle and crustal material differ in their LILE signatures, but in subduction settings it is difficult to trace the delicate differences in LILE ratios (e.g. U/Pb, Rb/Sr, Ba/Th), as they are masked by the high input of LILEs via slab-derived melt or fluid.
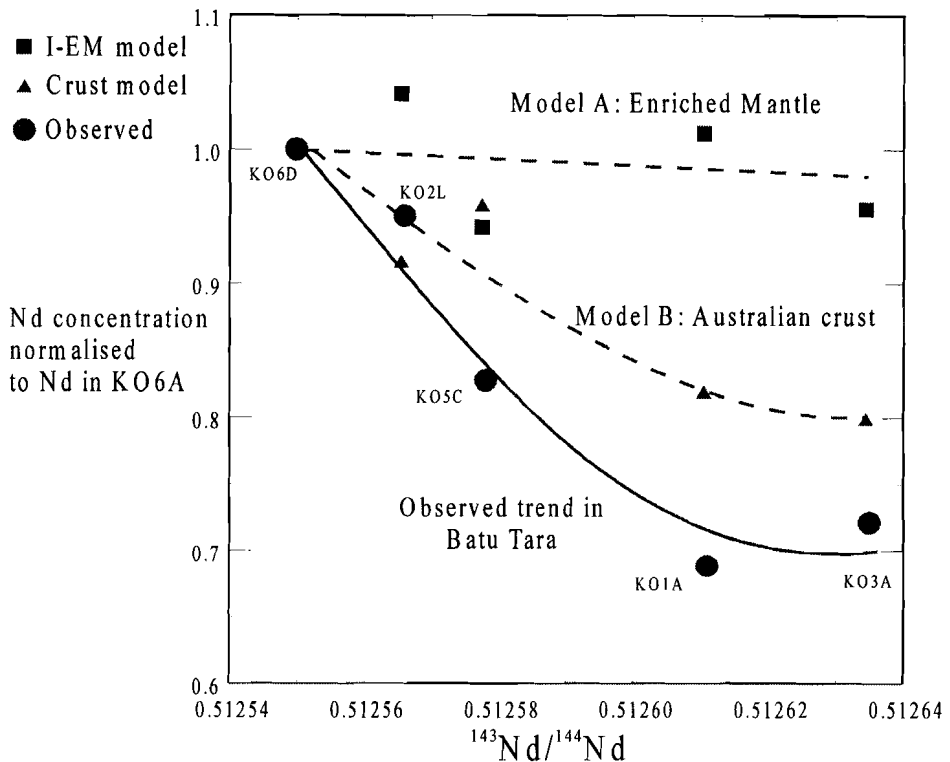
Figure 8.12. Inverse modelling results for Enriched Mantle (A) and Australian continental crust (B) scenarios, compared with the observed concentration trend in the Batu Tara samples. Neodymium concentrations are normalised to values in KO6A. The crust model approaches the observed trend best.

In conclusion, if fluid is included, a total of five components could be involved in the APS, the East Sunda Arc and the Banda Arc. Considering the documented inhomogeneity of the Indian Ocean *(Weis and Frey; 1996)* on scales less than 1000 km, there is also no reason to expect a completely homogenous sub-mantle in this region. Vroon *(1992)* suggested a systematic change in the mantle sources of the Banda Arc when approaching the collision zone. This systematic variation coincides with a change in the tectonic setting and with growing influence of the Australian continent, but the present analysis suggests that a more random variation of mantle components might be superimposed.

8.2.4 LILE/HFSE and LILE/REE systematics: an attempt to reconstruct the mineralogical composition of the frontal magma source

In the previous sections the nature of the different mantle and subduction-related sources and fluxes contributing to the magma source were studied. In this section an attempt is made to constrain the mineralogy of the frontal magma source region, starting from the components that have been identified.

The principal hydrous minerals found in metasomatized rocks have high LILE contents. In order to discriminate between the LILE signatures in the slab-derived melt and fluid fluxes, a three-dimensional plot is constructed with Yb/Ta versus Ce/Ta (Fig. 8.9 and 8.11) in the basal plane and LILE/HFSE ratios on the vertical axis. This plot comprises all the important chemical relations in magma genesis: LILE/HFSE (z-axis), LILE/LREE (projection on the right hand back surface), LILE/HREE (projection on the left hand back surface) and LREE/HREE (floor surface) and of course LREE/HFSE on the y-axis and HREE/HFSE on the x-axis.

In Figure 8.13 increasing LILE/HFSE and LILE/(H)REE ratios, relative to I-DM, I-EM, (N-MORB, OIB), SCM or crust, document the fractionation of the LILE from the HFSE and the (H)REE when the melt and fluid components are formed. From the extremely high LILE/Ta ratios it is clear that a little melt or fluid will already dominate the LILE abundance and hence the LILE/Ta ratio in the magma source.

The relations between the components that contribute to the frontal volcanoes are complex. The array of Sr/Ta combined with Yb/Ta of the frontal samples does not simply point to the Sr/Ta and Yb/Ta composition of the fluid component somewhere at the upper right hand side as is the case with the melt component, because almost no Yb and Ta are transported by the fluid. The variation of Yb/Ta was shown to depend on the depletion of the mantle wedge. Therefore the fluid endmember will lie somewhere high above the SCM or crustal fields.

Using the previously mentioned distribution coefficients, the following element ratios were calculated for melt and fluid that originate by melting and dehydration of an eclogitic assemblage:

Ratio	SCM	Melt component	Fluid component
Sr/Ta	113	2600-4400	850-950
Ba/Sr	2.8	7.4-8.1	34-80
Pb/Ta	33	1600-3000	2000-3000
Ba/Th	16	≈19	1000-2500
Th/U	6.6	≈7.4	≈3.2

Table 8.5 Calculated endmember compositions.

Fluid component

Sr/Ta

14000
12000
10000
8000
6000
4000
2000
400

Melt
component

Ce/Ta

300
200
100

20 40 60 80 100 120

Yb/Ta

Mantle

SCM or Crust

⊕ Mantle Sources
☒ SCM /Crust
■ Rear Arc
▲ Central Arc
● Frontal Arc
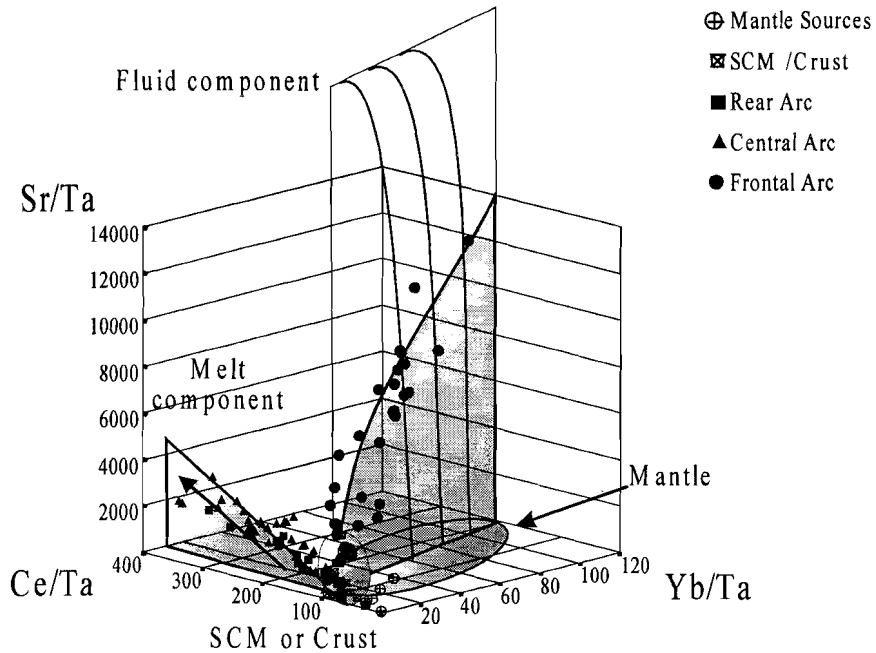
Figure 8.13. Sr/Ta systematics showing high Sr/Ta in the fluid component and less extreme Sr/Ta in the melt component. Yb/Ta is assumed to be dominated by compositional variation in the Depleted Mantle.

To explain the extreme Sr/Ta observed (13000) one could argue that the Sr of the fluid completely swamps the mantle wedge. Calculation of the Sr/Ta ratio of a 10% fluid, using the D's from Brenan et al. *(1995)* and assuming an eclogitic source (cpx:gn:rut:phlog =0.39:0.59:0.01:0.01; *adapted from Nichols et al., 1994*) with a cpx $D_{Sr}^{cpx/fluid}$ of 3.6 (average from Brenan et al. *(1995)*) yields a value of about 100, which is clearly much too low. Taking a $D_{Sr}^{cpx/fluid}$ of 0.48 from experiment 125 of Brenan et al. *(1995)* with eclogite composition, a value of 900 can be calculated for the Sr/Ta ratio in the fluid. However, the $D_{Sr}^{rutile/fluid}$ of 0.01 used in this calculation (see Table 8.3) is already low compared with what can be expected from the melt $D_{Sr}^{rutile/melt} / D_{Ta}^{rutile/melt}$ in Table 8.2. This would imply that a Sr/Ta ratio of 900 is a maximum estimate for the fluid. A larger amount of residual rutile could raise the calculated Sr/Ta in the fluid, but at least 10% rutile would be needed, which does not fit with the results in the previous sections. A smaller fluid fraction has negligible effect on Sr/Ta.

122
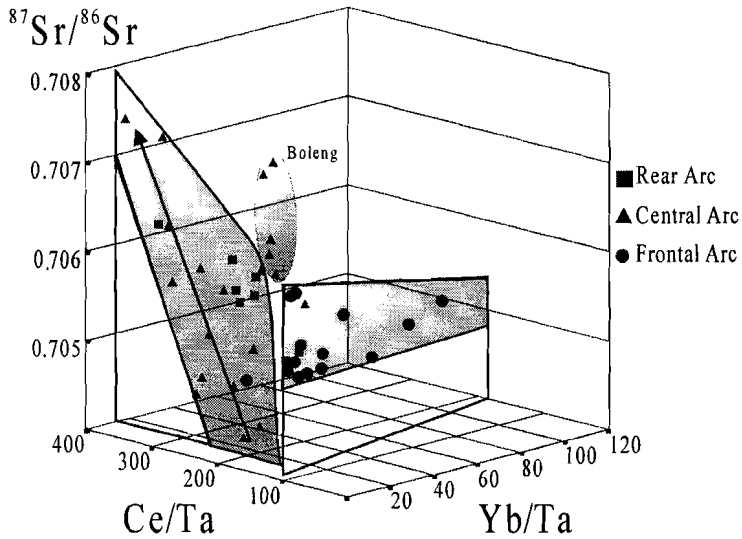
Figure 8.14. In the frontal fluid component only minor variations in $^{87}Sr/^{86}Sr$ are observed. In the CA and RA volcanoes an increase in $^{87}Sr/^{86}Sr$ correlates with increased Ce/Ta in the melt component.

Amphibole or biotite?

To check if amphibole or phlogopite control the LILE abundances, the mentioned procedure was used to calculate the expected Ba/Sr in the magma source. The ratio of $D_{Ba}^{phlog/melt} / D_{Ba}^{amf/melt}$ is much greater than 1 (25), whereas the $D_{Sr}^{phlog/melt} / D_{Sr}^{amf/melt}$ is close to unity (0.5). Therefore, if phlogopite is a residual phase in the magma source, a significant reduction of the Ba/Sr relative to the bulk mantle source can be expected. In cases where phlogopite is absent or amphibole is present, minor modification of the Ba/Sr ratio or significant enhancement can be expected, respectively.

The Ba/Sr ratio of I-DM is about 0.2 *(DSDP261; Weis and Frey, 1996)*. Addition of 0.5% fluid *(see Fig. 7.6)* from the eclogitic slab with Ba/Sr = 33-80 (with or without minor phlogopite in the slab) results in a metasomatized mantle with a Ba/Sr ratio of around 13 (Ba/Ta= 3800 and Sr/Ta=300). Batch melting (10%) of this source with garnet-, amphibole-, or phlogophite-peridotite assemblages would yield Ba/Sr ratios of 12, 16, and 1.0 respectively, and a $^{87}Sr/^{86}Sr$ ratio of 0.7053. In Figure 8.15 Ba/Sr and $^{87}Sr/^{86}Sr$ relations are presented. Clearly, the I-DM mantle with residual phlogopite fits the observations in the frontal APS rocks best. This model would also better explain the rather constant $^{87}Sr/^{86}Sr$ in Werung in Fig. 8.14.

123
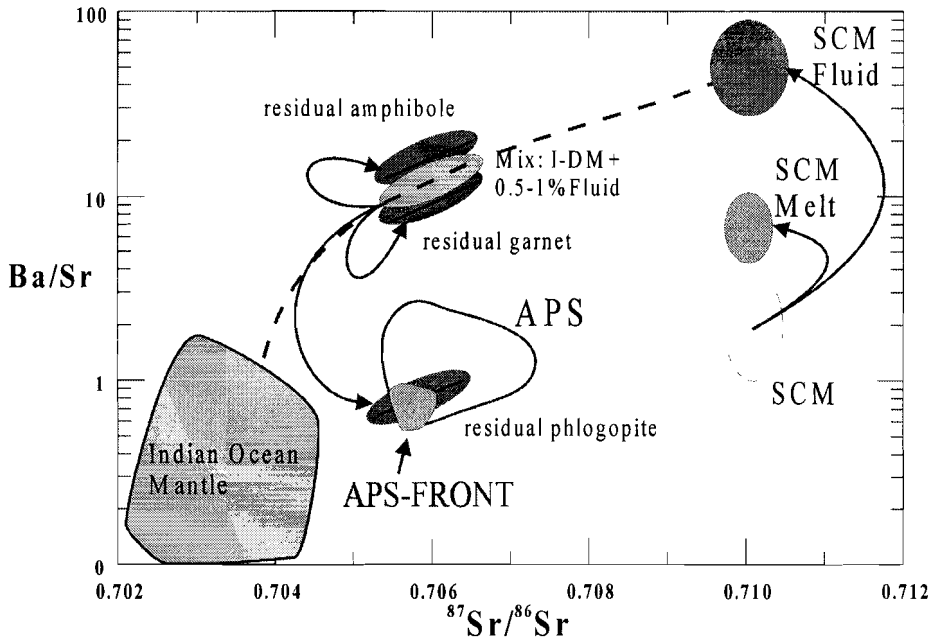
Figure 8.15. Two-stage models for Ba/Sr ratios, illustrating that phlogopite can be a residual mineral in sources at the volcanic front that have been infiltrated by SCM-derived fluid.

To test the validity of the Ba/Sr model, the results of a similar Ba-Th-U model are shown in Figure 8.16. This calculation uses the same constraints as in Figure 8.14. In contrast to the Ba/Sr systematics, amphibole seems the more likely residual hydrous phase in this case. Considering the high ^{226}Ra excess in Werung (see chapter 7), it is actually unlikely that a mineral with a high $D_{Ba}^{min/melt}$ is present in the magma source. On the other hand, this model would fit with results of Tatsumi et al. *(1992)*, who postulated amphibole under the volcanic front in the Izu-Bonin Arc and phlogopite under the central arc.

Both residual phlogopite and amphibole yield calculated Sr/Ta ratios of around 300, which is still too low compared with the observations. A Sr/Ta ratio of 13000 could be achieved with an extra 2% rutile present in the mantle wedge. The presence of a second titanate phase in the magma source region thus seems to be an option to be considered (cf., section 8.2.2.1 and *Foley and Wheller, 1990)*.

124
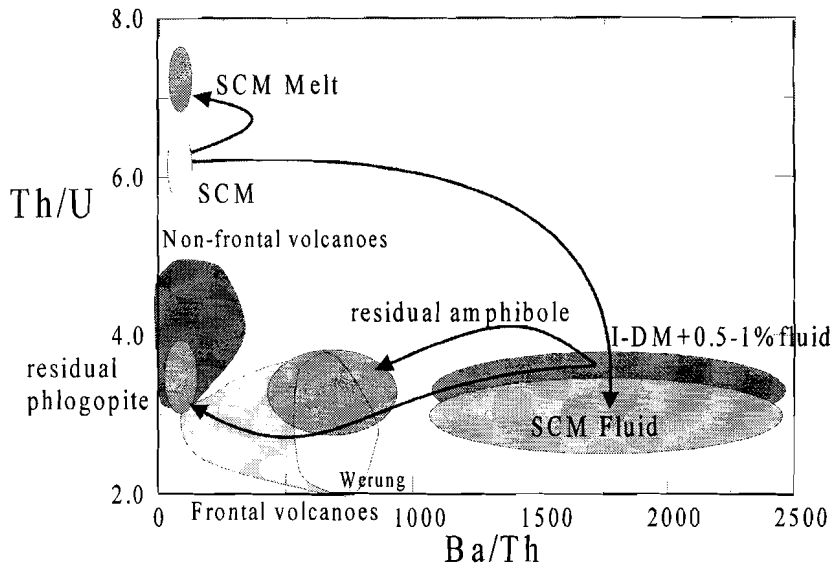
Figure 8.16. Ba/Th versus Th/U favouring residual amphibole (compare Figure 8.14) in the source of the frontal arc.

From these considerations it appears difficult to develop a robust model for all LILEs. A reason for this may be a chemically and/or mineralogically inhomogeneous mantle as a result of very localised metasomatism by the fluid component in particular. The variable amounts of U excess would support this. Another reason could be that the relations between the distribution coefficients assumed for Ba, Sr and Th are not valid in the APS magma source.

8.3 Conclusions

Due to crustal-type chemical signatures of Enriched Mantle, it is difficult to discriminate between contributions from Australian continental crust and an Indian Ocean Enriched Mantle component in the APS. In this chapter it has been demonstrated that an I-EM component is not needed to explain the observations in the APS, but its presence cannot be excluded on geochemical grounds. If I-EM does contribute, Nd-isotope systematics and HFSE/HFSE and REE/HFSE ratios indicate that the contribution from crystalline Australian crust is more important.

However, involvement of a crustal source different from the SCM-melt is required to explain the relations between the HFSE among themselves, between the HFSE and the REE, the extremely low He isotope ratios and $^{208}*Pb/^{206}*Pb$ ratios that are higher than I-EM. Although it has been suggested that the LREE are mobile in hydrous fluid, it seems that this is not the case in the APS. Only the LILE (and U) are enriched in the frontal fluids. The SCM melt phase is capable of transporting all incompatible elements (LILE, LREE and HFSE) from the slab to the magma source region.

An eclogite mineral assemblage of the SCM component, with additional rutile and possibly zircon, is capable of explaining most of the observed HFSE (Nb/Ta) and REE relations, both in the fluid and the melt. Recent Hf isotope work of P.Z. Vroon point to a combination of rutile and zircon.

It has not been possible to uniquely identify the most likely hydrous phase in the magma source region at the front. Although simple systems (e.g. HFSE, Ba-Sr or Ba-Th-U) give satisfactory results, they contradict each other. The most likely explanation is that a combination of mantle-wedge fertilisation and incongruent disequilibrium melting hampers a correct interpretation. Furthermore, distribution coefficients for solid/fluid and melt/fluid that were used may need revision when more data on trace element speciation at high temperatures and pressures become available.

126

8.4 Appendix

Inverse modelling of mixing relations.

A trace element ratio in a sample is assumed to be the same ratio as in its source and thus of weighed sums of trace element concentrations of the contributing endmembers. Fractionation after separation from the source might alter the concentration levels of the elements but it is assumed that for the carefully chosen elements it does not alter the ratio. In the formulas A, B, and C are elements, A_i is the concentration of element A in endmember i and X_i is the weighed fraction of the ith endmember. In a similar manner an isotopic ratio of a sample can be expressed as a function of the isotopic ratios of the contributing endmembers. The main constraint is the mass conservation equation taking care that all fractions should add up to 1.

Equations for trace element ratios:

$$(A/B)_{sample} = \sum_{1}^{i} (A_i . X_i) / \sum_{1}^{i} (B_i . X_i) \Leftrightarrow$$

$$\sum_{1}^{i} ((A/B)_{sample} . B_i . X_i) = \sum_{1}^{i} (A_i . X_i) \Leftrightarrow$$

$$\sum_{1}^{i} ((A_i - (A/B)_{sample} . B_i) . X_i) = 0$$

in similar fashion for isotopic ratios:

$$\sum_{1}^{i} ((R_i . A_i - R_{sample} . A_i) . X_i) = 0$$

with

$$R_i = \frac{^{p}A_i}{^{q}A_i}$$

p and q being different isotopes of the same element A in endmember i.

Mass conservation equation:

$$\sum_{1}^{i} X_i = 1$$

Example of a 3 component model in matrix notation with a trace element ratio, an isotopic ratio and the mass conservation equation:

$$\begin{bmatrix} A_1 - \left(\dfrac{A}{B}\right)_{sample} \cdot B_1 & A_2 - \left(\dfrac{A}{B}\right)_{sample} \cdot B_2 & A_3 - \left(\dfrac{A}{B}\right)_{sample} \cdot B_3 \\ R_1 \cdot C_1 - R_{sample} \cdot C_1 & R_2 \cdot C_2 - R_{sample} \cdot C_2 & R_3 \cdot C_3 - R_{sample} \cdot C_3 \\ 1 & 1 & 1 \end{bmatrix} \cdot \begin{bmatrix} X_1 \\ X_2 \\ X_3 \end{bmatrix} = \begin{bmatrix} 0 \\ 0 \\ 1 \end{bmatrix}$$

9 Conclusions

This thesis presents the results of a detailed trace element and isotope geochemistry study into the magmagenesis of volcanoes in the Adonara-Pantar Section (APS) of the East Sunda Arc in Indonesia, a setting where an oceanic island arc is colliding with a passive continental margin.

Sr, Nd, Pb, Ra, Th and U isotopes were analysed together with major and trace elements from five active and more than ten inactive volcanic centres on seven islands of the APS. In order to characterise the input into the subduction zone, literature data and additional analyses on samples of marine sediments from locations in front of the Timor Trough *(Vroon, 1982; Vroon et al., 1995)* were used.
The results of this study (1) identify different mantle and subduction-related components that contribute to the magma source region in the sub-arc mantle of the APS, (2) provide constraints for the mode of material transfer between the subducted slab and these magma sources, and (3) provide insight into spatial changes of this process as a function of the depth of the Benioff-Zone.

Careful consideration of isotope and trace element systematics suggests that one or two mantle components and three subduction-related components contribute to the magma generation in the APS. The mantle component consists of depleted Indian Ocean mantle (I-DM) which may contain enriched domains (I-EM), although their presence is not necessarily required to explain the observations. The subduction-related components consist of Subducted Continental Material (SCM), which changes systematically in composition from east to west, and crystalline Australian continental crust.

There appear to be different modes of mass transfer from the slab into the mantle wedge. At the frontal part of the APS arc, a hydrous fluid enriches the mantle wedge with only a selective group of elements. At the central and rear arc sections, the subducting slab partially melts and a siliceous liquid subsequently enriches the mantle wedge.
The mantle wedge in the frontal part of the APS is depleted in trace elements and has a HFSE, REE and Nd-isotopic composition similar to that found in depleted Indian Ocean mantle (I-DM) close to the APS *(e.g. DSDP261; Weis and Frey, 1996)*.

Pb isotopic signatures (e.g., elevated $^{208}Pb/^{204}Pb$ relative to I-DM) are difficult to explain by the subduction of sediments as represented by the cores taken in front of the arc. They can be attributed to local mantle characteristics or to involvement of subducted lithologies that have remained inaccessible for sampling. The presence of domains with the required I-EM-type signatures in the subarc-mantle would be consistent with mantle inhomogeneity in the NE part of the Indian Ocean as documented by Weis and Frey *(1996)*. Though theoretically conceivable, there is no need to invoke models for involvement of asthenospheric mantle that could rise through a slab window in response to incipient slab-detachment.
A more likely alternative to explain some of the more extreme lead isotopic data in the APS is involvement of subducted crystalline Australian crust. Evidence for subduction of the Australian continental margin is also provided by extremely radiogenic He-isotope ratios

observed in the frontal volcanoes, as we have argued in Hilton et al.*(1992)*. Furthermore, Nd-isotope systematics as well as HFSE/HFSE and REE/HFSE ratios are consistent with a contribution from this source, even if an I-EM-type mantle would be present.

Across-arc systematics in U-series and other trace elements reflect a progressive down-dip change in the nature of the SCM-derived subduction component: a high U/Th, Ra/Th and LILE-enriched hydrous fluid in the shallow parts, and a siliceous-melt with a U/Th similar to that of bulk SCM at greater depths.

Trace element modelling of the possible composition of slab-derived melt demonstrates that a residual eclogitic composition (garnet + clinopyroxene) in the subduction SCM, with additional rutile (and possibly zircon), is capable of explaining most of the observed HFSE (Nb/Ta) and REE signatures in the central and rear arc sections. The stability of residual rutile during melting or dehydration of subducted sediment may thus explain the low HFSE/LILE ratios that the APS has in common with other subduction settings.

The combined spatial geochemical systematics in the APS volcanoes document that these changes in magmagenetic regimes occur at depths of the subducted slab between 100 and 250 km. Material transfer processes at the slab-wedge interface during progressive dehydration and melting produce variations in magma compositions that are dominated by changing mobilities of trace elements. Unlike models for more common oceanic island arcs, these slab components are largely derived from subducted sediments and continental lithologies, reflecting a setting with collision-induced involvement of a passive continental margin.

130

Literature

Abbott M.J., and Chamalaun F.H., 1981. Geochronology of some Banda Arc volcanics. In: Geology and Tectonics of Eastern Indonesia (ed. A.J. Barber), Indonesian Geological Research and Development Center Special Publication No. 2: 253-268.

Adam J., Green T.H. and Sie S.H., 1993. Proton microprobe determined partitioning of Rb, Sr, Ba, Y, Zr, Nb, and Ta between experimentally produced amphiboles and silicate melts with variable F content. Chemical Geology 109: 29-49.

Albarede F. and Michard A. , 1987. Hydrothermal alteration of oceanic crust. In: crust/Mantle recycling at convergent zone: Ed's Hart. R.H. and Gulen L., NATO ASI series 258: 29-36.

Allègre C.J. , 1968. 230Th dating of volcanic rocks: a comment. Earth Planet. Sci. Lett. 5: 209-210.

Allègre C.J., Dupre B. and Lewin E., 1986. Thorium/Uranium ratio of the earth. Chemical Geology 56: 219-227.

Arculus R.J. , 1985. Arc magmatism - an unresolved problem of sources, material fluxes, tectonic evolution and thermochemical regions of subduction zones. In: Formation of active ocean margins. ed. Nasu N. et al. Terrapub., Tokyo. 367-397.

Arculus R.J. , 1994. Aspects of magma genesis in arcs. Lithos 33: 189-208.

Avdeiko G.P., Volynets O.N., Antonov A.Yu. and Tsvetkov A.A., 1991, Kurile island-arc volcanism: structural and petrological aspects. Tectonophysics 199: 271-287.

Ayers J.C., Dittmer S.K. and Layne G.D. , 1997. Partioning of elements between peridotite and H_2O at 2.0-3.0 GPa and 900-1100°C, and application to models of subduction processes. Earth Planet. Sci. Lett. 150: 381-398.

Bailey H.B. and Ragnarsdottir K.V. , 1994. Uranium and Thorium solubilities in subduction zone fluids. Earth Planet. Sci. Lett. 124: 119-129.

Bau M. and Knittel U. , 1993. Significance of slab-derived partial melts and aqueous fluids for the genesis of tholeiitic and calc-alkaline island-arc basalts: evidence from Mt. Arayat, Philippines. Chem. Geology 105: 233-251.

Beattie P. , 1993. The generation of uranium series disequilibria by partial melting of spinel periodotite: constraints from partitioning studies. Earth Planet. Sci. Let. 117: 379-391.

Bebout G.E. and Barton M.D., 1989. Fluid flow and metasomatism in a subduction zone hydrothermal system: Catalina schist terrain, California. Geology 17: 976-980.

Beckering J.D.H. , 1911. Beschrijving der eilanden Adonara en Lomblem, behoorende tot de Solor-groep. Tijdschrift Kon. Ned. Aard. Gen. 28: 67-202.

Beiersdorf H. and Hinz K. , 1979. Active ocean margins in south-east Asia. In: Mobile Earth, Final report geodynamics project D.F.G., eds.: Closs H. et al. Harald Boldt Verlag, Boppard : 121-125.

Ben Othman D. and Allègre C.J. , 1988. Th/U in oceanic basalts studied by $^{230}Th/^{238}U$. European Geochemists Conference Paris. Abstracts page : 30.

Ben Othman D. and Allègre C.J., 1990. U-Th isotopic systematics at 130N East Pacific Ridge segment. Earth Planet. Sci.Lett. 98: 129-137.

Ben Othman D., White W.M., and Patchett J., 1989. The geochemistry of marine sediments, island arc magma genesis, and crust-mantle recycling. Earth Planet. Sci. Lett. 34: 1-21.

Benioff H., 1954. Orogenesis and deep crustal structure – additional evidence from seismology. Bull. Geol. Soc. America 65: 385-400.

Bergman S.C., Coffield D.Q., Talbot J.P., and Garrard R.A., 1996. Tertiary Tectonic and magmatic evolution of western Sulawesi and the Makassar Strait, Indonesia: evidence for a Miocene continent-continent collision. In: Hall, R.& Blundell, D. (eds.), Tectonic Evolution of Southeast Asia, Geological Society Special Publication 106: 391-429.

Best M.G., 1975. Migration of hydrous fluids in the upper mantle potassium variation in calc-alkalic rocks. Geology 3: 429-432.

Bickle M.J., Bettenay L.F., Chapman H.J., Groves D.I., McNaughton N.J., Campbell I.H., and De Laeter J.R., 1989. The age and origin of younger granitic plutons of the Shaw Bathlith in the Archaean Pilbara Block, Western Australia. Contrib. Min. Petr. 101: 361-376.

Bowin C.O., Purdy G.M., Johnston C., Shor G.G., Lawver L., Hartono H.M.S. and Jezek P., 1980. Arc-continent collision in Banda Sea region. Bull. Am. Assoc. Pet. Geol. 64: 868-915.

Brenan J.M. and Watson E.B., 1991. Partitioning of trace elements between olivine and aqueous fluids at high P-T conditions: implications for the effect of fluid composition on trace element transport. Earth Planet. Sci.Lett. 107: 672-688.

Brenan J.M., Shaw H.F., Ryerson F.J. and Phinney D.L., 1995. Mineral-aqueous fluid partitioning of trace elements at 900°C and 2.0 GPa: Constraints on the trace element chemistry of mantle and deep crustal fluids. Geochim. Cosmochim. Acta 59: 3331-3350.

Brenan J.M., Shaw H.F., Phinney D.L. and Ryerson F.J., 1994. Rutile-aqueous fluid partitioning of Nb, Ta, Hf, U and Th: implications for HFSE depletions in island-arc basalts. Earth Planet. Sci.Lett. 128: 327-339.

Brenan J.M., Shaw H.F., Ryerson F.J. and Phinney D.L., 1995. Mineral-aqueous fluid partitioning of trace elements at 900°C and 2.0 GPa: Constraints on the trace element chemistry of mantle and deep crustal fluids. Geochim. Cosmochim. Acta 59: 3331-3350.

Brouwer H.A., 1940. Geological and petrological investigations on alkali and calc-alkali rocks of the islands Adonara, Lomblen and Batoe Tara. In: H.A. Brouwer, Geol. expedition of the University of Amsterdam to the Lesser Sunda Is-lands. North Holl. Pub. Co., Amsterdam 2: 1-94.

Cameron A.E., Smith D.H. and Waler R.L., 1969. Mass spectrometry of nanogram-size samples of lead. Anal. Chem. 41: 525-526.

Capaldi G., Cortini M., Gasparini P. and Pece R., 1976. Short lived radioactive disequilibria in freshly erupted volcanic rocks and their implication for the pre-eruption history of a magma. J. Geophys. Res 81: 350-358.

Carter D.J., Audley-Charles M.G., Barber A.J., 1976. Stratigraphical analysis of island arc-continental margin collision in eastern Indonesia. Geol. Soc. Lond. 132: 179-198.

Chabaux F. and Allègre C., 1994. ^{238}U-^{230}Th-^{226}Ra disequilibria in volcanics: A new insight into melting conditions. Earth Planet. Sci.Lett. 126: 61-74.

Chappell J and Veeh H.H., 1978. Late Quartenary tectonic movements and sea- level changes at Timor and Atauro Island. Geol. Soc. America Bull. 89: 356-368.

Charlton T.R., 1991. Postcollision extension in arc-continent collision zones eastern Indonesia. Geology 19: 28-31.

Condomines M. and Sigmarsson O., 1993. Why are so many arc magmas close to ^{238}U-^{230}Th radioactive equilibrium. Geochim. Cosmochim. Acta 57: 4491-4497.

Condomines M., Hemond Ch. and Allègre C.J., 1988. U-Th-Ra radioactive disequilibria and magmatic processes. Earth Planet. Sci.Lett. 90: 243-262.

Cox K.G., Bell J.D. and Pankhurst R.J., 1979. The interpretation of igneous rocks. George Allen & Unwin, London.

Davidsson J.P., Harmon R.S. and Wörner G., 1991. The source of central Andes magmas; some considerations . In: Andean magmatism and its tectonic setting. eds.: Harmon R.S. and Rapela C.W.. Geological Soc. of America special paper 265: 233-243.

Davies J.H. and Stevenson D.J., 1992. Physical model of source region of subduction zone volcanics. J. Geophys. Res. 97: 2037-2070.

De Bruin M., 1983. Instrumental neutron activation analysis - a routine method. Delftse Universitaire Press Delft : 270 pp.

De Hoog C-J., 1996. M. Sc. Thesis. University Utrecht

Desmet M.E.M., Fortuin A.R., Tjokrosapoetro S. and Van Hinte J.E., 1989. Late Cenozoic vertical movements of non-volcanic islands in the Banda Arc area. Neth. J. Sea Res. 24: 263-275.

Dickinson W.R., 1968. Circum Pacific andesite types. Journal of Geophysical Research 73: 2361-2369.

Dickinson W.R. and Hatherton T., 1975. Potash-Depth (K-h) relations in continental margin and intra oceanic arcs. Geology 3: 53-56.

Dickinson W.R. and Hatherton T., 1967. andesitic volcanism and seismicity around the Pacific. Science 157: 801-803.

Dosso L., Bougault H., Beuzart P., Calvez J-Y. and Joron J-L., 1988. The geochemical structure of the South-East Indian Ridge. Earth Plan. Sci. Lett. 88: 47-59.

Edwards C.M.H., Menzies M., and Thirlwall M.F., 1991. Evidence from Muriah, Indonesia, for the interplay of supra-subduction zone and intraplate processes in the genesis of potassic alkaline magmas. J. Petrol. 32: 555-592.

Edwards C.M.H., Menzies M.A., Thirlwall M.F., Morris J.D., Leeman W.P., and Harmon R.S., 1994. The Transition to Potassic Alkaline Volcanism in Island Arcs: The Ringgit-Beser Complex, East Java, Indonesia. Journal of Petrology 35: 1557-1595.

Edwards C.M.H., Morris J.D. and Thirlwall M.F., 1993. Separating mantle slab signatures in arc lavas using B/Be and radiogenic isotope systematics. Nature 362: 530-533.

Eggler D.E., 1987. Solubility of major and trace elements in mantle metasomatic fluids: experimental constraints. in Mantle Metasomatism (ed. Menzies M.A. & Hawkesworth C.J.) Acad. Press Inc., London : 21-41.

Ellam R.M. and Hawkesworth C.J., 1988. Elemental and isotopic variations in subduction related basalts: evidence for a three component model. Contrib. Mineral. Petrol. 98: 72-80.

Ewart A., Chappel B. W. and Menzies, M.A., 1988. An overview of the geochemical and Isotopic charateristics of the eastern Australian Cainozoic Volcanic provinces . J. Petrol. spec Vol: spec vol: 225-273.

Fletcher I.R, Myers J.S. and Ahmat A.L., 1991. Isotopic evidence on the age and origin of the Frase Complex Western Australia: a sample of Mid-Proterozoic lower crust. Chemical Geology 87: 197-216.

Foden J.D. and Green D.H., 1992. Possible role of amphibole in the origin of andesite: some experimental and natural evidence. Contrib. Mineral. Petrol. 109: 479-493.

Foley S.F. and Wheller G.E., 1990. Parallels in the origin of the geochemical signatures of island-arc volcanics and continental potassic igneous rocks: The role of residual titanates. Chem. Geol. 85: 1-18.

Fraser K.J., Hawkesworth C.J., Erlank A.J., Mitchell R.H. and Scott-Smith B.H., 1985/86. Sr Nd and Pb isotope and minor element geochemistry of lamproites and kimberlites. Earth Planet. Sci. Lett. 76: 57-70.

Gasparon M., 1993. Origin and evolution of mafic volcanics of Sumatra (Indonesia): their mantle sources, and the roles of subducted oceanic sediments and crustal contamination. Ph.D. thesis Univ. Tasmania.

Gasparon M., Hilton D.R. and Varne R., 1994. Crustal contamination processes traced by helium isotopes: Examples from the Sunda Arc, Indonesia. Earth Planet. Sci. Lett. 126: 15-22.

Gautier I., Weiss D., Mennessier J.P., Vidal P., Giret A. and Loubet M., 1990. Petrology and geochemistry of the Kerguelen Archipelago basalts (South Indian Ocean): evolution of the mantle sources from ridge to intraplate position . Earth Planet. Sci. Lett. 100: 59-76.

Gerbe M.C., Gourgaud A., Sigmarsson O., Harmon R.S., Joron J.L., Provost A., 1992. Mineralogical and geochemical evolution of the 1982-1983 Galunggung eruption (Indonesia). Bulletin of Volcanology 54: 284-298.

Gill J.B. and Condomines M., 1992. Short-lived Radioactivity and magma genesis. Science 257: 1368-1376.

Gill J.B. and Williams W.R., 1990. Th isotope and U-series studies of subduction-related volcanic rocks. Geochim. Cosmochim. Acta 54: 1427-1442.

Gill J.B., Morris J.D.and Johnson R., 1993. Timescale for producing the geochemical signature of island arc magmas: U-Th-Po and B-Be systematics in recent Papua-New Guinea lavas. Geochim. Cosmochim. Acta 57: 4269-4284.

Gill J.B., 1987. Early geochemical evolutionof an oceanic island arc and back arc: Fiji and the south Fiji bassin. J. Geol 95: 589-615.

Gill J.B., 1981. Orogenic andesites and plate tectonics. New York Springer-Verlag : 370 pp.

Gill J.B., 1984. Sr-Pb-Nd isotopic evidence that both MORB and OIB sources contribute to oceanic island arc magmas in Fiji. Earth Planet. Sci. Lett. 68: 443-458.

Govindaraju K., 1984. 1984 Compilation of working values and sample descriptions for 170 international reference samples of mainly silicate rocks and minerals. Geostandards Newsletter 8: Special July Issue.

Govindaraju K., 1989. Compilation of working values and sample descriptions for 272 geostandards. Geostandards Newsletter 13: 1-113.

Gradstein F.M., Ludden J.N., et al., 1990. Proceedings of the Ocean Drilling Program Scientific Results Vol. 123 College Station, TX.

Graustein W.C. and Turekian K.K., 1990. Radon fluxes from soils to the atmo-sphere measured by ^{210}Pb-^{226}Ra disequilibrium in soils. Geophys. Res. Let. 17: 841-844.

Green T.H., 1980. Island arc and continent-building magmatism- a review of petrogenetic models based on experimental petrology and geochemistry. In: Orthodoxy and creativity at the frontiers of the earth sciences. Tectonophysics 63: 367-385.

Green T.H. and Pearson N.J., 1986. Ti-rich accessory phase saturation in hydrous mafic-felsic compositions at high P T. Chem. Geol. 54: 185-201.

Green T.H., 1994. Experimental studies of trace element partitioning applicable to igneous petrogenesis - Sedona 16 years later. Chem. Geol. 117: 1-36.

134

Green T.H., 1995. Significance of Nb/Ta as an indicator of geochemical processes in the crust-mantle system. Chem. Geol. 120: 347-359.

Hamilton W., 1979. Tectonics of the Indonesian region. U.S. Geol. Surv. Prof. Pap. 1078: 345 pp.

Hart S.R. and Dunn T., 1993. Experimental cpx/melt partitioning of 24 trace elements. Contrib. Min. Petr. 113: 1-8.

Hart S.R. and Staudigel H., 1989. Isotopic characterisation ad identification of recycled components. NATO ASI Series, C: Math. and Phys. Sci 258: 15-28.

Hart S.R., 1988. Heterogeneous mantle domains: signatures genesis and mixing chronologies. Earth Planet. Sci. Lett. 90: 273-296.

Harte B., 1987. Metasomatic events recorded in mantle xenoliths: an overview. In: Mantle xenoliths. Ed.: Nixon P.H. John Wiley and Sons Ltd.

Hartman M.A., 1935. De werkende vulkanen van het eiland Lomblem (Solor archipel). Tijdschrift Kon. Ned. Aard. Gen. 52: 817-836.

Hartman M.A., 1936. Der taetige Feuerberg Siroeng auf Pantar. Natuurk. Tijdschr. Nederl. Indie 6: 89-121 6: 89-121.

Hartone H.M.S., 1990. Late Cenozoic tectonic development of the Southeast Asian continental margin of the Banda Sea area. Tectonophysics 181: 267-276.

Hatherton T. and Dickinson W.R., 1969. The relationship between andesitic volcanism and seismicity in Indonesia, the Lesser Antilles, and other island arcs. Journal of Geophysical Research 74: 5301-5310.

Hatherton T., 1967. The geophysical significance of calc-alkaline andesites in New Zealand. New Zealand J. Geol. Geophys., 12: 436-459.

Hawkesworth C.J., Hergt J.M., McDermott F., and Ellam R.M., 1991. Destructive margin magmatism and the contributions from the mantle wedge and subducted crust. Austr. J. Earth Sc. 38: 577-594.

Hawkesworth C.J., Gallagher K. Hergt J.M. and McDermott F., 1994. Destructive plate margin magmatism: Geochemistry and melt generation. Lithos 33: 169-188.

Hedeba E.H., Andriessen P.A.M. and Belle., 1988. Simultaneous isotope analysis of Nd and Sm with a fixed multicollector mass spectrometer. Fresenius Z. Anal. Chem. 331: 114-117.

Heitzler J.R., Cameron P., Cook P.J., Roeser H.E., Sukardi S. and Veevers J.J., 1978. The Argo abyssal plain. Earth Plan. Sci. Lett. 41: 21-31.

Hickey-Vargas R., 1992. A refractury HIMU component in the sources island-arc magma. Nature 360: 57-59.

Hilton D.R. and Graig H., 1989. A helium isotope transect along the Indonesian archipelago. Nature 342: 906-908.

Hilton D.R., Hoogewerff J.A., Van Bergen M.J. and Hammerschmidt K., 1992. Mapping magma sources in the east Sunda-Banda Arcs Indonesia: Constraints from helium isotopes. Geochim. Cosmochim. Acta 56: 851-859.

Hofman A.W., Jochum K.P., Seufert M. and White W.M., 1986. Nb and Pb in oceanic basalts: new constraints on mantle evolution. Earth Planet. Sci. Lett. 79: 33-45.

Holloway J., 1987. Igneous Fluids . In: Reviews in mineralogy 17 Eds Carmichael I.S.E. and Eugster H.P. : 211-234.

Hoogewerff J.A., Van Bergen M.J., Vroon P.Z., Hertogen J., Wordel R., Sneyers A., Nasution A., Varekamp J.C., Moens H.L.E., and Mouchel D., 1997. U-series, Sr-Nd-Pb isotope and trace element systematics across an active island arc-continent collision zone: Implications for element transfer at the slab-wedge interface. Geochim. Cosmochim Acta 61: 1057-1072.

Huang W.L., Wyllie P.J and Nehru C.E., 1980. Subsolidus and liquidus phase relations in the system CaO-SiO$_2$-CO$_2$ to 30 kbar with geological applications. American Mineralogist 65: 285-301.

Hutchison C.S. and Jezek P.A., 1978. Banda Arc of eastern Indonesia: Petrography mineralogy and chemistry of the volcanic rocks. Proceedings of the third regional conference on geology and mineral resources of S.E. Asia (ed. Prinya Nutalaya) Asian Institute of Technology Bangkok : 607-619.

Ionov D.A. and Hofman A.W., 1995. Nb-Ta-rich mantle amphiboles and micas: Implications for subduction-related metasomatic trace element fractionations. Earth Planet. Sci. Lett. 131: 341-356.

Irifune T., Ringwood A.E. and Hibberson W.O., 1994. Subduction of continental crust and terrgenous and pelagic sediments: an experimental study. Earth Planet. Sci. Lett. 126: 351-368.

Ishikawa I. and Nakamura E., 1994. Origin of the slab component in arc lava's from across-arc variation of B and Pb isotopes. Nature 370: 205-208.

Ito E., White W.M. and Gospel C., 1987. The O, Sr, Nd and Pb isotope geochemistry of MORB. Chem. Geol. 62: 157-176.

Jacobson R.S., Shor G.G., Kieckhefer R.M. and Purdy G.M., 1978. Seismic refraction and reflection studies in the Timor-Aru Trough system and Australian continental shelf. Am. Ass. Petrol. Geol. Mem. 29: 209-222.

Jâkes P. and White A.J.R., 1972. Major and trace elements abundance's in volcanic rocks of orogenic areas. Geol. Soc. America Bull. 83: 29-40.

Jenner G.A., Foley S.F., Jackson S.E., Green T.H., Fryer B.J. and Longerich H.P. 1993 Determination of partition coefficients for trace elements in high pressure-temperature experimental run products by LAM-ICP-MS. Geochim. Cosmochim. Acta 57: 5099-5103.

Jochum K.P., Seufert H.M. and Thirlwall M.F., 1990. High-sensitivity Nb analysis by spark-source mass spectrometry (SSMS) and calibration of XRF Nb and Zr. Chemical Geology 81: 1-16.

Johnson M.C. and Planck T., 1993. Experimental constraints on sediment melting during subduction. EOS 74: 680.

Karig D.E., Barber A.J., Charlton T.R., Klemperer S. and Hussong D.H., 1987. Nature and distribution of deformation across the Banda Arc-Australian collision at Timor. Geol. Soc. Am. Bull. 98: 18-32.

Kay R.W., 1980. Volcanic arc magma. implications of a melting-mixing model for element recycling in the crust upper mantle system. J. Geol. 88: 497-522.

Kelemen P.B., Johnson K.T.M., Kinzler R.J. and Irving A.J., 1990. High-field-strength element depletions in arc basalts due to mantle-magma interaction. Nature 345: 521-524.

Kelemen P.B. and Dunn T., 1992. Depletion of Nb relative to other highly incompatible elements by rock/melt reaction in the upper mantle . EOS 73: 656-657.

136

Kepezhinskas P., Defant M.J. and Drummond M.S., 1996. Progressive enrichment of island arc mantle by melt-peridotite interaction inferred from Kamchatka xenoliths. Geochim. Cosmochim. Acta 60: 1217-1229.

Keppler H. and Wyllie P.J., 1990. Role of fluids in transport and fractionation of uranium and thorium in magmatic processes. Nature 348: 531-533.

Keppler H. and Wyllie P.J., 1991. Partitioning of Cu, Sn, Mo, W, U and Th between melt and an aqueous fluid in the systems haplogranite-H_2O and haplogranite-H_2O-HF. Contrib. Mineral. Petrol. 109: 139-150.

Klein M. Stosch H.-G. and Seck H.A., 1997. Partitioning of high field-strength and rare-earth elements between amphibole and quartz-dioritic to tonalitic melts: an experimental study. Chemical Geology 138: 257-271.

Krishnaswami S., Turekian K.K. and Bennett J.T., 1984. The behaviour of the ^{232}Th and the ^{238}U chain nuclides during magma formation and volcanism. Geochim. Cosmochim. Acta 48: 505-511.

Kuno, H., 1959. Origin of Cenozoic petrographic provinces of Japan and surrounding areas. Bull. Volcanologique, 20: 37-76.

Lapouille A., Haryono H., Larue M., Pramuwijoyo S. and Lardy M., 1985. Age and origin of the seafloor of the Banda Sea (eastern Indonesia). Oceanol. Acta 8: 379-389.

Latourette T., 1994. Trace element partioning between amphibole, phlogopite, and hydrous basanite melt. EOS 75: 693.

Lee C.S. and McCabe R., 1986. The Banda-Celebes-Sula basin: a trapped piece of Cretaceous-Eocene oceanic crust. Nature 322: 51-54.

Lin P.N., Stern, R.J. and Bloomer S.H., 1989. Shoshonitic volcanism in the Northern Mariana arc:2. Large-ion lithophile and rare earth element abundances-evidence for the source of incompatible element enrichments in intra-oceanic arcs. J. Geo-phys. Res. 94: 4497-4514.

Lin P.N., Stern R.J., Morris J. and Bloomer S.H., 1990. Nd- and Sr-isotopic compositions of lavas from the northern Mariana and southern Volcano arcs: implications for the origin of island arc melts. Contrib. Mineral. Petrol. 105: 381-392.

MacKenzie W.S., Donaldson C.H. and Guilford C., 1987. Atlas of igneous rocks and their textures. 3rd Edition. Longman Scientific & Technical, Harlow, United Kingdom. 148 pages.

Margaritz M. Whitford D.J. and James D.E., 1978. Oxygen isotopes and the origin of high-$^{87}Sr/^{86}Sr$ andesites. Earth Planet. Sci. Lett. 40: 220-230.

Maury R.C., Defant M.C. and Joron J.L., 1992. Metasomatism of the sub-arc mantle inferred from trace elements in Philipine xenoliths. Nature 360: 661-663.

McCaffrey R., Molnar P., Roecker S. and Joyodiwiryo Y., 1985. Microearthquake seismicity and fault plane solutions related to arc-continent collision in the Eastern Sunda Arc, Indonesia. J. Geo-phys. Res. 90: 4511-4528.

McCaffrey R., 1989. Seismological constraints and speculations on Banda Arc tectonics. Neth. J. Sea Res. 24: 141-152.

McCulloch. M.T. and Gamble J.A., 1991. Geochemical and geodynamical constraints on subduction zone magmatism. Earth Planet. Sci. Lett. 102: 358-374.

McCulloch M.T., Jaques A.L., Nelson D.R., and Lewis J.D., 1983. Nd and Sr isotopes in kimberlites and lamproites from Western Australia: An enriched mantle origin. Nature 302: 400-403.

McDermott F. and Hawkesworth C.J., 1991. Th, Pb and Sr isotopes variations in young island arc volcanics and oceanic sediments. Earth Planet. Sci.Lett. 104: 1-15.

McDermott F., Defant M.J., Hawkesworth C.J., Maury R.C. and Joron J.L., 1993. Isotope and trace element evidence for three component mixing in the genesis of the North Luzon arc lavas (Philippines). Contrib. Mineral. Petrol. 113: 9-23.

Mckenzie D. and O'nions R.K., 1991. Partial melt distributions from inversion of rare earth element concentrations. J. Petrol. 32: 1021-1091.

Mckenzie D., 1985. ^{230}Th-^{238}U disequilibrium and the melting processes beneath ridge axes. Earth Planet. Sci. Lett. 72: 149-157.

Michard A., R. Montigny and Schlich R., 1986. Geochemistry of the mantle beneath the Rodriquez Triple Junction and the South-East Indian Ridge. Earth Planet. Sci. Lett., 78: 104-114.

Minster J.B. and Jordan T.H., 1978. Present-day plate motions. J. Geophys. Res. 83: 5331-5354.

Morrice M.G., Jezek P.A., Gill J.B., Whitford D.J. and Monoarfa M., 1983. An introduction to the Sanghi Arc: Volcanism accompanying arc-arc collision in the Molucca Sea, Indonesia. J. of Volcanology and Geothermal Res. 19: 135-165.

Morris J.D. and Hart S.R., 1983. Isotopic and incompatible element constraints on the genesis of island arc volcanics from Cold Bay and Amak Island Aleutians and implications for mantle structure. Geochim. Cosmochim. Acta 47: 2015-2030.

Morris J. D., Leeman W.P. and Tera F., 1990. The subducted component in island arc lavas: Constraints from Be isotopes and B-Be systematics. Nature 344, 31-36 344: 31-36.

Morris J.D., Jezek P.A., Hart S.R., and Gill J.B., 1983. The Halmahera island arc Molucca Sea collision zone Indonesia: a geochemical survey. In: The Tectonic and Geologic Evolution of Southeast Asian Seas and Islands Part 2 (ed. D.E. Hayes) Am. Geophys. Union Geophys. Monogr. Ser. 27: 373-387.

Morris J.D., Gill J.B., Schwartz D. and Silver E.A., 1984. Late Miocene to Recent Banda Sea volcanism III: Isotopic compositions . EOS Trans. AGU 65: 1135.

Morris J.D., 1984. Enriched geochemical signatures in Aleutian and Indonesian arc lavas: an isotopic and trace element investigation. Ph.D. thesis Mass. Inst. Technol. Cambridge : 320 pp.

Nelson D. McCulloch M.T. and Sun S.S., 1986. The origins of ultrapotassic rocks as inferred from Sr, Nd, and Pb isotopes. Geochim. Cosmochim. Acta 50: 231-245.

Nelson B.K., 1995. Fluid flow in subduction zones: evidence from Nd- and Sr-isotope variations in metabasalts of the Franciscan complex, California. Contrib. Min. Petrol. 119: 247-262.

Newman S., Macdougall J.D. and Finkel R.C., 1984. ^{230}Th-^{238}U disequilibrium in island arcs: evidence from the Aleutians and the Marianas. Nature 308: 268-270.

Nichols G.T., Wyllie P.J. and Stern Ch. R., 1994. Subduction zone melting of pelagic sediments constrained by melting experiments. Nature 371: 785-788.

Noya Y. and Koesoemadinata S., 1986. Report on the geology of the Lomblem quadrangle, east Nusatenggara. Open file report, Geological research and development centre, Bandung Indonesia.

Oliver J. and Isacks B., 1967. Deep earthquake zones, anomalous structures in the upper mantle, and the lithosphere. J. Geophys. Res 72: 4259-4275.

138

O'reilly S.Z. and Griffin W.L., 1988. Mantle metasomatism beneath western Victoria, Australia: I. Metasomatic processes in Cr-diopside lherzolites. Geochim. Cosmochim. Acta 52: 433-447.

Peacock S.M., 1993. Large-scale hydration of the lithosphere above subducting slabs. Chem. Geology 108: 49-59.

Peacock S.M., Rushmer T. and Thompson A.B., 1994. Partial melting of subducting oceanic crust. Earth Planet. Sci. Lett. 121: 227-244.

Peacock S.M., 1990. Fluid processes in subduction zones. Science 248: 329-337.

Pearce J.A. and Parkinson I.J., 1993. Trace element models for melting: application to volcanic arc petrogenesis. In: Magmatic processes and plate tectonics. Eds: Prichard et al.. Geol. Soc. Special Publ. 76: 373-403.

Pearce J.A. and Peate D.W., 1995. Tectonic implications of the composition of volcanic arc magmas. Annu. Rev. Earth Planet. Sci. 23: 251-285.

Pedersen R.B. and Hertogen J., 1990. Magmatic evolution of the Karmoy Ophiolite Complex, SW Norway: relationships between MORB-IAT-boninitic-calc-alkaline and alkaline magmatism. Contrib. Mineral. Petrol. 104: 277-293.

Perfit M.R., Gust D.A., Bence A.E., Arculus R.J. and Taylor S.R., 1980. Chemical characteristics of island-arc basalts: implications for mantle sources. Chemical Geology 30: 227-256.

Perring, C.S., and Rock N.M.S., 1991. Relationships between calc-alkaline acidic and basic (mantle derived) magmas in the late archean composite dykes, Kambalda Goldfield , Western Australia. Precambriam Res. 52: 245-273.

Philippot P. and Selverstone J., 1991. Trace element-rich brines in eclogitic veins: implications for fluid composition and transport during subduction. Contrib. Mineral. Petrol. 106: 417-430.

Philippot P., 1995. Fluid composition and evolution in coesite-bearing rocks (Dora-Maira massif, Western Alps): Implications for element recycling during subduction. Contrib. Mineral. Petrol. 121: 29-44.

Plank T. and Langmuir C.H., 1993. Tracing trace elements from sediment input to volcanic output in subduction zones. Nature 362: 739-743.

Plank T., Elliot T. and White W., 1994. Nb anomalies in arc lavas: insight from the Marianas. EOS 75: 730.

Poli S. and Schmidt M.W., 1995. H_2O transport and release in subduction zones: Experimental constraints on basaltic and andesitic systems. J. Geophys. Res. 100: 22299-22314.

Poorter R.P.E., Varekamp J.C., Sriwana T., Van Bergen M.J., Erfan R.D., Suharyono K., Wirakusumah A.D. and Vroon P.Z., 1989. Geochemistry of hot springs and fumarolic gases from the Banda Arc. Neth. J. Sea Res. 24: 323-331.

Poorter R.P.E., Varekamp J.C., Poreda R.J., Van Bergen M.J., and Kreulen. R., 1991. Chemical and isotopic compositions of volcanic gases from the east Sunda and Banda Arcs Indonesia. Geochim. Cosmochim. Acta 55: 3795-3807.

Poreda R. and Craig H., 1989. Helium isotope ratios in circum-Pacific volcanic arcs. Nature 338: 473-478.

Powell D.E. and Mills S.J., 1978. Geological evolution and hydrocarbon prospects of contrasting continental margin types Southwest Australia. In: Regional conference on Geology and Mineral Resources of SE Asia Proceedings Jakarta Indonesia (eds. S. Wiryosujono and A. Sudradjat) Association of Indonesian Geologists : 77-100.

Price N.J. and Dudley-Charles M.G., 1987. Tectonic collision processes after plate rupture. Tectonophysics 140: 121-129.

Qin Z., 1992. Disequilibrium partial melting model and its implications for trace element fractionations during mantle melting. Earth Planet. Sci. Lett. 112: 75-90.

Reagan M.K., Morris J.D., Herrstrom E.A. and Murrell M.T., 1994. Uranium series and beryllium isotope evidence for an extended history of subduction modification of the mantle below Nicaragua. Geochim. Cosmochim. Acta 58: 4199-4212.

Ringwood A.E., 1990. Slab-mantle interactions. 3. Petrogenesis of intraplate magmas and structure of the upper mantle. Chem. Geol. 82: 187-207.

Rittman, A., 1953. Magmatic character and tectonic position of the Indonesian Volcanoes. Bull. Volcanologique 14: 45-58.

Rohi W., 1978. Pemeriksaan Kawah-Kawah G. Ili Boleng, G. Ili Werung dan G. Sirung. Direktorat Vulkanologi Indonesia.

Rosenbaum J.M. and Wilson M., 1993. Mantle phlogopite: fingerprint of subduction? . EOS 74: 680.

Rubin K.H., Wheller G.E., Tanzer J.D., Macdougall J.D. Varne R. and Finkel R.C., 1989. ^{238}U decay series systematics of young lavas from Batur volcano Sunda Arc. J. Volcanol. Geotherm. Res. 38: 215-226.

Rudnick R. L., and Goldstein S.L. 1990. The Pb isotopic composition of lower crustal xenoliths and the evolution of lower crustal Pb. Earth Plan. Sci. Lett. 98: 192-207.

Ryan J.G., Morris J., Tera F., Leeman W.P. and Tsretkov A., 1995. Cross-arc geochemical variations in the Kurile Arc as a function of slab depth. Science 270: 625-627.

Ryerson F.J. and Watson E.B., 1987. Rutile saturation in magmas: implications for Ti-Nb-Ta depletion in island-arc basalts. Earth Plan. Sci. Lett. 86: 225-239.

Salters V.J.M. and Hart S.R., 1991. The mantle sources of ocean ridges, islands and arcs: the Hf-isotope connection. Earth Plan. Sci.Lett. 104: 364-380.

Saunders A.D., Tarney J. and Weaver S.D., 1980. Transverse geochemical variations across the antarctic peninsula: implications for the genesis of calcalkaline magmas. Earth Plan. Sci. Lett. 46: 344-360.

Schouten 1775. Schouten's Reistogt naar en door Oost-Indien. 78-80.

Shaw D.M., 1970. Trace element fractionation during anatexis. Geochim. Cosmochim. Acta 34: 237-243.

Sigmarsson O., Condomines M., Morris J.D. and Harmon R.S., 1990. Uranium and ^{10}Be enrichment by fluids in andean arc magmas. Nature 346: 163-165.

Sorensen S.S. and Barton M.D., 1987. Metasomatism and partial melting in a subduction complex: Catalina Schist, Southern California. Geology 15: 115-118.

Sorensen S.S. and Grossman J.N., 1989. Enrichment of trace elements in garnet amphibolites from a paleo-subduction zone: Catalina Schist, southern California. Geochim. Cosmochim. Acta 53: 3155-3177.

Spiegelman M. and Elliott T., 1993. Consequences of melt transport for uranium series disequilibrium in young lavas. Earth Plan. Sci. Lett. 118: 1-20.

Spiegelman M. and Kenyon P., 1992. The requirements for chemical disequilibrium during magma migration. Earth Plan. Sci. Lett. 109: 611-620.

Staudigel H., Plank T., White B. and Schminke H-U., 1996. Geochemical fluxes during seafloor alteration of the upper oceanic crust: DSDP sites 417 and 418. In: Subduction, top to bottom. Bebout G.E. et al. (Eds.) Geophysical monograph AGU 96: 19-38.

Stern R.J., and Ito E., 1983. Trace element and isotopic constraints on the source of magmas in the active Volcano and Mariana Island Arcs, Western Pacific. J. Volcanol. Geotherm. Res. 18: 461-482.

Stern R.J., Morris J., Bloomer S.H. and Hawkins J.W., 1991. The source of the subduction component in convergent margin magmas: trace element and radiogenic isotope evidence fromEoncene bononotes, Mariana Fore arc. Geochim. Cosmochim. Acta 55: 1467-1481.

Stern R.J., Jackson M.C., Fryer P. and Ito E., 1993. O, Sr, Nd and Pb isotopic composition of the Kasuga Cross-chain in the Mariana arc: A new perspective on the K-h relationship. Earth Planet, Sci. Lett. 119: 459-475.

Stolper E. and Newman S., 1994. The role of water in the petrogenesis of Mariana trough magmas. Earth Planet, Sci. Lett. 121: 293-325.

Stolz A.J. and Davies G.J., 1988. Chemical and isotopic evidence from spinel lherzolite xenoliths for episodic metasomatism of the upper mantle beneath south-east Australia. J. Petrol spec Vol. spec. vol.: 303-330.

Stolz A.J., Varne R., Wheller G.E., Foden J.D. and Abbott M.J., 1988. The geochemistry and petrogenesis of K-rich alkaline volcanics from the Batu Tara volcano, eastern Sunda Arc. Contrib. Mineral. Petrol. 98: 374-398.

Stolz A.J., Varne R., Davies G.R., Wheller G.E. and Foden J.D., 1990. Magma source components in an arc-continent collision zone: the Flores-Lembata sector, Sunda Arc, Indonesia. Contrib. Mineral. Petrol. 105: 585-601.

Stolz A.J., Jochum K.P., Spettel B. and Hofmann A.W., 1996. Fluid- and melt-related enrichment in the subarc mantle: evidence from Nb/Ta variations in island-arc basalts. Geology 24: 587-590.

Sugimura A., 1960. Zonal arrangement of some geophysical and petrological features in Japan and its environs. J. Fac. Sci. Univ. of Tokyo 12: 133-153.

Sun S.S. and McDonough W.F., 1989. Chemical and isotopic systematics of oceanic basalts: implications for mantle composition and processes in Magmatism in the Oceanic Basins. edited by A.D. Saunders and M.J. Norry. Geol. Soc. Spec. Publ. 42: 313-145.

Tatsumi Y., Hamilton D.L. and Nesbitt R.W., 1986. Chemical characteristics of fluid phase released from a subducted lithosphere and origin of arc magmas: evidence from high-pressure experiments and natural rocks. J. Volcanol. Geotherm. Res. 29: 293-309.

Tatsumi Y. Murasaki M. Arsadi E.M. and Nohda S., 1991. Geochemistry of quaternary lavas from N.E. Sulawesi: transfer of subduction components into the mantle wedge. Contrib. Mineral. Petrol. 107: 137-149.

Tatsumi Y., Murasaki M. and Nohda S., 1992. Across arc variation of the lava chemistry in the Izu-Bonin arc: identification of of subduction components. J. Volcanol. Res. 49: 179-190.

Tatsumi Y., 1989. Migration of fluid phases and genesis of basalt magmas in subduction zones. J. Geophys. Res. 94: 4697-4707.

Taylor S.R. and McLennan S.M., 1985. The continental crust: its composition and evolution 312 pp. Blackwell Oxford. 212 pp.

Thirlwall M.F., Hough R., Vroon P.Z. and Wills J., 1993. Trace element partitioning during mantle melting. Terra Nova 5: 585.

Thirlwall M.F., Smith T.E., Graham A.M., Theodorou N., Hollings P., Davidson J.P. and Arculus R.J., 1994. High Field Strength element anomalies in arc lavas: source or process. J. Petrol. 35: 819-838.

Thirlwall M.F., Jenkins C., Vroon P.Z. and Mattey D.P., 1996. Crustal interaction during construction of ocean islands: Pb-Sr-Nd-O isotope stratigraphy of the shield basalts of Gran Canaria. Chemical Geology (in press).

Tomita, T., 1935. On the chemical composition of the Cenozoic alkaline suite of the circum Japan Sea region. Shanghai Sci. Inst. Jour., sect 2 1: 227-306.

Tomkeiff S. I., 1949. The volcanoes of Kamchatka. Bull. Volcanologique 8: 87-114.

Valbracht P.J. 1991. The origin of the continental crust of the Baltic shield, as seen through Nd and Sr isotopic variations in 1.89-1.85 Ga old rocks from Western Bergslagen, Sweden. PhD thesis, GUA papers of geology Series 1, 29: pp222.

Van Bergen M.J., Vroon P.Z., Varekamp J.C. and Poorter R.P.E., 1992. The Origin of the Potassic rock suite from Batu Tara volcano (East Sunda Arc, Indonesia). Lithos 28: 261-282.

Van Bergen M.J., Vroon P.Z. and Hoogewerff J.A., 1993. Geochemical and tectonic relationships in the east Indonesian arc-continent collision region: implications for the subduction of the Australian passive margin. Tectonophysics 223: 97-116.

Vanlerberghe L., 1987. Geochemische studie van de Nyiragongo vulkaan d.m.v. x-stralen-fluorescentienanalyse, neutronenactiveringsanalyse en U-Th alfaspectrometrie. Ph.D. Thesis University Leuven, Belgium.

Varekamp J.C., Van Bergen M.J., Vroon P.Z., Poorter R.P.E., Wirakusumah A.D., Erfan R., Suharyono K. and Sriwana T., 1989. Volcanism and tectonics in the Eastern Sunda Arc, Indonesia. Neth. J. Sea Res. 24: 303-312.

Varne R. and Foden J.D., 1986. Geochemical and isotopic systematics of Eastern Sunda Arc volcanics: implications for mantle sources and mantle mixing processes. In: The Origin of Arcs (ed. F.C. Wezel) Elsevier Amsterdam: 159-189.

Varne R., 1985. Ancient subcontinental mantle: a source for K-rich orogenic volcanics. Geology 13: 405-408.

Veevers J.J., Heirtzler J.R., et al., 1974. Site 262 . In: Initial reports on the Deep Sea Drilling Project (eds. J.J. Veevers J.R. Heirtzler et al.) Vol. 27 Washington U.S. Government Printing Office 27: 193-278.

Vidal Ph., Dupuy C., Maury R., Richard M., 1989. Mantle metasomatism above subduction zones: Trace element and radiogenic isotope characteristics of peridotite xenoliths from Batan Island (Philippines). Geology 17: 1115-1118.

Vielzeuf D., Clemens J.D., Pin C. and Moinet E., 1990. Granites, granulites and crustal evolution. In: Granulites and crustal evolution (eds. D. Vielzeuf and Ph. Vidal). Kluwer Acad. Publ., the Netherlands : 59-85.

Volmer R., 1987. Metasomatism of the continental lithosphere: simulation of isotope and element abundance behaviour and case studies. H.C. Helgeson (ed.), Chemical Transport in Metasomatic Processes : 53-90.

Vroon P.Z., Nowell G., Hoogewerff J.H. and Van Bergen M.J., 1998. HFSE mobility at the slab-wedge interface: Hafnium-isotope evidence from the east Sunda-Banda Arc. Min. Mag. 62A: 1717-1618.

142

Vroon P.Z., Van Bergen M.J., Klaver G. and White W.M., 1995. Sr, Nd and Pb isotopic and trace element signatures of the East Indonesian sediments: provenance and implications for Banda Arc magma genesis . Geochim. Cosmochim. Acta 59: 2573-2598.

Vroon P.Z., Lowry D., and Van Bergen M.J., 1994. Oxygen- and Strontium-Isotope systematics of the Banda Arc volcanics (Indonesia): Evidence for the subduction of continental material. Min. Mag. 58A: 945-946.

Vroon P.Z., Van Bergen M.J., White W.M. and Varekamp J.C., 1993. Sr-Nd-Pb isotope systematics of the Banda Arc, Indonesia: combined subduction and assimilation of continental material. J. Geophys. Res. 98: 22349-22366.

Vroon P.Z., 1986. Volcanism in the Eastern Sunda and Banda Arc. M.Sc. Thesis, Utrecht University unpublished.

Vroon, P.Z., 1992. Subduction of continental material in the Banda Arc, Eastern Indonesia . Geologica Ultraiectina, Ph.D. Thesis University Utrecht, The Netherlands 90: 205 pp.

Vukadinovic D. and Nicholls I.A., 1989. The petrogenesis of island arc basalts from Gunung Slamet volcano, Indonesia: Trace element and $^{87}Sr/^{86}Sr$ contraints. Geochim. Cosmochim. Acta 53: 2349-2363.

Vukadinovic D. and Sutawidjaja I., 1995. Geology, mineralogy and magma evolution og Gunung Slamet Volcano, Java, Indonesia. Journal of Southeast Asian Earth Sciences 11: 135-164.

Wadati K., 1928. On shallow and deep earthquakes. Geophys. Mag. 1: 162-202.

Wadati K. and Iwai Y., 1954. The minute investigation of seismicity in Japan. Geophys. Mag. 25: 167-174.

Weaver B.L., 1991. The origin of ocean island basalt endmember compositions: trace element and isotopic constraints. Earth Planet. Sci. Lett. 104: 381-397.

Weiss D. and Frey F.A., 1996. Role of the Kerguelen plume in generating the eastern Indian Ocean seafloor. J. Geophys. Res. B1 101: 13,831-13,849.

Wheller G.E., Varne R., Foden J.D. and Abbott M.J., 1987. Geochemistry of Quaternary volcanism in the Sunda-Banda Arc, Indonesia, and three-component genesis of island-arc basaltic magmas. J. Volcanol. Geotherm. Res. 32: 137-160.

Wheller G.E. and Varne R., 1986. Genesis of dacitic magmatism at Batur volcano, Bali, Indonesia: Implications for the origins of stratovolcano calderas. J. Volcanol. Geotherm. Res. 28: 363-378.

White W.M. and Dupre B., 1986. Sediment subduction and magma genesis in the Lesser Antilles: Isotopic and trace element constraints. Geoph. Res. 91: 5927-5941.

White W.M. and Patchett J., 1984. Hf Nd Sr isotopes and incompatible element abundances in island arc: Implications for magma origins and crust mantle evolution. Earth Planet. Sci. Lett. 67: 167-185.

Whitford D.J. and Jezek P., 1979. Origin of the late Cenozoic lavas from the Banda Arc, Indonesia: Trace element and Sr isotope evidence. Contrib. Mineral. Petrol. 68: 141-150.

Whitford D.J. and Jezek P., 1982. Isotopic constraint on the role of subducted sialic material in Indonesian island-arc magmatism. Geol. Soc. Am. Bull. 93: 504-513.

Whitford D. J., Compston W., Nicholls I.A. and Abbott M.J., 1977. Geochemistry of late Cenozoic lavas from eastern Indonesia: Role of subducted sediments in petrogenesis. Geology 5: 571-575.

Whitford D.J., Nicholls I.A. and Taylor S.R., 1979. Spatial Variations in the Geochemistry of Quaternary Lavas Across the Sunda Arc in Java and Bali. Contrib. Mineral. Petrol. 70: 341-356.

Whitford D.J., White W.M. and Jezek P.A., 1981. Neodymium isotopic composition of Quaternary island arc lavas from Indonesia. Geochim. Cosmochim. Acta 45: 989-995.

Whitford D.J., 1975. Strontium isotopic studies of the volcanic rocks of the Sunda Arc, Indonesia, amd their petrogenetic implications. Geochim. Cosmochim. Acta 39: 1287-1302.

Williams R.W. and Gill J.B., 1989. Effects of partial melting on the uranium decay series. Geochim. Cosmochim. Acta 53: 1607-1619.

Wilson M., 1989. Igneous Petrogenesis. Unwin Hyman Ltd. London : 466 pp.

Wiriosoemarto A., 1960a. Laporan Ili Lewotolo. Direktorat Vulkanologi Indonesia (72).

Wiriosoemarto A., 1960b. Laporan Ili Werung. Direktorat Vulkanologi Indonesia (74).

Wood B.J. and Fraser D.G., 1976. Elementary thermodynamics for geologists. Oxford, Oxford University Press.

Woodhead J.D., 1989. Geochemistry of the Mariana arc (western Pacific). Chem. Geology 76: 1-24.

Woodhead J.D. and Johnson R.W., 1993. Isotopic and trace element profiles across the New Britain island arc, Papua New Guinea. Contrib Mineral Petrol 113: 479-491.

Woodhead J., Eggins S. and Gamble J., 1993. High field strength and transition systematics in island arc and back-arc basin basalts: evidence for multiple-phase melt extraction and a depleted mantle wedge . Earth Planet. Sci. Lett. 114: 491-504.

Woodhead J.D., 1989. Geochemistry of the Mariana arc (western Pacific). Chem. Geology 76: 1-24.

Wordel R., Mouchel D., Solé V.A., Hoogewerff J.A. and Hertogen J., 1994. Investigation of the natural radioactivity of volcanic rock samples using a low background gamma-ray spectrometer. Nucl. Instr. Meth. Phys. Res. A 339, 322-328 339: 322-328.

Wyllie P.J. and Wolf M.B., 1993. Amphibolite dehydration-melting: sorting out the solidus. In: Magmatic Processes and Plate Tectonics. Eds: Prichard H.M. et al. Geological Society Special Publications 76: 405-416.

Appendix 1: Sampling

Locations

In this appendix sketch maps show the locations of all the samples collected during the expeditions of 1989 and 1990. Note that within the framework of this study only a selection of samples have been analysed and their results can be found in appendix 2 and following. For the sample locations of the SNELLIUS II expedition the reader is referred to Varekamp et al. *(1989)* and references therein. Sample locations of the Brouwer collection can be found in Brouwer *(1940)*. An overview of the different sampling areas is given in Figure 4.1.

The maps used are the "Verkenningskaart van de onderafdeling Oost-Flores en Solor-eilanden, oostblad" (1:100,000) from the Dutch colonial topographic service in Batavia (Jakarta) printed in 1931. This map is used in the Figures A1.1, A1.2, A1.3a, A1.4a, A1.4b, A1.5 and A1.7. For the island of Pantar (Fig. A1.8) and the small islands in the Strait of Pantar (Fig. A1.8) we used the "blad 88-89/XLIII-XLIV, Algemene Schetskaart van Nederlands Indië, 1:200,000, 1940" . Detailed sketch maps were available from reports of the Indonesian Volcanological Survey for the Werung (Fig. A1.3b) and Lewotolo (Fig. A1.6) volcanoes (Wiriosoemarto, 1960a and Wiriosoemarto, 1960b) and the Sirung volcano (Fig. A1.9) *(Rohi, 1978)*. The maps from Figure A1.10 are personal field sketches. The map of the island of Alor (Fig. A1.11) is from Oemar Ali (date unknown but available at the Volcanological Survey in Bandung).

Sampling procedures

The samples were gathered during fieldwork in the springs of 1989 and 1990. Large rock specimen were collected with as little as possible evidence of alteration. The outer sides of the fragments were removed and the resulting sample (about one kilogram) was packed in plastic bags. At the Department of Earth Sciences in Utrecht the samples were sawed to remove possible weathered parts. After rinsing with demineralized water a part of the sample was taken apart for the preparation of thin sections. The other part of the sample was further split and about 500 gram were grinned in a tungsten-carbide grinder to a size less than 5 millimetre. A representative split of 100 gram was used to prepare a powdered sample for chemical analysis using an agate grinding mill. All apparatus used, was cleaned between milling cycles with distilled water and acetone.

Figure A1.1 Sample locations Boleng volcano
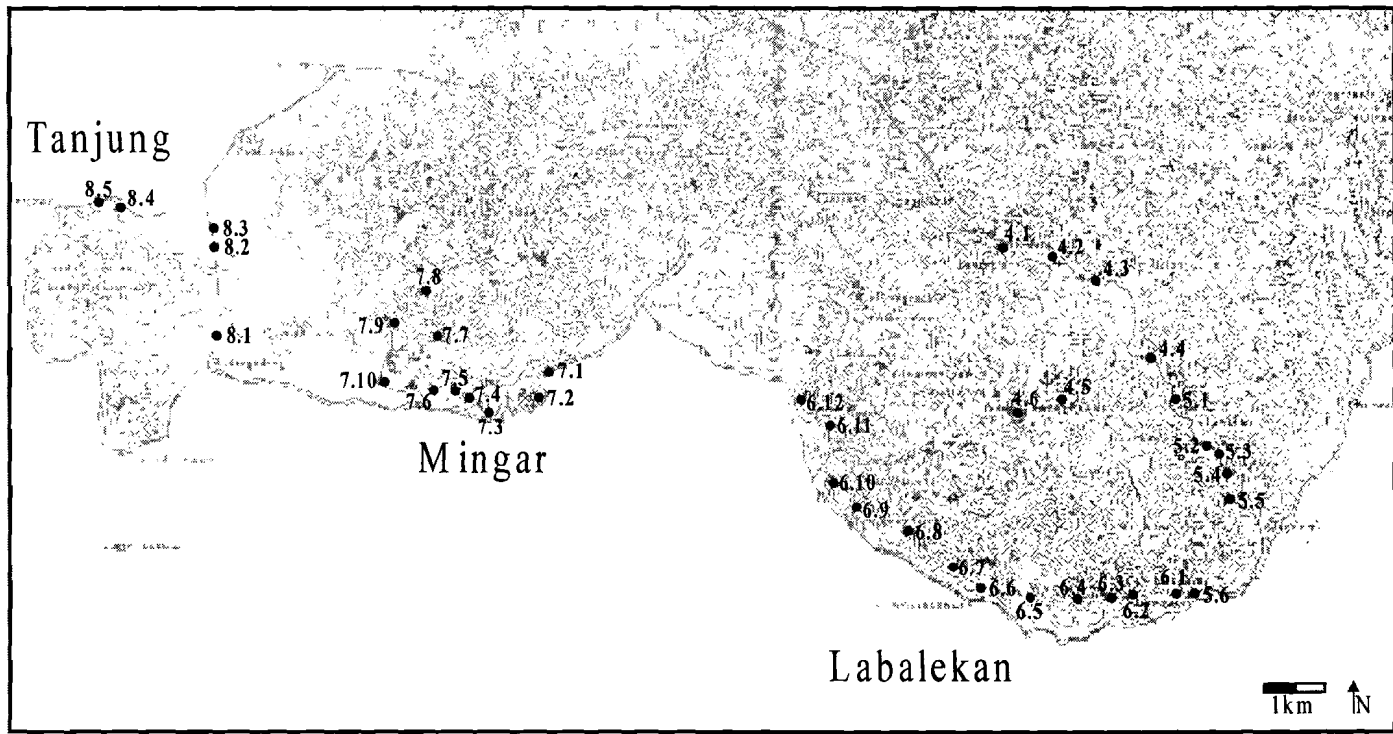
Figure A1.2 Sample locations South-West Lembata
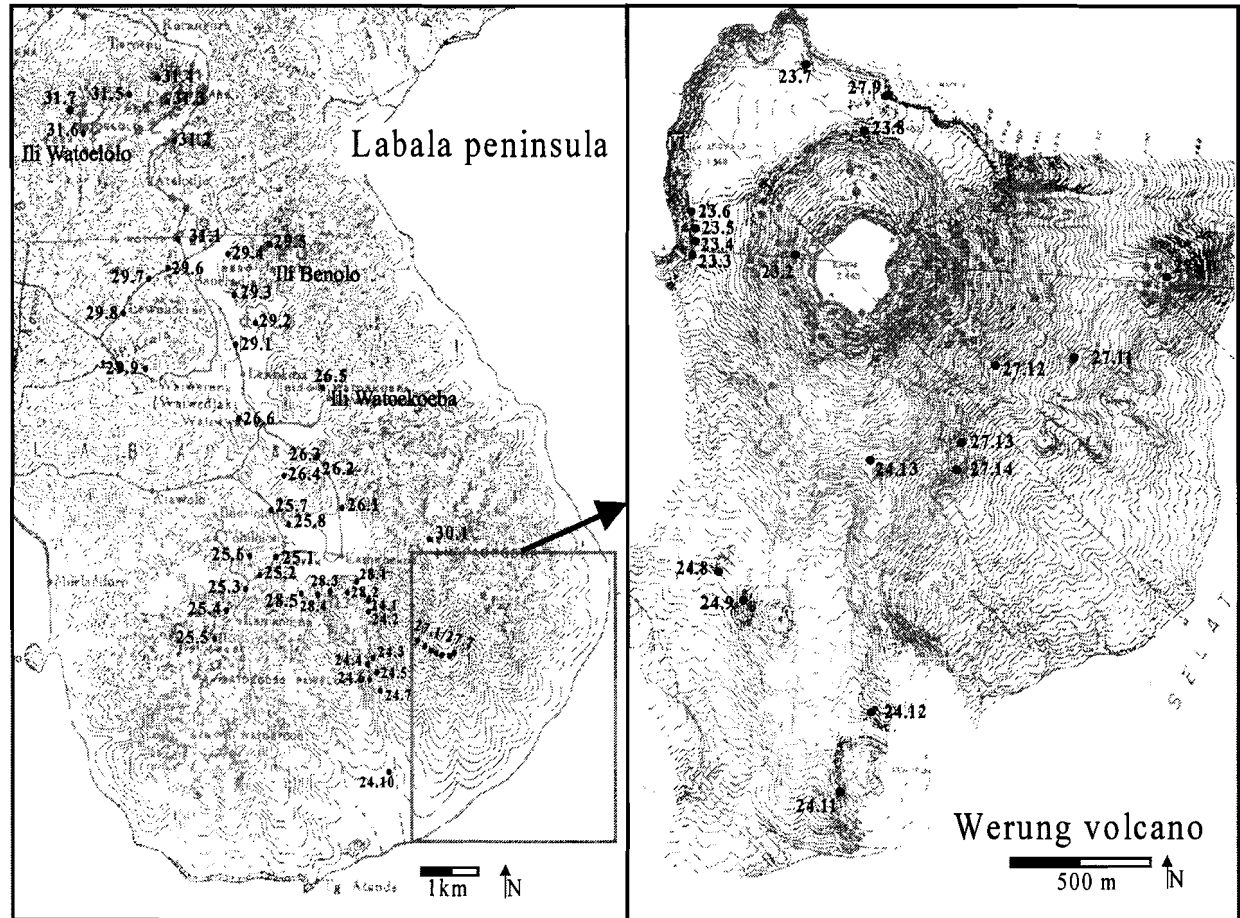
Figure A1.3 Sample locations Labala peninsula and Werung volcano
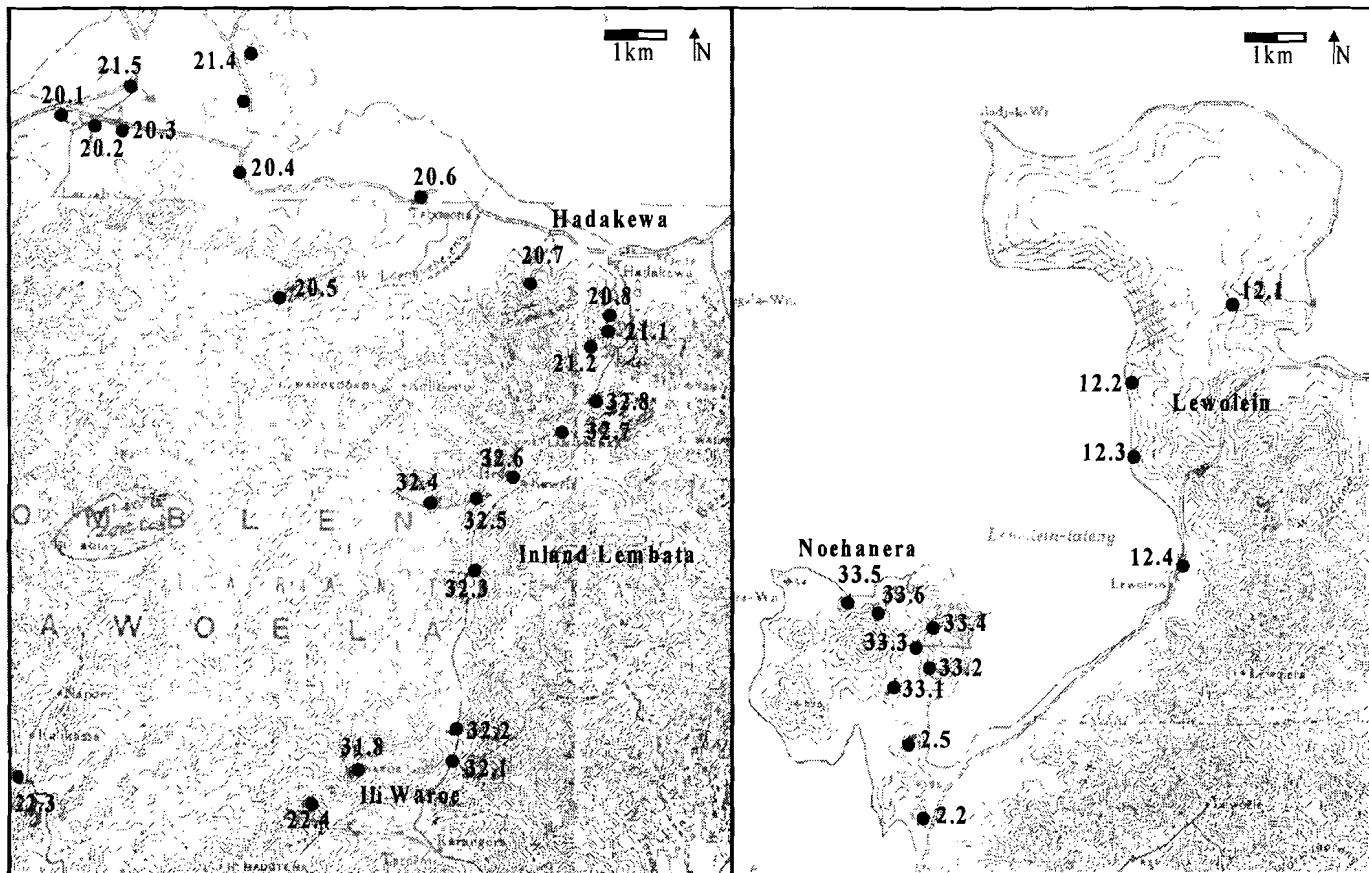
Figure A1.4 Sample locations Lembata centre and peninsulas

Figure A1.5 Sample locations Lewotolo
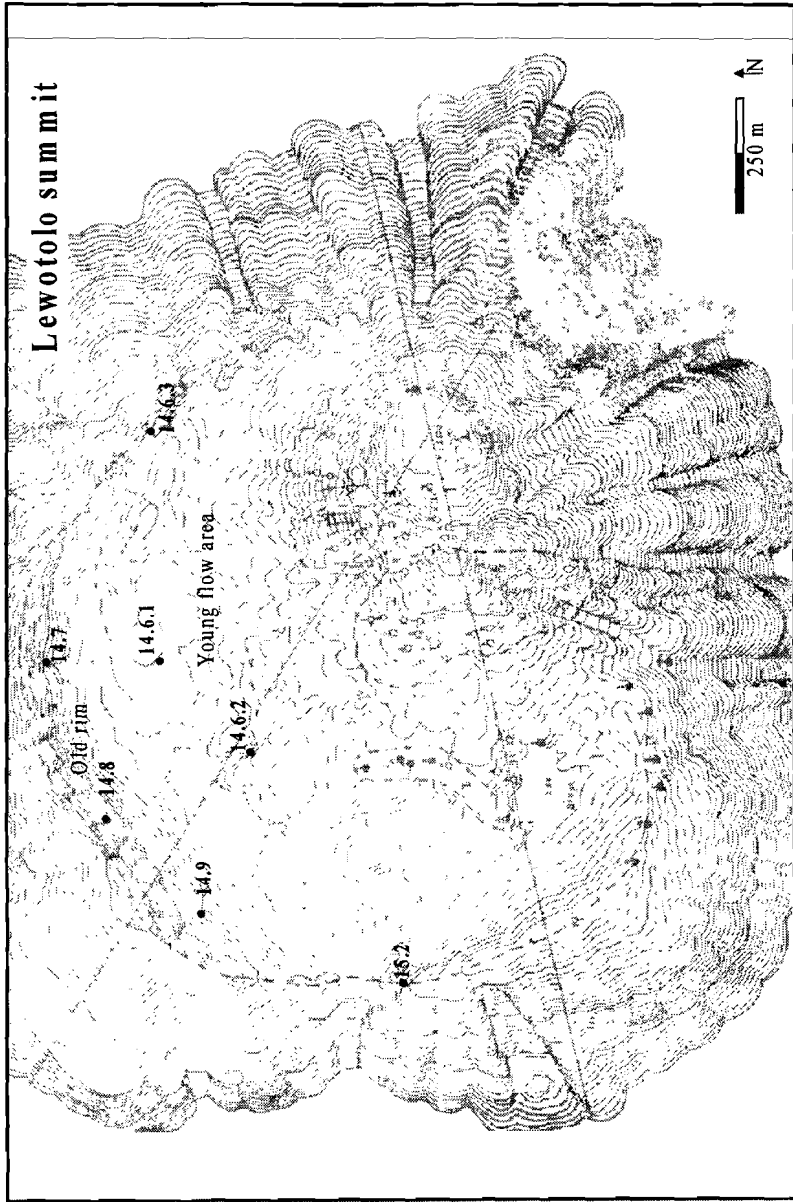
Figure A1.6 Sample locations summit crater Lewotolo
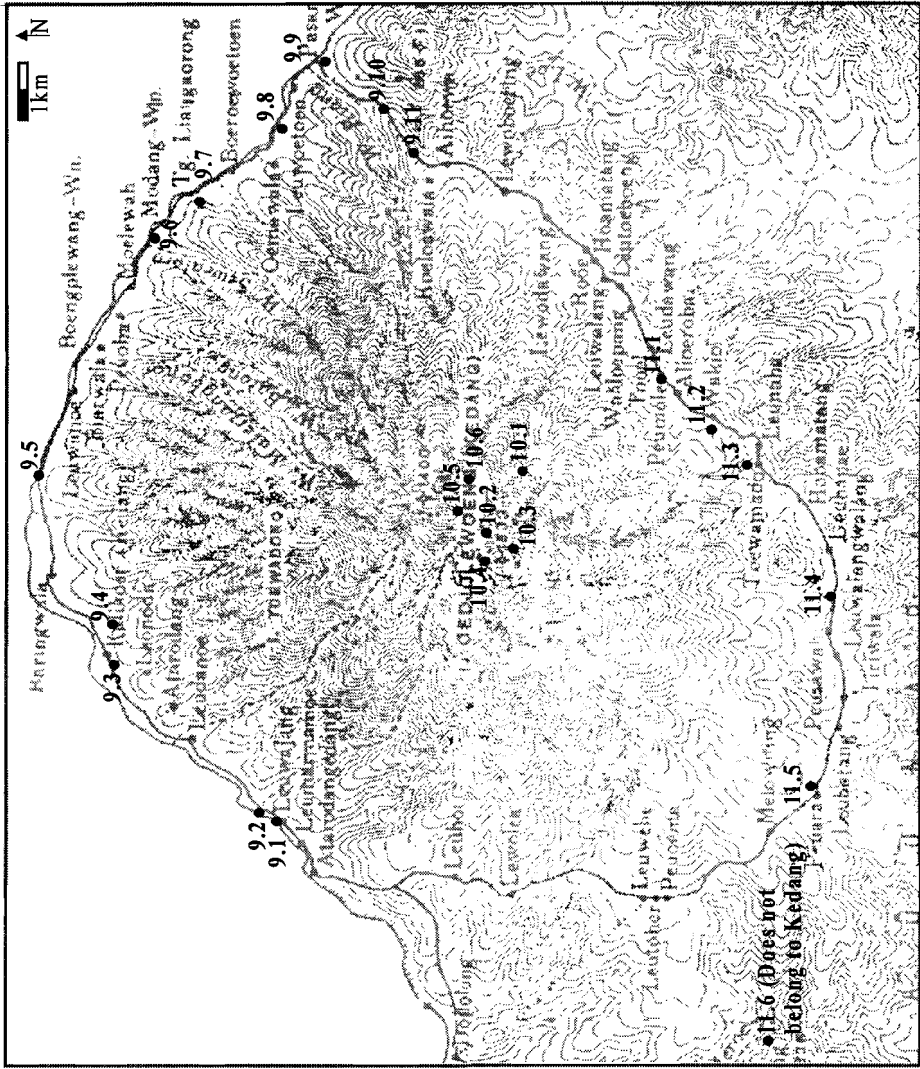
Figure A1.7 Sample locations Kedang

Figure A1.8 Sample locations Pantar and Treweg
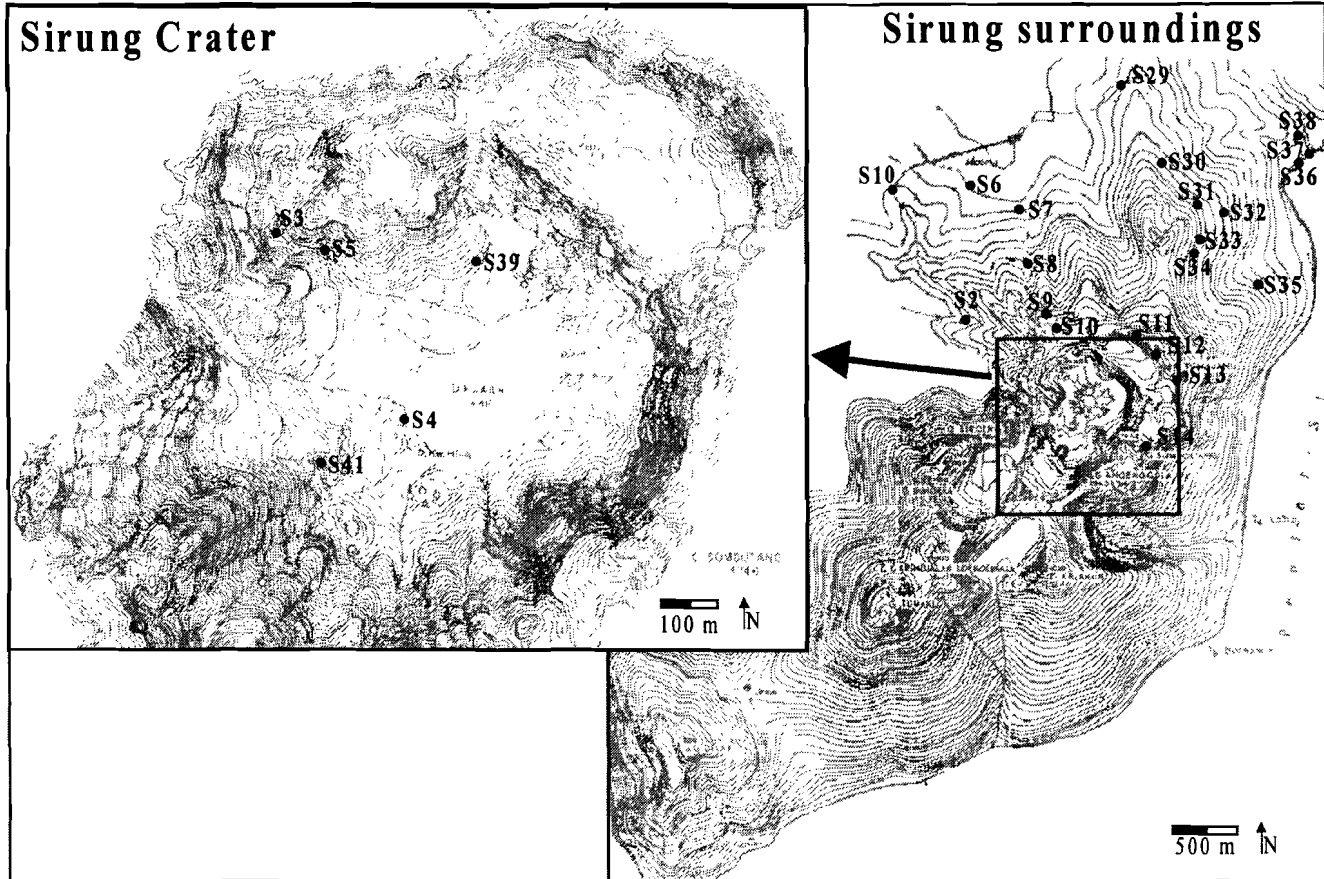
Figure A1.9 Sample locations Sirung surroundings and crater
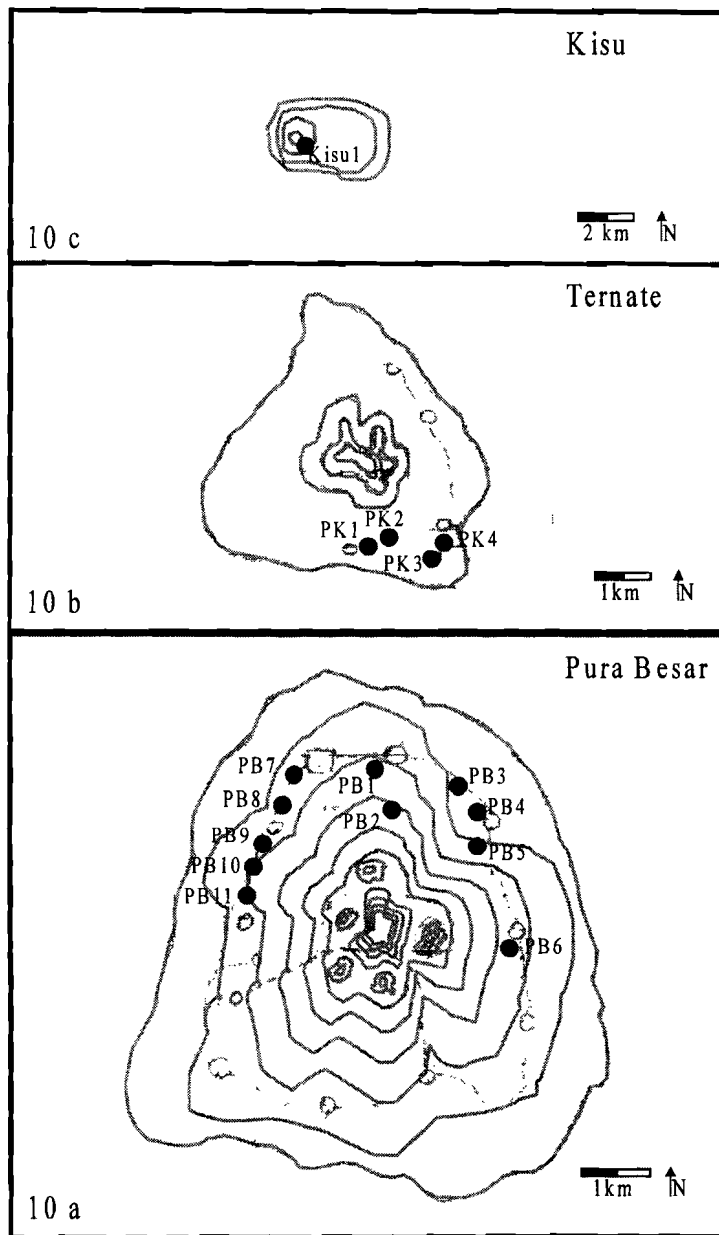
Figure A1.10 Sample locations Pura Besar, Ternate and Kisu
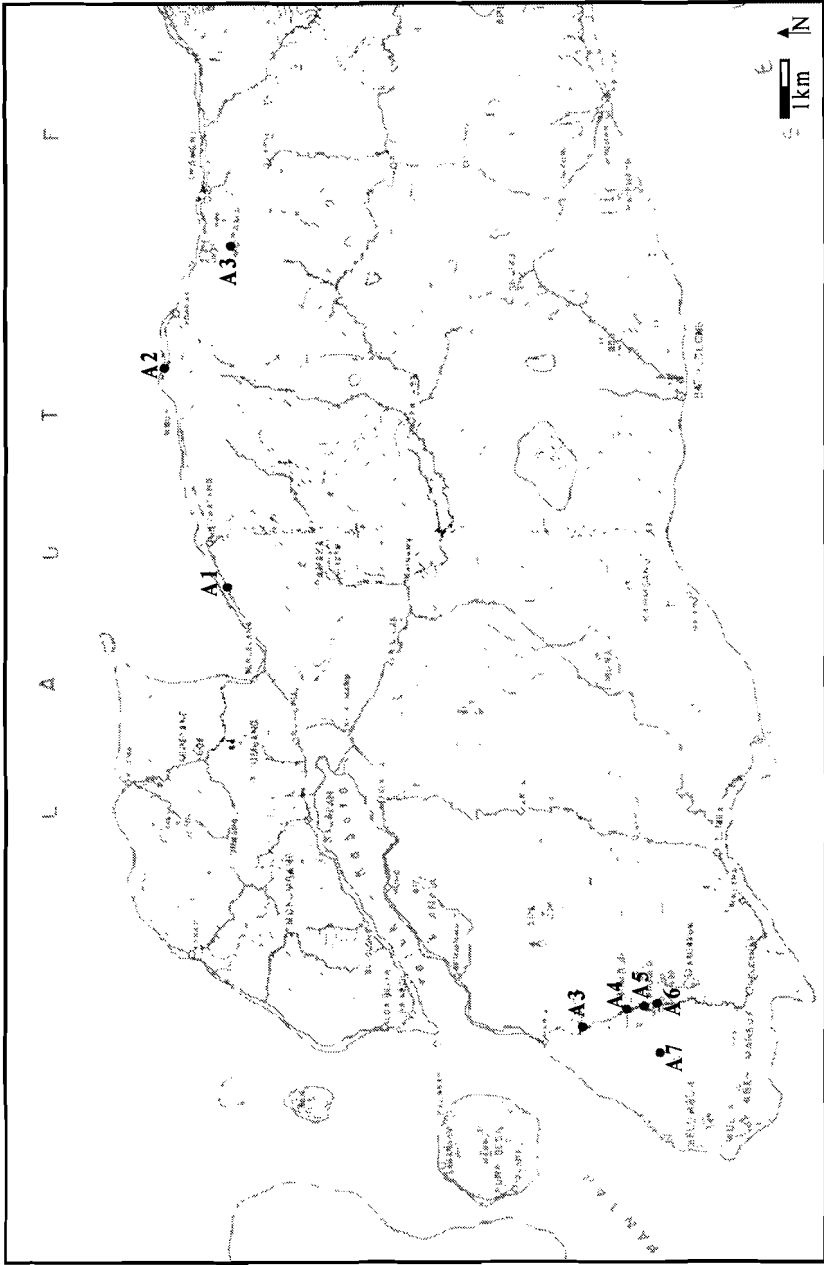
Figure A1.11 Sample locations Alor

Appendix 2 Sample Description

In this appendix the type of rock to which the samples belong and its microscopic characteristics are described.

Terminology used:
Location: the volcano, volcanic complex or region to which the samples belong.
Sample number: numbers used in text to denote the different samples in the field.
Laboratory number: numbers used to archive the samples in the collection at the Geochemistry Department in Utrecht.
Type: Field classification:

> lava sample comes from a clearly distinguishable lava flow,
> dome: sample comes from a dome structure,
> pumice or breccia: if a sample is such,
> inclusion: if the sample is found as an inclusion in host rock,
> Block in case of the Tanjung samples means that these samples come from boulders and not from well defined outcrops.

Minerals present: Ol= olivine, Cpx= clinopyroxene, Opx= orthopyroxene, Plag= plagioclase, Amph= amphibole, Phl = phlogopite, Op= dark opaque minerals present.
Signs: + = present, +++ = relatively large amount of this mineral, ± = present but altered and ? questionable remnants present.
Remarks: Porph, Seriate or Glom: lavas have porphyritic, seriate or glomero-porphyritic character *(according to Mackenzie et al., 1982)*. Agglo: indicates that agglomerates of pheno- or xenocrystal origin are present. Vesic hints at vesicular structure of the sample. Glassy indicates absence of phenocrysts.

Location	Sample	Lab. Nr.	Type	Ol	Cpx	Opx	Plag	Hbl	Phl	Op	Ap	Remarks
Labalekan												
	4-3-1	12M324	Lava		+	+	+			+		porf
	4-6-1	12M327	Lava		+		+			+		porf
	4-6-2	12M328	Lava		+	+	+			+		porf
	4-6-3	12M329	Lava	±	+	+	+			+		porf
	4-6-4	12M330	Lava	±	+	+	+			+		seriate
	4-6-5	12M331	Lava	+	+	+	+			+		seriate
	5-2-1	12M333	Lava	+	+	+	+			+		porf
	5-4-1	12M334	Lava		+	+	+			+		porf
	5-5-4	12M337	Lava		+	+	+			+		porf
	5-5-5	12M338	Lava		+	+	+			+		porf
	5-6-1	12M339-2	Lava		+	+	+			+		porf
	6-10-1	12M340	Lava	+		+	+			+		porf
	6-3-1	12M345	Lava	+	+	+	+			+		porf
	6-6-1	12M348-3	Lava		+	+	+			+		porf
Mingar												
	7-5-1	12M355	Lava	+	+	+	+			+		porf
	7-5-2	12M356	Lava	±	+	+	+			+		porf
	7-7-1	12M358	Lava		+	+	+			+		seriate
	7-9-1	12M360	Lava	+	+	+	+			+		seriate
Labala peninsula												
	24-2-1	12M224	Lava	±		+	+			+		seriate
	24-4-1	12M226	Lava		+	+	+			+		seriate
	32-6-1	12M227	Lava		+	+	+					seriate
	24-10-1	12M228	Lava				+			+		glassy no phenocrists
	24-6-1-1	12M243	Lava		+	+	+			+		seriate
	24-6-1-2	12M244	Lava		+	+	+			+		seriate
	25-2-1	12M252	Lava		+	+	+			+		porf
	25-3-1	12M253-2	Lava	+	+	+	+			+		seriate
	25-4-1	12M254	Lava		+	+	+			+		seriate
	25-5-1	12M255	Lava		+	+	+			+		porf
	25-5-2	12M256	Lava	+	+	+	+			+		porf, glassy
	25-7-1	12M260	Lava	±	+	+	+			+		seriate
	25-8-1	12M261	Dome		+	+	+			+		porf
	26-3-1	12M264	Dome ?	±	+	+	+			+		porf
	26-4-1	12M265	Dome	±	+	+	+			+		porf, vesic
	26-4-2	12M266	dome		+	+	+			+		porf
	26-5-1	12M267	Lava		+	+	+			+		porf
	26-5-2	12M268	Lava	±	+	+	+			+		porf
	28-1-1	12M271	Dome		+	+	+			+		porf
	28-2-1	12M272	Lava		+		+			+		porf
	28-3-1	12M273	Lava			+	+			+		porf
	28-4-1	12M274	Lava			+	+			+		seriate
	28-5-1	12M275	Lava		+	+	+			+		seriate
	29-1-1	12M276	Lava		+	+	+			+		porf
	29-2-1	12M277	Lava	±	+	+	+			+		porf

158

Location	Sample	Lab. Nr.	Type	Ol	Cpx	Opx	Plag	Hbl	Phl	Op	Ap	Remarks
Labala peninsula												
	29-3-1	12M278	Lava	±	+	+	+			+++		porf
	29-3-2	12M279	Lava		+	+	+	±		+		seriate
	29-3-4	12M281	Incluision	±	+	+	+					Large XX
	29-5-1-1	12M283	Lava	+	+	+	+			+		porf, vesic
	29-5-1-3	12M285	Lava	±	+	+	+			+		porf
	29-6-1	12M286	Breccia	±	+	+	+			+		porf
	29-7-1	12M287	Lava	±	+	+	+			+		porf, incl
	29-8-1	12M288	Lava		+	+	+			+		porf, incl,Q
	29-9-1	12M290	Lava	+	+	+	+			+		porf
	31-1-1	12M294	Lava		+	+	+			+		porf
	31-2-1	12M295	Lava		+	+	+			+		porf
	31-3-1	12M296	Lava		+	+	+			+		porf
	31-4-1	12M297	Lava		+	+	+			+		porf
	31-5-1	12M298	Lava	+	+	+	+			+		porf
	31-6-1	12M299	Lava		+	+	+			+		porf
	31-7-1	12M300	Lava		+	+	+			+		porf,incl
	31-8-1	12M301	Lava		+	+	+			+		porf
Tandjung												
	8-1-2	12M362	block		+	+	+			+		porf
	8-5-1	12M366	block	±	+		+			+		porf
	8-5-2	12M367	block	+	+	+	+			+		porf
	8-5-3	12M368	block	+	+	+	+			+		porf
Werung												
	27-1-1	12M179	Lava		+	+	+			+		seriate
	27-1-2	12M180	Lava		+	+	+			+		glassy
	27-2-1	12M181	Lava	+	+	+	+			+		porf, agglo
	27-3-1	12M182	Lava		+	+	+			+		seriate
	27-4-1	12M183	Lava		+	+	+			+		seriate
	27-5-1	12M184	Lava		+	+	+			+		seriate
	27-6-1	12M185	Lava		+	+	+			+		porf
	27-7-1	12M186	Lava		+	+	+			+		porf
	27-8-1	12M187	Lava		+	+	+			+		porf
	27-9-1	12M188	Lava		+	+	+			+		porf
	27-10-1	12M191	Lava	±	+	+	+			+		seriate
	27-10-2	12M192-2	Lava		+	+	+			+		porf
	27-10-3	12M193	Lava		+	+	+			+		seriate, large XX
	27-10-4	12M194	Lava		+	+	+			+		seriate
	27-12-1	12M196	Lava		+	+	+			+		seriate
	27-13-1	12M197	Lava	±	+	+	+			+		porf ,agglo
	27-14-1	12M198	Lava		+	+	+			+		
	23-2-1	12M199	lava		+	+	+			+		porf
	23-2-3-1	12M201	Dome	±	+	+	+			+		glom
	23-3-1	12M205	Dome	+	+	+	+			+		glom
	23-5-1	12M206	Lava		+	+	+			+		porf
	23-5-2	12M207	Lava	±	+	+	+			+		glom
	23-5-3	12M208	Lava	±	+	+	+			+		glom

Location	Sample	Lab. Nr.	Type	Ol	Cpx	Opx	Plag	Hbl	Phl	Op	Ap	Remarks
Werung	23-5-4	12M209	Lava	±	+	+	+			+		glom
	23-5-5	12M210	Lava	±	+	+	+			+		porf
	23-6-1-1	12M211	Lava	±	+	+	+			+		seriaat
	23-7-1	12M213	Lava	±	+	+	+			+		glom
	23-7-6	12M218	Lava		+	+	+			+		Cumu
	23-8-1	12M219	Dome	+	+	+	+			+		porf
	24-3-1	12M225	Lava		+	+	+			+		seriaat
	24-11-1	12M229	Dome	±	+	+	+			+		porf
	24-11-2	12M230	Dome	+	+	+	+			+		porf
	24-12-1	12M231-2	Dome	+	+	+	+			+		porf
	24-12-2	12M232	Dome	+	+	+	+			+		porf
	24-13-1-2	12M234	Dome	+	+	+	+			+		porf
	24-13-4	12M239	dome		+	+	+			+		glassy
	24-13-5	12M240	Pumice		+	+	+			+		Porf, vesic
	24-5-1	12M242	Lava		+	+	+			+		seriaat
	24-8-1	12M245	Lava	±	+	+	+			+		porf,vesiccles ,agglo
	24-8-2	12M246-2	Lava	±	+	+	+			+		porf,vesiccles ,agglo
	24-8-6	12M250	Lava	±	+	+	+			+		porf,vesiccles ,agglo
	24-9-1	12M251	Lava		+	+	+			+		porf
	30-1-1-2	12M293	Lava	+	+	+	+			+		porf
Boleng												
	34.3.1	12M498	Lava	+	+	+	+			+		seriate
	34.4.1	12M499-T	Lava		+	+	+			+		glassy
	B4202BO	B4202	Lava		+	+	+			+		glassy
	B4203BO	B4203										
	B4205BO	B4205										
	B4206BO	B4206										
	B4208BO	B4208										
	B4209BO	B4209										
	B4210BO	B4210										
	B4212BO	B4212										
	B4214BO	B4214										
	B4215BO	B4215										
Hadakewa												
	20-5-1	12M479	Lava	±	+	+	+			+		porf
	20-8-1	12M481										
	20-3-1	12M482										
	20-7-1	12M483										
Lewotolo												
	14-3-1	12M400	Lava		+	+	+	+		+		seriate
	14-6-1-3	12M407	Lava	+	+	+	+			+		porf
	14-6-2	12M408	Lava	+	+	+	+			+		porf
	14-6-3	12M409	Lava	+	+	+	+			+		porf
	14-7-1	12M410	Lava	+	+	+	+			+		seriate
	14-7-2	12M411	Lava		+		+	+		+		porf
	14-7-3	12M412	Lava		+		+	+		±		porf
	14-7-5	12M414	Lava		+	+	+	+		+		Seriate

160

Location	Sample	Lab. Nr.	Type	Ol	Cpx	Opx	Plag	Hbl	Phl	Op	Ap	Remarks
Lewotolo	14-8-1	12M415	Lava		+	+	+	+		+		porf
	15-2-1	12M417	Lava				+	+		+		glassy
	15-3-1	12M418	Lava		+	+	+			+		glassy
	15-4-1	12M419	Lava	+	+	+	+			+		glassy
	16-10-1	12M420	Lava	+			+			+		seriate, vesic
	16-10-2	12M421	Lava	+	+		+			+		seriate
	16-10-2	12M422	Lava	+	+	+	+			+		seriaat
	16-11-1	12M423	Lava	+	+	+	+		+	+		porf
	16-12-1	12M424	Lava	+	+	+	+		+	+		porf
	16-13-1	12M425	Lava		+	+	+	+		+		porf
	16-14-1	12M426	Lava	+	+	+	+	+		+		porf
	16-16-1	12M427	Lava	+	+		+	+		+		porf
	16-15-1	12M433	Lava		+		+			+		seriate
	16-2-1-1	12M434	Lava	−	+	+	+			+		seriate
	16-3-1	12M436	Lava	+	+	+	+	+		+		porf
	16-3-2	12M437	Lava	+	+	+	+			+		porf
	16-3-3	12M438	Lava		+	+	+			+		seriate, vesic
	16-4-1	12M439	Lava	+	+	+	+			+		seriate
	16-5-1	12M443	Lava		+		+			+		porf
	16-6-1	12M444	Lava	±	+	+	+	?		+		porf
	16-7-1	12M445	Lava		+	+	+	+		+		porf
	16-8-1	12M446	Lava		+	+	+			+		seriate
	16-8-2	12M447	Lava	+	+		+	+		+		porf
	16-9-1	12M448	Lava		+	+	+	+		+		porf
	17-1-1	12M449	Lava	+	+		+			+		porf
	17-2-6	12M450	Lava	+	+	+	+			+		porf
	17-2-9	12M451	Lava	+	+		+			+		vesic
	17-3-1-2	12M452	Lava	+	+	+	+			+		porf
	17-4-1	12M453	Lava	+	+		+			+		porf ,carb sec?
	17-5-1	12M454	Lava	+	+	+	+			+		porf
	17-7-1	12M455	Lava		+	+	+	+		+		seriate
	17-8-1	12M456	Lava	+	+	+	+		+	+		porf
	17-9-1	12M457	Lava	+	+	+	+		+	+	seriate	porf
	17-10-1	12M458	Lava	+	+	+	+	+		+		seriate
	17-12-1	12M459	Lava		+		+		+	+		porf
	17-13-1	12M460	Lava		+		+		+	+		porf
	17-14-1	12M461	Lava		+	+	+		+	+		seriate
	17-15-1	12M462	Lava		+	ı	+	+	+	+		seriate
	17-16-1	12M463	Lava	+	+		+			+		porf
	17-17-1	12M464	Lava	+	+	+	+		+	+		porf
	17-18-1	12M465	Lava	+	+		+	+		+		porf
	17-19-1	12M466	Lava		+		+	+		+		porf
	18-1-1	12M467	Lava	+	+		+			+		porf
	18-3-1	12M468	Lava		+		+	+		+		porf
	18-5-1	12M469	Lava	+	+		+			+		seriate, vesic
	18-8-1	12M470	Lava		+		+			+		seriate, vesic
	18-9-1	12M471	Lava		+		+	+	+	+		porf
	18-10-1	12M472	Lava	+	+	+	+			+		Seriate

Location	Sample	Lab. Nr.	Type	Ol	Cpx	Opx	Plag	Hbl	Phl	Op	Ap	Remarks
Lewotolo	19-1-1	12M473	Lava	+	+	+	+			+		seriate
	19-3-1	12M474	Lava	+	+	+	+			+		seriate
	19-7-1	12M475	Lava	+	+	+	+			+		porf
	19-8-1	12M476	Lava	+	+	+	+			+		seriate
	19-9-1	12M477	Lava	+	+	+	+			+		porf
	19-10-1	12M478	Lava		+	+	+	+		+		porf
	17-8-2	12M489	Lava		+	+	+	+	+	+		porf
	17-10-2	12M490	Lava		+		+	+		+		seriate
SE of Lewotolo	16-1-1	12M428	Lava		+	+	+		+	+		seriate, quartz?
	16-1-2	12M429	Lava		+	+	+		+	+		seriate, quartz!
	16-1-3	12M430	Lava		+		+		+	+		seriate, quartz!
	16-1-4-1	12M431	Lava		+		+		+	+		seriate, quartz!
Noehanera	33-1-1	12M485	Lava	+	+	+	+					seriate
	33-2-1	12M486	Lava	+	+	+	+					seriate
	33-3-1	12M487	Lava	+	+	+	+					seriate
	33-4-1	12M488	Lava	+	+	+	+					seriate
Inland Lembata	32-1-1-1	12M305	Lava	+	+	+	+			+		seriate
	32-2-1	12M307	Lava	+	+	+	+			+		porf
	32-3-1	12M309	Lava	+	+	+	+		±	+		porf
	32-3-2	12M310	Lava		+	+	+			+		porf
	32-3-3	12M311	Inclusion	+	+	+	+			+		porf
	32-3-4	12M312	Lava	+	+	+	+			+		porf
	32-5-1	12M314	Lava		+	+	+		+	+		porf
	32-5-6	12M319	Lava		+	+	+			+		porf
	32-8-1	12M322	Lava		+	+	+			+		porf
	32-9-1	12M323	Lava		+	+	+			+		porf
Sirung	PA1	PA1	Lava			+	+			+		porf
	PA4A2	PA4A2	Lava	±		+	+			+		glassy
	PA5	PA5	Lava	±	+	+	+			+		seriate
	S10.1	12M520	Lava		+	+	+			+		seriate
	S14.2.2	12M521	Lava	+		+	+			+		seriate
	S41.1	13M953-D	Lava	+	+	+	+			+		seriate
в.Waspila	B2.1	12M506	Lava		+	+	+			+		seriate
	B3.1	12M507	Lava	+	+	+	+			+		seriate
	B5.1	12M508	Lava	±	+	+	+			+		seriate
Dalaleng	12-1-2	12M381	Lava	+	+	+	+			+		porf
	12-2-1	12M382	Lava	+	+	+	+			+		porf
	12-4-1	12M385-3	Lava	+	+	+	+			+		porf

162

Location	Sample	Lab. Nr.	Type	Ol	Cpx	Opx	Plag	Hbl	Phl	Op	Ap	Remarks
Kedang												
	10-2-1	12M369	Lava	±	+	+	+		+	+		seriate
	10-4-1	12M371	Lava	+	+	+	+			+		seriate
	10-6-1	12M373	Lava		+	+	+		+	+		seriate
	11-3-1	12M376	Lava		+	+	+			+		seriate
	11-5-1	12M378	Lava			+	+	+++		+		seriate
	9-10-1	12M386	Lava	+	+	+	+			+		seriate
	9-1-1	12M388	Lava	+	+	+	+		±	+		seriate
	9-3-1	12M392-3	Lava	+	+	+	+	+		+		seriate
	9-4-1	12M393	Lava		+	+	+	+		+		porf
	9-6-1	12M395	Lava		+	+	+	+		+		seriate
	9-8-1	12M397	Lava		+	+	+	+	+	+		seriate
Treweg												
	TR1.2.1	12M522	Lava	+	+	+	+			+		seriate
	TR2.1.1	12M523-T	Lava	±	+	+	+			+		seriate
	TR5.1.1	12M524	Lava	+	+	+	+			+		seriate
Kisu												
	BUA1.2.3	12M509	Lava		+	+	+	+	+	+		porf
	BUA2.1	12M510	Lava		+	+	+	+	±	+		porf
Pura Besar												
	PB10.1.1	12M511-T	Lava	±	+	+	+			+		seriate
	PB11.1.3	12M512	Lava	±	+	+	+	±		+		seriate
	PB2.2	12M513	Lava	±	+	+	+			+		seriate
	PB3.1	12M514	Lava		+	+	+			+		seriate
	PB7.1	12M515	Lava	±	+	+	+			+		seriate
	PB8.1	12M516	Lava		+	+	+	+	±	±		seriate
Ternate												
	PK2.1	12M517	Lava		+	+	+	+		+	±	porf
	PK3.1.2	12M518	Lava		+		+	+	+	+		porf
	PK3.1.3	12M519	Lava			+	+	+	+	+		seriate
Alor												
	A1	12M500	Lava	±	+	+	+			+		seriate
	A10	12M505	Lava		+	+	+	+	+	+		seriate
	A11.1.1	12M501	Lava			+	+	+	+	+		seriate
	A2	12M502	Lava		+	+	+	+	+	+		seriate
	A4	12M503	Lava			+	+			+		seriate
	A5	12M504	Lava	±		+	+			+		seriate

163

Appendix 3.1 XRF analysis: sample preparation and standard measurements

Major elements

About 5 gram of powder were used to determine the loss on ignition (LOI) at 900 °C. Glass beads, containing 0.5 gram of ignited powder sample and 5.00 g $LiBO_2$-LiB_4O_7 (66/34) were fused at 1100 °C in a Herzog HAG 1200 automated furnace. Measurements were performed with a Philips PW 1400 XRF. The USG standards AGV-1, BCR-1, BHVO-1, G-2, GSP-1 were used to test accuracy and reproducibility. Accuracy and reproducibility are presented in Table A3.1 for the major elements. Results show very good reproducibility and accuracy for most elements, acceptable accuracy for P_2O_5 and a rather poor average accuracy for L.O.I.-number, which can be explained by the fact that the L.O.I. of the standards material is determined by heating from room temperature to 900 °C without an intermediate step at 120°C *(pers. comm. G.Eussen, 1990)*. Iron is calculated as Fe_2O_3 and oxides are normalised to 100% dry weight. Literature values (XXX-LIT) are from Govindaraju *(1989)*.

Sample	SiO_2	TiO_2	Al_2O_3	Fe_2O_3	MnO	MgO	CaO	Na_2O	K_2O	P_2O_5	L.O.I.	Total
AGV-1 avg. n=3	59.72	1.07	17.33	6.87	0.10	1.51	4.99	4.25	2.92	0.48	1.75	100.98
AGV-LIT	58.79	1.05	17.14	6.75	0.09	1.53	4.94	4.26	2.91	0.49	1.78	99.73
Reproducibility	1.0	1.1	0.5	1.1	0.0	2.7	1.4	2.5	1.0	4.3	20.2	0.6
Precision	1.6	1.6	1.1	1.7	8.7	-1.1	1.0	-0.3	0.2	-1.4	-1.9	1.3
BCR-1 avg. n=3	54.17	2.25	13.58	13.52	0.18	3.40	7.05	3.19	1.76	0.37	1.67	101.12
BCR-LIT	54.06	2.24	13.64	13.35	0.18	3.48	6.95	3.27	1.69	0.36	1.56	100.78
Reproducibility	1.1	1.2	0.8	0.9	0.0	1.5	0.7	0.5	0.9	0.0	0.0	0.9
Precision	0.2	0.4	-0.5	1.2	1.7	-2.4	1.4	-2.5	4.3	2.8	7.1	0.3
BHVO-1 avg. n=3	49.80	2.75	13.73	12.45	0.17	7.09	11.68	2.21	0.54	0.28	0.28	100.97
BHVO-LIT	49.94	2.71	13.80	12.34	0.17	7.23	11.40	2.26	0.52	0.27	0.21	100.85
Reproducibility	0.6	0.0	1.2	0.7	0.0	0.6	0.4	1.7	0.0	5.4	0.0	0.3
Precision	-0.3	1.5	-0.5	0.9	1.2	-2.0	2.5	-2.4	3.8	3.8	33.3	0.1
G-2 avg. n=3	69.48	0.50	15.48	2.71	0.03	0.82	1.89	4.10	4.46	0.15	0.81	100.44
G-2-LIT	69.08	0.48	15.38	2.69	0.03	0.75	1.96	4.08	4.48	0.14	0.62	99.69
Reproducibility	0.1	0.0	0.1	0.9	0.0	0.7	0.0	0.6	0.0	7.5	0.0	0.1
Precision	0.6	4.2	0.7	0.6	-6.3	9.8	-3.6	0.6	-0.4	9.5	30.6	0.7
GSP-1 avg. n=3	67.58	0.67	15.13	4.35	0.04	0.99	1.99	2.77	5.49	0.30	1.02	100.33
GSP-LIT	67.15	0.65	15.10	4.35	0.04	0.96	2.07	2.80	5.51	0.28	0.62	99.42
Reproducibility	0.8	0.9	0.9	0.7	0.0	3.3	0.3	4.7	0.8	3.3	0.0	0.9
Precision	0.6	3.6	0.2	-0.1	0.0	2.8	-3.7	-1.0	-0.4	7.1	64.5	0.9
Avg. reproducibility	0.8	0.6	0.7	0.8	0.0	1.7	0.6	2.0	0.5	4.1	4.0	0.6
Avg. precision	0.5	2.3	0.2	0.9	1.1	1.4	-0.5	-1.1	1.5	4.4	26.7	0.7

Table A3.1 Reproducibility and precision of major element analysis.

Trace elements

Eight grams of powder were mixed with 2 ml elvacite solution (elvacite: aceton=1:5) as a binding agent and pressed to pellets under 20 ton/cm2 for 1 minute.
The USG standards AGV-1, BCR-1, BHVO-1, GSP-1 were used to test accuracy and reproducibility (Table A3.2). In addition 11 duplicate- and 18 triplicate samples were analysed to test the homogeneity of the powdered samples and the reproducibility of the pellet preparation. Literature values (XXX-LIT) are from Govindaraju (*1989*).
In all Ba, Sc, V, Co, Cu, Ga, Nb, Ni, Pb, Rb, Sr, Th, Y, Zn, Zr have been measured.
The standard samples show good average accuracy for Ba, Sc, V, Ga, Rb, Sr, Th, Y, Zn and Zr (less than 5% error on average). Cu and Nb have slightly lower accuracy. The low average accuracy for lead is due to the low Pb concentration in the BHVO standard which is close to the detection limit of 5 ppm. The error in the measurement of Ni is large at concentrations below 20 ppm. The reproducibility of the duplicates and triplicates is good except for concentrations of Co below 20 ppm, Nb, Pb and Th below 10 ppm. The good overall reproducibility implies sample homogeneity. (ppm = mg/kg)

The accuracy is defined as (ValueSample-ValueStandard)/ValueStandard * 100%.
The reproducibility is defined as StandardDeviationOfSamples/AverageOfSamples * 100%.

Sample	Ba	Sc	V	Co	Cu	Ga	Nb	Ni	Pb	Rb	Sr	Th	Y	Zn	Zr
AGV-1 avg n=4	1174	13 6	126	15 2	60.0	20 3	14 3	22.9	36.9	68.3	655	7 22	20 8	86.0	234
AGV-LIT	1226	12.2	121	15 3	60 0	20.0	15 0	16.0	36 0	67 3	662	6.50	20.0	88.0	227
precision	-4.2	11.6	4.1	-0.8	0.0	1.5	-4.4	43.3	2.4	1.5	-1.1	11.0	3.8	-2.3	3.2
reproducibility	0.5	3.7	9.7	8.1	2.3	-5.2	3.8	5.5	7.5	1.0	0.4	17.2	5.3	1.6	2.0
BCR-1 avg. n=4	699	32.0	432	39 6	23.5	23.4	12.3	15.1	12.9	49.1	336	6 13	37.2	124 7	197
BCR-LIT	681	32.6	407	37 0	19.0	22.0	14 0	13.0	13.6	47.2	330	5 98	38.0	129.5	190
precision	2.7	-1.9	6.1	7.0	23.6	6.4	-12.1	16.2	-5.2	3.9	1.8	2.6	-2.1	-3.7	3.7
reproducibility	0.3	4.3	1.7	1.5	3.7	5.1	2.3	12.8	16.0	2.7	0.6	23.8	5.7	1.0	0.3
BHVO-1 avg n=4	129	30.6	277	44.5	141.4	23.0	18 5	120.8	4.8	10.4	399		27.0	104 0	178
BHVO-LIT	139	31 8	317	45 0	136.0	21.0	19 0	121.0	2.6	11 0	403	1.08	27.6	105 0	179
precision	-7.0	-3.9	-12.5	-1.2	4.0	9.5	-2.8	-0.2	83.5	-5.7	-1.0		-2.2	-0.9	-0.8
reproducibility	2.3	2.2	2.4	7.2	1.8	5.8	2.9	1.1	27.3	1.3	1.1		6.8	1.1	1.2
GSP-1 avg. n=4	1251		53	7 0	32 1	21.3	25 1	14 9	58.6	257	236	98.3	30.6	103	509
GSP-LIT	1310	6.2	53	6.6	33.0	23.0	27 9	8 8	55 0	254	234	106.0	26.0	104	530
precision	-4.5		0.9	6.2	-2.6	-7.5	-10.1	69.5	6.5	1.0	0.9	-7.3	17.7	-1 0	-4.0
reproducibility	0.4		10.5	8.5	1.4	4.3	1.2	9.9	2.5	0.4	0.4	5.6	13.3	0.4	3.1
Avg. precision	-3.3	1.4	-0.4	2.8	6.2	2.5	-7.3	32.2	21 8	0.2	0.2	1.6	4.3	-2.0	0.6
Avg. reproducibility	0.9	2.6	6.1	6.3	2.3	5.1	2.6	7.3	13.3	1.3	0.6	11.7	7.8	1.1	1.7

Average reproducibility 11 duplicates and 18 triplicates															
	Ba	Sc	V	Co	Cu	Ga	Nb	Ni	Pb	Rb	Sr	Th	Y	Zn	Zr
reproducibility	0.8	2.0	4.8	10.0	2.1	2.5	5.5	5.9	8.7	2.0	0.4	9.2	2.0	0.8	0.9
between 1 and 10 ppm			12(1-20 ppm)				6.0		17			15			
above 10 ppm			5(>20 ppm)				3 7		6			6			

Table A3.2 Reproducibility and precision of trace element analysis.

Appendix 3.2: INA analysis: standard measurements

Table A3.3 shows the precision of the INAA (Instrumental Neutron Activation Analysis) measurements performed by J. Hertogen in Leuven, Belgium. Table A3.4 shows the precision of the INAA by T. van Meerten at IRI in Delft, the Netherlands.

	AN-G			BCR-1			BE-N		
	Measured	2 SEM	Recommended	Measured	2 SEM	Recommended	Measured	2 SEM	Recommended
Sc	10	0.1	10	32.3	0.3	33	22	0.3	22
Cr	44	2	50	13	1	17.6	350	7	360
Co	25.3	0.5	25	38.2	0.5	38	63.4	1.1	61
La	2.2	0.2	2	25.1	0.4	26	79	2	82
Ce	4.6	0.2	4.7	55.1	0.9	53.9	150	4	152
Nd	2.3	0.2	2	28.3	0.7	29	63	2	70
Sm	0.68	0.03	0.7	6.53	0.06	6.6	11.7	0.3	12
Eu	0.37	0.01	0.37	1.99	0.03	1.94	3.63	0.08	3.6
Tb	0.18	0.01	0.2	1.04	0.03	1	1.29	0.07	1.3
Yb	0.82	0.03	0.85	3.35	0.08	3.36	1.76	0.09	1.8
Lu	0.12	0.01	0.12	0.52	0.03	0.55	0.24	0.04	0.24
Hf	0.38	0.02	0.38	4.8	0.1	4.7	5.5	0.2	5.4
Ta	0.18	0.02	0.2	0.85	0.02	0.91	6.4	0.1	5.5
Th	<0.1	-	-	6.1	0.1	6	10.7	0.2	11
U	<0.1	-	-	1.66	0.08	1.74	2.2	0.5	2.4

Table A3.3 Results from geostandards as measured by Pedersen and Hertogen *(1990)* in Leuven. Recommended values from Govindaraju *(1984)*. SEM: standard error of the mean.

	BCR-1			BHVO			SCO-1		
	Measured	1 S	Recommended	Measured	1 S	Recommended	Measured	1 S	Recommended
Sc	33.24	0.62	32.6	32.13	0.66	31.8	12.00	0.38	10.8
Cr	13.8	1.24	16	292.63	8.13	289	71.17	2.12	68
Co	37.63	0.25	37	45.74	0.9	45	11.31	0.58	10.5
La	29.42	1.24	24.9	17.33	1.29	15.8	29.21	1.96	29.5
Ce	52.84	2.34	53.7	38.87	1.27	39	57.92	3.06	62
Sm	6.66	0.33	6.59	6.03	0.17	6.2	5.38	0.22	5.3
Eu	2.00	0.04	1.95	2.07	0.03	2.06	1.19	0.05	1.19
Tb	1.09	0.15	1.05	0.91	0.06	0.96	0.72	0.07	0.7
Yb	3.28	0.24	3.38	1.93	0.17	2.02	2.12	0.05	2.27
Lu	0.63	0.11	0.51	0.38	0.08	0.29	0.37	0.03	0.34
Hf	5.08	0.09	4.95	4.45	0.15	4.38	4.71	0.16	4.6
Ta	0.56	0.12	0.81	1.04	0.15	1.23	0.76	0.07	0.92
Th	5.80	0.15	5.98	1.12	0.08	1.08	9.47	0.28	9.7
U	1.71	0.12	1.75	-	-	0.42	3.36	0.32	3.0

Table A3.4 Results from geostandards measured in Delft according to de Bruin *(1983)* and published by Vroon *(1992)*. Recommended values from Govindaraju *(1989)*. S is standard deviation.

Appendix 3.3: Sr, Nd and Pb analysis: sample preparations and standard measurements

Sr, Nd and Pb analysis were performed at the Free University Amsterdam in 1992 except for Pb isotopes of the Werung samples which were analysed at Cornell, Ithaca by P.Z. Vroon *(Vroon et al., 1993)*.

Strontium isotopes

For the Sr isotopes approximately 0.5 gram were dissolved in HF-HNO$_3$ 1:1. After complete destruction and evaporation an aliquot was dissolved and Sr was isolated in a two step method on ion-exchange columns. Samples were run on a Finnigan MAT261 using double jumps on fixed multicollectors with double Re-filaments. NBS987 runs yielded a ^{87}Sr/^{86}Sr 0.710264±18 n=7, blanks average at 0.9 ng Sr.

Neodymium isotopes and Sm and Nd abundances

About 0.25 g of sample for Nd isotopes and Sm, Nd isotope dilution was dissolved in 1:1 HF-HNO$_3$. Using standard ion-exchange techniques *(c.f. Valbracht, 1991)* Nd and Sm were separated from the matrix. Using double jumps the La Jolla standard yielded a ^{143}Nd/^{144}Nd of 0.511841±12 n=5 using exponential correction.
Blanks showed less than 1 ng of both elements. Sm and Nd were measured simultaneously on the MAT261 using the method of Hebeda et al. *(1988)*. Precision of the measurements is better than 1% *(Valbracht, 1991)*.

Lead isotopes

For the Pb isotopes ca. 0.5 g of sample was dissolved in 1:1 HF-HNO$_3$ and separated from the matrix using ion-exchange columns. About 1mg Pb was loaded on a single Re-filament using phosphoric-acid and silica-gel *(Cameron et al., 1969)*. Filament temperature was slowly raised to 1300 °C. Mass fractionation correction was based on replicate analyses of NBS981 (0.088% per amu). Blanks for Pb showed less than 0.5 ng.

Appendix 4: Analytical results

In Table A4.1 the XRF results for major and trace elements are presented. The columns INAA and isotopes indicate that additional INAA respectively isotope measurements have been performed and the reader is referred to the Tables A4.2 and A4.3 for the results.

The LOI is the weight loss on ignition starting from room temperature except for those cases where data is to be found in the H_2O-column. In those cases LOI is weight loss on ignition starting at 120 °C. H_2O- is weight loss on drying at 120 °C starting from room temperature. Fe_2O_3 equals all iron.

Additional high-precision Nb XRF analyses of 'low-abundance' samples from Werung were carried out at Royal Holloway, following Jochum et al. *(1990)* by P. Vroon. The values determined in this manner are denoted in italics.

Table A4.2 shows the results of the INAA (Instrumental Neutron Activation Analysis) performed by J. Hertogen in Leuven, Belgium and T. van Meerten at IRI in Delft, the Netherlands. Because Nd is not measured at IRI, Nd-values for the samples measured in Delft were interpolated from weighted Ce and Sm values (italics in Table 4.2).

Table A4.3 contains the results of the Nd-, Sm-, Sr-, Pb isotope and trace element results. Errors in Table A4.3 indicate one standard deviation.

Volcano	Labalekan									
Sample	4-3-1	4-6-1	4-6-2	4-6-3	4-6-4	4-6-5	5-2-1	5-4-1	5-5-4	5-5-5
Lab. Nr.	12M324	12M327	12M328	12M329	12M330	12M331	12M333	12M334	12M337	12M338
Latitude	8.53	8.53	8.53	8.53	8.53	8.53	8.53	8.53	8.53	8.53
INAA	+		+		+					
Isotopes	+				+					
SiO_2	54.5	58.4	62.3	55.2	56.1	54.2	62.4	58.6	58.8	50.3
TiO_2	0.79	0.72	0.69	0.74	0.73	0.79	0.68	0.71	0.73	0.90
Al_2O_3	17.6	20.2	16.8	17.0	16.8	17.8	15.9	19.1	18.8	19.5
Fe_2O_3	9.58	6.91	7.20	9.55	9.38	9.66	7.82	7.19	7.30	11.41
MnO	0.17	0.14	0.16	0.18	0.18	0.18	0.16	0.15	0.15	0.19
MgO	4.46	1.53	1.90	4.81	4.42	4.48	1.98	1.73	1.71	3.87
CaO	9.28	7.80	5.87	9.01	8.62	9.43	5.98	7.97	7.98	11.04
Na_2O	2.61	3.04	3.55	2.51	2.70	2.52	3.69	3.38	3.45	2.17
K_2O	0.88	1.15	1.40	0.91	0.97	0.78	1.34	0.89	0.89	0.49
P_2O_5	0.10	0.14	0.16	0.12	0.12	0.11	0.14	0.19	0.18	0.10
H_2O-										
LOI	-0.16	0.86	1.29	0.33	-0.09	0.05	0.45	0.46	0.35	-0.36
Ba	495	668	837	534	582	451	778	536	543	347
Sc	30	22	22	29	27	31	27	30	28	37
V	222	62	73	169	190		97	98	105	290
Co	21.1	10.1	9.3	24.0	20.0	24.4	12.6	9.6	13.0	27.6
Cu	44	44	27	51	38	68	27	34	23	79
Ga		18	17	17	16	15	17	20	20	21
Nb	1.7	3.5	3.5		2.1		3.3	3.1		
Ni	19.7			23.8	20.6	19.0				
Pb	17	16	21	15	13	16	30	18	14	12
Rb	21	26	38	24	26	21	31	20	20	13
Sr	309	340	287	328	330	313	275	383	385	424
Th								8.5		
Y	27	23	37	25	27	25	46	32	33	19
Zn	69	62	68	64	65	71	69	77	70	75
Zr	81	99	117	86	91	82	114	77	77	43

Table A4.1 Major and trace element results XRF.

Volcano	Labalekan				Mingar				Labala Penin.	
Sample	5-6-1	6-3-1	6-6-1	6-10-1	7-5-1	7-5-2	7-7-1	7-9-1	24-10-1	24-2-1
Lab. Nr.	12M339-2	12M345	12M348-3	12M340	12M355	12M356	12M358	12M360	12M228	12M224
Latitude	8.53	8.53	8.53	8.53	8.52	8.52	8.52	8.52	8.52	8.52
INAA		+			+	+			+	+
Isotopes										
SiO_2	57.2	48.8	58.2	57.3	57.5	57.9	55.9	52.3	55.0	51.9
TiO_2	0.83	0.86	0.94	0.74	0.75	0.76	0.88	0.92	0.96	0.73
Al_2O_3	18.1	18.0	16.3	16.6	16.8	16.9	16.8	17.7	16.9	20.0
Fe_2O_3	9.10	11.93	9.53	9.87	8.34	8.33	9.55	11.09	11.21	9.90
MnO	0.14	0.20	0.20	0.14	0.16	0.17	0.18	0.19	0.20	0.20
MgO	2.46	4.78	3.01	3.61	3.63	3.49	3.75	4.60	3.56	3.91
CaO	7.94	12.87	7.32	8.06	8.37	8.15	8.76	9.57	8.42	10.79
Na_2O	3.28	2.04	3.36	2.50	2.93	3.02	2.84	2.56	2.56	2.17
K_2O	0.82	0.42	0.94	1.09	1.38	1.22	1.17	0.91	1.09	0.33
P_2O_5	0.15	0.10	0.17	0.07	0.13	0.13	0.14	0.16	0.14	0.11
H_2O-									0.05	0.22
LOI	1.11	0.61	-0.32	0.15	0.67	0.22	0.13	0.04	-0.43	-0.29
Ba	426	325	631	749	645	661	584	507	361	226
Sc	37	38	34	28	29	28	32	35	41	37
V	155	295	157		178	174	224	248	277	245
Co	13.8	29.7	15.9	6.5	17.3	17.0	22.0	27.0	25.9	24.4
Cu	32	57	13		34	38	39	55	50	38
Ga	18	17	17	16	16	16	18	17	19	19
Nb	3.4		4.0	4.2	5.1	4.0	4.3	4.6		
Ni					10.1	10.1		11.1		
Pb	12	8	15	16	18	19	15	11	11	-6
Rb	22	9	21	25	34	34	28	24	44	8
Sr	356	412	381	368	382	383	396	452	263	288
Th									2.6	4.1
Y	24	18	32	41	27	29	28	24	26	20
Zn	79	72	82	73	64	64	76	73	87	76
Zr	63	38	83	107	86	88	80	62	79	38

Table A4.1 Major and trace element results XRF, continued.

Volcano	Labala peninsula									
Sample	24-4-1	24-6-1-1	24-6-1-2	25-2-1	25-3-1	25-4-1	25-5-1	25-5-2	25-7-1	25-8-1
Lab. Nr.	12M226	12M243	12M244	12M252	12M253-2	12M254	12M255	12M256	12M260	12M261
Latitude	8.52	8.52	8.52	8.52	8.52	8.52	8.52	8.52	8.52	8.52
INAA	+									+
Isotopes										
SiO_2	53.6	54.2	54.1	53.5	53.8	53.4	59.0	59.1	52.0	53.5
TiO_2	0.85	0.84	0.86	0.87	0.81	0.84	0.60	0.60	0.85	0.75
Al_2O_3	18.2	18.0	17.9	20.6	20.2	18.0	19.5	20.1	17.9	19.6
Fe_2O_3	10.95	10.73	10.82	9.12	8.97	11.06	6.18	6.16	12.03	9.30
MnO	0.23	0.23	0.23	0.17	0.17	0.19	0.10	0.10	0.21	0.18
MgO	4.12	3.93	3.99	2.53	2.76	4.14	2.05	1.72	4.20	3.40
CaO	9.04	9.03	8.98	9.51	9.58	9.19	8.46	7.99	10.15	9.93
Na_2O	2.57	2.56	2.59	2.68	2.77	2.23	2.87	2.84	2.04	2.67
K_2O	0.36	0.38	0.37	0.82	0.80	0.81	1.12	1.26	0.49	0.47
P_2O_5	0.10	0.12	0.13	0.15	0.15	0.11	0.14	0.14	0.10	0.11
H_2O-	0.08	0.14	0.16	0.05	0.25	0.70	0.73	0.78	0.80	0.41
LOI	-0.28	-0.46	-0.48	0.37	0.14	0.16	0.62	0.77	0.45	-0.18
Ba	221	239	240	323	324	297	364	368	316	254
Sc	32	32	32	33	30	44	22	21	39	35
V	175	195	199	182	176	281	102	89	275	213
Co	16.1	18.2	18.9	17.2	18.0	20.7	6.6	7.4	24.3	19.4
Cu	29	22	22	44	62	38	27	26	54	40
Ga	16	15	16	19	19	19	16	17	16	17
Nb							4.0	3.4		
Ni										
Pb	10	15	14	10	8	11	13	13	10	8
Rb	10	9	10	30	29	32	49	50	17	13
Sr	331	325	328	336	347	240	331	323	276	353
Th				2.4	3.2	3.2	5.2	5.9		3.9
Y	22	23	22	26	32	22	23	25	23	22
Zn	72	68	70	72	66	74	41	46	81	66
Zr	39	38	39	63	61	59	80	80	52	52

Table A4.1 Major and trace element results XRF, continued.

Volcano	Labala peninsula									
Sample	26-3-1	26-4-1	26-4-2	26-5-1	26-5-2	28-1-1	28-2-1	28-3-1	28-4-1	28-5-1
Lab. Nr.	12M264	12M265	12M266	12M267	12M268	12M271	12M272	12M273	12M274	12M275
Latitude	8.52	8.52	8.52	8.52	8.52	8.52	8.52	8.52	8.52	8.52
INAA										
Isotopes										
SiO_2	54.7	54.7	54.5	55.9	57.1	55.4	54.9	53.4	53.5	54.2
TiO_2	0.80	0.74	0.71	0.75	0.77	0.71	0.84	0.83	0.82	0.79
Al_2O_3	19.9	20.1	21.2	16.4	16.6	20.0	18.1	20.5	20.6	19.7
Fe_2O_3	9.25	8.45	7.63	10.90	10.00	8.51	10.02	9.01	8.98	9.30
MnO	0.16	0.18	0.14	0.18	0.14	0.17	0.19	0.17	0.17	0.15
MgO	2.55	1.99	2.23	4.34	4.36	2.87	3.68	2.61	2.64	3.20
CaO	9.30	10.28	10.04	8.40	7.66	9.12	8.94	9.78	9.80	9.17
Na_2O	2.69	2.73	2.82	2.30	2.41	2.67	2.70	2.78	2.62	2.65
K_2O	0.50	0.74	0.61	0.70	0.86	0.47	0.54	0.77	0.75	0.79
P_2O_5	0.14	0.14	0.13	0.09	0.11	0.12	0.11	0.15	0.14	0.12
H_2O-	1.44	0.38	0.72	0.56	1.83	0.22	0.25	0.30	0.15	0.49
LOI	1.17	0.91	0.82	1.07	2.27	0.20	-0.23	-0.13	-0.12	0.03
Ba	302	303	436	404	415	281	293	311	312	294
Sc	40	32	30	35	37	29	33	30	30	37
V	201	175	138	240	195	160	204	179	170	210
Co	18.3	17.6	13.6	23.6	26.1	13.1	18.8	13.2	13.1	21.3
Cu	56	41	51	51	32	35	36	32	40	69
Ga	17	18	18	19	16	18	18	19	20	18
Nb	3.3	3.1	3.2		3.1					
Ni										
Pb	9	9	11	93	51	18	12	13	13	11
Rb	10	24	18	22	29	12	17	30	28	27
Sr	336	341	370	244	240	325	332	349	350	268
Th	3.5	3.7	2.5	3.8	3.6	2.7	2.5	2.6	2.8	6.1
Y	24	23	25	24	27	30	27	27	27	25
Zn	74	64	68	229	144	62	68	69	65	74
Zr	62	60	64	65	68	54	57	60	60	66

173

Table A4.1 Major and trace element results XRF, continued.

	Labala peninsula									
Volcano										
Sample	29-1-1	29-2-1	29-3-1	29-3-2	29-3-4	29-5-1-1	29-5-1-3	29-6-1	29-7-1	29-8-1
Lab. Nr.	12M276	12M277	12M278	12M279	12M281	12M283	12M285	12M286	12M287	12M288
Latitude	8.52	8.52	8.52	8.52	8.52	8.52	8.52	8.52	8.52	8.52
INAA				+						
Isotopes				+						
SiO_2	56.0	56.6	59.2	60.9	53.1	58.7	58.6	59.1	60.2	55.8
TiO_2	0.78	0.78	0.68	0.66	0.79	0.68	0.68	0.75	0.74	0.74
Al_2O_3	16.7	16.5	17.0	16.3	17.6	16.5	16.6	16.4	15.8	17.1
Fe_2O_3	10.38	10.19	8.93	8.22	11.10	8.96	8.95	9.24	8.92	9.51
MnO	0.19	0.20	0.17	0.17	0.20	0.18	0.18	0.19	0.18	0.17
MgO	4.35	4.06	3.13	2.85	4.41	3.40	3.46	3.60	2.93	4.39
CaO	8.36	8.33	6.96	6.90	9.76	7.84	7.88	6.94	7.05	8.73
Na_2O	2.36	2.45	2.88	3.01	2.37	2.77	2.69	2.50	2.91	2.53
K_2O	0.74	0.79	1.01	0.94	0.57	0.88	0.83	1.21	1.23	0.92
P_2O_5	0.11	0.11	0.11	0.10	0.11	0.10	0.11	0.10	0.12	0.13
H_2O-	1.29	0.88	0.21	0.11	0.08	0.16	0.17	0.95	0.19	0.61
LOI	0.29	0.10	2.77	0.21	0.23	0.14	0.26	0.74	0.00	0.29
Ba	462	382	382	542	301	476	497	551	652	425
Sc	34	34	33	27	35	31	29	30	28	28
V	215	211	203	178	292	230	224	196	221	193
Co	22.3	23.9	21.0	19.2	26.9	17.7	17.5	15.9	16.8	20.3
Cu	23	41	38	33	47	41	43	61	26	48
Ga	15	16	16	17	20	18	17	15	16	16
Nb			3.5	3.5						
Ni										13.5
Pb	11	14	10	9	10	11	11	8	12	11
Rb	23	24	24	22	13	26	23	36	36	30
Sr	261	252	249	226	244	243	246	245	260	308
Th		4.8	2.2	2.8	3.3		3.5	5.2	5.2	4.4
Y	24	24	24	28	22	26	25	31	37	25
Zn	69	68	67	67	92	69	69	59	60	65
Zr	63	65	66	87	53	76	76	87	97	73

Table A4.1 Major and trace element results XRF, continued.

Volcano	Labala peninsula									
Sample	29-9-1	31-1-1	31-2-1	31-3-1	31-4-1	31-5-1	31-6-1	31-7-1	31-8-1	32-6-1
Lab. Nr.	12M290	12M294	12M295	12M296	12M297	12M298	12M299	12M300	12M301	12M227
Latitude	8.52	8.52	8.52	8.52	8.52	8.52	8.52	8.52	8.52	0.00
INAA			+							
Isotopes			+							
SiO_2	51.3	59.2	61.0	58.0	62.1	60.8	59.7	60.8	63.1	54.2
TiO_2	0.93	0.76	0.67	0.70	0.67	0.67	0.72	0.71	0.63	0.83
Al_2O_3	18.3	16.3	16.4	16.7	16.2	16.5	16.5	16.6	16.1	17.8
Fe_2O_3	11.62	9.18	7.95	8.88	7.59	7.97	8.53	7.75	6.76	9.90
MnO	0.20	0.18	0.16	0.17	0.15	0.16	0.17	0.15	0.14	0.18
MgO	4.70	3.29	2.87	3.83	2.67	2.76	3.19	2.61	2.18	4.21
CaO	10.16	7.11	6.76	7.80	6.19	6.79	6.85	6.76	5.70	9.17
Na_2O	2.20	2.73	2.95	2.88	3.12	3.08	2.81	2.94	3.41	2.73
K_2O	0.52	1.14	1.17	0.93	1.25	1.11	1.34	1.56	1.84	0.85
P_2O_5	0.10	0.11	0.13	0.13	0.12	0.15	0.13	0.13	0.17	0.16
H_2O-	0.30	0.22	0.31	0.07	0.23	0.40	0.45	0.05	0.47	0.50
LOI	-0.04	0.67	0.43	0.30	0.29	0.34	0.44	-0.30	0.33	0.49
Ba	276	584	525	445	583	593	641	721	880	495
Sc	41	28	26	29	21	25	28	22	17	33
V	286	197	155	182	129	159	183	149	128	232
Co	27.5	19.6	17.1	17.3	13.1	14.3	14.1	13.4	12.6	21.5
Cu	96	63	35	24	31	29	54	38	33	47
Ga	18	16	16	16	16	16	17	15	15	18
Nb		3.6	4.4	3.2	3.8	3.5	3.7	4.6	3.6	
Ni										
Pb	10	12	10	11	14	12	10	18	12	11
Rb	14	36	44	32	43	32	47	56	61	25
Sr	340	270	279	302	259	279	272	299	339	407
Th	2.4	6.1	5.3	4.7	5.7	6.3	5.0	7.1	5.6	3.1
Y	23	41	28	26	28	36	44	36	31	27
Zn	77	74	62	64	52	57	63	55	48	72
Zr	50	94	97	85	104	100	102	115	120	80

175

Table A4.1 Major and trace element results XRF, continued.

Volcano	Tandjung				Werung					
Sample	8-1-2	8-5-1	8-5-2	8-5-3	23-2-1	23-2-3-1	23-3-1	23-5-1	23-5-2	23-5-3
Lab. Nr.	12M362	12M366	12M367	12M368	12M199	12M201	12M205	12M206	12M207	12M208
Latitude	8.51	8.51	8.51	8.51	8.55	8.55	8.55	8.55	8.55	8.55
INAA		+	+		+					+
Isotopes										+
SiO_2	64.0	69.4	56.3	55.5	53.0	57.4	55.6	52.7	49.0	49.8
TiO_2	0.84	0.52	0.83	0.82	0.72	0.66	0.78	0.84	0.70	0.80
Al_2O_3	15.8	15.1	17.0	17.3	18.8	17.9	18.9	17.9	21.7	18.3
Fe_2O_3	6.74	3.94	9.79	9.82	10.29	8.69	9.24	11.37	10.58	12.38
MnO	0.18	0.17	0.19	0.20	0.22	0.22	0.21	0.23	0.19	0.22
MgO	1.60	0.98	3.59	3.59	4.07	3.23	3.03	4.31	4.02	5.21
CaO	5.19	4.01	8.73	8.94	10.05	8.33	8.98	9.70	11.93	11.06
Na_2O	4.20	4.43	2.83	3.04	2.37	2.90	2.73	2.46	1.59	1.92
K_2O	1.18	1.27	0.59	0.60	0.41	0.53	0.42	0.37	0.15	0.20
P_2O_5	0.21	0.13	0.15	0.15	0.10	0.14	0.12	0.10	0.07	0.10
H_2O-					0.06	0.05	0.92	0.32	1.96	0.36
LOI	0.97	0.41	0.08	0.17	-0.34	-0.24	-0.46	0.38	1.52	0.00
Ba	1034	752	605	453	262	342	243	199	145	142
Sc	33	15	34	33	34	28	32	40	45	47
V			223	205	183	117	136	243	259	348
Co	17.3		18.9	19.3	17.3	13.6	12.3	18.1	22.5	30.5
Cu	63		29	16	37	16	38	57	43	53
Ga	16	14	17	17	17	17	18	19	18	20
Nb	3.6	4.1			4.4	3.6				0.5
Ni	11.4									
Pb	12	17	11	7	9	9	8	7	7	7
Rb	27	25	15	13	12	14	12	11	7	6
Sr	299	290	336	337	288	293	272	264	255	242
Th							3.8	3.6	3.6	4.5
Y	29	41	31	31	20	23	25	24	17	19
Zn	62	54	67	64	81	74	76	85	81	91
Zr	91	132	73	71	43	52	43	42	28	30

Table A4.1 Major and trace element results XRF, continued.

Volcano	Werung									
Sample	23-5-4	23-5-5	23-6-1-1	23-7-1	23-7-6	23-8-1	24-11-1	24-11-2	24-12-1	24-12-2
Lab. Nr.	12M209	12M210	12M211	12M213	12M218	12M219	12M229	12M230	12M231-2	12M232
Latitude	8.55	8.55	8.55	8.55	8.55	8.55	8.55	8.55	8.55	8.55
INAA	+		+	+	+		+		+	+
Isotopes	+									
SiO_2	49.8	51.5	52.9	56.6	52.5	53.2	52.8	52.7	55.1	52.9
TiO_2	0.79	0.89	0.79	0.70	0.84	0.69	0.72	0.69	0.70	0.72
Al_2O_3	18.9	18.1	17.5	19.1	18.3	19.2	19.5	19.8	19.4	19.2
Fe_2O_3	12.09	11.94	11.37	8.24	11.11	9.80	10.14	9.80	8.84	10.18
MnO	0.22	0.23	0.20	0.21	0.28	0.22	0.21	0.20	0.21	0.21
MgO	5.09	4.54	4.58	2.96	4.34	3.79	3.76	3.74	3.14	3.78
CaO	11.02	10.13	9.64	8.76	9.89	10.29	9.95	10.22	9.18	9.93
Na_2O	1.84	2.19	2.51	2.90	2.35	2.28	2.45	2.38	2.87	2.51
K_2O	0.20	0.31	0.39	0.44	0.29	0.41	0.40	0.39	0.48	0.41
P_2O_5	0.11	0.16	0.13	0.12	0.09	0.12	0.10	0.11	0.12	0.10
H_2O-	0.28	1.41	0.78	0.07	0.09	0.05	0.08	0.03	0.06	0.04
LOI	0.01	0.62	0.04	-0.22	-0.10	-0.34	0.03	-0.22	-0.25	-0.21
Ba	138	144	242	306	229	273	247	239	289	246
Sc	46	44	40	28	32	34	33	33	31	32
V	308	413			181	195	212	207	171	202
Co	30.0	21.5	23.4	12.3	16.2	18.2	18.3	21.4	12.9	18.3
Cu	51	42	69	17	45	28	35	33	23	41
Ga	19	18	19		20	19	19	19	19	18
Nb	*0.6*									
Ni										
Pb	9	11		10		10	12	7	8	9
Rb		9	10	12	7	11	11	11	12	11
Sr	241	263	265	325	321	301	291	295	304	291
Th		2.5			2.8	2.2	4.0	3.7	2.4	2.5
Y	19	24	22	24	20	19	21	20	25	21
Zn	91	85	80	72	85	75	79	77	74	81
Zr	31	40	44	46	33	39	42	40	51	41

Table A4.1 Major and trace element results XRF, continued.

Volcano	Werung									
Sample	24-13-1-2	24-13-4	24-13-5	24-3-1	24-5-1	24-8-1	24-8-2	24-8-6	24-9-1	27-1-1
Lab. Nr.	12M234	12M239	12M240	12M225	12M242	12M245	12M246-2	12M250	12M251	12M179
Latitude	8.55	8.55	8.55	8.55	8.55	8.55	8.55	8.55	8.55	8.55
INAA	+							+	+	+
Isotopes								+		
SiO_2	57.1	54.6	59.4	55.3	54.1	55.6	53.5	53.7	52.5	57.0
TiO_2	0.66	0.72	0.67	0.95	0.87	0.68	0.71	0.69	0.80	0.70
Al_2O_3	17.9	18.9	17.3	17.3	18.0	18.6	18.8	18.9	18.8	18.4
Fe_2O_3	8.85	9.67	8.21	10.39	10.98	9.21	10.16	9.91	10.58	8.38
MnO	0.22	0.20	0.23	0.23	0.23	0.22	0.22	0.22	0.22	0.22
MgO	3.43	3.44	2.84	3.09	3.91	3.47	4.10	4.00	4.07	2.97
CaO	8.47	9.42	7.70	9.06	8.92	9.07	9.69	9.70	10.08	8.83
Na_2O	2.76	2.48	2.99	3.07	2.49	2.63	2.31	2.41	2.40	2.92
K_2O	0.53	0.42	0.59	0.42	0.38	0.49	0.46	0.42	0.40	0.46
P_2O_5	0.11	0.11	0.13	0.14	0.12	0.10	0.09	0.11	0.10	0.13
H_2O-	0.02	0.09	0.05	0.09	0.11	0.08	0.05	0.05	0.05	0.03
LOI	-0.28	-0.07	-0.04	-0.34	-0.38	-0.34	-0.42	-0.40	-0.21	-0.31
Ba	348	271	392	240	248	309	258	263	241	318
Sc	29	33	28	37	32	32	34	34	34	28
V	136	187	72	177	179	147	188	165	200	128
Co	13.4	17.6	10.5	18.2	20.3	15.2	21.7	17.0	20.3	13.0
Cu	19	30	32	39	27	24	28	36	33	16
Ga	18	18	18	19	16	17	17	18	19	19
Nb	*1.2*		3.1						*0.9*	
Ni										
Pb	10	11	15	11	8	12	8	13	8	8
Rb	14	11	16	10	10	13	12	12	13	12
Sr	298	281	293	279	328	290	293	291	297	323
Th				2.9	3.5	2.3		3.3		2.7
Y	23	24	26	29	23	22	21	20	21	25
Zn	73	83	78	85	66	82	84	82	81	72
Zr	50	44	56	47	38	47	42	43	44	47

Table A4.1 Major and trace element results XRF, continued.

Volcano	Werung									
Sample	27-1-2	27-10-1	27-10-2	27-10-3	27-10-4	27-12-1	27-13-1	27-14-1	27-2-1	27-3-1
Lab. Nr.	12M180	12M191	12M192-2	12M193	12M194	12M196	12M197	12M198	12M181	12M182
Latitude	8.55	8.55	8.55	8.55	8.55	8.55	8.55	8.55	8.55	8.55
INAA		+				+			+	+
Isotopes		+				+				
SiO_2	55.9	60.1	55.1	53.2	59.8	53.0	57.3	54.5	53.4	53.9
TiO_2	0.74	0.64	0.67	0.76	0.63	0.73	0.67	0.71	0.88	0.86
Al_2O_3	18.3	17.3	18.9	18.7	17.5	19.5	18.3	19.2	17.7	18.1
Fe_2O_3	9.16	7.86	9.17	10.24	7.81	9.67	8.55	8.96	11.51	10.85
MnO	0.22	0.21	0.22	0.20	0.21	0.20	0.22	0.21	0.23	0.23
MgO	3.42	2.60	3.40	4.05	2.48	3.88	3.17	3.26	4.24	3.86
CaO	8.91	7.30	9.36	10.00	7.42	10.06	8.28	9.77	9.23	9.18
Na_2O	2.82	3.20	2.60	2.35	3.44	2.43	2.86	2.75	2.27	2.55
K_2O	0.48	0.62	0.46	0.38	0.65	0.37	0.52	0.44	0.43	0.38
P_2O_5	0.13	0.16	0.11	0.10	0.14	0.10	0.11	0.12	0.10	0.12
H_2O-	0.06	0.15	0.03	0.02	0.03	0.02	0.03	0.04	0.05	0.04
LOI	-0.05	0.10	-0.33	-0.42	-0.23	-0.41	-0.16	-0.04	-0.22	-0.32
Ba	311	421	299	240	415	268	349	302	231	238
Sc	34	28	32	33	28	35	31	28	34	33
V	163	123	179	227	93	197	131	136	231	198
Co	15.2	10.1	16.5	19.8	9.1	19.5	10.5	14.7	22.7	16.9
Cu	27	12	32	38	15	41	18	24	35	31
Ga	19	18	18	18	17	18	18	19	18	17
Nb	3.2					*0.8*		3.8		
Ni										
Pb	10	20	11	7	13	7				7
Rb	13	17	13	10	16	10	14	12	12	10
Sr	303	295	295	298	296	289	297	327	299	333
Th				3.3	4.5		4.2			
Y	25	27	23	21	29	28	25	22	28	20
Zn	83	75	82	73	74	75	76	75	78	70
Zr	47	60	46	38	59	41	52	43	38	37

Table A4.1 Major and trace element results XRF, continued.

Volcano	Werung							Boleng		Hadakewa
Sample	27-4-1	27-5-1	27-6-1	27-7-1	27-8-1	27-9-1	30-1-1-2	34.3.1	34.4.1	20-3-1
Lab. Nr.	12M183	12M184	12M185	12M186	12M187	12M188	12M293	12M498	12M499-T	12M482
Latitude	8.55	8.55	8.55	8.55	8.55	8.55	8.55	8.42	8.42	8.41
INAA	+	+	+	+	+	+	+	+	+	+
Isotopes								+	+	
SiO_2	53.9	54.1	54.7	54.2	54.6	56.0	53.6	52.6	62.5	73.9
TiO_2	0.86	0.86	0.80	0.80	0.71	0.76	0.74	1.26	0.85	0.22
Al_2O_3	17.9	18.2	17.9	18.0	19.9	18.5	19.8	17.2	16.4	13.7
Fe_2O_3	10.90	10.72	10.45	10.76	8.60	8.98	9.32	10.87	5.96	1.62
MnO	0.23	0.23	0.22	0.22	0.21	0.22	0.20	0.20	0.16	0.12
MgO	3.95	3.85	3.68	3.78	3.24	3.25	3.40	4.08	1.76	0.41
CaO	9.08	9.09	9.03	9.14	9.49	8.93	9.89	8.72	4.81	1.60
Na_2O	2.62	2.53	2.66	2.60	2.69	2.78	2.55	3.14	4.23	3.11
K_2O	0.39	0.38	0.44	0.44	0.42	0.44	0.38	1.63	2.96	5.16
P_2O_5	0.12	0.12	0.11	0.11	0.11	0.11	0.11	0.34	0.36	0.14
H_2O-	0.10	0.08	0.29	0.10	0.06	0.03	0.09			
LOI	-0.41	-0.39	-0.29	-0.28	-0.29	-0.35	-0.37	0.10	-0.04	2.97
Ba	244	240	271	282	294	304	261	820	1318	1584
Sc	34	33	37	36	32	30	34	30	15	
V	194	184	202	198	141	184	213	240	62	
Co	20.4	17.1	18.0	20.1	15.1	12.3	19.7	22.2	8.3	
Cu	26	32	36	44	24	29	41	45	11	
Ga	16	17	19	18	19	18	19	17	15	11
Nb			3.8	3.7	3.0		1.0	7.9	11.4	8.5
Ni								8.9	8.2	
Pb	8	10	12	17	11	7	7	30	44	21
Rb	9	10	9	11	10	11	9	40	79	115
Sr	326	325	295	292	329	322	295	618	526	264
Th	3.0				2.3	3.2		10.5	22.7	23.3
Y	22	23	25	24	24	24	23	34	41	18
Zn	69	71	77	76	75	74	74	74	66	36
Zr	38	38	48	46	41	44	42	129	225	123

Table A4.1 Major and trace element results XRF, continued.

Volcano	Hadakewa					Lewotolo				
Sample	20-5-1	20-7-1	20-8-1	21-2-1	21-2-3	14-3-1	14-6-1-3	14-6-2	14-6-3	14-7-1
Lab. Nr.	12M479	12M483	12M481	12M484	12M480	12M400	12M407	12M408	12M409	12M410
Latitude	8.41	8.41	8.41	8.41	8.41	8.31	8.31	8.31	8.31	8.31
INAA		+					+	+		
Isotopes							+			
SiO_2	52.2	74.2	73.7	73.4	73.6	53.6	53.8	51.4	53.6	57.4
TiO_2	0.85	0.22	0.22	0.23	0.21	0.73	0.68	0.90	0.75	0.68
Al_2O_3	19.6	13.8	14.0	14.1	14.1	19.5	21.3	19.4	19.5	19.8
Fe_2O_3	10.61	1.67	1.67	1.81	1.60	7.80	6.52	9.19	7.82	6.45
MnO	0.17	0.12	0.12	0.12	0.11	0.15	0.13	0.17	0.16	0.15
MgO	3.31	0.43	0.52	0.55	0.44	3.15	2.36	3.89	3.13	2.32
CaO	10.00	1.69	1.55	1.67	2.06	8.49	8.63	9.38	8.43	6.10
Na_2O	2.55	3.61	3.34	3.67	2.95	3.24	3.22	3.02	3.32	3.38
K_2O	0.57	4.22	4.72	4.40	4.88	3.04	2.92	2.35	2.96	3.45
P_2O_5	0.14	0.10	0.10	0.10	0.08	0.35	0.35	0.36	0.33	0.29
H_2O-										
LOI	0.81	4.44	3.86	3.62	4.27	-0.02	0.21	0.05	0.09	1.74
Ba	443	1649	1596	1644	1691	1238	1333	1138	1236	1265
Sc	42					16	13	20	16	13
V										
Co	23.1					15.4	9.7	17.3	12.1	8.5
Cu	34			23		47	31	54	40	43
Ga	18	11		11		17	18	19	18	16
Nb		8.3	8.0	8.4	8.4	8.6	9.0	7.1	9.8	9.9
Ni										
Pb	10	21	23	20	21	28	23	21	27	33
Rb	15	119	112	116	113	80	80	62	80	92
Sr	368	248	260	258	250	955	1053	986	952	694
Th		22.8	22.0	21.9	24.4	25.6	20.9	10.0	24.5	25.6
Y	21	19	18	20	19	27	26	26	29	25
Zn	77	34	36	36	34	66	54	65	66	55
Zr	46	122	128	130	125	137	132	118	136	157

Table A4.1 Major and trace element results XRF, continued.

Volcano	Lewotolo									
Sample	14-7-2	14-7-3	14-7-5	14-8-1	15-2-1	15-3-1	15-4-1	16-10-1	16-10-2	16-10-2
Lab. Nr.	12M411	12M412	12M414	12M415	12M417	12M418	12M419	12M420	12M421	12M422
Latitude	8.31	8.31	8.31	8.31	8.31	8.31	8.31	8.31	8.31	8.31
INAA										
Isotopes										
SiO_2	57.7	57.5	57.4	57.3	61.5	56.8	57.5	56.2	55.8	56.1
TiO_2	0.69	0.68	0.68	0.67	0.48	0.71	0.62	0.75	0.73	0.74
Al_2O_3	18.6	19.3	19.8	19.3	18.5	19.2	17.8	18.9	19.4	18.8
Fe_2O_3	6.46	6.53	6.43	6.41	4.82	6.71	7.30	7.11	7.02	7.15
MnO	0.16	0.15	0.15	0.15	0.15	0.15	0.16	0.17	0.17	0.16
MgO	2.34	2.30	2.26	2.18	1.48	2.45	3.01	2.57	2.54	2.62
CaO	6.58	6.50	6.03	6.69	4.92	6.96	7.40	6.93	6.95	6.99
Na_2O	3.53	3.22	3.50	3.56	3.95	3.22	3.02	3.57	3.68	3.67
K_2O	3.55	3.47	3.49	3.47	4.03	3.52	2.96	3.35	3.34	3.30
P_2O_5	0.30	0.30	0.29	0.30	0.27	0.30	0.25	0.45	0.43	0.44
H_2O-										
LOI	0.88	1.33	1.53	0.33	0.85	0.32	0.06	0.10	0.23	-0.10
Ba	1254	1273	1286	1274	1362	1237	1068	1365	1356	1368
Sc	12	13	11	12		14	14	12	12	13
V										
Co	9.1	11.8	15.0	13.0	6.9	11.7	14.5	12.8	13.2	16.7
Cu	34	32	26	35	16	37	59	45	46	40
Ga	18	19	18	17	15	17	16	18	19	18
Nb	10.1	9.3	9.0	8.9	9.1	9.0	7.5	9.6	8.9	9.3
Ni							10.5			
Pb	34	27	22	34	31	33	25	30	30	28
Rb	100	98	93	95	112	96	90	93	92	86
Sr	735	723	711	736	683	765	735	919	919	921
Th	27.3	27.9	25.0	27.1	34.1	30.2	25.5	21.9	23.9	24.0
Y	30	31	28	31	25	28	24	29	29	29
Zn	62	67	56	65	59	61	61	69	73	67
Zr	162	158	152	159	177	161	141	159	160	159

Table A4.1 Major and trace element results XRF, continued.

Volcano	Lewotolo									
Sample	16-11-1	16-12-1	16-13-1	16-14-1	16-15-1	16-16-1	16-2-1-1	16-3-1	16-3-2	16-3-3
Lab. Nr.	12M423	12M424	12M425	12M426	12M433	12M427	12M434	12M436	12M437	12M438
Latitude	8.31	8.31	8.31	8.31	8.31	8.31	8.31	8.31	8.31	8.31
INAA										
Isotopes										
SiO_2	57.0	56.6	60.6	54.9	55.9	61.4	55.1	49.9	50.1	52.8
TiO_2	0.66	0.68	0.49	0.72	0.73	0.49	0.82	1.03	1.02	0.77
Al_2O_3	17.1	17.1	18.0	17.5	19.4	18.0	17.5	19.8	20.0	18.8
Fe_2O_3	7.43	7.63	5.45	8.55	6.99	4.99	8.66	9.90	9.79	8.00
MnO	0.17	0.18	0.13	0.18	0.17	0.15	0.18	0.19	0.19	0.16
MgO	3.49	3.71	1.85	3.59	2.50	1.57	3.83	3.93	3.83	3.44
CaO	7.45	7.58	5.66	8.01	6.89	5.21	8.34	10.05	9.90	9.77
Na_2O	3.07	2.91	3.65	2.96	3.69	3.61	2.84	3.04	2.99	2.90
K_2O	3.35	3.37	3.91	3.22	3.33	4.23	2.48	1.85	1.89	2.89
P_2O_5	0.28	0.28	0.28	0.33	0.44	0.29	0.27	0.35	0.35	0.47
H_2O-										
LOI	0.67	0.87	0.18	0.21	0.13	1.10	0.60	0.41	0.35	1.33
Ba	1114	1159	1371	1140	1378	1356	1021	837	836	939
Sc	14	14		19	13		21	22	22	19
V										
Co	11.5	11.9	8.4	15.1	11.1	6.6	14.7	16.9	18.6	18.1
Cu	27	36	21	69	55	16	50	46	49	64
Ga	18	17	16	18	18	17	17	18	18	17
Nb	8.6	8.3	8.8	7.9	9.8	9.3	8.2	7.3	6.1	7.2
Ni	20.9	19.7		14.6			10.2			13.5
Pb	28	31	32	20	31	31	22	23	11	21
Rb	105	99	114	92	92	112	62	44	44	87
Sr	705	719	758	947	920	696	806	948	951	993
Th	30.6	29.7	30.6	24.4	23.5	29.3	21.4	11.9	18.2	18.7
Y	28	29	26	31	29	24	28	28	28	28
Zn	61	62	48	63	68	58	59	76	67	62
Zr	152	153	182	171	159	172	126	85	84	137

183 **Table A4.1** Major and trace element results XRF, continued.

	Lewotolo									
Volcano										
Sample	16-4-1	16-5-1	16-6-1	16-7-1	16-8-1	16-8-2	16-9-1	17-1-1	17-10-1	17-10-2
Lab. Nr.	12M439	12M443	12M444	12M445	12M446	12M447	12M448	12M449	12M458	12M490
Latitude	8.31	8.31	8.31	8.31	8.31	8.31	8.31	8.31	8.31	8.31
INAA					+					
Isotopes				+	+					
SiO_2	54.4	54.9	54.5	62.0	56.2	55.9	62.3	52.7	57.0	49.4
TiO_2	0.79	0.95	0.93	0.53	0.75	0.73	0.53	0.89	0.65	0.98
Al_2O_3	17.7	18.5	18.5	17.3	18.8	19.4	17.1	18.4	17.5	18.2
Fe_2O_3	8.60	8.11	8.22	5.45	7.08	7.04	5.42	9.44	7.75	11.39
MnO	0.17	0.19	0.19	0.16	0.17	0.17	0.15	0.18	0.17	0.24
MgO	3.60	3.12	3.21	1.80	2.56	2.55	1.70	4.25	2.82	5.29
CaO	8.39	7.43	7.58	4.88	6.94	6.91	4.76	8.90	7.47	9.70
Na_2O	3.03	3.48	3.42	3.64	3.56	3.52	3.74	2.85	3.05	2.60
K_2O	3.02	2.99	3.02	3.94	3.40	3.35	3.99	2.15	3.24	1.93
P_2O_5	0.31	0.32	0.34	0.31	0.45	0.44	0.31	0.31	0.28	0.28
H_2O-										
LOI	-0.09	0.42	0.18	0.05	0.42	0.21	0.09	-0.08	0.21	1.34
Ba	1209	1082	1090	1266	1377	1380	1286	867	1203	1009
Sc	16	20	19		13	13		21	13	27
V										
Co	18.3	14.2	12.6	7.5	10.8	14.2	8.3	20.7	13.3	35.2
Cu	46	37	36	19	45	36	18	49	33	52
Ga	18	18	17	15	17	17	16	19	17	20
Nb	8.0	6.1	6.9	10.2	11.0	10.8	9.7	6.6	10.9	6.0
Ni	10.5							13.0		14.1
Pb	22	34	32	32	29	21	34	16	19	62
Rb	86	77	79	115	92	91	112	57	97	55
Sr	848	781	782	678	918	914	677	766	898	877
Th	25.7	23.3	23.1	31.2	20.9	24.3	30.0	16.5	28.9	21.6
Y	27	30	30	29	28	29	29	28	31	26
Zn	59	81	76	67	70	67	64	67	60	76
Zr	132	126	123	179	158	157	180	129	187	99

Table A4.1 Major and trace element results XRF, continued.

Volcano	Lewotolo									
Sample	17-12-1	17-13-1	17-14-1	17-15-1	17-16-1	17-17-1	17-18-1	17-19-1	17-2-6	17-2-9
Lab. Nr.	12M459	12M460	12M461	12M462	12M463	12M464	12M465	12M466	12M450	12M451
Latitude	8.31	8.31	8.31	8.31	8.31	8.31	8.31	8.31	8.31	8.31
INAA								+		
Isotopes										
SiO_2	56.0	56.6	53.3	59.8	53.7	54.7	61.1	61.1	54.7	54.1
TiO_2	0.60	0.62	0.76	0.53	0.71	0.71	0.49	0.50	0.75	0.85
Al_2O_3	18.3	18.2	18.7	16.8	21.0	20.3	18.6	18.1	18.0	17.7
Fe_2O_3	7.50	7.68	8.95	6.47	6.88	6.94	4.95	4.96	8.52	9.17
MnO	0.18	0.19	0.18	0.15	0.15	0.17	0.16	0.15	0.18	0.18
MgO	2.77	2.62	3.71	2.72	2.58	2.56	1.52	1.60	3.65	3.94
CaO	7.46	7.48	8.32	6.19	8.24	7.59	5.04	5.28	8.22	8.42
Na_2O	3.29	3.07	2.81	3.19	3.18	3.27	3.75	3.73	2.98	2.73
K_2O	3.62	3.20	2.90	3.92	3.09	3.28	4.11	4.25	2.67	2.61
P_2O_5	0.27	0.31	0.40	0.23	0.49	0.47	0.28	0.28	0.37	0.29
H_2O-										
LOI	0.37	0.45	1.11	0.56	0.17	0.14	1.17	0.18	0.32	0.91
Ba	1073	1213	1277	1301	1062	1115	1364	1376	850	1013
Sc	13	11	16	12	17	16			20	18
V										
Co	15.4	11.6	18.0	10.0	13.1	11.0	6.6	6.8	17.5	16.3
Cu	44	33	42	42	57	40	13	15	57	47
Ga	19	18	18	15	19	19	16	16	18	15
Nb	13.7	11.7	9.6	10.4	8.4	8.8	9.7	9.5	8.3	8.1
Ni	10.6		11.9	13.0					11.0	10.0
Pb	31	29	22	30	21	25	32	31	25	23
Rb	109	99	83	121	90	96	113	114	72	77
Sr	1143	905	875	752	1086	1025	688	699	750	787
Th	28.4	25.6	29.8	40.5	24.1	26.7	29.6	28.9	19.5	18.9
Y	35	33	28	27	28	31	26	26	28	27
Zn	65	66	62	55	61	63	59	58	69	71
Zr	231	185	135	181	144	149	176	175	142	145

Table A4.1 Major and trace element results XRF, continued.

Volcano	Lewotolo									
Sample	17-3-1-2	17-4-1	17-5-1	17-7-1	17-8-1	17-8-2	17-9-1	18-1-1	18-10-1	18-3-1
Lab. Nr.	12M452	12M453	12M454	12M455	12M456	12M489	12M457	12M467	12M472	12M468
Latitude	8.31	8.31	8.31	8.31	8.31	8.31	8.31	8.31	8.31	8.31
INAA	+	+								
Isotopes		+								
SiO_2	47.2	48.9	54.2	56.1	58.5	58.3	60.4	56.5	57.2	61.0
TiO_2	1.05	0.88	0.84	0.61	0.70	0.70	0.54	0.71	0.71	0.51
Al_2O_3	18.1	18.1	18.0	18.3	17.2	17.6	17.1	19.1	18.6	18.1
Fe_2O_3	11.93	10.43	8.46	7.72	7.13	7.10	6.39	6.79	6.77	5.15
MnO	0.19	0.19	0.17	0.18	0.16	0.15	0.16	0.16	0.14	0.15
MgO	5.84	5.68	3.58	3.44	2.78	2.81	2.16	2.58	2.45	1.63
CaO	11.74	11.23	8.42	7.88	6.67	6.61	6.05	7.01	6.92	5.27
Na_2O	2.24	2.36	3.00	2.83	3.23	3.20	3.24	3.18	3.51	3.76
K_2O	1.46	1.84	3.02	2.66	3.38	3.32	3.66	3.61	3.40	4.10
P_2O_5	0.25	0.33	0.27	0.27	0.25	0.26	0.25	0.30	0.29	0.28
H_2O-										
LOI	-0.17	-0.07	0.21	0.47	0.68	-0.10	0.08	0.50	2.98	0.84
Ba	784	762	1143	931	1184	1233	1249	1228	1288	1357
Sc	33	28	19	14	13	12		14	13	
V										
Co	28.5	29.0	14.0	14.2	10.1	12.0	7.7	9.3	12.6	6.9
Cu	61	51	49	29	26	25	34	30	33	14
Ga	18	18	17	18	16	16	16	16	16	17
Nb	3.7	5.2	8.5	9.3	9.1	10.0	10.3	9.3	8.6	9.6
Ni	18.0	18.2								
Pb	19	17	30	22	24	19	30	32	23	32
Rb	31	45	85	78	103	96	119	95	94	110
Sr	856	821	769	709	675	696	742	764	768	702
Th	10.5	10.6	22.7	22.4	31.1	27.8	32.9	27.5	22.1	26.5
Y	24	25	28	24	26	26	26	28	27	26
Zn	71	69	62	66	52	44	56	59	54	57
Zr	61	87	139	136	164	167	183	159	156	176

Table A4.1 Major and trace element results XRF, continued.

Volcano	Lewotolo									SE of Lewotolo
Sample	18-5-1	18-8-1	18-9-1	19-1-1	19-10-1	19-3-1	19-7-1	19-8-1	19-9-1	16-1-1
Lab. Nr.	12M469	12M470	12M471	12M473	12M478	12M474	12M475	12M476	12M477	12M428
Latitude	8.31	8.31	8.31	8.31	8.31	8.31	8.31	8.31	8.31	8.37
INAA										
Isotopes										
SiO_2	54.6	52.7	61.3	56.8	53.3	56.3	53.9	55.3	56.0	63.2
TiO_2	0.72	0.79	0.54	0.70	0.79	0.62	0.70	0.63	0.66	0.52
Al_2O_3	20.1	18.5	18.8	19.0	18.7	17.5	20.8	17.8	17.5	15.8
Fe_2O_3	7.02	9.16	4.75	6.65	7.97	7.61	6.76	8.28	7.87	6.48
MnO	0.16	0.19	0.15	0.15	0.16	0.17	0.15	0.18	0.17	0.13
MgO	2.58	3.81	1.46	2.50	3.58	3.36	2.58	3.59	3.61	2.64
CaO	7.72	9.02	4.94	6.97	9.29	8.39	8.49	8.18	8.28	6.26
Na_2O	3.19	3.03	3.92	3.32	2.86	2.90	3.04	2.76	2.88	2.86
K_2O	3.41	2.52	3.92	3.53	2.89	2.85	3.10	2.96	2.72	2.01
P_2O_5	0.51	0.30	0.27	0.31	0.46	0.26	0.46	0.35	0.25	0.10
H_2O-										
LOI	0.42	0.59	0.48	0.33	0.65	0.66	0.30	0.29	0.32	1.12
Ba	1122	960	1406	1235	948	1053	1024	1128	966	2017
Sc	14	18		14	19	13	16	15	15	21
V										
Co	12.7	18.1	5.8	13.3	16.5	13.8	12.0	15.8	15 3	14.7
Cu	57	55	18	29	38	27	46	34	30	30
Ga	18	17	15	17	17	16	16	14	16	15
Nb	9.1	7.4	10.6	9.3	7.7	7.5	7.9	9.3	7.5	3.3
Ni					14.5	10.1		11.4	11.3	
Pb	27	23	40	29	16	21	21	29	26	12
Rb	106	68	109	96	93	88	94	91	80	61
Sr	1013	896	701	758	988	756	1066	865	749	306
Th	24.9	19.4	30.9	24.2	19.1	25.6	20.3	30.0	23.2	11.6
Y	30	28	25	28	29	24	30	27	23	28
Zn	59	75	47	60	63	56	70	64	61	40
Zr	156	118	176	159	136	134	142	141	126	75

Table A4.1 Major and trace element results XRF, continued.

Volcano	SE of Lewotolo			Noahanera				Inland Lembata		
Sample	16-1-2	16-1-3	16-1-4-1	33-1-1	33-2-1	33-3-1	33-4-1	32-1-1-1	32-2-1	32-3-1
Lab. Nr.	12M429	12M430	12M431	12M485	12M486	12M487	12M488	12M305	12M307	12M309
Latitude	8.37	8.37	8.37	8.33	8.33	8.33	8.33	8.48	8.48	8.48
INAA	+			+	+		+	+		
Isotopes								+		
SiO_2	63.1	63.6	61.6	68.9	58.4	56.5	55.0	58.9	61.0	63.7
TiO_2	0.53	0.53	0.55	0.35	0.67	0.70	0.84	0.81	0.72	0.48
Al_2O_3	15.6	15.6	15.7	15.1	17.7	17.5	17.3	16.3	16.6	14.5
Fe_2O_3	6.55	6.34	7.11	3.42	7.72	7.90	9.12	8.27	7.65	5.76
MnO	0.13	0.12	0.13	0.10	0.15	0.17	0.16	0.16	0.16	0.14
MgO	2.75	2.72	3.16	1.10	2.92	3.10	4.13	3.22	2.78	3.33
CaO	6.32	5.96	6.91	3.87	6.87	8.65	8.33	7.29	6.20	5.84
Na_2O	2.89	2.92	2.86	3.82	3.21	3.21	3.11	3.25	3.15	2.98
K_2O	2.04	2.11	1.81	3.28	2.10	1.99	1.71	1.49	1.55	3.07
P_2O_5	0.10	0.09	0.10	0.16	0.28	0.29	0.28	0.29	0.17	0.18
H_2O-								0.16	0.27	0.12
LOI	0.85	1.52	1.53	1.05	0.82	1.79	1.47	-0.09	0.34	1.34
Ba	1248	1286	1039	1554	1231	989	2020	797	818	1464
Sc	21	21	24		17	16	22	22	22	16
V								167	146	109
Co	15.4	12.2	14.8	5.4	13.4	14.9	20.4	19.3	17.9	15.6
Cu	29	29	28		37	36	47	26	35	32
Ga	14	13	14	12	19	17	15	16	16	14
Nb	4.9	4.7	3.1	7.2	5.9	5.1	4.7	4.2	3.8	5.8
Ni							14.6			20.5
Pb	11	14	11	21	15	17	16	11	11	21
Rb	62	63	55	95	59	55	44	43	41	82
Sr	281	273	284	427	664	667	752	549	376	424
Th	10.3	11.6	11.6	18.8	10.2	11.3	-7.8	6.5	7.9	18.5
Y	24	20	17	26	26	26	26	31	33	28
Zn	41	41	45	33	55	56	60	55	56	48
Zr	73	76	68	154	145	131	104	109	113	119

Table A4.1 Major and trace element results XRF, continued.

Volcano	Inland Lembata							Sirung		
Sample	32-3-2	32-3-3	32-3-4	32-5-1	32-5-6	32-8-1	32-9-1	S10.1	S14.2.2	S41.1
Lab. Nr.	12M310	12M311	12M312	12M314	12M319	12M322	12M323	12M520	12M521	13M953-D
Latitude	8.48	8.48	8.48	8.48	8.48	8.48	8.48	8.46	8.46	8.46
INAA	+	+	+			+		+	+	+
Isotopes								+	+	+
SiO_2	55.2	56.0	59.6	61.0	69.2	58.7	60.3	61.5	50.8	47.5
TiO_2	0.83	0.83	0.55	0.72	0.53	0.72	0.68	0.83	0.77	0.72
Al_2O_3	16.7	16.7	14.5	15.8	13.0	16.6	16.5	15.7	17.2	19.2
Fe_2O_3	9.53	9.52	7.24	7.50	6.33	8.72	7.91	7.90	11.29	11.24
MnO	0.17	0.16	0.15	0.15	0.09	0.17	0.14	0.17	0.20	0.18
MgO	4.78	4.45	4.82	2.66	1.97	3.09	2.93	1.94	6.24	6.14
CaO	8.70	7.91	7.63	6.31	5.32	7.87	7.00	5.75	10.47	12.73
Na_2O	2.44	2.50	2.59	3.16	2.30	2.83	3.07	3.49	2.02	1.72
K_2O	1.48	1.64	2.66	2.47	1.17	1.13	1.37	2.44	0.83	0.44
P_2O_5	0.23	0.21	0.23	0.24	0.10	0.13	0.13	0.23	0.14	0.11
H_2O-	0.31	0.60	0.12	0.09	1.43	0.43	0.71			
LOI	0.24	0.80	0.99	1.40	1.45	0.14	0.53	1.06	-0.35	0.17
Ba	876	1138	1444	1060	486	547	738	809	334	254
Sc	27	28	22	19	19	29	26	25	40	43
V	217	215	161	155	100	211	206	130	250	285
Co	25.0	26.7	21.3	11.2	10.3	19.7	15.4	11.5	38.2	36.5
Cu	58	52	52	29	29	76	36	31	106	46
Ga	16	16	13	15	12	16	16	17	17	19
Nb	4.1	4.3	5.4	6.9	3.5	3.2	3.2	7.6	2.3	1.1
Ni	23.6	24.6	29.3						26.0	15.6
Pb	15	18	17	17	10	16	16	22	7	5
Rb	37	41	73	67	39	39	40	86	28	14
Sr	518	468	511	460	249	326	350	345	382	384
Th	10.1	7.5	21.3	12.2	3.8	6.5	6.1	12.2		
Y	29	31	24	31	21	33	36	40	22	15
Zn	65	67	57	57	41	60	53	86	78	71
Zr	99	98	108	126	71	73	86	161	63	38

Table A4.1 Major and trace element results XRF, continued.

Volcano	B. Waspila			Dalaleng			Kedang			
Sample	B2.1	B3.1	B5.1	12-1-2	12-2-1	12-4-1	9-1-1	9-3-1	9-4-1	9-6-1
Lab. Nr.	12M506	12M507	12M508	12M381	12M382	12M385-3	12M388	12M392-3	12M393	12M395
Latitude	8.28	8.28	8.28	8.27	8.27	8.27	8.21	8.21	8.21	8.21
INAA	+	+	+	+		+				
Isotopes	+	+								
SiO_2	59.0	52.1	51.5	51.1	54.6	53.1	55.8	53.6	61.1	55.0
TiO_2	0.68	0.91	0.95	1.05	1.02	0.89	0.78	0.74	0.64	0.81
Al_2O_3	16.5	19.4	18.3	18.9	17.9	16.1	17.5	17.9	17.5	16.1
Fe_2O_3	7.78	9.78	10.62	10.15	9.51	9.20	8.24	8.95	5.52	8.27
MnO	0.15	0.19	0.19	0.19	0.20	0.16	0.15	0.19	0.17	0.18
MgO	3.13	3.42	4.18	4.48	2.92	5.48	3.24	3.69	1.52	4.09
CaO	6.98	10.13	10.01	9.51	7.60	10.20	7.70	8.84	5.19	8.66
Na_2O	2.93	3.00	2.75	2.99	3.72	2.36	3.18	3.14	4.32	2.67
K_2O	2.65	0.88	1.18	1.27	2.14	2.17	3.12	2.66	3.70	3.53
P_2O_5	0.24	0.22	0.29	0.32	0.41	0.32	0.31	0.35	0.32	0.63
H_2O-										
LOI	1.14	0.07	0.23	-0.10	0.39	1.94	0.10	0.07	0.40	0.44
Ba	1094	449	562	807	1077	850	1439	1401	1511	1168
Sc	18	29	31	27	19	25	16	16		17
V	136	215	287	229	165	192	190	177	75	173
Co	16.9	22.0	26.3	21.6	15.0	26.4	16.7	16.0	7.4	16.5
Cu	30	53	71	52	17	62	18	42		44
Ga	16	19	18	17	15	13	15	17	13	15
Nb	8.1	4.5	6.0	5.4	6.1	8.5	8.6	6.4	9.8	10.2
Ni	10.0		9.1	10.4		41.3				20.5
Pb	16	8	9	11	13	16	15	21	15	14
Rb	83	19	28	24	48	46	83	72	94	135
Sr	511	608	610	768	748	815	841	878	799	755
Th	17.2	5.7			12.6	17.6	26.1	20.2	24.3	15.4
Y	28	28	27	26	34	29	27	27	30	30
Zn	54	73	79	66	78	68	54	58	52	62
Zr	150	71	95	84	111	151	142	113	156	173

Table A4.1 Major and trace element results XRF, continued.

Volcano	Kedang							Treweg		
Sample	9-8-1	10-2-1	10-4-1	10-6-1	11-3-1	11-5-1	9-10-1	TR1.2.1	TR2.1.1	TR5.1.1
Lab. Nr.	12M397	12M369	12M371	12M373	12M376	12M378	12M386	12M522	12M523-T	12M524
Latitude	8.21	8.21	8.21	8.21	8.21	8.21	8.21	8.39	8.39	8.39
INAA	+	+	+	+				+	+	+
Isotopes			+	+				+		
SiO_2	64.0	57.7	54.4	59.2	58.3	59.5	55.0	55.7	56.0	56.8
TiO_2	0.46	0.74	0.82	0.72	0.74	0.63	0.78	0.82	0.82	0.76
Al_2O_3	17.2	17.2	18.0	16.8	17.2	17.1	17.9	18.0	17.8	17.8
Fe_2O_3	4.54	7.87	8.78	7.27	7.69	7.04	8.47	8.83	8.66	8.24
MnO	0.14	0.17	0.18	0.16	0.16	0.16	0.17	0.20	0.19	0.20
MgO	1.02	3.36	3.67	2.77	3.08	2.62	3.30	3.37	3.35	3.19
CaO	3.93	7.22	7.90	6.08	6.93	6.33	7.84	8.29	8.27	7.92
Na_2O	4.06	3.09	3.17	3.64	3.26	3.32	3.23	3.43	3.41	3.37
K_2O	4.43	2.30	2.71	3.05	2.36	3.01	2.96	1.15	1.30	1.41
P_2O_5	0.23	0.32	0.33	0.31	0.30	0.26	0.35	0.28	0.24	0.27
H_2O-										
LOI	0.47	0.68	0.69	-0.06	-0.08	0.14	0.31	0.21	0.86	0.50
Ba	1651	1202	1438	1492	1240	1396	1419	737	536	592
Sc		18	18	12	17	14	16	20	19	16
V	55	156	190	155	154	154	174	167	175	134
Co		14.1	17.4	8.7	14.6	13.2	15.9	16.2	16.2	13.6
Cu		29	27	16	26	22	28	37	24	22
Ga	13	15	15	15	18	15	15	17	16	16
Nb	12.4	7.7	8.3	8.6	9.4	8.6	9.0	4.5	6.0	5.7
Ni		12.7			12.3					
Pb	19	17	18	19	19	18	20	22	14	17
Rb	130	58	68	78	61	74	88	37	39	42
Sr	682	699	875	714	695	678	843	664	657	660
Th	44.3	18.8	19.1	20.8	19.1	21.1	32.5		5.4	
Y	36	29	28	28	29	24	29	27	23	25
Zn	41	61	63	45	57	50	61	51	53	49
Zr	202	171	131	161	178	146	144	83	84	90

Table A4.1 Major and trace element results XRF, continued.

Volcano			ı Besar						ıate	
Sample	1.2.3	A2.1	0.1.1	1.1.3	!.2	i.1	'.1	i.1	?.1	?.1.2
Lab. Nr.	1509	1510	1511-T	1512	1513	1514	1515	1516	1517	1518
Latitude	8.09	8.09	8.22	8.22	8.22	8.22	8.22	8.22	8.15	8.15
INAA	+	+	+	+	+	+	+	+	+	+
Isotopes	+				+				+	
SiO_2	58.0	58.6	55.9	58.3	55.6	56.8	56.6	57.2	59.6	57.8
TiO_2	0.61	0.59	0.82	0.60	0.78	0.69	0.72	0.69	0.55	0.63
Al_2O_3	17.8	18.2	17.5	18.1	17.2	17.7	17.5	17.7	17.0	17.3
Fe_2O_3	6.65	6.38	8.89	6.49	9.05	7.87	8.16	7.80	6.72	7.80
MnO	0.18	0.19	0.19	0.18	0.19	0.18	0.19	0.18	0.16	0.17
MgO	2.06	1.80	3.38	1.85	3.69	3.52	3.54	3.49	2.56	2.98
CaO	6.41	6.08	7.60	6.23	8.01	7.64	7.54	7.44	6.43	6.73
Na_2O	3.68	3.66	3.41	3.74	3.18	3.39	3.52	3.35	3.58	3.53
K_2O	4.28	4.08	1.98	4.18	1.96	1.82	1.89	1.83	3.09	2.83
P_2O_5	0.28	0.41	0.29	0.38	0.28	0.34	0.33	0.34	0.26	0.26
H_2O-										
LOI	0.38	0.55	0.63	0.36	0.24	0.10	-0.50	0.83	0.66	0.67
Ba	1782	1693	1076	1075	1112	1121	1130	1009	1785	1218
Sc	9	8	16	16	16	17	17	16	11	14
V	146	136	154	162	164	121	149	162	192	124
Co	11.3	10.8	16.9	17.2	20.1	12.7	15.6	17.0	12.6	15.9
Cu	21	18	33	21	35	33	30	32	23	27
Ga	16	16	15	14	15	16	17	15	14	16
Nb	8.0	8.6	8.0	8.6	7.0	8.3	8.1	7.4	7.4	6.7
Ni	8.8	8.8	8.8	9.0	9.5	16.3	15.6	8.1	10.0	8.6
Pb	14	16	17	14	14	21	17	18	13	16
Rb	120	119	52	54	52	52	56	50	92	79
Sr	857	838	765	734	815	733	723	771	663	674
Th	31.5	32.6	12.0	14.1	17.3	15.2	17.6	13.6	25.7	21.4
Y	30	30	27	24	23	24	25	27	21	23
Zn	65	61	53	50	54	56	56	53	49	58
Zr	169	168	115	121	110	131	132	118	141	129

Table A4.1 Major and trace element results XRF, continued.

Volcano	Ternate	Alor					
Sample	PK3.1.3	A1	A10	A11.1.1	A2	A4	A5
Lab. Nr.	12M519	12M500	12M505	12M501	12M502	12M503	12M504
Latitude	8.15	8.29	8.29	8.29	8.29	8.29	8.29
INAA	+	+	+	+	+	+	+
Isotopes					+	+	
SiO_2	57.9	51.6	61.3	60.5	56.9	56.4	59.4
TiO_2	0.65	0.79	0.81	0.66	0.77	0.64	0.76
Al_2O_3	17.3	17.1	17.9	16.5	17.5	16.9	16.8
Fe_2O_3	7.87	8.68	6.33	6.72	8.19	7.53	7.43
MnO	0.17	0.15	0.09	0.13	0.15	0.15	0.15
MgO	2.96	5.87	1.54	3.24	3.41	3.98	3.20
CaO	6.68	10.98	6.19	6.90	7.94	7.89	6.87
Na_2O	3.41	2.73	3.58	2.88	3.46	3.04	3.13
K_2O	2.79	1.81	2.12	2.27	1.54	3.19	2.11
P_2O_5	0.26	0.28	0.23	0.16	0.20	0.28	0.18
H_2O-							
LOI	0.67	1.00	1.22	1.22	1.42	1.07	1.83
Ba	1188	1010	618	566	1517	494	555
Sc	14	28	24	20	18	23	21
V	162	229	120	182	197	172	153
Co	15.8	30.5	11.7	15.2	22.1	20.0	17.3
Cu	25	66	18	43	50	36	34
Ga	16	16	19	16	18	18	17
Nb	6.1	8.0	9.8	6.9	12.0	7.2	7.3
Ni	8.8	38.7	8.7	10.7	24.2	17.4	12.8
Pb	12	20	12	20	28	15	17
Rb	80	60	72	94	119	197	123
Sr	683	630	383	288	697	337	285
Th	21.9	17.0	11.9	11.6	35.9	9.1	9.0
Y	24	22	30	26	20	25	29
Zn	60	67	67	60	61	62	59
Zr	130	110	169	153	141	136	159

Table A4.1 Major and trace element results XRF, continued.

Volcano	Sample	Lab.	Sc	Cr	Co	La	Ce	Nd	Sm	Eu	Tb	Yb	Lu	Hf	Ta	Th	U
Labalekan	4-3-1	L	29.2	47	26.5	6.5	15.3	9.24	2.92	0.91	0.62	2.56	0.42	2.12	0.085	1.55	0.43
	4-6-2	D	23.7	1.4	12.6	9.6	23.2	*15.8*	4.63	1.24	1	3.66	0.64	3.26	-	2.67	-
	4-6-4	L	28.2	62	25.8	7.9	18.8	10.7	3.18	0.95	0.66	2.74	0.41	2.24	0.11	2.07	0.64
	6-3-1	D	40	25	32.9	3.06	7.3	*5.8*	1.96	0.78	0.48	1.75	0.27	1.04	-	0.35	-
Mingar	7-5-1	L	30.5	25	21.8	9.5	21.5	12.2	3.53	1.07	0.69	2.83	0.45	2.39	0.15	2.8	0.86
	7-5-2	L	30.6	26	22	9.4	20.8	11.9	3.5	1.06	0.7	2.8	0.43	2.3	0.15	2.7	0.92
Labala Pen.	24-10-1	L	40	-	27.3	10.1	21.7	11.2	3.2	1.03	0.67	2.62	0.39	2.1	0.19	4.6	0.79
	24-2-1	L	35.7	10	24.2	1.87	5.8	4.7	1.83	0.77	0.46	2.05	0.31	0.91	0.033	0.39	-
	24-4-1	L	30.7	3	22	2.3	6.2	4.7	2	0.87	0.5	2.19	0.32	0.92	0.037	0.41	-
	25-8-1	L	32.6	8	22.7	4.7	10.8	7.7	2.39	0.89	0.54	2.25	0.33	1.35	0.094	1.07	0.19
	29-3-2	L	31.5	-	20.7	6	13.7	8.1	2.76	0.87	0.64	2.92	0.44	2.36	0.1	2.58	0.5
	31-2-1	L	27.7	7	19.1	9.3	19.5	12	3.31	0.96	0.67	2.78	0.41	2.54	0.16	3.33	0.59
Tandjung	8-5-1	D	14	2.7	3.8	12.4	26.5	*17.2*	4.78	1.38	0.9	4.05	0.67	3.82	-	2.75	-
	8-5-2	D	36.7	13.4	24.3	6.9	15.1	*11.2*	3.55	1.26	0.79	2.89	0.47	2.15	-	0.98	-
Werung	23-2-1	D	35.1	5.5	21.8	2.5	6.4	*5.2*	1.84	0.82	0.46	1.8	0.34	1.16	-	0.27	-
	23-5-3	L	46.1	5	34.6	1.19	3.6	3.8	1.53	0.69	0.41	1.84	0.25	0.68	0.027	0.28	-
	23-5-4	L	45.4	7	34	1.27	3.5	4.1	1.54	0.71	0.44	1.87	0.28	0.7	0.019	0.29	-
	23-6-1-1	L	40.5	8	28.7	2.5	6.6	5.7	2.05	0.81	0.49	2.19	0.32	1.11	0.041	0.43	-
	23-7-1	D	30.2	-	15	2.8	7.3	*5.5*	2.27	0.94	0.56	2.49	0.36	1.15	0.049	0.56	-
	23-7-6	L	39.4	3	22	2	5.2	3.9	1.82	0.78	0.48	2.12	0.33	0.89	0.042	0.4	-
	24-11-1	L	34.5	5	23.6	2.2	6.1	5.2	1.89	0.79	0.46	2.05	0.3	1.03	0.038	0.41	-
	24-12-1	L	31.4	-	18.4	3.6	9.1	6.3	2.33	0.94	0.57	2.46	0.36	1.3	0.1	0.76	-
	24-12-2	L	35.2	6	23.3	2.3	6.2	5.1	1.99	0.82	0.49	2.14	0.32	1.05	0.036	0.39	-
	24-13-1-2	L	30.9	5	18.2	3.4	8.5	6.5	2.29	0.9	0.55	2.46	0.4	1.26	0.055	0.58	-
	24-8-6	L	34.7	8	24.2	2.65	7.3	6.2	1.93	0.8	0.47	2.11	0.33	1.1	0.04	0.48	-
	24-9-1	L	35.6	7	23.2	3	7.7	4.9	2.01	0.82	0.5	2.18	0.32	1.09	0.083	0.59	-
	27-1-1	D	30.7	4.3	13.9	3	7.6	*7.2*	2.9	1.03	0.54	2.26	0.38	1.25	-	0.42	-
	27-10-1	D	29	4.4	13.5	3.8	9.1	*7.5*	2.65	1.06	0.61	2.96	0.43	1.58	-	0.52	-
	27-12-1	D	35.4	11	23.8	2.2	5.9	*5.1*	2	0.84	0.51	2.2	0.33	1.04	0.04	0.38	0.12
	27-2-1	D	37.7	4	22.8	2.3	6.6	*6.0*	2.33	1.01	0.65	2.55	0.43	0.78	-	0.38	0.12
	27-3-1	L	30.7	-	21.9	2.25	5.9	5.3	1.99	0.88	0.5	2.25	0.33	1.01	0.03	0.37	-
	27-4-1	D	29.5	4.2	19.8	1.93	6.1	*5.2*	1.87	0.85	0.49	2.14	0.332	0.88	-	0.34	-
	27-5-1	D	30.3	3.2	20	2.33	6	*5.2*	1.96	0.91	0.49	2.13	0.3	0.9	-	0.28	-

Table A4.2 INAA results. Lab. Indicates laboratory where measurement was performed, L: Leuven and D: Delft

Volcano	Sample	Lab.	Sc	Cr	Co	La	Ce	Nd	Sm	Eu	Tb	Yb	Lu	Hf	Ta	Th	U
Werung	27-6-1	D	34.7	4.4	20.4	2.5	6.9	*6.0*	2.26	0.94	0.58	2.29	0.35	1.34	-	0.34	-
	27-7-1	D	37	3.9	22.8	2.7	6.6	*6.0*	2.33	0.87	0.54	2.16	0.36	1.25	-	0.45	0.18
	27-8-1	D	30.7	3	16.3	2.8	6.7	*5.8*	2.16	0.91	0.51	2.2	0.36	1.26	-	0.38	-
	27-9-1	D	33.5	-	17.4	2.7	7.4	*6.3*	2.28	0.95	0.56	2.54	0.35	1.19	0.05	0.48	0.14
	30-1-1-2	L	35	7	20.9	2.2	6.3	5.4	2.05	0.86	0.5	2.29	0.34	1.1	0.036	0.36	0.14
Boleng	34.3.1	L	30.2	6	25.4	30.9	60.8	28.7	6.4	1.84	1	3.2	0.5	3.1	0.38	10.3	2.7
	34.4.1	L	14.4	6	8.2	50	93	38	8.1	1.92	1.16	4	0.62	5.3	0.67	20.4	5.1
Hadakewa	20-3-1	D	2.13	-	0.96	43.3	71.4	*26*	4.04	0.855	0.54	2.21	0.35	0.35	-	20	-
	20-7-1	D	2	1.1	0.98	41.9	69	*25*	3.86	0.8	0.5	2.18	0.36	3.11	-	19.4	-
Lewotolo	14-6-1-3	L	14.7	3	14.6	62.7	110	41.1	7.52	2.03	0.85	2.33	0.35	3.27	0.38	22.6	4.7
	14-6-2	L	23.4	5	23.6	48.5	90	35.9	7.14	2	0.86	2.29	0.36	2.93	0.34	13.1	3
	16-8-1	L	13.1	3	15.1	63.2	115	42.6	8.17	2.12	0.96	2.63	0.41	3.8	0.5	21.9	5.1
	17-19-1	D	6.74	-	8.14	58	97.8	*38*	6.2	1.54	0.65	2.5	0.4	4.11	-	27.2	-
	17-3-1-2	D	37.6	20.6	34.5	30.4	56	*27*	5.7	1.58	0.64	2.01	0.29	0.29	-	8.6	-
	17-4-1	L	32.7	26	32.8	37.6	72.4	32	6.58	1.88	0.88	2.19	0.35	2.28	0.23	11	2.6
SE of Lewo.	16-1-2	L	24.3	18	17.9	25.7	34	18.7	4.26	1.23	0.69	2.33	0.36	1.94	0.28	9.5	2.2
Noehanera	33-1-1	D	6.59	3.4	6.19	50.1	78	*31*	5.4	1.46	0.79	2.75	0.452	3.98	-	17.6	-
	33-2-1	L	17.7	11	18.4	35.1	62.8	25.3	5.19	1.46	0.75	2.42	0.38	3.39	0.36	9.2	2.2
	33-4-1	D	23.3	24	22.3	29.5	52.2	*23*	4.22	1.55	0.65	2.38	0.4	2.74	-	6.82	-
Inl.Lembata	32-1-1-1	L	24	19	19.8	24.6	47.9	22.4	5.26	1.46	0.82	2.86	0.43	2.82	0.24	5.5	1.24
	32-3-2	L	30.4	72	27.6	23.7	44.3	20.1	4.9	1.38	0.79	2.55	0.37	2.4	0.22	7.4	1.4
	32-3-3	L	30.6	74	28.5	27.8	47.9	24.1	5.6	1.55	0.88	2.79	0.39	2.5	0.22	7.4	1.4
	32-3-4	L	25.4	164	24.7	43.1	76	28.6	6.03	1.53	0.76	2.14	0.36	2.6	0.32	17.1	3.2
	32-8-1	L	30.4	17	23	10.2	19.8	11.5	3.57	1.15	0.75	3.2	0.48	1.91	0.19	2.7	0.87
Sirung	S10.1	L	24.6	5	13.5	28.1	55.1	26.1	6.2	1.49	1.07	3.9	0.59	4.2	0.51	11	2.8
	S14.2.2	L	38.2	31	40	8.9	18.8	10.3	2.83	0.89	0.53	1.95	0.32	1.56	0.16	2.95	0.99
	S41.1	L	42.9	48	39.1	4.2	9.9	6	1.87	0.7	0.38	1.44	0.22	0.88	0.07	1.08	0.21
B. Waspila	B2.1	L	21.3	15	19.4	39.5	71	27.9	5.7	1.47	0.78	2.66	0.43	3.6	0.43	14.3	2.9
	B3.1	L	27.6	8	24	12.5	27.8	16.3	4.2	1.39	0.73	2.67	0.41	1.9	0.14	2.9	0.73
	B5.1	L	30.7	14	28.4	20.8	42.8	21.6	4.9	1.47	0.76	2.57	0.38	2.3	0.23	4.5	0.99
Dalaleng	12-1-2	D	29	17.5	26.7	24.5	47.1	*25*	5.5	1.66	0.6	2.51	0.44	0.44	-	4.86	-
	12-4-1	D	30.5	180	30.5	39.1	76	*35*	7.1	2.02	0.76	2.62	0.42	0.42	-	14.9	-

Table A4.2 INAA results, continued.

Volcano	Sample	Lab.	Sc	Cr	Co	La	Ce	Nd	Sm	Eu	Tb	Yb	Lu	Hf	Ta	Th	U
Kedang	9-8-1	D	5.88	1.8	5.6	89.7	158	*58*	9.05	1.99	0.85	3.4	0.54	5.7	-	46.3	-
	10-2-1	D	20.2	18.1	20	55.4	101	*40*	6.88	1.93	0.8	2.7	0.46	4.41	-	15.8	-
	10-4-1	L	19.5	9	22.3	54	95	36.9	7	1.86	0.86	2.46	0.4	3.25	0.39	16.2	3.4
	10-6-1	L	14.9	4	15.8	52	92	34.6	6.71	1.73	0.84	2.56	0.41	3.89	0.48	9.7	4.2
Treweg	TR1.2.1	L	20.4	8	19.2	25.6	46.9	25	5.2	1.55	0.73	2.45	0.36	2.1	0.25	5.5	1.8
	TR2.1.1	L	19.9	6	18.2	22.9	46.5	22.2	4.7	1.46	0.67	2.2	0.32	2.17	0.26	5.5	1.6
	TR5.1.1	L	18.1	7	16.9	24.1	45.9	23.1	5	1.5	0.69	2.34	0.35	2.2	0.27	5.6	1.8
Kisu	BUA1.2.3	L	10.9	-	13.4	77.4	137	51	8.9	2.25	1.03	2.4	0.38	3.8	0.38	31.9	5.9
	BUA2.1	L	10.9	6	13.8	78.8	135	49	9	2.26	1.02	2.44	0.38	3.6	0.38	31.4	6.4
Pura Besar	PB10.1.1	L	17.8	-	20.8	44.2	78.6	32.2	6.2	1.72	0.78	2.5	0.37	2.83	0.35	12.7	2.7
	PB11.1.3	L	16.9	-	19.2	41.7	75	30.4	5.9	1.61	0.74	2.33	0.36	2.91	0.35	12.9	2.9
	PB2.2	L	18.7	5	21.9	45.5	81	30.9	6	1.65	0.74	2.2	0.37	2.7	0.32	14.9	2.9
	PB3.1	L	17.6	36	19.2	51.6	91	33	6.2	1.7	0.73	2.37	0.36	3	0.39	14.8	3.4
	PB7.1	L	17.4	33	19.1	52	92	36	6.1	1.71	0.75	2.37	0.38	3	0.38	14.9	3.4
	PB8.1	L	17.4	-	20.5	42.1	77	31.7	6.1	1.67	0.78	2.51	0.39	2.9	0.34	12.3	2.7
Ternate	PK2.1	L	13.1	9	16.6	54.4	92	29.2	5.5	1.48	0.67	1.97	0.33	3.2	0.38	23.2	4.8
	PK3.1.2	L	14.6	7	19.2	47.7	82	29.1	5.5	1.53	0.66	2.02	0.32	3	0.34	19.5	3.8
	PK3.1.3	L	14.4	5	18.8	46.6	79	27.7	5.4	1.5	0.65	1.97	0.32	2.9	0.33	18.9	4.1
Alor	A1	L	32.2	137	31.5	46	83	31	5.7	1.54	0.66	1.89	0.3	2.7	0.39	16.3	3.7
	A10	L	18.3	-	11.5	33	61.5	27.8	5.9	1.47	0.84	2.62	0.4	4	0.65	9.9	2.1
	A11.1.1	L	23.1	13	19.4	24.4	44.2	17.9	4.4	0.94	0.62	2.25	0.41	3.6	0.48	11	3.3
	A2	L	20.3	55	22.6	70.7	120	38.6	6.7	1.62	0.71	1.76	0.33	3.6	0.68	31.1	6.5
	A4	L	23.5	19	21.4	21.4	43.3	19.8	4.4	1.15	0.69	2.53	0.35	3.4	0.44	8.9	2.2
	A5	L	21.9	17	18.7	23.9	47.9	21.2	4.8	1.14	0.76	2.74	0.42	4	0.51	10.9	2.8

Table A4.2 INAA results, continued.

Volcano	Sample	^{143}Nd/^{144}Nd	error	^{87}Sr/^{86}Sr	error	Nd ppm	Sm ppm	^{147}Sm/^{144}Nd	error	^{206}Pb/^{204}Pb	^{207}Pb/^{204}Pb	^{208}Pb/^{204}Pb
Labalekan	4-3-1	0.512881	0.000007	0.705884	0.000036	10.16	2.98	0.17728	0.00016	19.001	15.669	39.322
	4-6-4	0.512860	0.000004	0.705895	0.000015	11.39	3.20	0.16983	0.00015	18.993	15.662	39.301
Labala pen.	29-3-2	0.512840	0.000004	0.705507	0.000018	10.00	2.78	0.18462	0.00022			
	31-2-1	0.512740	0.000011	0.705528	0.000016	6.29	1.73	0.16664	0.00024			
Werung	23-5-3	0.512912	0.000007	0.705637	0.000029	3.91	1.56	0.24118	0.00041			
	23-5-4	0.512914	0.000006	0.705623	0.000012	3.89	1.55	0.24133	0.00010	19.008	15.665	39.302
	24-8-6	0.512873	0.000004	0.705690	0.000014	5.57	1.92	0.20867	0.00007	19.041	15.669	39.344
	27-10-1	0.512865	0.000008	0.705693	0.000052	12.54	4.19	0.20211	0.00017	19.041	15.675	39.352
	27-12-1	0.512910	0.000004	0.705476	0.000014	5.52	2.02	0.22073	0.00011	19.048	15.668	39.329
Boleng	34.3.1	0.512695	0.000006	0.706087	0.000021	28.89	1.33			19.021	15.692	39.425
	34.4.1	0.512685	0.000003	0.706206	0.000013	39.49	8.05	0.12327	0.00014	19.019	15.691	39.417
Lewotolo	14-6-1-3	0.512584	0.000006	0.705907	0.000013	41.99	7.54	0.10854	0.00011	19.153	15.671	39.399
	16-7-1	0.512635	0.000007	0.705398	0.000015	38.67	6.83	0.10676	0.00029	19.147	15.666	39.381
	16-8-1	0.512608	0.000007	0.705669	0.000022	44.56	8.06	0.10940	0.00011	19.116	15.670	39.381
	17-4-1	0.512576	0.000006	0.706686	0.000026	31.50	6.48	0.12442	0.00028	19.083	15.674	39.354
Inl. Lembata	32-1-1-1	0.512718	0.000007	0.705099	0.000011	23.81	5.25	0.13319	0.00012			
Sirung	S10.1	0.512617	0.000005	0.705638	0.000009	26.94	6.14	0.13768	0.00023	19.227	15.693	39.519
	S14.2.2	0.512654	0.000006	0.705527	0.000017	11.08	2.81	0.15350	0.00155	19.203	15.685	39.463
	S41.1	0.512658	0.000011	0.705659	0.000014	6.29	1.83	0.17623	0.00052	19.125	15.695	39.385
B. Waspila	B2.1	0.512620	0.000007	0.705645	0.000015	28.98	5.68	0.11845	0.00011	19.165	15.683	39.506
	B3.1	0.512740	0.000005	0.705143	0.000012	16.43	4.22	0.15527	0.00038	19.252	15.727	39.681
Kedang	10-4-1	0.512616	0.000007	0.705411	0.000008	39.09	7.12	0.11003	0.00010	19.159	15.657	39.415
	10-6-1	0.512631	0.000007	0.705419	0.000018	36.81	6.74	0.11075	0.00013	19.169	15.704	39.557
Treweg	TR1.2.1	0.512628	0.000016	0.705449	0.000018	24.46	5.14	0.12701	0.00013	19.358	15.718	39.677
Kisu	BUA1.2.3	0.512496	0.000010	0.706758	0.000013	51.34	9.04	0.10642	0.00009	19.217	15.690	39.499
Pura Besar	PB2.2	0.512654	0.000007	0.705304	0.000016	32.01	5.93	0.11196	0.00016	19.351	15.720	39.714
Ternate	PK2.1	0.512555	0.000007	0.706033	0.00002	31.96	5.56	0.10511	0.00015	19.259	15.681	39.533
Alor	A2	0.512495	0.000007	0.707353	0.000022	41.36	6.71	0.09804	0.00010	19.245	15.719	39.628
	A4	0.512444	0.000008	0.707444	0.000017	19.91	4.40	0.13368	0.00013	19.441	15.750	39.935

Table A4.3 Nd-,, Sm-, Sr-, Pb isotope and trace element results.

CURRICULUM VITAE

Jurian Adriaan Hoogewerff werd op 25 Juni 1960 geboren te Utrecht. In 1984 behaalde hij behaalde hij het diploma ''ongedeeld VWO'' door middel van een staatsexamen bij de Leidse Onderwijs Instellingen.

In dat zelfde jaar begon hij met de studie geologie aan de Universiteit Utrecht. Na de propaedeuse koos hij voor het hoofdvak endogene geochemie met de bijvakken thermodynamica en informatica. Het afstudeeronderzoek concentreerde zich op het gedrag van gasholten in explosief magma dat bestudeerd werd aan de hand van puimsteenafzettingen op het eilandje Yali in de oostelijke Aegeïsche Zee.Van 1989 tot en met 1993 was Hoogewerff verbonden als Onderzoeker in Opleiding (O.I.O.) aan het Instituut voor Aardwetenschappen. In deze periode werd het onderzoek voor dit proefschrift gedaan in Indonesië, Utrecht, Amsterdam, Leuven en Berlijn.

In 1993 aanvaarde de auteur een positie als Universitair Docent Milieukunde aan de Universiteit Maastricht bij de vakgroep Gezondheids Risico Analyse en Toxicologie. In 1996 vetrok hij naar Arsenal Research in Wenen om voor twee jaar jaar als Marie Curie Fellow, gesubsidieerd door de Europeesche Unie, zijn eigen onderzoek naar geochemische fingerprintmethoden te kunnen doen. Sinds 1998 is Hoogewerff verbonden als projectleider aan Arsenal Research alwaar hij zich bezighoudt met het verder ontwikkelen van fingerprintmethoden middels sporenelementen en isotopen voor milieuonderzoek en toxicologische, forensische, anthropologische en aardwetenschappelijke toepassingen.